TETRATHIAFULVALENE DERIVATIVES AND THEIR APPLICATIONS IN MATERIALS CHEMISTRY

MIN SHAO


CENTRE FOR NFLD. STUDIES
MEMORIAL UNIVERSITY
OF NEWFOUNDLAND

Tetrathiafulvalene Derivatives and Their Applications in Materials Chemistry

by

©Min Shao

A thesis submitted to the

School of Graduate Studies

in partial fulfillment of the

requirements for the degree of

Doctor of Philosophy

Department of Chemistry

Memorial University of Newfoundland

April 2010

St. John's Newfoundland

Abstract

The projects outlined in this thesis were aimed at the synthesis and characterization of π-extended tetrathiafulvalene (TTF) derivatives, and exploration of their applications in materials chemistry. In these five projects, the synthetic targets have been successfully synthesized, and their electronic and electrochemical properties have been extensively explored and elucidated by CV, UV-Vis and fluorescence techniques.

The donor-acceptor (D-A) systems containing anthraquinone-type TTF analogues in the first and fourth projects exhibited obvious electronic push-pull effect within the molecules. This property renders them potential candidates for intramolecular charge-transfer and nonlinear optical materials. In these two projects, a TTFAQ donor was attached to a series of D/A groups such as anthraquinone, *t*-butylthiophenyl, amino and carboxyl ester groups via two acetylene bridges.

In the third project, thiophene was employed as π-spaces to spatially expand the conjugation paths between TTFs. It was expected that this could contribute many beneficial molecular properties, such as increased dimensionality, improved donor ability, intimate solid-state packing, minimized on-site Coulombic repulsion in the di- or polycationic states, and enhanced stability of the corresponding cation radical or dication species.

The fourth chapter focused on developing effective saccharide sensors using a TTFAQ-boronic acid as a platform. The work has demonstrated that phenylboronic acid and TTFAQ moieties can be efficiently tethered together via the CuAAC (click) reaction and TTFAQ-diboronic acid was found to give different voltammetric responses to the four saccharides tested.

The fifth and sixth chapters are concerned with TTF-based chemical sensors for metal cations. The signal transduction mechanism adopted in the fifth project is an internal charge-transfer mechanism (ICT), while a photoinduced electron-transfer mechanism (PET) in the system is described in the sixth chapter. The products in the fifth project displayed high sensitivity and selectivity for Cu^{2+} cation. The crown ether-annulated TTFAQ prepared in the sixth project showed decent sensitivity to Ag^{+}, Mg^{2+}, Li^{+} and Ba^{2+}, and particularly high selectivity for Ba^{2+} ion.

Acknowledgements

I would like to express my sincere gratitude to my supervisor, Dr. Zhao, Yuming, for his offering me this precious opportunity to get a doctoral education.

I would like to express my deeply and sincere thanks to Dr. Graham Bodwell for his teaching how to study organic chemistry and how to read organic books.

I would like to thank Dr. David Tompson for correcting my thesis; and my committee member, Dr. Christina Bottaro, for her valuable opinions on my research work and thesis.

I also want to acknowledge the staff in the chemistry department who have helped me during these four years, especially Mary Flinn who is working in the general office.

Table of Contents

List of Tables

List of Figures

List of Schemes

List of Symbols, Nomenclature or Abbreviations

A	acceptor
Å	angstrom
APCI	atmospheric pressure chemical ionization
aq	aqueous
Bu	butyl
BEDO	bis(ethylenedioxy)
BEDT	bis(ethylenedithio)
cm	centimeter
CT	charge-transfer
CuAAC	Cu-catalyzed alkyne-azide cycloaddition
CV	cyclic voltammetry
d	doublet
D	donor
D-A	donor-acceptor
DBU	1,8-diazabicycloundec-7-ene
DMDCNQI	dimethyldicyanoquinonediimine
dmit	4,5-dimercapto-1,3-dithiole-2-thione
DMSO	dimethylsulfoxide
DPV	differential pulse voltammetry
DTT-TTF	dithienothiophene tetrathiafulvalene
EA	electron affinity
EC	a chemical reaction (*c*) that may follow an electron transfer (*e*) step

EDG	electron donating group
EWG	electron withdrawing group
EPR	electron paramagnetic resonance
equiv	equivalent
Et	ethyl
exTTFs	π-extended TTF analogues
GC	gas chromatography
h	hour(s)
HOMO	highest occupied molecular orbital
Hz	hertz
IR	infrared (spectroscopy)
ICT	intramolecular charge-transfer or internal charge-transfer
J	coupling in hertz
L	liter
LCMSD	liquid chromatography quadrupole mass spectrometer
LUMO	lowest unoccupied molecular orbital
m	multiplet
MALDI-TOF	matrix-assisted laser desorption/ionization time-of-flight mass
MDT	methylenedithio
Me	methyl
mg	milligram(s)
min	minute(s)
mL	milliliter

mmol	millimole
mM	millimole/litre
Mp	melting point
mol	mole
MS	mass spectrometry
m/z	mass to charge ratio
NBS	*N*-Bromosuccinimide
NLO	nonlinear optical
nm	nanometer
NMR	nuclear magnetic resonance
o	*ortho*
p	*para*
PET	photoinduced electron transfer
Ph	phenyl
rt	room temperature
s	second or singlet
t	triplet
TBAF	tetra-*n*-butylammonium fluoride
TCNAQ	7,7,8,8-tetracyano-*p*-anthraquinodimethane
TCNQ	7,7,8,8-tetracyano-*p*-quinodimethane
Tf	trifluoromethanesulfonyl
TFA	trifluoromethanesulfonic acid
THF	tetrahydrofuran

TLC	thin-layer chromatography
TMS	trimethylsilyl
TMSA	trimethyklsilylacetylene
TMTSF	tetramethyltetraselenafulvalene
TTeF	tetratellurafulvalene
TTF	tetrathiofulvalene
TTFAQ	tetrathiofulvalene anthaquinone
T-TTF	thiophene tetrathiafulvalene
TT-TTF	thienothiophene tetrathiafulvalene
UV-Vis	ultraviolet-visible
V	volt
δ	chemical shift
μM	micromole/litre
λ_{max}	maximum absorption wavelength
ε	molar extinction coefficient

Chapter 1

Introduction

1.1 A historical overview of TTF

Tetrathiafulvalene (TTF) has attracted great attention as an organic π-electron donor since the discovery of high electrical conductivity in a chloride salt of TTF,[1] and metallic behaviour in the charge-transfer complex TTF-TCNQ (TCNQ = 7,7,8,8-tetracyano-*p*-quinodimethane).[2] In 1972, Wudl demonstrated that TTF chloride salt was an excellent organic solid-state semiconductor with a resistivity of 3.7±1 Ω cm (E = 10 V) at room temperature. Furthermore, they found that compressed pellets of TTF chloride salt did not lose conductivity or visibly degrade even after 10^3 mol equiv of current was passed through the pellets. These studies showed that TTF chloride salt had properties comparable to mixed valence organometallics, such as biferrocenium picrate (Figure 1.1). In 1973, another new highly conductive organic based TTF:TCNQ (1:1) charge-transfer (CT) complex was reported by Cowan and co-workers.[2] In their experiments, highly pure TTF and TCNQ were combined in acetonitrile resulting in a precipitate of 1:1 TTF/TCNQ complex. This complex retained ohmic conductivity properties over a wide temperature range and was regarded as the first true organic metal. The breakthrough immediately drew attention from the scientific community.

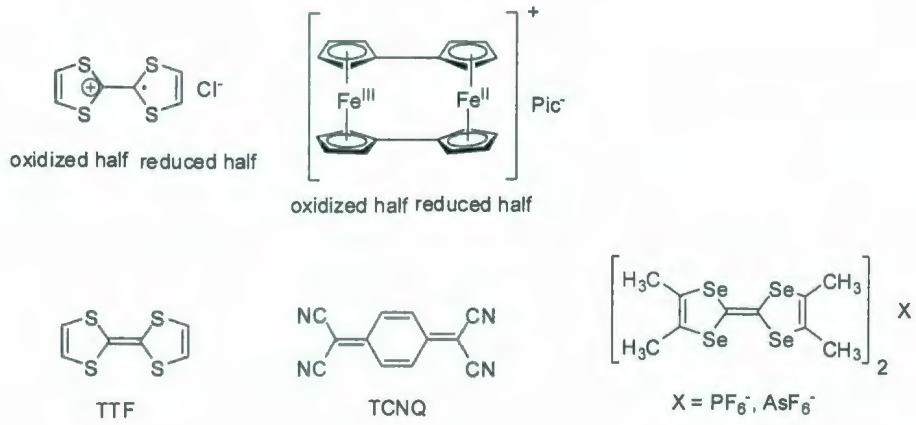

Figure 1.1: Structures of TTF chloride salt, TTF/TCNQ (1:1) complexes and the Bechgaard salts.

In the following two decades, enormous attention was focused on the synthesis and characterization of organic charge-transfer salts with unusual solid-state properties, metallic conductivity and superconductivity. In 1979, the first molecule-based superconductor was prepared by mixing Bechgaard salts $[TMTSF]_2X$ ($X = PF_6^-$, AsF_6^-)[3] (Figure 1.1) with a selenium-containing TTF derivative, namely tetramethyltetraselenafulvalene (TMTSF). Since then, a great deal of work has been carried out to enhance the electron-donating ability of TTF derivatives in order to improve the conductivities of salts and charge-transfer complexes derived from them. Important events in the development of organic conductors based on CT complexes and ion radical salts are listed in Table 1.1.[4]

Table 1.1: Major landmarks in the development of organic conductors based on CT complexes and ion radical salts.

Year	Event
1973	TTF-TCNQ prepared the first organic metal; σ_{rt} = 500 Scm^{-1}; T_{M-I} at 53 K.
1980	$(TMTSF)_2X$ salts: organic superconductivity first reported at 0.9 K and 12 kbar for $X = PF_6^-$, and at 1.4 K and ambient pressure for $X = ClO_4^-$.
1982	$(BEDT\text{-}TTF)_2$ ClO_4 (1,1,2-trichloroethane): metallic conductivity over temperature range 294-1.4 K in a sulphur-based system.
1983	$(BEDT\text{-}TTF)_2$ ReO_4: the first sulphur-based organic superconductor; T_c = 1.4 K at 4 kbar.
1984	β-$(BEDT\text{-}TTF)_2I_3$: T_c at 1.4 K and ambient pressure.
1986	β-$(BEDT\text{-}TTF)_2I_3$: T_c raised to 8 K under anisotropic pressure.
1986	$TTF[Ni(dmit)_2]_2$: the first superconducting system based on a CT salt of a π-anion molecule; T_c = 1.6 K at 7 kBar.
1987	$Cu(2,5\text{-}DMDCNQI)_2$ extremely high conductivity for a radical ion salt, metallic behaviour between 295-13 K with $\sigma = 5 \times 10^5$ Scm^{-1} at 35 K.
1987	$Me_4N[Ni(dmit)_2]_2$ superconductivity in a π-anion molecule having a closed shell cation, T_c = 50 K at 7 kBar.
1988	TTeF-TCNQ synthesized, σ_{rt} = *ca.*2000 Scm^{-1}.
1988	$(MDT\text{-}TTF)_2$ AuI_2 sulphur-based superconductivity observed with an unsymmetrical unsymmetrical donor, T_c = 35 K at ambient pressure.
1988	κ-$(BEDT\text{-}TTF)_2Cu(SCN)_2$ ambient pressure superconductivity at 104 K.
1990	$(BEDO\text{-}TTF)_{24}I_3$ the first organic metal of an oxygen-containing donor,

	σ_{rt} = 100-280 Scm^{-1}.
1990	$(BEDO\text{-}TTF)_2Cu(NCS)_3$ superconductivity observed in an oxygen-containing donor, T_c = 10 K at ambient pressure.
1990	k-$(BEDT\text{-}TTF)_2Cu(N(CN)_2)$ X, X = Br, Cl currently the highest T_c organic superconductors, T_c = 116 K at ambient pressure for X = Br, T_c = 125 K at 3 kbar for X = Cl.

In the next 20 years, interest has been directed toward novel magnetic and optical properties of functionalized TTF derivatives, and application of TTF derivatives as versatile building blocks in cation sensors, liquid crystals, intramolecular charge-transfer and nonlinear optical materials, supramolecular switches and devices, and redox polymers.

1.2 Synthesis of various TTF derivatives

The TTF framework has been modified by different strategies, which has led to a large number of functionalized TTF derivatives. The focus of these studies is aimed at a synthetic control over the energies of the HOMO-LUMO (highest occupied molecular orbital-lowest unoccupied molecular orbital) gap. It is well-known that low band gaps are very important characteristics to organic electronic materials, since band gap is a standard to evaluate their abilities to donate (from HOMO) or accept (to LUMO) electrons. There are two distinct synthetic approaches to achieve this goal at the molecular level: (1) extending π-conjugation in the molecule; (2) construction of molecular D-spacer-A systems (where D is an electron donor and A is an electron acceptor) in which electron-

donating and electron-withdrawing substituents are placed at appropriate sites to finely tune HOMO and LUMO levels.[6] Both principles have been successfully utilized in the design of π-conjugated polymers. Many TTF-spacer-A systems functionalized with electron-donating groups (EDG) and electron-withdrawing groups (EWG) exhibit lower HOMO-LUMO gaps. A variety of π-conjugated oligmers, polymers and TTF-spacer-A systems has been designed and synthesized, and their electrochemical properties were explored for potential applications in materials chemistry.

A number of versatile synthetic routes to TTF with yields up to 90% have been reported. Fanghaenel and co-workers gave a detailed review on this subject (Scheme 1.1).[7] Among these approaches, A, B, C are the most popular synthetic paths to the TTF structure. Methods A and B are the most straightforward and widely adopted methods to synthesize symmetrical TTF. For asymmetric TTFs, method C, a base-promoted Wittig coupling, is commonly used.

Two most important TTF precursors 1,3-dithiole-2-thione and 1,3-dithiolium salts can be prepared by numerous ways as shown in Schemes 1.2 and 1.3.[7]

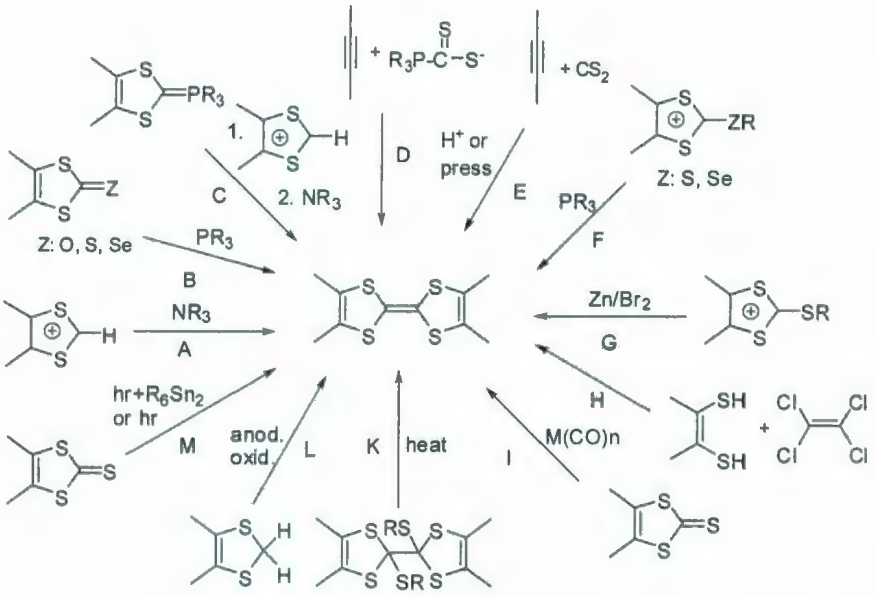

Scheme 1.1: Synthetic routes to the TTF skeleton.

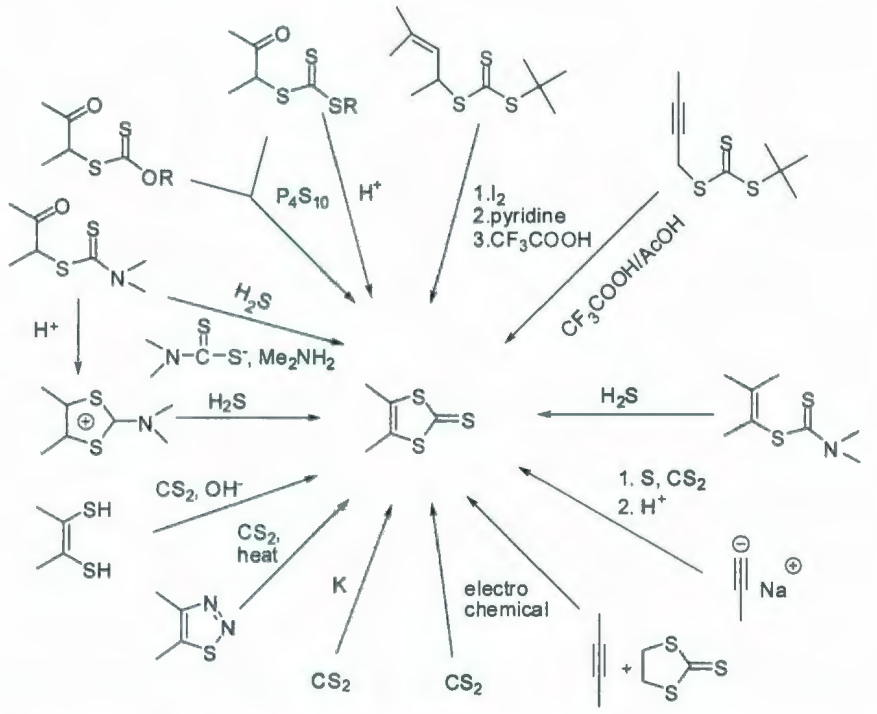

Scheme 1.2: Synthetic routes to TTF precursors: 1,3-dithiole-2-thione.

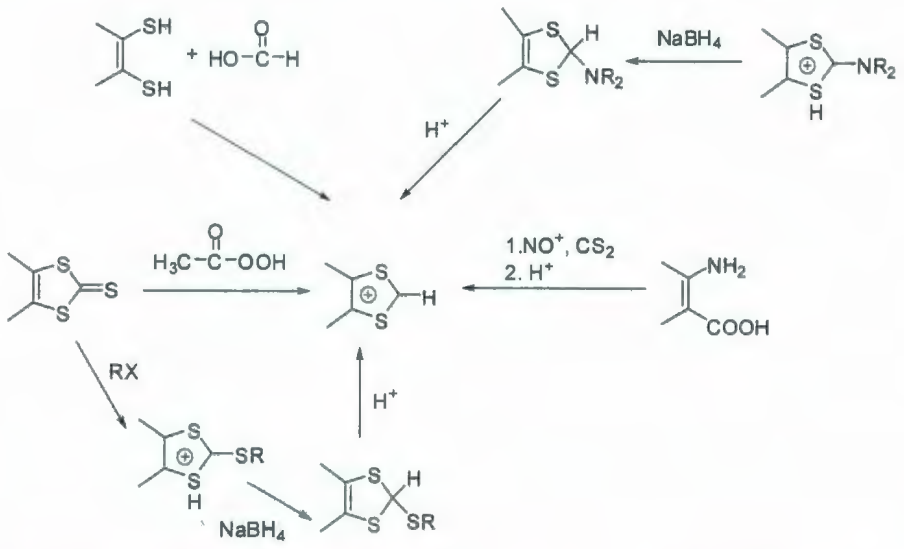

Scheme 1.3: Synthetic routes to TTF precursors: 1,3-dithiolium salt.

With the TTF precursors and TTF in hand, functionalization of TTF derivatives can be performed via two different synthetic methodologies: (1) construction of the TTF skeleton from functionalized precursors; (2) direct functionalization of complete TTF compound.[6]

Based on the first strategy, numerous organic metals and π-extended TTF derivatives have been reported. In a highly π-extended system containing two or more 1,3-dithiol-2-ylidene moieties, the use of a phosphonate synthon seems to be efficient. Wittig olefination under basic conditions easily affords π-extended TTF derivatives by using ylide **4** generated from phosphonium salt **1**.[8] The phosphonium salt **2** is another reagent that undergoes Wittig olefination.[9] Alternative ylide **5** from phosphonate **3**[10] can be employed in a Horner-Witting. The phosphorus salt **2** and phosphonate **3** can be respectively prepared by reacting an aromatic 1,3-dithiolium salt with triphenylphosphine or with trialkyl phosphite in the presence of sodium iodide. Access to the target π-

extended TTF derivatives can be achieved by reaction between the olefination reagents **4** or **5** and a suitable (poly)ketonic or polyaldehydic derivative (Scheme 1.4).

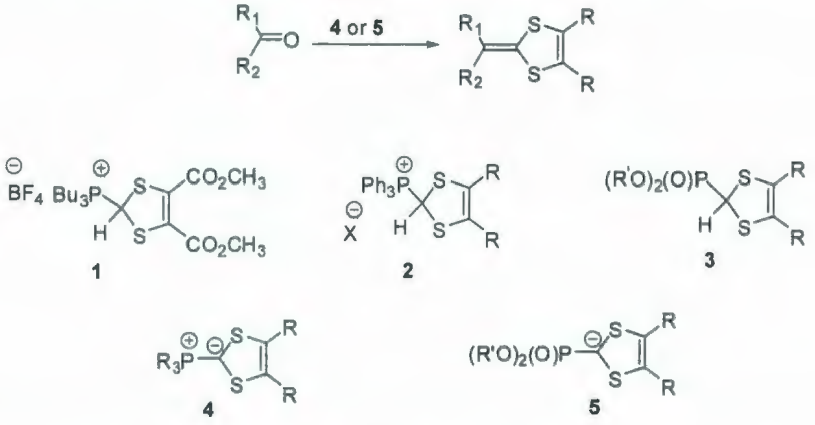

Scheme 1.4: Synthesis of 1,3-dithiol-ylidene via Wittig-Olefination.

The above methods for the syntheses of π-extended TTF derivatives based on the Wittig-type reaction are generally preceded by multi-step syntheses of the starting materials, and all reagents need to be compatible with basic conditions. In addition to those methods, Iijima *et al.* developed a novel and simple olefination methodology to π-extended TTF derivatives (Scheme 1.5).[11] It employs direct triethyl phosphate-mediated coupling between a conjugated ketone and a 2-thione-1,3-dithiole derivative. This reaction allows the access to π-extended TTF derivatives containing substituents that are incompatible with Wittig reaction conditions. The only limitation of this method is that the reagents should be amenable to use at high temperatures (Scheme 1.5).

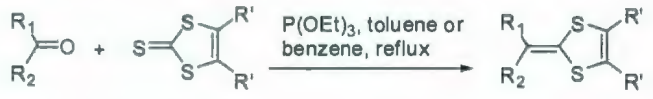

Scheme 1.5: Olefination methodology of ketones and 2-thione-1,3-dithiole derivatives.

Based on previous reports on synthesizing π-extended TTF derivatives, an efficient and reliable route to π-extended TTF analogues has been established by Zhao *et al.* (Scheme 1.6). TTFAQs are a large and important series of the π-extended TTF family. They were generated by coupling TTF and anthracene. The first TTFAQ was reported in 1978 by Akiba *et al.*[9] However, intensive studies of the electronic properties of this family of compounds were carried out by Bryce, who demonstrated the unique redox behavior of TTFAQs.

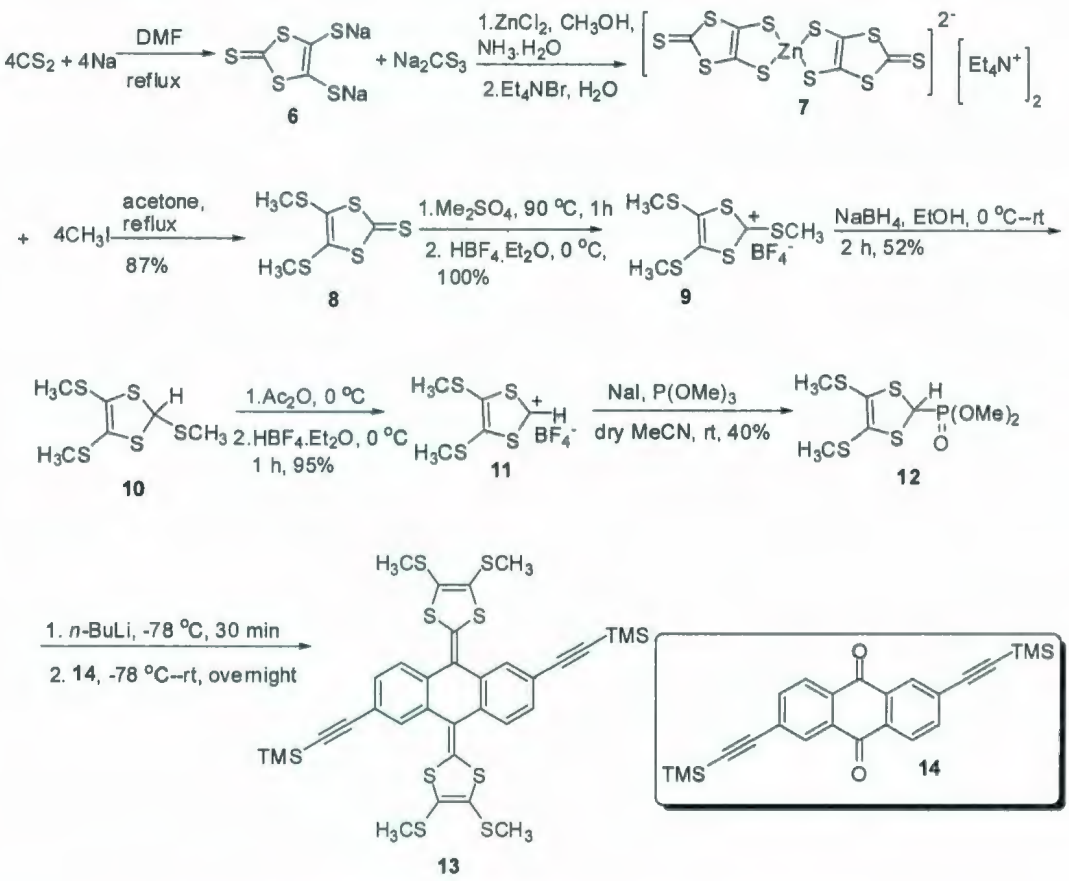

Scheme 1.6: Synthetic route to π-extended TTF analogues TTFAQ.

For the second strategy, four approaches have been employed frequently to functionalize TTF (Scheme 1.7).[6] They include: deprotonation of *S*-(β-cyanoethyl)thio-

TTF, followed by alkylation of the resulting thiolate;[12] lithiation of the TTF molecule followed by reaction with a number of electrophilic reagents, affording aldehydes, alcohols and carboxylic acids, which are convenient synthons for further functionalization;[13] the Diels-Alder reaction of dimethylene generated *in situ* from bis(bromomethyl)TTF or 3-sulfolenoTTF with different dienophiles, which was used in the synthesis of several annulated TTF-quinones and TTF-fullerene conjugates; and *N*-alkylation of mono-/bis-pyrrolo-TTF compounds, which was particularly effective in supramolecular chemistry.[14]

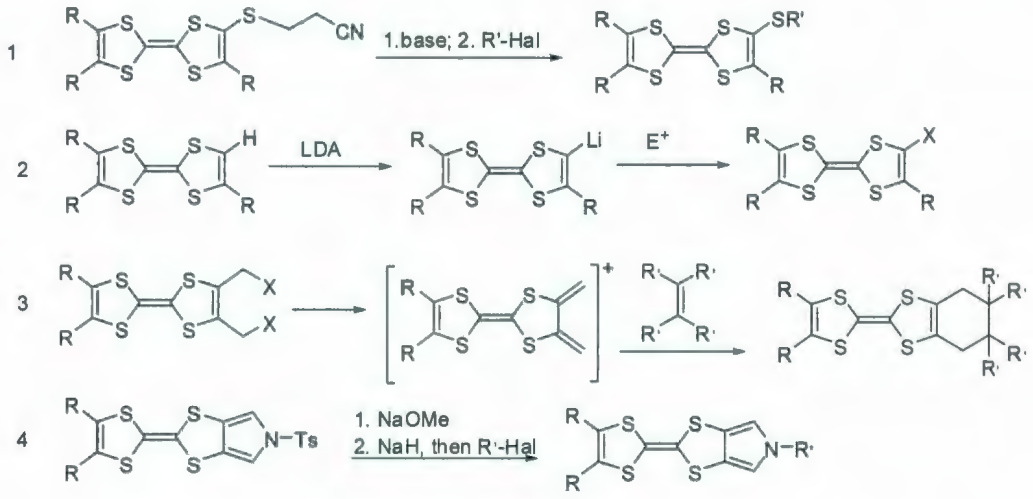

Scheme 1.7: Four general approaches to functionalize TTFs.

1.3 Properties of TTF derivatives and their applications in materials science

TTF has many unique properties which make it an ideal and versatile building block for new materials. It has a boat-like geometry and is a 14-π-electron system in the ground state. TTF can be sequentially and reversibly oxidized to the cation radical and dication at

relatively low potentials[15] ($E_{1/2}^1$ = +0.34 V and $E_{1/2}^2$ = +0.78 V, vs. Ag/AgCl in acetonitrile) (Figure 1.2). The oxidation potentials can be finely tuned by the attachment of electron-donating or electron-withdrawing substituents. The dithiolium rings in the cation radical or dication of TTF resulting from oxidation are planar and aromatic. Due to the small difference between planar and boat-like conformations, TTF is very flexible and can appear in various conformations, depending on the donor-acceptor interactions in the crystals. It is very stable to many synthetic transformations, except strongly acidic or strongly oxidizing conditions. Owing to intermolecular π-π interactions and non-bonded sulfur-surfur interactions, TTF and its derivatives can form dimers, highly ordered stacks, or two-dimensional sheets.

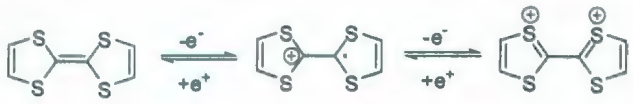

Figure 1.2: TTF in neutral, cation radical and dicationic forms.

The field of TTF synthetic chemistry continues, even after 40 years, resulting in a large number of TTF derivatives and systems that span molecular, supramolecular and macromolecular sized domains. In the past two decades, attention has focused on the synthesis and characterization of organic charge-transfer salts, which display unusual solid-state properties, metallic conductivity and superconductivity. The focus on the development of molecular devices with novel magnetic and optical properties of functionalized TTF derivatives is a relatively new research direction. These derivatives were widely applied in the fields of supramolecular chemistry, molecular switches, nonlinear optics, molecular sensors, and photovoltaics. In the following sections, with the exception of conventional applications as molecular conductors, new applications of

functionalized TTF derivatives as versatile π-electron systems in materials chemistry will be discussed in detail.

1.3.1 TTF-spacer-A systems for intramolecular charge transfer and nonlinear optical materials

Although TTF and its derivatives have been studied over 30 years as π-electron donors in intermolecular charge-transfer materials, the potential of TTF as a donor in functional molecular devices is still a target application. One of the original purposes for the synthesis of TTF D-A system was aimed at searching for novel charge-transfer materials with predefined D/A stoichiometeries. According to the published literature, a wide range of functionalized TTF moieties covalently linked to a π-acceptor moiety through σ or π-bonded bridges possess intramolecular charge-transfer (ICT) properties. The absorption of a photon yields excited states which differ dramatically from the ground state. Electron acceptors include TCNQ, quinone, electron-deficient aryl, pyridinium and bipyridinium fullerene, phthalocyanine, conjugated carbonyl, thiocarbonyl, ester, and related acceptor groups. They can be divided into several groups according to their structural characteristics: nonconjugated TTF-σ-A systems; conjugated TTF-π-A systems; and π-extended TTFs.

1.3.1.1 Nonconjugated TTF-σ-A systems

Covalent attachment of donor/acceptor systems was an extremely important development in the field of electron transfer because the spatial control of D-A components allowed new insights into electron transfer dynamics. In 1974, Aviram and Ratner[16] proposed a

TTF-σ-TCNQ compound **15** (Figure 1.3), in which a strong donor TTF is covalently connected to a strong acceptor moiety TCNQ as a strategy to lower the HOMO-LOMO energy gap by creation of a covalent bond ion-pair. Although this compound has not been prepared so far, the idea has inspired several groups to pursue other readily accessible TTF-σ-TCNQ systems. Compound **16**[17] (Figure 1.3) was the first TTF-σ-TCNQ system made; however, the difficulty of synthesis and purification thwarted further studies on this material. Infrared (IR) and Electron Paramagnetic Resonance (EPR) data of compound **16** showed an ionic ground state. Compound **17**[18] (Figure 1.3) with easy synthesis and purification allowed for detailed characterization by cyclic voltammetry (CV), EPR and IR. This compound exhibited a typical redox wave of the TTF system, two reversible, one-electron oxidation waves, and one, reversible, two-electron wave corresponding to the reduction of the TCNAQ system to the dianion. Simultaneous electrochemistry and EPR provided qualitative evidence for intramolecular interaction between the TTF and TCNAQ groups in compound **17**.

Compounds **18** and **19**[19] (Figure 1.3) were synthesized by Cava, Metzger and co-workers. CV data for compound **18** showed no interaction between the TTF and quinone moieties, but compound **19** was observed to show remarkably large positive shifts (>400 mV in dichloromethane) for both TTF oxidation waves compared to its precursor, which was ascribed to the inductive effect of a strong electron withdrawing group through σ bonds.

The macrocyclic compound **20**[20] (Figure 1.3) contains a TTF donor and a quinone acceptor unit. The charge-transfer properties mimic intermolecular systems rather than

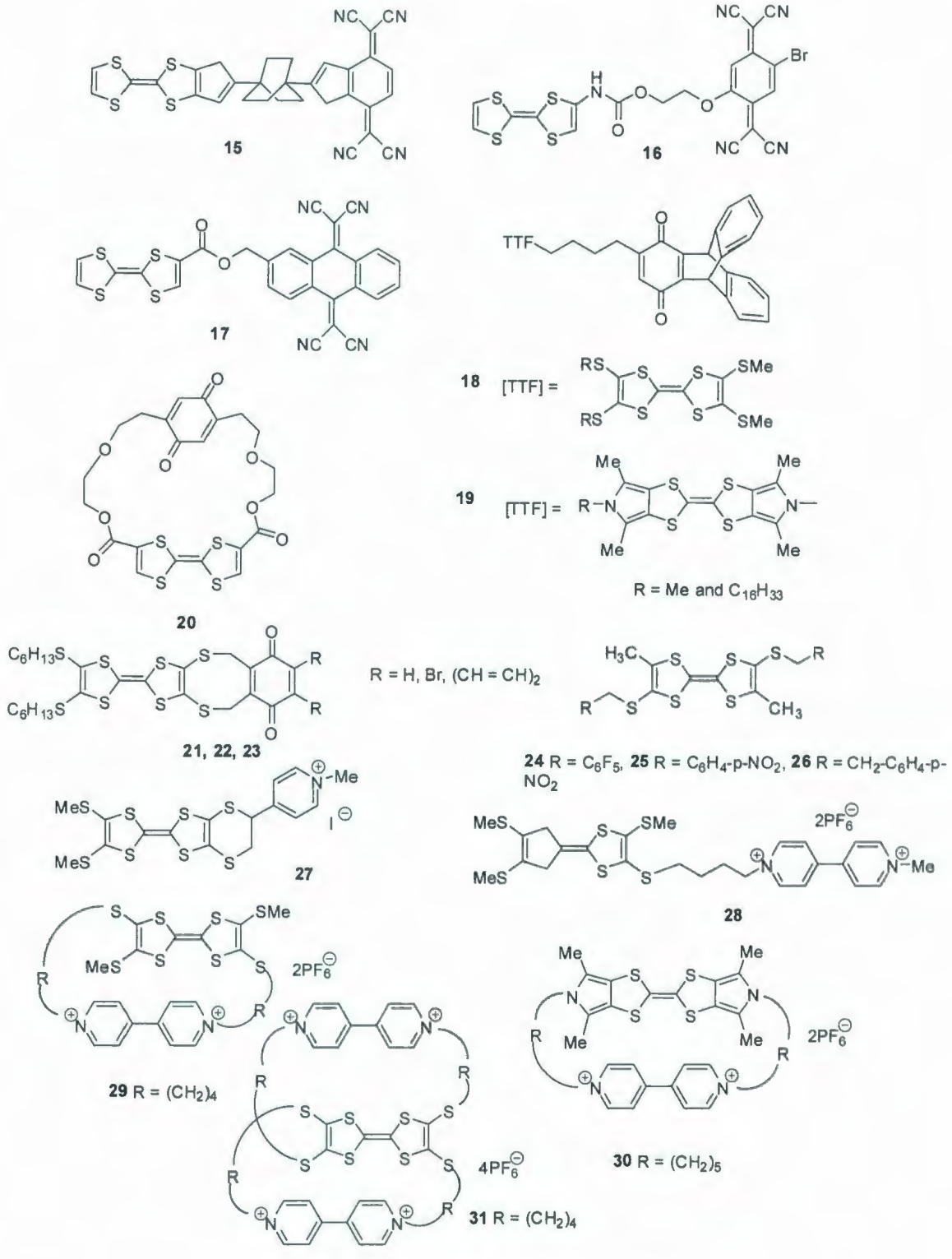

Figure 1.3: Structures of compounds **15-31**.

intramolecular adducts. A series of compounds **21-23**[21] (Figure 1.3) were prepared by the Martín group. Optical and electrochemical data for these compounds demonstrated that the TTF units and quinone units acted independently without significant electronic coupling in the ground state. It was argued that the rigid structure of $-S-CH_2-$ units with σ bonds prevented strong polarization of electron density between donor and acceptor units. The absence of an ICT band was consistent with expectations based on weak electronic coupling.

Several compounds **24-26**[22] (Figure 1.3) with σ bridges between TTF and electron-deficient aryl groups with known redox properties were prepared by Robert and co-workers. The oxidation potential $E_2^{1/2}$ was raised as much as 190 mV for compound **24** relative to that of R = H, and the oxidation potential was remarkably greater for **25** with the shorter chain ($\Delta E_1^{1/2}$ = 50 mV; $\Delta E_2^{1/2}$ = 140 mV) than **26** ($\Delta E_1^{1/2}$ = 20 mV; $\Delta E_2^{1/2}$ = 110 mV), consistent with an increase in the charge-transfer character of the compounds.

The above electron-deficient aryl substituents are all weak acceptor moieties. Significantly stronger acceptor moieties, pyridinium and bipyridinium groups were employed as acceptors in the following compounds. Becher and co-workers prepared compound **27**.[23] A weak ICT absorption at $\lambda_{max} \approx$ 665 nm was observed, although the pyridinium cation is an extremely strong acceptor. In 1997, Cava, Becher, and coworkers synthesized a number of TTF-σ-bipyridinium compounds **28-30** (Figure 1.3).[24] These three compounds had broad ICT bands λ_{max} at 624, 673 and 640 nm respectively. Compound **29** has the highest extinction coefficient since its conformation is more rigid than compounds **28** and **30**. The conformation of compound **28** is flexible and compound **30** has a longer R group. The strong electron affinity (EA) of the bipyridinium moiety

generated a distinct amphoteric multiredox electrochemical behavior in these molecules, with an electrochemical gap between the first oxidation and the first reduction potential lower than 1 eV. Compound **31**[25] was also observed to have an ICT band in the UV-Vis spectrum. Anodic shifts (70-90 mV) in both of the oxidation potentials of **31** were ascribed to a combined effect of ICT interactions and electrostatic repulsion between the four pyridinium cations and the oxidized TTF cations.

Fullerene C_{60} has been used as an acceptor in TTF-σ-A systems due to its low HOMO-LUMO gap, which is the result of its extended conjugated π-electronic structure. Compounds **32**,[26] **33**,[27] **34**[28] and **35**[29] (Figure 1.4) were synthesized via [3+2] dipolar cycloaddition reaction of a TTF-substituted azomethine ylide or Diels-Alder reaction of 4,5-dimethylene TTF on C_{60}. UV-Vis and CV data for these compounds showed no electron transfer within these molecules. Rovira and co-workers have synthesized and performed more detailed experiments on the series of compounds **34, 36, 37** and **38**.[30] Electronic spectra of **34, 36** and **37** implied weak inter- or intramolecular interactions between the donor and acceptor moieties.

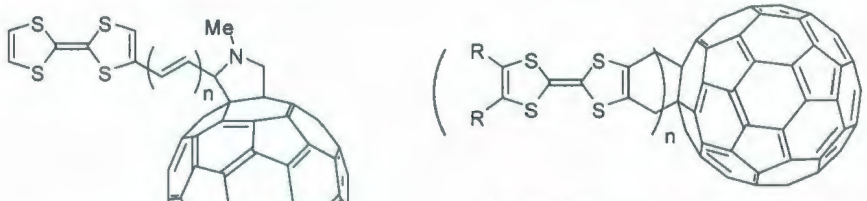

Figure 1.4: Structures of compounds **32-38**.

The acceptor groups mentioned above possess moderate electron affinity. It is very difficult to incorporate a strong acceptor moiety in TTF-σ-A type compounds. For

example, the conversion of TTF-benzoquinone dyads in the TTF-TCNQ derivatives failed due to the intolerance of TTF to highly acidic reaction conditions. It is known that condensation of poly(nitrofluoren-9-one)s with malononitrile occurs under milder conditions and the resulting dicyanomethylene derivatives are very strong acceptors. Upon this consideration, the Bryce group synthesized a series of novel donor-acceptor dyads[31] **39-43** (Figure 1.5) in a motif of TTF-σ-A architecture. Electrochemical data of these compounds showed that the TTF-fluorenone dyads are amphoteric compounds, displaying five reversible redox waves (two oxidations due to TTF and three reductions due to fluorenone), with a HOMO-LUMO gap as low as 0.5-0.6 eV. The electron affinity of the fluorenone moiety can be easily enhanced by conversion of fluorenone to dicyanomethylene derivatives. The reduction waves of the 9-dicyanomethylene derivatives are shifted to more positive potentials by around 300 mV, leading to a reduced HOMO-LUMO energy gap.

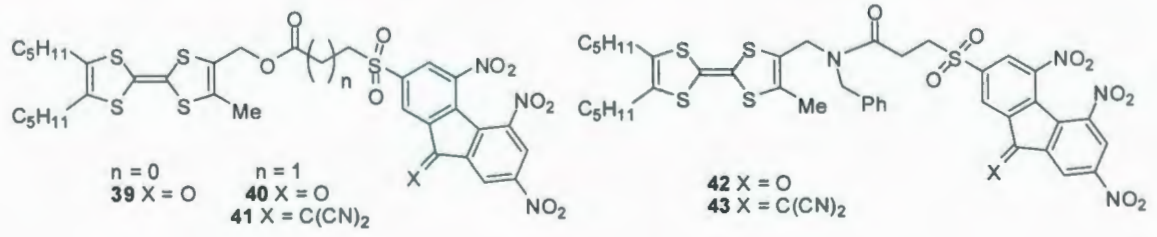

Figure 1.5: Structures of compounds of **39-43**.

1.3.1.2 Conjugated TTF-π-A systems

One of the original purposes for the synthesis of TTF D-A systems was to explore novel charge-transfer materials with predefined D/A stoichiometries for optoelectronic applications, such as nonlinear optical materials (NLO). An approach toward NLO

chromophores, based on aldehydes, has been employed widely. The moderate acceptor properties of the aldehyde group in compound **44**[32] can be easily enhanced by conversion into dicyanomethylene derivatives **45**.[33] Later, conversion of TTF-aldehydes into nitrophenyl **46**,[34] nitrophenylimine **47**,[34] oxazolone **48**,[33] 3-dicyanomethyleneindan-1-one **49**,[33,35] barbituric acid **50**,[36] and thiobarbituric acid **51**[33] were accessible with large hyperpolarizability. Experimental data of these compounds indicate that increasing the electron-withdrawing properties of the accepter can reduce both the electrochemical and optical gaps and provides higher hyperpolarizability. Although the TTF-π-A system with the thiobarbituric acceptor group has the lowest HOMO-LUMO gap and good hyperpolarizabilities (180-45) $\times$ 10^{-48} esu, the system with the oxazolone and dicyanomethyleneindanone acceptor groups obtained the highest hyperpolarizabilities, (259-611) $\times 10^{-48}$ esu. In many, but not all, cases, the elongation of the π-linker between the donor and acceptor results in small, but consistent, hypsochromic shifts of the long-wavelength absorption with a reduced electrochemical gap. On the other hand, the hyperpolarizability of all TTF-π-A compounds increases with elongation of the π-linker.

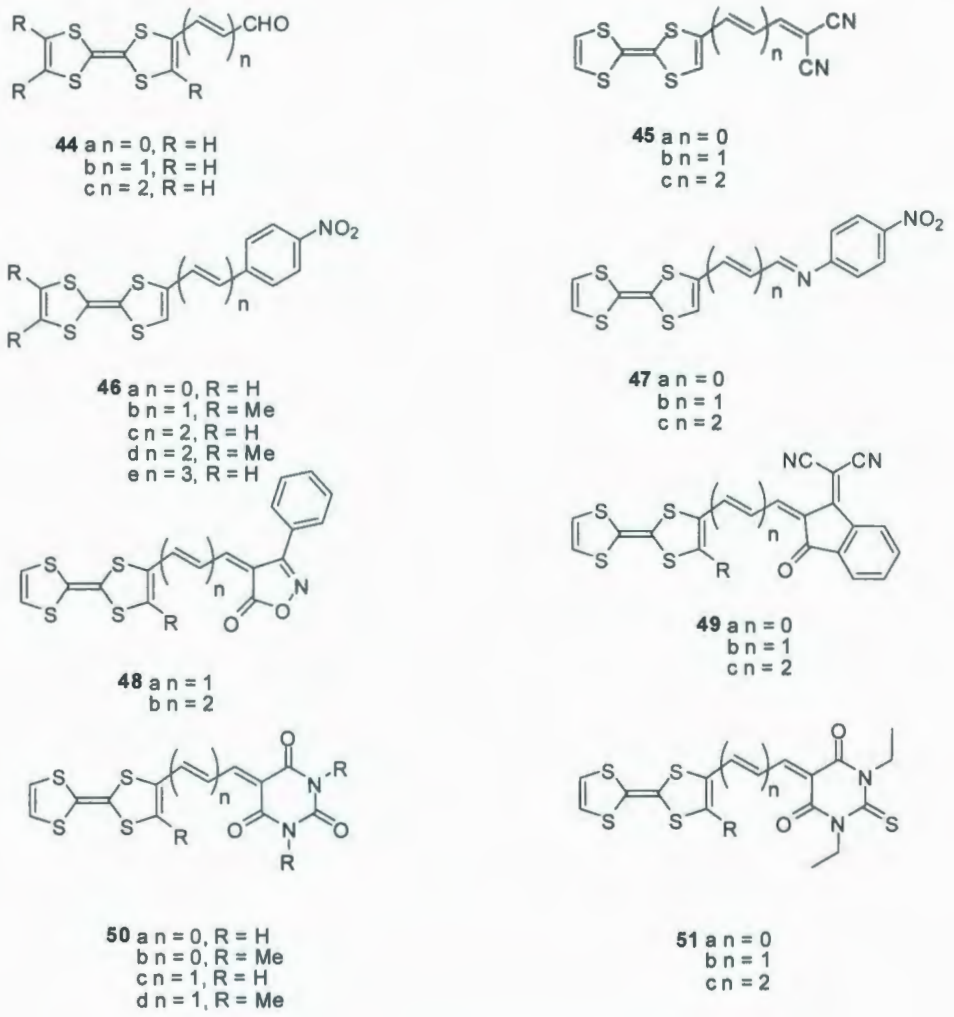

Figure 1.6: Structures of compounds **44-51**.

1.3.1.3 TTFAQ-A systems

In the above TTF-σ-A systems and TTF-π-A systems, TTFAQ-spacer-A systems were not mentioned. Since these TTF analogues with a central *p*-quinonedimethane spacer constitute a compelling and separate branch within the rapidly expanding TTF family, a separate review is outlined as follows.

The use of various π-spacers to extend the π-conjugation between the two dithiole rings has become an important approach to create the so-called π-extended TTF

analogues. In order to enhance solid-state contact, increase dimensionality and produce better electron-donating and charge-transfer properties, anthraquinone was chosen as an ideal π-space to separate the two dithole rings. These TTF analogues, termed TTFAQs, were oxidized at lower potential values owing to charge delocalization and to the decrease of the intramolecular on-site Coulombic repulsion. In contrast to parent TTF, which sequentially forms stable radical cation and dication states, *p*-TTFAQs are characterized by a single, two-electron oxidation wave in the CV to yield thermodynamically stable dications (E_{pa}^{ox} = +0.40 V, R = H, vs. Ag/AgCl).[37] TTFAQ possesses a saddle-shaped structure in the neutral state, due to the steric hindrance caused by benzanulation of the quinoid moiety. This conformation contrasts with the almost planar structure of the TTF moiety. The large structure change that accompanies the oxidation to the dictation introduces a significant reorganization energy, and the central anthracene moiety becomes aromatic and plannar and the 1,3-dithiolium cations are orthogonal to the anthrancene plane (Figure 1.7). Functionalization at both the anthracene and dithiole units has enabled the preparation of more sophisticated electron donor TTF derivatives and novel electroactive donor-acceptor systems.

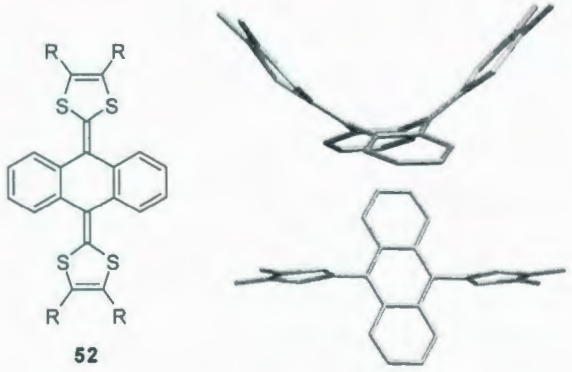

52

Figure 1.7: Chemical structure of TTFAQ and crystal structures of TTFAQ and $[TTFAQ]^{2+}$.

The first TTFAQ, reported by Akiba *et al.*,[9] stimulated intensive and systematic investigations of the electronic properties of these compounds which were initiated by the Bryce group in the 1980s.[37] The Bryce group also first discovered and reported the particular redox behaviour of TTFAQ derivatives. In this aspect, the Bryce group made a significant contribution to the development of TTFAQ chemistry. Nazario Martín also has extensively studied push-pull chromophores for NLO materials derived from π-extended TTFs. Over the past several years, the Zhao group has invested a significant amount of effort to develop highly π-extended analogues of TTFAQ.

Multi-stage organic redox systems, and electrochemically amphoteric compounds, for which both oxidized and reduced states are easily accessible within a potential window, may have potential applications in molecular electronic and optoelectronic devices. In order to get highly amphoteric compounds, strong electron-donor and electron-acceptor segments should be linked together. The Bryce group tried to connect TTFAQ and polynitrofluorene together in order to access TTFAQ-σ-A systems with high amphotericity. Compounds **53**, **54**, **55**, **56**[38] (Figure 1.8) were synthesized and analyzed by CV, UV-Vis and EPR. Electrochemical measurements revealed three reversible, single-electron reduction waves (corresponding to the fluorene moiety) and one two-electron, quasi-reversible oxidation of the TTFAQ fragment. Five redox states have been observed, neutral (D°/A°), dication (D^{2+}/A°), radical anion ($D^{\circ}/A^{\cdot-}$), dianion (D°/A^{2-}), radical trianion ($D^{\circ}/A^{\cdot 3-}$) for **53** and **54**; $A^{\circ}/D^{\circ}/A^{\circ}$, $A^{\circ}/D^{2+}/A^{\circ}$, $A^{\cdot-}/D^{\circ}/A^{\cdot-}$, $A^{2-}/D^{\circ}/A^{2-}$, $A^{\cdot 3-}/D^{\circ}/A^{\cdot 3-}$ states for **56** (for **55**, possessing the lower EA, the radical trianion state is not stable). From the analysis of the data, compound **54** showed an ideal quality as electronic and optoelectronic materials, since the E_{pa}^{ox}-E_{pa}^{red} gap was as low as 0.25 V, which was,

the lowest known value for closed shell D-σ-A systems, while compounds **53**, **55** and **56** possess weaker acceptor moieties.

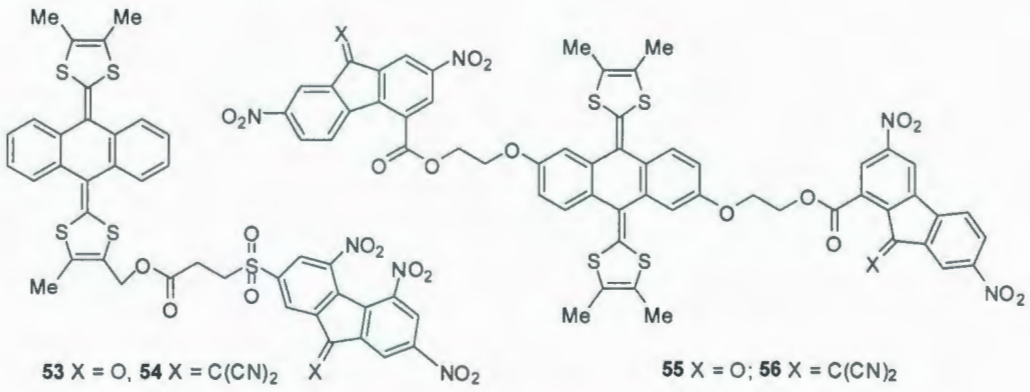

Figure 1.8: Structures of compounds **53-56**.

In order to further investigate the properties of TTFAQ derivatives, a range of new functionalized TTFAQ derivatives were synthesized and investigated by the Bryce group. In principle, the incorporation of a *p*-quinodimethane spacer into TTF should lead to reduced on-site Coulombic repulsion and stabilization of the oxidized states, a requirement for NLO materials and charge-transfer salts. In 2003, Bryce and co-workers prepared compounds **57** and pyrrolo-annulated TTFAQs **58-64**,[39] and characterized their electrochemical and structural properties by CV, UV and X-ray analysis (Figure 1.9). All these TTFAQ derivatives showed the typical quasi-reversible two-electron oxidation wave of the TTFAQ at potentials which varied slightly depending on the substituents. An increase in the oxidation potential was observed when electron withdrawing groups were attached. The CV of the conjugated TTFAQ dimer **57** showed two, two-electron oxidation waves corresponding to the sequential formation of dication $\mathbf{57}^{2+}$ and tetracation $\mathbf{57}^{4+}$ (ΔE^{ox} = 130 mV). The difference in oxidation potentials for the two TTFAQ moieties is more likely due to a significant intramolecular electron interaction.

After one TTFAQ unit in **57** was oxidized, it became a good electron acceptor, thus raising the oxidation potential of the second (neutral) TTFAQ unit in the molecule. A strong intramolecular charge transfer band at λ_{max} 538 nm was observed in the UV-Vis spectra of compounds **63** and **64**. The X-ray crystal structures of compounds **58**, **61** and **62** showed significant intermolecular interactions.

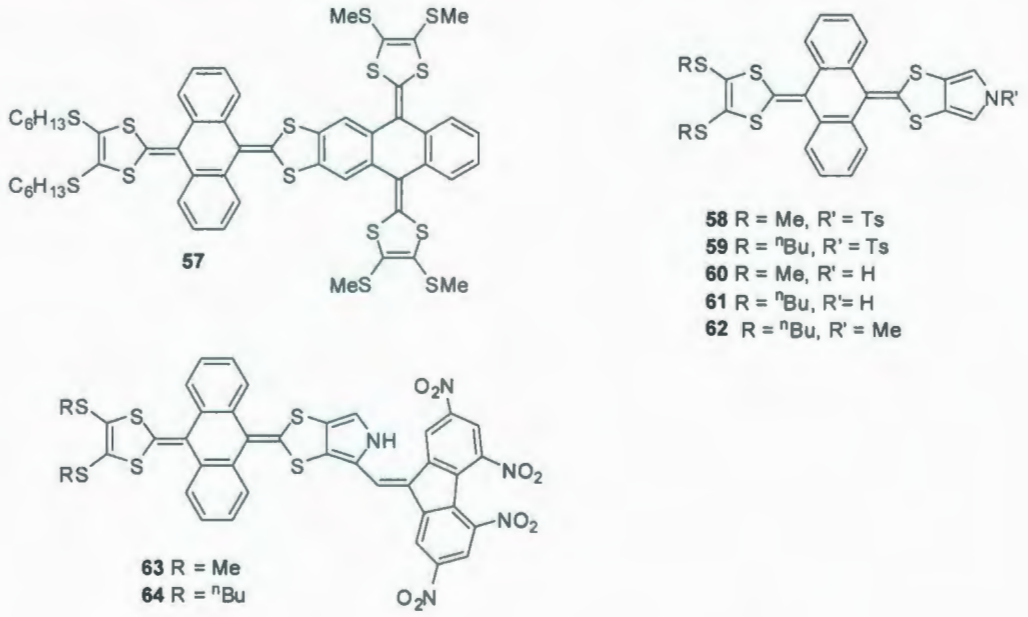

Figure 1.9: Structures of compounds **57-64**.

In order to study the effect of conformational changes on the redox behaviour in TTFAQs, extended TTF was incorporated to cyclophane structures. From 1999 to 2006, the Bryce group carried out a series of systematic studies where singly, doubly, and triply bridged cyclophanes were synthesized and their properties were investigated. The bridged cyclophanes **65**, **66**[40] displayed an irreversible two-electron oxidation wave at E^{ox} +0.69 V and +0.74 V, respectively. The oxidation wave of the bridged systems **65** and **66** showed a significant positive shift (+200-+300 mV) compared to their non-bridged analogues. Compounds **67** and **68**,[41] **69** and **70**[42] were subsequently prepared, which

contained bridges on different units of the TTFAQ system. In the CV, **67** and **68** displayed a quasi-reversible two-electron oxidation wave at E_{pa}^{ox} = +0.70-+0.72 V (for **67**) and E_{pa}^{ox} = +0.47 V (for **68**). The oxidation potential of **67** was raised significantly (ca. 300 mV), while **68** with longer bridge showed no effect on the oxidation value. This is likely due to the shorter bridge on **67** which hindered the marked conformational change which accompanies oxidation to the dication. Compounds **69** and **70** have bridges on anthracene group instead of dithiole ring. They also showed a quasi-reversible two-electron oxidation wave at E_{pa}^{ox} = +0.47-+0.52 V in the CV, respectively. Their CV data showed that bridging the anthracene unit had less effect compared to linking the dithiole ring. Compound **69** had a positive shift around 50 mV compared to its precusor, while **70** remained the same as its precursor. In 2006, the Bryce group synthesized doubly and triply bridged cyclophanes **71-74**.[43] The oxidation potentials of the doubly and triply bridged cyclophanes are raised considerably compared to those of their precursors. Unlike all previous bridged systems, these compounds displayed two reversible, one-electron oxidation waves. Because of their very rigid structures, these compounds had little or no conformation change can accompany the oxidation of the doubly or triply bridged cyclophanes. The radical cation species gave rise to a very broad, low-energy band (λ_{max} = 2175 and 2040 nm for **71** and **73** respectively), assigned to an intramolecular interaction. The steric constraints imposed by multiple bridging render remarkable optical and redox behaviours which are different from those of typical ex-TTF systems.

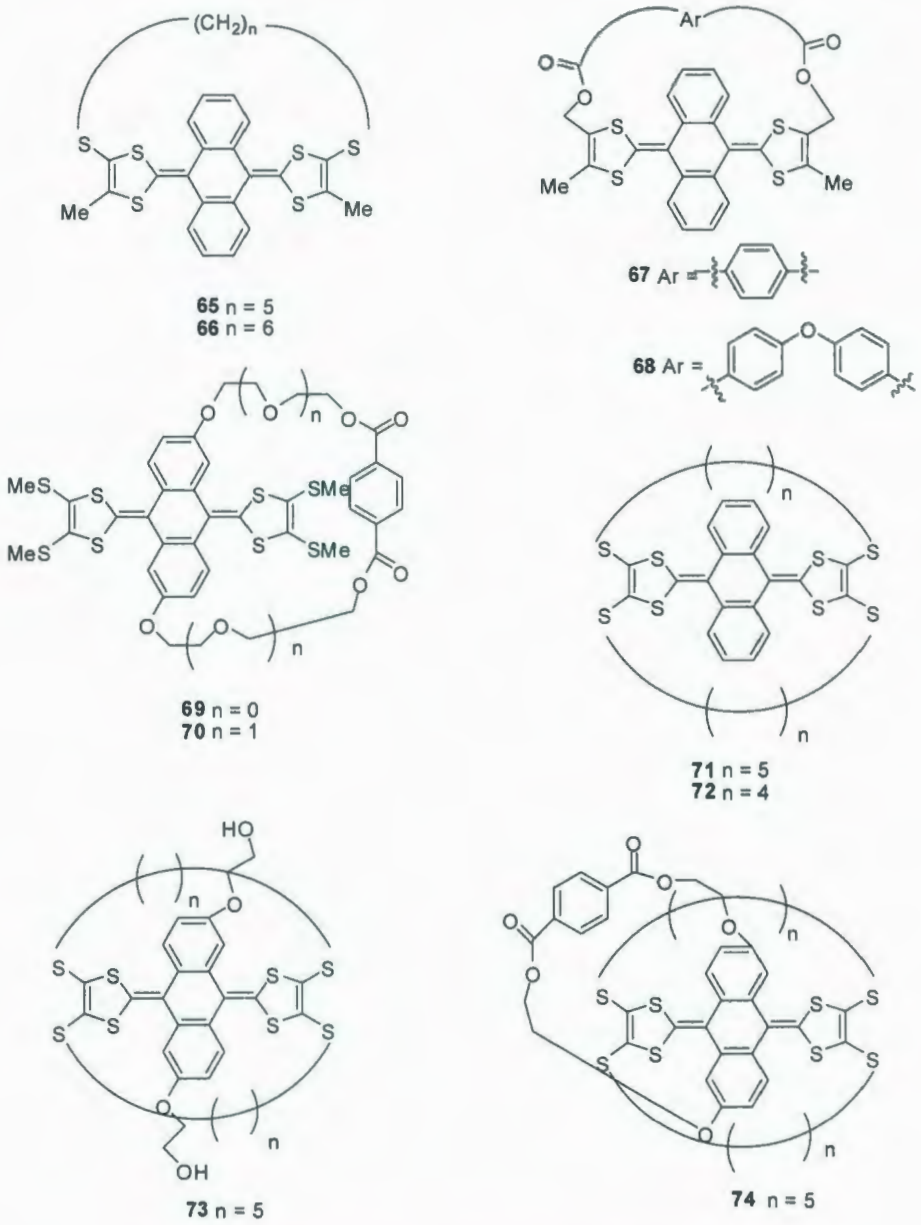

Figure 1.10: Structures of bridged TTFAQs **65-74**.

In 2007, the Bryce group also prepared and investigated macromolecular exTTFAQs **75, 76** and **77** (Figure 1.11).[44] In the CV, each unit in these compounds behaved as an independent two-electron redox system, giving rise to a single, quasi-reversible wave respectively, indicating that there was no ICT interaction in those compounds.

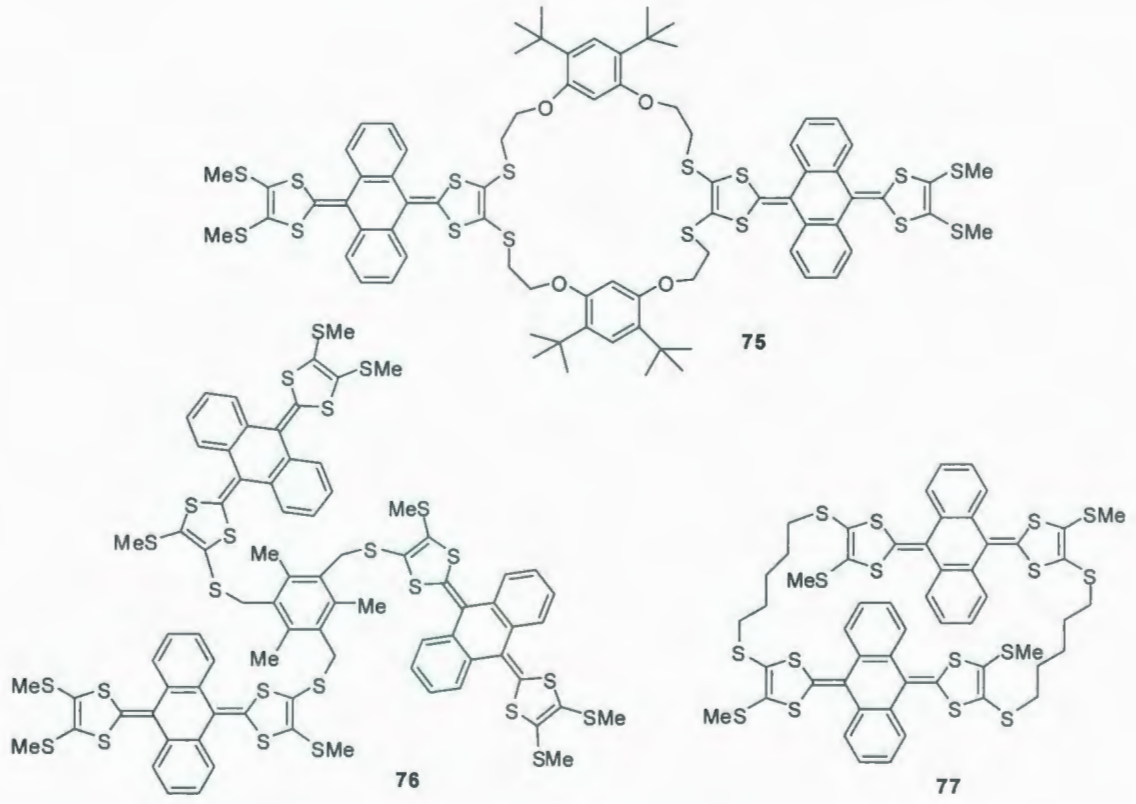

Figure 1.11: Structures of compounds **75-77**.

In the mean time, the Martín group also developed systematic studies of π-extended TTFs. They were not just satisfied with investigation of the well-known π-extended analogues bearing only one anthraquinoid structure with strong acceptor moieties. They have also examined systems containing two or more highly conjugated TTFAQ units. This kind of systems may display multi-stage redox behaviour which might provide the possibility to control the stoichiometry, band filling and molecular assembly in the desired conductive complexes.

In order to increase the dimensionality in the donor systems, oxygen was used as a bridge to connect two TTFAQ units. It was expected that oxygen would participate in inter- and intra-stack interactions. Compounds **78-80**[45] (Figure 1.12) were made by the

Martín group in 1997. The CV data of these compounds showed only one oxidation wave involving four electrons to form the corresponding dication in both monomeric units of the dimer, indicating that the oxo-bridged donor fragments behaved independently. The oxidation potentials of the oxo-bridged system were greater than the corresponding monomer due to the electron-withdrawing oxygen atom linking both donor units, indicating weak electronic coupling in the ground state.

The oxygen bridge did not facilitate conjugation, presumably due to the lack of π-bonding across the oxo-bridge between the two electron-donor units. The Martín group then developed a series of new hybrid TTF dimers (Figure 1.12) which were connected through a conjugated vinyl spacer. The presence of the double bond in the vinylene allows for electronic interactions by extended π-bonding, and serves to lower bond distortions and electron-electron repulsion by charge delocalization in the oxidized species. Compounds **81-83**[46] were synthesized and characterized by UV-Vis spectroscopic and electrochemical techniques. In the CV, **81** displayed a two-electron wave and two one-electron oxidative waves. Compounds **81** and **83** exhibited one three-electron and an one-electron anodic waves at more positive potentials. These successive electrochemical oxidations are indicative of intramolecular electronic interactions between the two different TTF units under the neutral and oxidative states. The anodic shifts at the first and second oxidation potentials became more positive when compared to monomeric TTF moieties. Red shifts for all these compounds compared to other related TTF moieties were observed by spectroscopic studies.

BisTTFAQ **84-86** (Figure 1.12) were prepared in which a vinyl group was employed as a π bridge.[47] Compounds **84** and **85** exhibited only one oxidation wave involving 4e$^-$ at

values similar to those for the respective monomer components, while compound **86** displayed two oxidation waves corresponding to the formation of the dication and tetracation species of the two different exTTF units. The first oxidation wave corresponded to the oxidation of the exTTF unit with the unsubstituted dithiole rings, and the second redox process was assigned to the exTTF unit bearing the SCHS groups. Upon comparing their CV data with those of their related monomers, it was obvious that the dimers was distinctly different from the sum of related monomers. This behaviour is accounted for by the π-bond mediated electronic interactions between the two donor groups in the ground state.

In 2006, the Martín group prepared the first TTFAQ dimer **87**[48] in which the two TTFAQ units are covalently connected by 1,3-dithiole rings. From the CV data, this dimer displayed two consecutive $2e^-$ processes D^o- $D^o \rightarrow D^{2+}$- $D^o \rightarrow D^{2+}$-D^{2+} suggesting a significantly different electronic structure in these systems, where the π-bonding orbitals were spread over several nuclear coordinates.

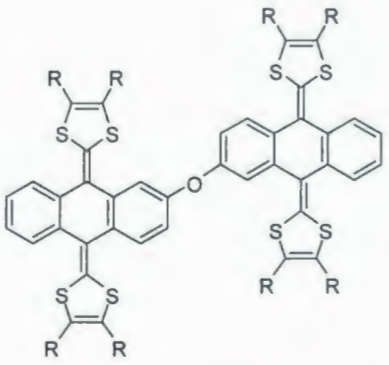

78 R = H, **79** R = SMe, **80** R = SCH_2CH_2S

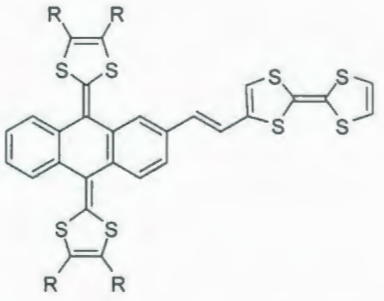

81 R = H, **82** R = SMe, **83** R = SCH_2CH_2S

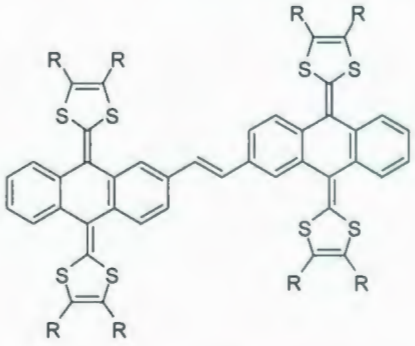

84 R = H, **85** R = SCH_3

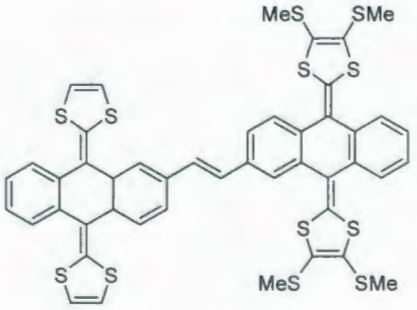

86

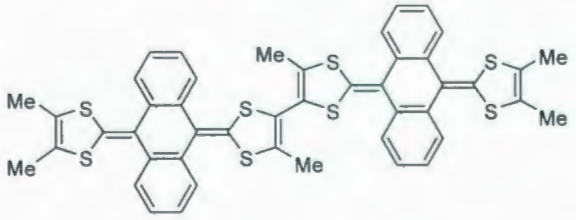

87

Figure 1.12: Structures of compounds **78-87**.

Martín *et al.* have also studied the TTFAQ-σ-C_{60} dyad species **88-90**[49] (Figure 1.13). Their CV data consistently show a single, two-electron oxidation wave at E^{ox} = +0.46V, revealing independant redox processes between the donor and C_{60} moieties.

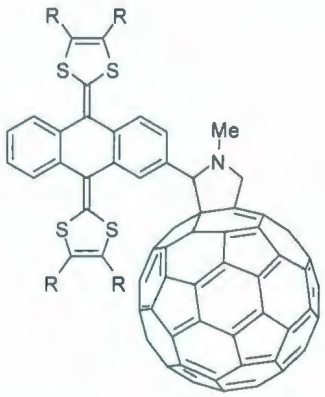

88 R = H
89 R = SMe
90 R = $S(CH_2)_2S$

Figure 1.13: Structures of compounds **88-90**.

The organic materials reported by Martín possessed highly polarizable electron density around the molecules, a prerequisite for non-linear optical (NLO) properties. NLO effects have applications in laser technology and other photonic devices. The Martín group explored a series of systematic studies to understand property-structure correlations. To achieve high molecular hyperpolarizability, nonlinear optical chromophores (NLO-phores) containing a strong donor and acceptor units bonded through a conjugated spacer have been widely investigated. A series of derivatives in which the TTFAQ is linked to different acceptors, such as carbonyl, dicyanovinyl and nitro groups through olefinic spacers have been synthesized and investigated. NLO-phores **91**(a-c), **92**(a-c),[50] **93**(a-c), **94**(a-c) and **95**(a-c)[51], reported in 1997 and 2002 , respectively, are shown in Figure 1.14. All of the compounds investigated displayed similar properties with respect to the conjugation length as well as the substituents on the exTTF moiety: the presence of the substituents on the TTF units resulted in an enhancement of molecular hyperpolarizability; the increase of conjugation length also resulted in an increase of molecular hyperpolarizability. All these compounds showed a two-electron quasi-reversible oxidation wave from CV experiments. TTF units bearing

substituents had more positive oxidation values with SMe and $S(CH_2)_2S$ groups than unsubstituted TTF, signifying the relatively poorer donor properties compared with unsubstituted exTTF.

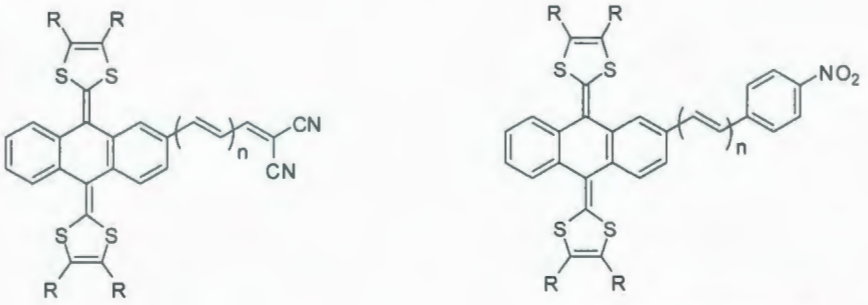

Figure 1.14: Structures of compounds **91-95**.

From the above discussions, it is well known that TTFAQs are better electron donors compared to its parent TTF. In recent years, the Zhao group has designed a new TTFAQ core, **96** (Figure 1.15), as a building block for a series of exTTFs with improved donor properties. The central anthracene moiety served as a π-extended conjugation path between the two dithiole ring, and the acetylenic linkages were employed to connect donors and acceptors. Based on this building block, a series of alkyne-TTFAQ derivatives have been synthesized, and the results provide the basis of this dissertation.

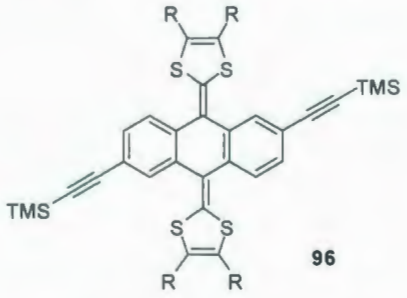

Figure 1.15: 2,6-Dialkynlated TTFAQ **96**.

1.3.2 TTF-based chemical sensors, molecular switches, wires and shuttles

Molecular systems which incorporate a redox-active component and a host unit capable of selectively binding with cations, anions, and neutral molecules can be employed as electrochemical sensors as well as redox-switchable ligands. In a sensor system, the redox-active unit will respond to the change in physical properties of the host, resulting in changes of color, redox-properties, and fluorescence emission. In a redox-switchable ligand system, the roles of the two parts in a sensor system are reversed. As such, the physical properties of the redox-active units are changed by an external stimulus, such as electrochemical or light, then the binding abilities of the ligand part will be changed, thereby influencing the uptake and release of guest molecules (Figure 1.17).[52]

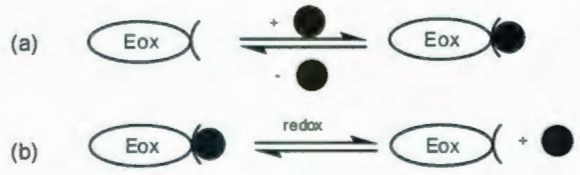

(a) Redox-detected sensor molecule; (b) Redox-controlled ligand system.

Figure 1.16: Mechanisms of electrochemical sensors and redox-switchable ligands.

Crown ether annulated TTFs was first synthesized by Otsubo and Ogura in 1985,[53] and their metal-binding characteristics were investigated by Becher *et al.* in 1992.[54] Since then, TTF has been incorporated in a wide range of different macrocyclic molecules, aiming at molecular sensors, switches, wires and shuttles. In the case of crown ether annulated TTFs, the TTF unit functions as a redox-active fragment and the crown ether acts as a host unit capable of cation binding. Such molecular systems can be employed as

cation sensors

The synthesis of crown ether annulated TTFs generally started from the readily available salt 1,3-dithiole-2-thione-4,5-dithiolate. It can be coupled with a range of electrophiles to prepare a series of thiones, which were then subjected to a standard coupling reaction with trialkyl phosphites to afford the desired crown ether annulated TTFs (Scheme 1.8).

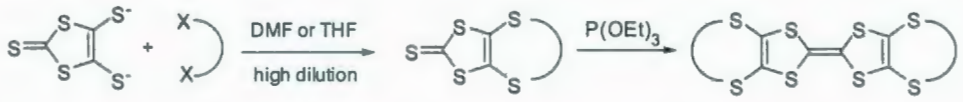

Scheme 1.8: Preparation of planar macrocyclic TTF derivatives.

In order to investigate π-extended TTF systems, modifying the TTF units to attain vinylogous TTF systems appeared to be a tenable methodology. Key intermediates in this type of reactions are Horner-Wittig reagents, phosphonate esters, which can be generated from thiones. After phosphonate esters are treated with LDA at -78 °C to generate carbanions, bis-aldehyde or ketone substrates in dry THF are added to form desired products through olefination reactions. The route is depicted in Scheme 1.9.

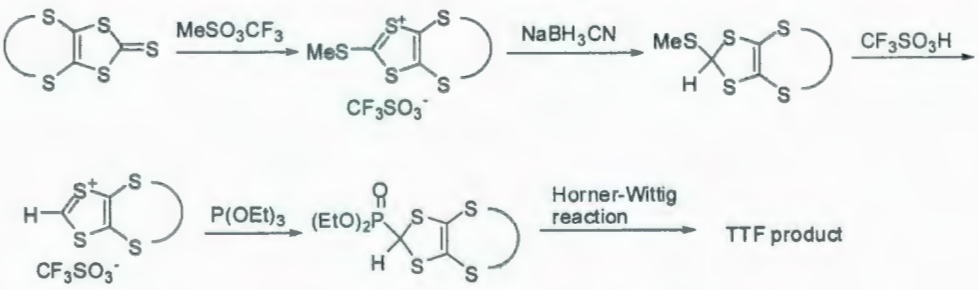

Scheme 1.9: Synthetic route to crown-ether phosphonate ester.

In a review by Jørgensen,[52] it was pointed out that the crown ether annulated TTFs

97-98 showed a positive shift of the first oxidation potential after binding the metal cations Li^+, Na^+ and K^+. The second oxidation potential of the TTF remained unchanged and acts as a convenient internal reference, which was explained by expulsion of the cations after the first oxidation. According to this paper, 250 equivalents of cations were required to observe shifts of redox potential for the ligands. Compound **99**[55] showed a positive shift of both oxidation waves on addition of Ag^+ ions, while compound **100**[55] had an anodic shift in the first oxidation wave upon addition of Ag^+ up to 1 equiv. Self-assembled monolayers of **101**, **102** and **103**[56] were also sensitive to metal cations. They showed a small positive response to Li^+ and K^+ (10-20 mV), a significant response to Na^+ and Ba^{2+} (45-55 mV) and a greater response to Ag^+ (60-90 mV). But these self-assembled monolayers (SAMs) were unstable under different experimental conditions. Another two self-assembled monolayers of **104** and **105**[57] were found to be robust on gold and showed positive shifts for the first and second oxidation potentials.

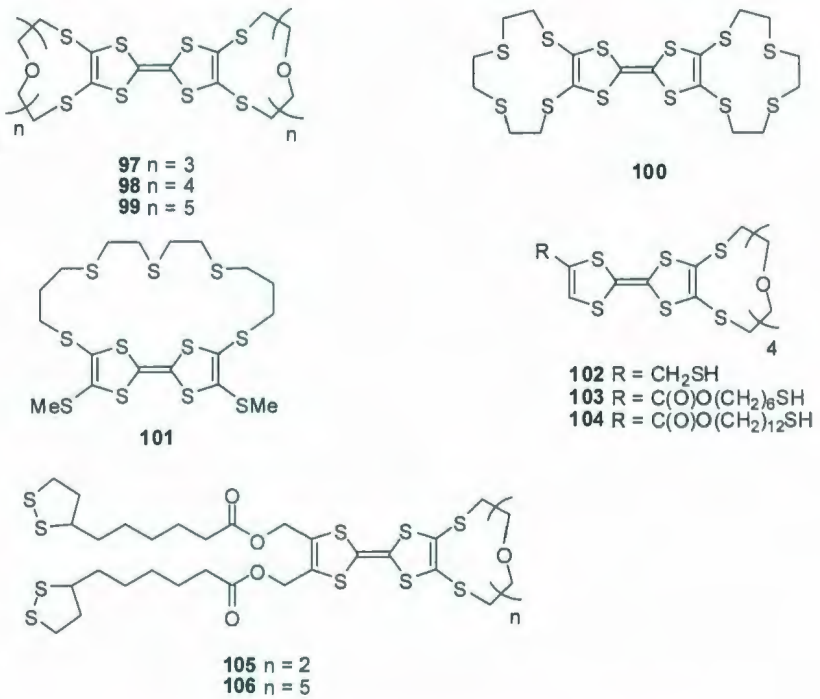

Figure 1.17: Structures of compounds **97-106**.

Other interlocking molecular systems containing TTF unit and π-electron accepting cyclophane cyclobis(paraquat-*p*-phenylene) have been studied. Becher and coworkers synthesized compound **107a**[58] as a thermally-controlled switch. Once tethered, the cyclobis(paraquat-*p*-pheynylene) π-acceptor and the TTF unit associated together to afford the "self-complexing" compound, resulting in an ICT band. Refluxing the green-colored equilibrium solution of **107a** caused almost complete disappearance of this ICT band, converting to the orange-coloured decomplexed form **107b**. Storing the solution at room temperature for ca. 20 h re-established the green colour. This cycle could be repeated for many times with a small decrease in the equilibrium absorbance after each experiment.

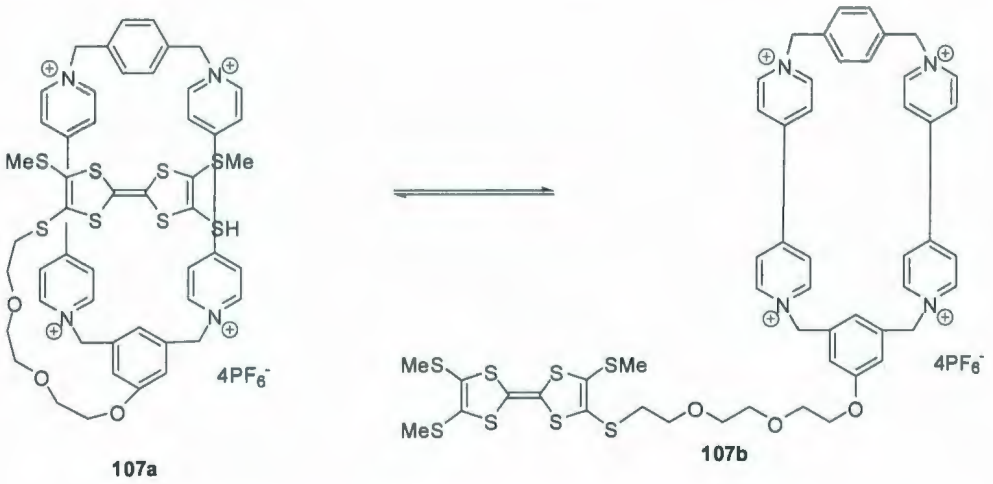

107a **107b**

Figure 1.18: Thermally-controlled switch **107**.

Balzani, Stoddart and coworkers synthesized chemically and electrochemically-switchable $\mathbf{108}^{4+}$.[59] This compound contains two different electron-rich fragments (a disubstituted TTF and a 1,5-alkoxynaphthalene ring). The TTF unit is located inside the cyclophane in $\mathbf{108}^{4+}$. Chemical or electrochemical oxidation of the TTF unit into the

cation radical or dication led to electrostatic repulsion of the tetracationic acceptor macrocycle and displacement of the TTF unit by the naphthalene system inside the cavity. This reversible process was accompanied by a color change from green ($\mathbf{108}^{4+}$) to maroon ($\mathbf{108}^{5+\cdot}/\mathbf{108}^{6+}$).

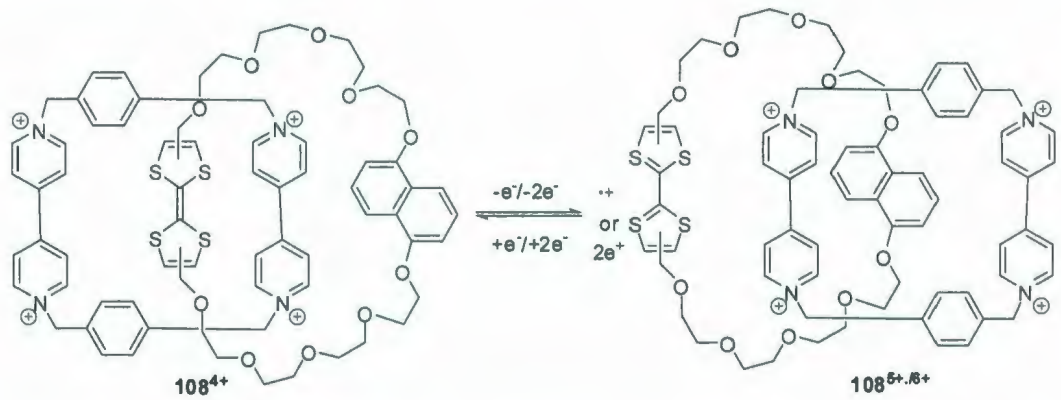

Figure 1.19: Chemical and electrochemical-switching of **108**.

The Zhu group has recently reported fluorescent sensors for metal cations and saccharides based on a motif of fluorophore-TTF-receptor, in which a photoinduced electron-transfer mechanism was fully employed to operate the molecular systems. In these molecular systems $\mathbf{109}^{60}$ and $\mathbf{110}^{61}$, TTF was used as a wire to link signal reporter and receptor instead of a traditional signal reporter. For compound **109**, the addition of Na^+ and C_{60} gave rise to enhanced fluorescence intensity. Compound **110** showed a very good selectivity for fructose. These two examples will be discussed in detail in Chapter 6.

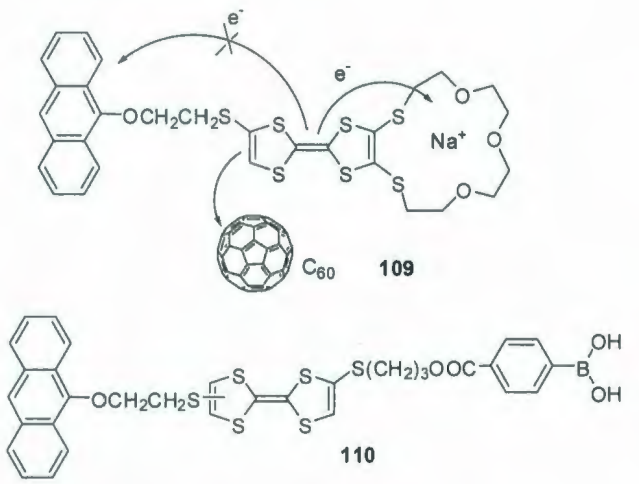

Figure 1.20: Structures of **109** and **110**.

1.3.3 TTF macromolecular systems

TTF macromolecular systems include systems containing one or more TTF units, TTF-containing dendrimers, and TTF-containing polymers. The major interest in these compounds lies in their multi-stage redox behavior which provides the possibility of controlling the stoichiometry, band filling, and molecular assembly. In addition, the increased dimensionality of their charge transfer salts is also an advantage.

Compounds **111**,[62] **112**,[63] **113**,[64] and **114**[65] (Figure 1.21), which contain three TTF moieties joined by non-conjugated linkages, showed no intermediate oxidation states by CV analysis. Only two oxidation waves were observed, corresponding to the oxidation to the respective trications and hexacations. These findings suggested that there were no Coulombic repulsion effects between the charged TTF moieties, and that the individual TTF units behaved independently and did not interact with each other. Compound **115**[66] with a high number of TTF units in which TTF units are also linked through nonconjugated bonds showed no interaction among the TTF moieties. Compound **115a**

exhibited four reversible redox waves. The first one corresponded to the formation of the radical cation of the central TTF unit; the second redox wave can be assigned to the formation of the pentacation by the loss of one electron from each of the four peripheral TTF units; the third redox couple corresponded to the formation of the dication of the central TTF unit, and the fourth redox couple arised from the second oxidation of the peripheral TTF units. While **115b** was only observed to show two reversible redox waves, probably because the central and the peripheral TTF moieties were almost equivalent in terms of redox behaviour. Compound **116**[67] made by the Becher group also showed two oxidation waves, indicating no intramolecular interactions among TTF units.

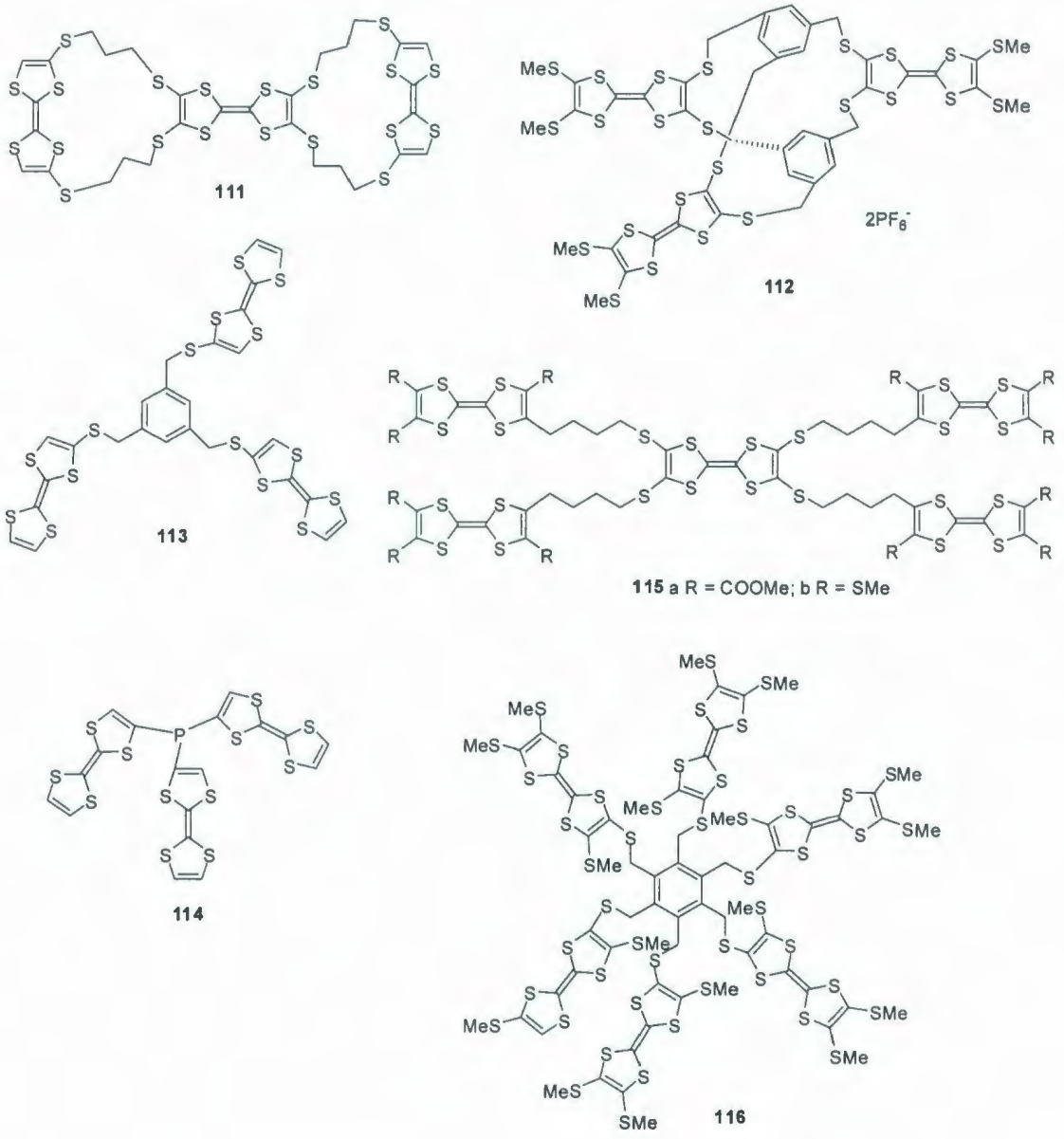

Figure 1.21: Structures of compounds **111-116**.

Dendrimers possess well-defined, three-dimensional structural order, and their size and architecture can be finely controlled in synthesis, providing unique molecular frameworks for the disposition of functional groups in predetermined spatial arrangements. Many groups have been interested in the synthesis and characterization of

soluble dendrimeric materials containing TTF. Focus has been placed on synthesizing structurally well-defined multi-electron redox systems, as well as exploring the known solubility enhancement in highly-branched macromolecules, compared to their linear counterparts. The Bryce group synthesized dendritic TTF derivatives **117**[68] containing 12 TTF units at the periphery of the dendrimer framework, and charge-transfer complex **118**,[69] which replaces some TTF units in compound **117** with the electron acceptor, anthraquinone. The CV data of compound **118** showed clear amphoteric redox behaviour with reversible switching between (+16, +8, 0, -4 and -8 charged states). This study provided the possibility of incorporating stronger π-acceptor groups in conjugation with TTF, and enabled the study of intramolecular charge transfer within a dendritic microenvironment. Such materials could be useful as electrooptical switches.

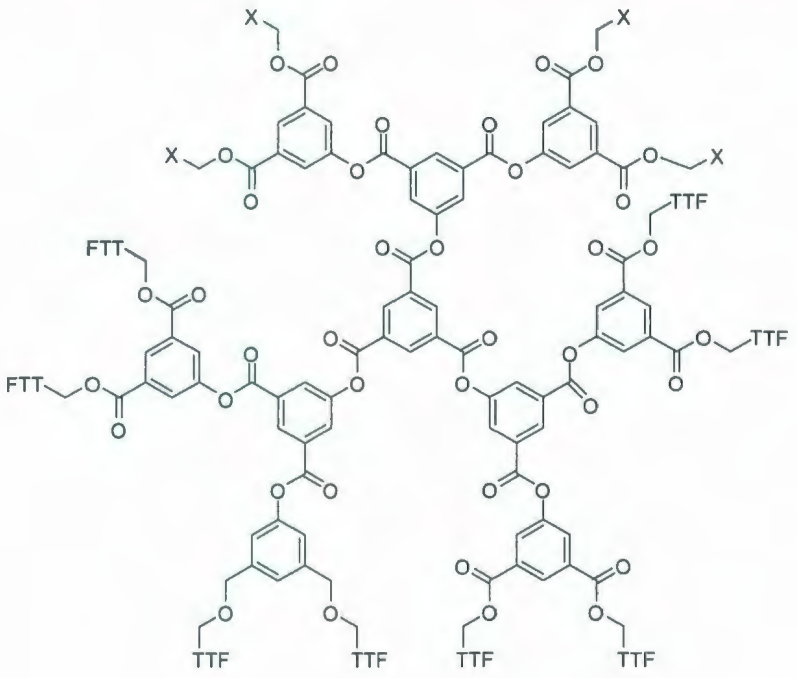

117 X= TTF; **118** X= Anthraquinone

Figure 1.22: Structures of **117** and **118**.

1.3.4 TTF polymers

CT complexes and radical cation salts of TTF tend to be brittle and intractable materials. This problem could be overcome by the incorporation of TTFs in polymers which are well known for their favorable rheological properties. These TTF polymers could be made in two motifs: in-chain TTF polymers and TTF-pendant polymer.[70]

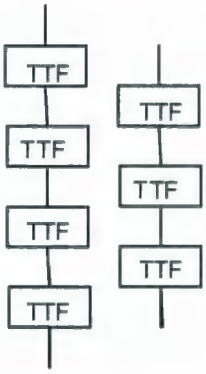

main-chain polymer

side-chain polymer

Initial synthetic experiments, where polymers with spacers such as polyamide, polyurethane, polyphenylene, polystyrene or polyesters were used, did not ensure a well-defined orientation of the TTF groups. The difficulties of controlling torsional angles around the bridging bonds proved to be a challenging problem. Hence, these poorly characterized polymers **119a-e**[71] (Figure 1.23) were unsucessful both in achieving order of the TTF sub-units, and dimensionality of the conduction process in the doped state. An attractive structure would incorporate π-conjugated TTF-based conductor. These TTF derivatives combine the unique properties of high molecular weight and processibility of polymers. The electron donating properties of TTF allowed the polymers to be doped by strong acceptors. Moreover, the propensity of TTF to form ordered stacks could be used to control the long-range order of a conjugated backbone within the supramolecular assembly. The combination of TTF with a conjugated polymer chain can increase in the

dimensionality of the conduction process and might eventually lead to materials with hydrid conduction.

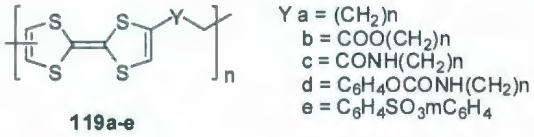

Figure 1.23: Structures of compounds **119a-c**.

In 1997, Yamamoto *et al.* synthesized polymers **120-123**[72] (Figure 1.24), which contain TTF units in the π-conjugated main chain. Those compounds showed both chemical and electrochemical activities. Even in the presence of electron-withdrawing acetylenic groups, two-step oxidation was detected.

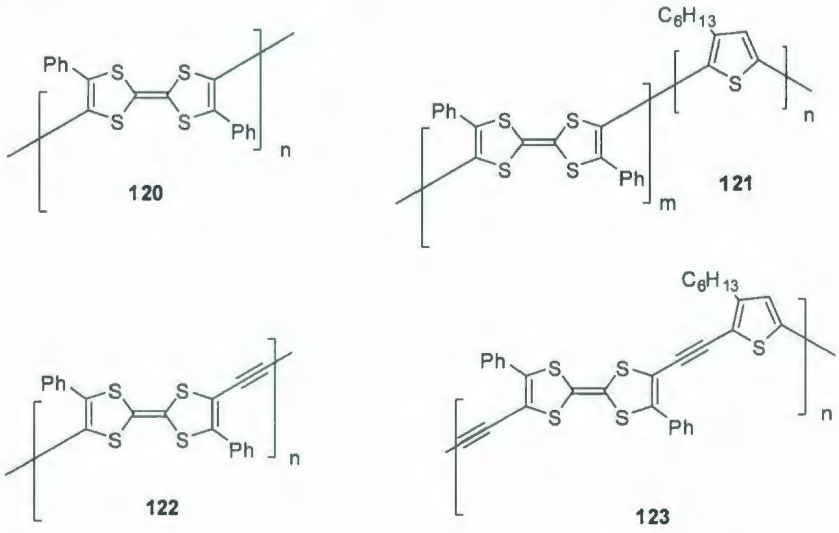

Figure 1.24: Structures of compounds **120-123**.

Roncali and coworkers successfully electropolymerized TTF-derivatized thiophene monomers. These two extensively π-conjugated TTF-derivatized polythiophenes **124** and **125**[73] (Figure 1.25) showed interesting electrochemical properties with a much lower

electropolymerization potential than their precusors. They revealed a previously unknown additional oxidation wave at a potential intermediate between those corresponding to the generation of the TTF radical cation and dication.

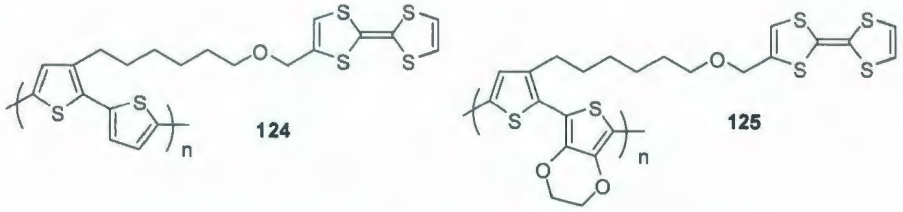

Figure 1.25: Structures of compounds **124** and **125**.

1.4 Outline of this thesis

This thesis describes five major projects concerning the syntheses and properties of π-extended TTF derivatives. The details of these studies are elaborated in Chapters 2 to 6.

In Chapter 2, the syntheses and electronic properties of conjugated trimer and donor-acceptor essembles of TTFAQ and anthraquinone are described. In this project, CV and UV-Vis studies have been conducted, demonstrating that TTFAQ is a better electron donor than its parent TTF. Experiments investigating electronic donor-acceptor interactions are described.

In Chapter 3, the focus is on the syntheses and properties of thiophene functionalized π-extended tetrathiafulvalenes. Extention of the distance of two dithiole rings reduced the intramolecular Coulombic repulsion, rendering these TTF derivatives as good organic electron donors. Thiophene is the essential repeat unit for a class of well-known conducting polymers, poly/oligothiophene. Attempted electropolymerization and detailed electrochemical and spectroscopic properties are described.

In Chapter 4, a modular synthesis of phenylboronic acid functionalized TTFAQ derivative and its applications in electrochemical recognition of saccharides are described. The synthesis was accomplished through an efficient click reaction. Under weakly basic conditions, this derivative showed distinct binding abilities for different saccharides, providing the basis to create a selective electrochemical sensor for saccharide detection.

In Chapter 5, focus is on the investigation of the potential of using two new D/A-substited TTFAQ derivatives as redox active ligands to recognize transition metal ions. The decrease of current intensity of these two compounds with the increasing addition of metal ion indicates that these two compounds probably can be employed as electrochemical sensors for some metal ions.

The last project, outlined in Chapter 6, involves the synthesis of crown ether-annulated TTFAQ and the investigation of the fluorescence properties before and after complexation with some metal cations. Without complexation with metal ions, photoinduced electron transfer from the electron-rich TTFAQ to the anthracene group effectively quenched the fluorescent emission of the anthracene group. When complexed with alkali metal ions, intermolecular and intramolecular photoinduced electron transfer (PET) occurred efficiently between cations and TTFAQ, thereby increasing the fluorescence of the anthracene group.

Chapter 2

Conjugated Push-Pull TTFAQ Triads

2.1 Introduction

Many groups have been active in the synthesis of TTF-based D-D-D, D-A-D and A-D-A (D: donor; A: acceptor) triads for use in various functions including photonic materials, nonlinear optics (NLO) and media for long range electron transfer. The present challenge is the ability to manipulate the components of molecular assemblies with appropriate donor (D) and acceptor (A) partners for specified applications.[74,5,15] It was anticipated that such molecular systems could lend themselves to be utilized in technically evolving device applications in supramolecular chemistry, molecular switches, nonlinear optics, moleculor sensors, and photovoltaics.

In 1996, the Müllen group synthesized compounds **126** and **127**[75] (Figure 2.1) which were TTF-based D-A-D triads. The electrochemical studies of compound **126** revealed a one-electron reduction of the quinone unit ($E_{1/2}^{red}$ = -0.27 V, vs. Ag/AgCl in $C_2H_2Cl_4$) and two reversible two-electron oxidation waves. The first oxidation potential was at higher potential, $E_{1/2}^{ox}$ = +0.60 V, compared with its precursor TTF ($E_{1/2}^{1}$ = +0.34 V, $E_{1/2}^{2}$ = +0.78 V, vs. Ag/AgCl in acetonitrile). The increase of first oxidation potential results from a destabilization of the radical cation by the electron withdrawing effect of the carbonyl moieties. The second redox potential appeared at $E_{1/2}^{ox}$ = +1.02 V. The fact that the oxidation processes occurred stepwise rather than simultaneously suggests the occurrence of intramolecular charge-transfer within these molecular systems. UV-Vis

spectra of compound **127** also showed significant intramolecular electonic interactions. Compound **127,** measured in solvents with different polarity, showed a shift of λ_{max} by up to 90 nm (1,4-dioxane λ_{max} = 787 nm, toluene λ_{max} = 819 nm and dichloromethane λ_{max} = 877 nm), leading to the conclusion that the long-wavelength absorption was an intramolecular charge-transfer band from the donor to the acceptor moiety.

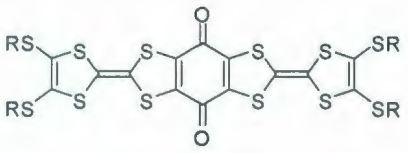

126 R = *n*-Bu, **127** R = *n*-hexyl

Figure 2.1: Structures of compounds **126** and **127.**

Müllen reported the synthesis of **128**[76] in 1994 (Figure 2.2). These TTF assemblies have three TTF moieties. Six possible electrochemical processes were observed, indicating strong interactions among these conjugated TTF units. This compound was the first example of a fully reversible stepwise oxidation in a TTF trimer.

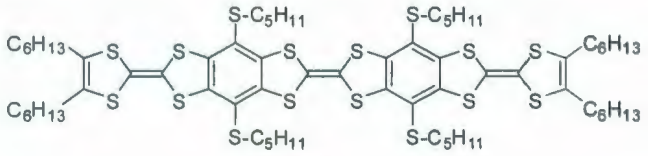

128

Figure 2.2: Structure of compound **128.**

In 1996, Yamabe *et al.* reported the synthesis and characterization of compound **129**[77] (Figure 2.3) which is structurally similar to compound **128**. Its cyclic voltammogram consists of two pairs of quasi-reversible waves and an irreversible wave. Compared to its smaller analogues, compound **130** and TTF **131,** the redox processes of compound **129**

involved three stages of two-electron transfer to form a hexacation, which is in agreement with the fact that **129** has six redox-active TTF rings.

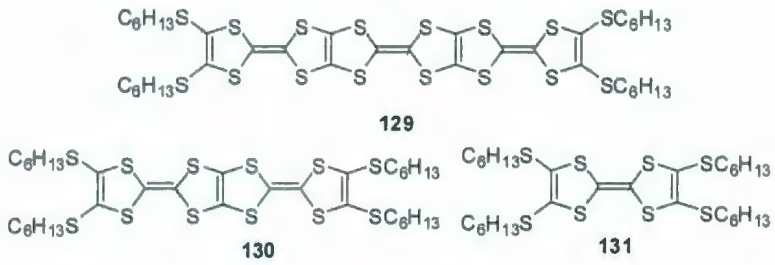

129

130 **131**

Figure 2.3 Structures of compounds **129**, **130** and**131**.

In 1994, the Iyoda group synthesized TTF compound **132**[78] (Figure 2.4) in which the TTF units were located at the 1,3,5-positions of a benzene ring. Electrochemical characterization revealed two three-electron processes, consistent with weak electron coupling between the TTF cations as a consequence of the lack of conjugation through the *meta*-positions of the benzene ring.

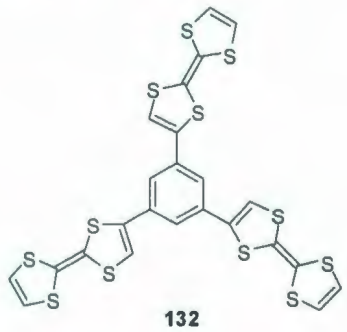

132

Figure 2.4: Structure of compound **132**.

In 2000, the Martín group reported the synthesis of systems containing more TTF units as well as star-shaped TTF oligomers. The structures of **133**, **134** and **135**[79] are shown in Figure 2.5. In the cyclic voltammograms of these compounds, only two redox

processes were observed, corresponding to the simultaneous oxidation of the three TTF units to the tris-(radical cation) (+0.48 V) and hexacation (+0.85 V). These observations indicate that the three TTF units behaved independently, and were electronically "isolated".

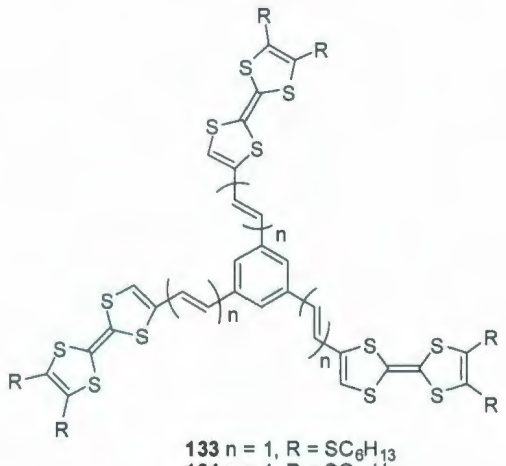

133 n = 1, R = SC_6H_{13}
134 n = 1, R = $SC_{12}H_{25}$
135 n = 2, R = $SC_{12}H_{25}$

Figure 2.5: Structures of compounds **133**, **134** and **135**.

In 2004, the Hudhomme group successfully synthesized TTF D-D-D and A-D-A triads **136** and **137**. In triad **136**[80] (Figure 2.6), three pairs of one-electron reversible oxidation waves were observed at E^{ox} = +0.43, +0.49, and +0.60 V, which correspond to the successive formation of the cation radical for each TTF unit. Two other reversible waves at E^{ox} = +0.84 V and +1.00 V were related to the generation of a dication on each TTF, the second wave being attributed to both equivalent TTF moieties. These results are consistent with the multiple redox steps shown below,

$$\mathbf{136} \underset{+e^-}{\overset{-e^-}{\rightleftharpoons}} \mathbf{136}^{+\cdot} \underset{+e^-}{\overset{-e^-}{\rightleftharpoons}} \mathbf{136}^{2+} \underset{+e^-}{\overset{-e^-}{\rightleftharpoons}} \mathbf{136}^{3+\cdot} \underset{+e^-}{\overset{-e^-}{\rightleftharpoons}} \mathbf{136}^{4+} \underset{+e^-}{\overset{-e^-}{\rightleftharpoons}} \mathbf{136}^{6+}$$

This study confirmed that there were significant intramolecular interactions between the TTF units. In compound **137**,[81] UV-Vis spectral analysis confirmed the intramolecular

interaction between both D and A moieties. A broad and strong absorption band around 808 nm in CS_2 was observed. In cyclic voltammetry, the *p*-benzoquinone moiety was characterized by a two-electron reversible reduction wave E^{red} = -0.25 V. Two one-electron reversible oxidative waves E^{ox1} = +0.99 V, E^{ox2} = +1.36 V, are ascribed to the successive generation of the cation and dication radicals, respectively of the TTF moiety. Compared with parent TTF, its oxidative potentials were clearly anodically shifted. The electron-withdrawing effect of the quinone group was presumably responsible for this phenomenon.

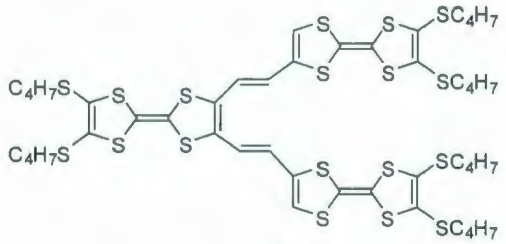

136

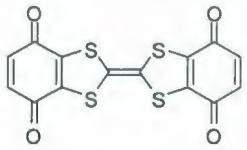

137

Figure 2.6: Structures of compounds **136** and **137**.

All examples introduced above are TTF-based compounds. As mentioned in Chapter 1, TTFAQ is a stronger two-electron donor than TTF. This is due to the strongly inter-related redox and structural properties of TTFAQ, which favor a simultaneous two-electron oxidation accompanied by dramatic conformational changes in the molecule. Compared to the dication of TTF, the dication of TTFAQ is considerably stabilized by the aromaticity gained at the central anthracene moiety and reduced Coulombic repulsion between the two dithiolium rings. These properties attracted several research groups to synthesize and investigate different π-extended TTFAQs. The Zhao group has been especially interested in such π-extended TTFAQ derivatives as those with an anthracene

between two dithiole rings (Figure1.76), further π-extended along the anthracene direction via two conjugated acetylenic bridges. By employing this type of exTTFs as building blocks, a series of A-π-D-π-A, D-π-A-π-D, and D-π-D-π-D triads have been synthesized in the Zhao lab. These investigations have been driven by the need to understand the structure-property relations for intramolecular charge-transfer interactions.

2.2 Results and Discussion

2.2.1 Synthesis

2.2.1.1 Conjugated TTFAQ trimer and doner-acceptor ensembles of TTFAQ and anthraquinone

To construct the synthetic targets D-D-D **138**, D-A-D **139** and A-D-A **140** (Scheme 2.2) conjugated acetylene-bridged TTFAQ triads, sequential Sonogashira and Horner-Wittig reactions were employed. From the starting materials, 2,6-diaminoanthraquinone **141** and 2-aminoanthraquinone **142** (Scheme 2.1), Sandmeyer-type reactions afforded iodo products **143** and **144** respectively. The two iodides **143** and **144** were then subjected to Sonogashira coupling with trimethylsilylacetylene (TMSA) under the catalysis of Pd/Cu, giving ethynylated anthraquinones **145** and **146**. In this reaction, the solution needed to be degassed completely at the beginning. These two compounds then underwent Horner-Wittig reaction with a phosphonate ylide **147** to afford TTFAQs **148a** and **149a**. In this reaction, after phosphonate ylide **147** was deprotonated by *n*-BuLi for 0.5 h at -78 °C, anthraquinone was added dropwise to the solution. After complete addition, this mixture was allowed to warm up to rt and stirred overnight. The yields of these two compounds **148a** and **149a** were satisfactory, 85% and 55% respectively. Compounds of **148a** and

149a could be easily desilylated with K_2CO_3 to afford free terminal alkynes **148b** and **149b**. Generally, the yields of desilylation were very high, above 80%.

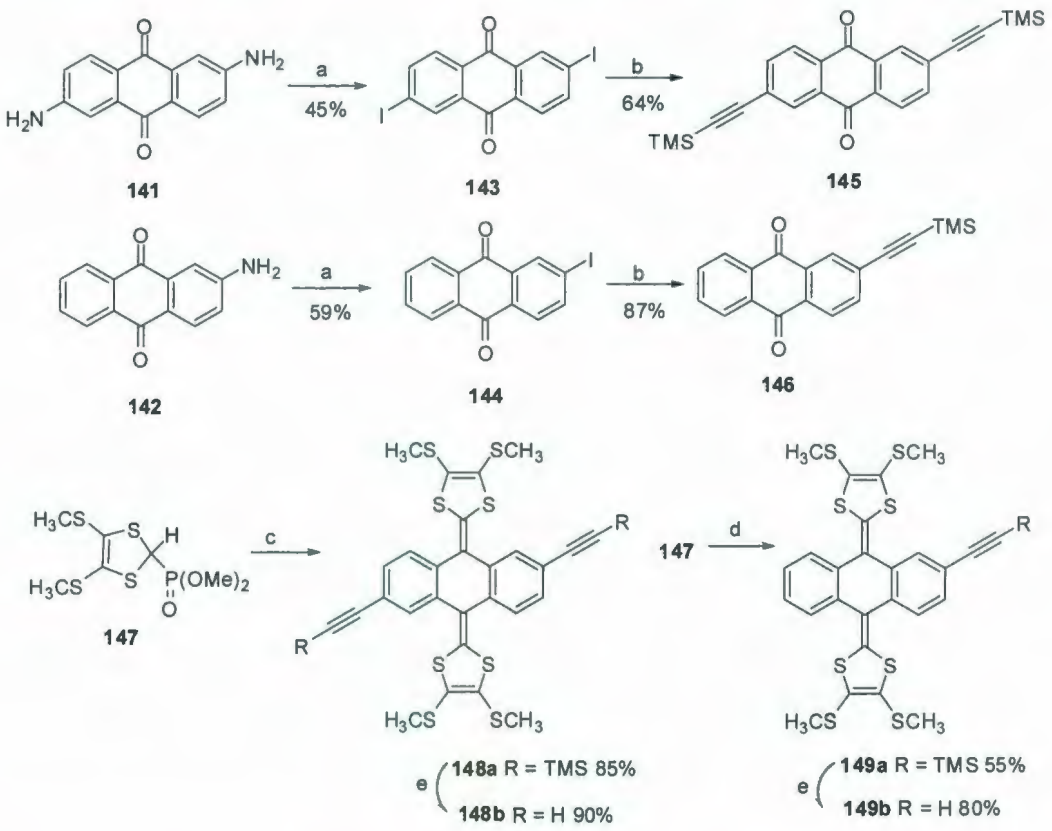

Scheme 2.1: Synthesis of TTFAQ **148a** and **149a**. Reagents and conditions: (a) (i) $NaNO_2$, H_2SO_4, 0 °C; (ii) KI, rt, overnight; (b) TMSA, $Pd(PPh_3)_4$, CuI, Et_3N, THF, rt, overnight; (c) (i) *n*-BuLi, THF, –78 °C, 30 min; (ii) **145**, –78 °C to rt, overnight; (d) (i) *n*-BuLi, THF, –78 °C, 30 min; (ii) **146**, –78 °C to rt, overnight; (e) K_2CO_3, THF/MeOH; wet THF.

With these precursors in hand, several routes involving sequential Sonogashira and Horner-Wittig reactions can be envisioned to construct the skeleton of the targeted trimer **138**, and TTFAQ-anthraquinone ensembles **139** and **140**, depending on their structures. In our experiments, however, the route given in Scheme 2.2 proved to be efficient,

whereas our other attempts involving Sonogashira couplings between a monoiodo-substituted TTFAQ and a diiodo-substituted TTFAQ with respective alkyne counterparts resulted in either sluggish reactions or no products at all.

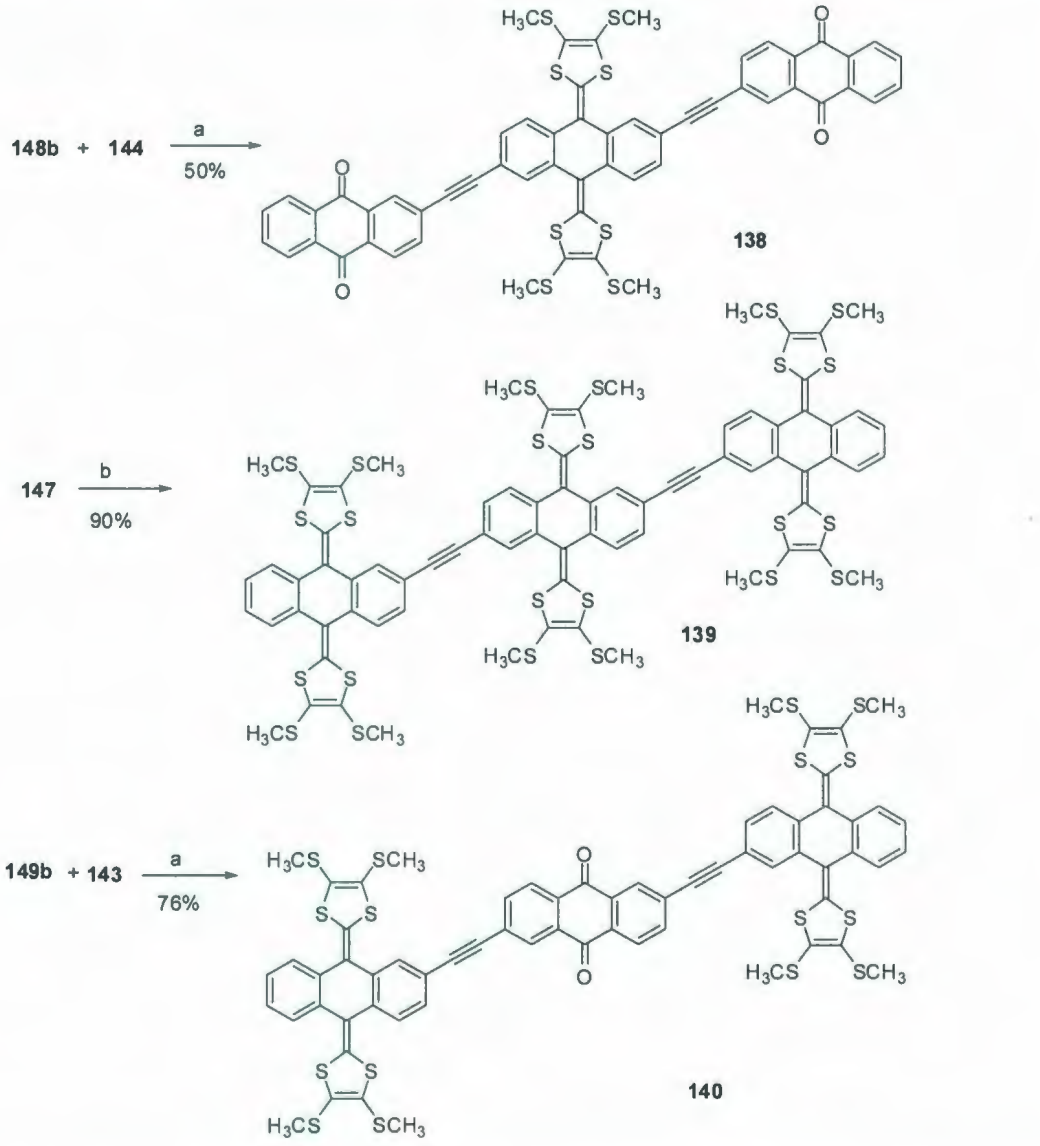

Scheme 2.2: Synthesis of triads **138**, **139** and **140**. Reagents and conditions: (a) $Pd(PPh_3)_4$, CuI, Et_3N, THF, rt, overnight; (b) (i) *n*-BuLi, THF, –78 °C, 30 min; (ii) **138**, –78 °C to rt, overnight.

Diethynyl-TTFAQ **148b** was cross-coupled with 2 equiv of 2-iodoanthraquinone **144**, affording compound **138** in 50% yield. Compound **138** was then subjected to a Horner-Wittig olefination reaction with the ylide that was prepared from **147**, yielding the desired TTFAQ trimer **139** in 90% yield. 2,6-Diiodoanthraquinone **143** was cross-coupled with 2 equivalents of TTFAQ **149b** under the same catalytic conditions as employed in the synthesis of **138**, giving ensemble **140** in a yield of 76%.

Compound **139** is an orange solid, while **138** and **140** are dark brown solids. They all show moderate solubility in organic solvents such as chloroform and methylene chloride. Through silica column chromatography, compounds **138-140** were thoroughly purified and their structures were clearly elucidated by NMR, IR, and MALDI-TOF MS analyses.

2.2.1.2 2,6-Disubstituted TTFAQ triads

The synthetic target **150** is a 2,6-disubstituted TTFAQ triad. The synthetic approach to **150** is shown in Scheme 2.3. *t*-Butyl alcohol **151** was chlorinated by reacting with concentrated HCl. After **152** was obtained, an S-alkylation of compound **153** was conducted with **152** in the presence of $AlCl_3$. The thiol group of **153** was alkylated with *t*-butyl in a yield of 86%. The crude product **154** was pure enough, so that it was used directly in the next step without further purification. After lithiation of **154**, aldehyde **155** was produced after addition of DMF. Corey-Fuchs reaction of aldehyde with $PPh_3.CHBr_3$ afforded alkyne **156** under basic conditions. Terminal alkyne **156** was reacted with **144** via a Sonogashira reaction to afford ketone **157**. Finally, compound **150** was synthesized throught a Horner-Wittig reaction between ketone **157** and phosphonate **147**.

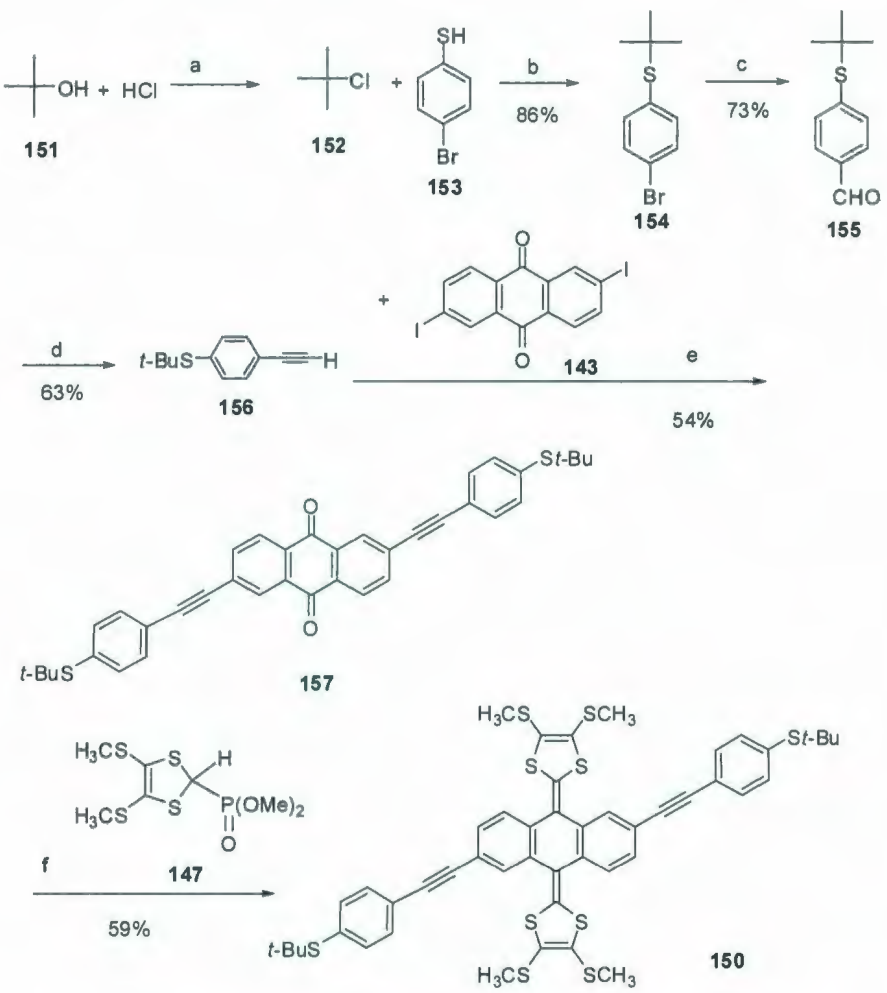

Scheme 2.3: Synthesis of compound **150**. Reagents and conditions: (a) HCl, rt, 15 min; (b) $AlCl_3$, rt, 5 h; (c) *n*-BuLi, -78 °C, 15 min; then DMF, rt, 30 min; (d) $PPh_3.CHBr_3$, ^tBuOK, rt, 35 min; (e) $Pd(PPh_3)_4$, CuI, Et_3N, THF, rt, overnight; (f) (i) *n*-BuLi, THF, –78 °C, 30 min; (ii) **156**, –78 °C to rt, overnight.

2.2.2 Electronic and electrochemical properties of TTFAQs

Electronic absorption properties of these new TTFAQ derivatives were studied by UV-Vis spectroscopy. Figure 2.7 (a) compares the UV-Vis absorption profiles of compounds **138-140**. In the spectra, the trimeric TTFAQ **139** shows a prominent low-energy absorption band at 458 nm accompanied by another band at 391 nm, assigned to $\pi \rightarrow \pi^*$

transitions. Compared with the spectrum of monomer TTFAQ **148a**, no noticeable shift is observed for the $\pi \rightarrow \pi^*$ bands. This result suggests insignificant intramolecular electronic interactions among the three TTFAQ donor units, despite that they are connected through conjugated ethynyl linkages. The nonplanar conformation of the TTFAQ core in the ground state[82] and the relatively weak orbital interactions through the C≡C bonds[83] presumably account for such electronic features as found in **139**. Compound **140** consists of a symmetric array of D-A-D groups, in which a strong π-electron-accepting anthraquinone unit is flanked by two TTFAQ donors via ethynyl bridges. An electron 'push-pull' effect is therefore expected to exert a significant impact on its UV-Vis absorption energies and intensity of the spectral bands.[84] Indeed, the two low-energy $\pi \rightarrow \pi^*$ transitions of **140** at 449 and 372 nm are greatly blueshifted relative to those of TTFAQ trimer **139**. Moreover, an appreciable absorption tail emerges in the spectrum of **140**, extending from ca. 490 to 600 nm. This tail is ascribed to the charge-transfer absorption from the ground state to the dication. In compound **138**, the array of D-A groups assumes an A-D-A motif. Likewise, strong D-A interactions are observed in its UV-Vis spectrum. Interestingly, unlike **140**, the low-energy $\pi \rightarrow \pi^*$ band of **138** at 460 nm shows no significant shift relative to trimer **139**, whereas the second $\pi \rightarrow \pi^*$ band that appears as a discernible shoulder does blueshift to 372 nm. Of note is the considerably intensified charge-transfer band in **138** compared to that of **140**, implying greater electronic communications between the two anthraquinone and the central TTFAQ. To further understand the change of electronic properties in response to electron transfers (i.e. oxidation), a solution of **139** was progressively titrated with an oxidant solution containing $PhI(OAc)_2$ and TfOH (1:4 molar ratio). The titration was monitored by UV-

Vis and the results are given in Figure 2.7 (b). Theoretically, consumption of six π-electrons from TTFAQ trimer **139** to form a dication on each of the TTFAQ units needs three equivalents of oxidant. In the titration profiles, three isosbestic points are clearly observed, which are similar to the titration outcomes of the TTFAQ monomer reference compound **148a**. The oxidation of trimer **139** in theory should undergo sequential dication formations, that is, **139** → $[\mathbf{139}]^{2+}$ → $[\mathbf{139}]^{4+}$ → $[\mathbf{139}]^{6+}$. In Figure 2.7 (b), the increasing low-energy band beyond 500 nm is attributed to the characteristic absorption of the cationic products from oxidative titration, while the two decreasing bands at ca. 470 and 395 nm are likely associated with π→π* transitions on the neutral TTFAQ and the π-conjugated framework. At this juncture, clear spectral assignments on specific cationic products are not tenable and await further spectroelectrochemical investigations. The electrochemical redox properties of **148a** and **138-140** were investigated by cyclic voltammotry and the results are shown in Figure 2.8. The detailed redox potential data are summarized in Table 2.1. The cyclic voltammogram of TTFAQ trimer **139** shows only one significant quasi-reversible redox wave pair at $E_{1/2}^{ox}$ = +0.44 V (vs. Ag/AgCl), along with several weak irreversible anodic and cathodic peaks in the range of +0.74-+1.3 V, consistent with the UV-Vis oxidative titration data, indicating that the oxidation processes on the three TTFAQ units occur simultaneously rather than successively because of the insignificant electronic interactions among the three TTFAQ units. In comparison to the cyclic voltammogram of **148a**, the first oxidation potential of trimer **139** is relatively lowered by ca. 0.1 V, signifying a better electron-donating ability. This shift is likely due to electronic interactions among the three TTFAQ units through conjugated acetylenic bonds. Compound **138** shows a quasi-reversible wave at $E_{1/2}^{ox}$ =

+0.50 V ascribed to oxidation at the TTFAQ unit. This value is greater than that of **139**, which can be rationalized by the strong electron-withdrawing effect from the two adjacent anthraquinone units. Scanning cathodically, the two anthraquinone moieties gave rise to two quasi-reversible waves at $E_{1/2}^{red}$ = –0.79 V and –1.21 V, corresponding to the formation of a radical anion and a dianion on each anthraquinone unit.[85] For compound **140**, the two TTFAQ units lead to one quasi-reversible wave at $E_{1/2}^{ox}$ = +0.48 V, a value in between those of **139** and **138**. In the negative potential region, the central anthraquinone moiety of **139** gave one quasi-reversible wave at $E_{1/2}^{red}$ = –0.77 V, while the second reduction wave became only vaguely discernible.

In summary, the first conjugated TTFAQ trimer **139** and two TTFAQ-anthraquinone molecular ensembles, **138** and **140** have been successfully synthesized using a Sonogashira/Horner-Wittig strategy. Trimer **139** shows rather insignificant electronic communication among the TTFAQ units, whereas the D-A molecules **138** and **140** display appreciable electronic interactions among the electroactive groups. Our results manifest the effectiveness of the Sonogashira/Horner-Wittig protocol in creating extended π-conjugated systems involving TTFAQ and anthraquinone moieties.

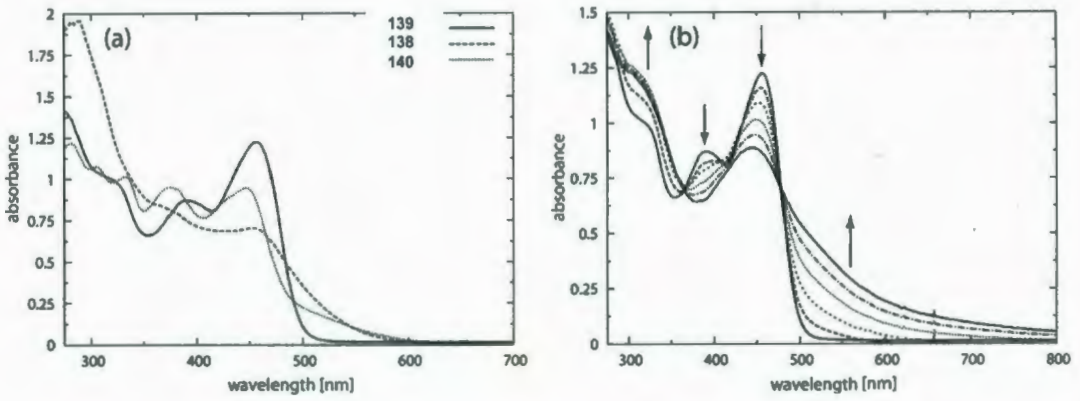

Figure 2.7: (a) UV-Vis absorption spectra of **138-140** measured in $CHCl_3$ at rt (b) UV-Vis oxidative titration profiles of trimer **140**. The arrows indicate the progression of adding oxidant $PhI(OAc)_2$ from 0-3 equivalents. Note that one molar equivalent of oxidant consumes two moles of electrons.

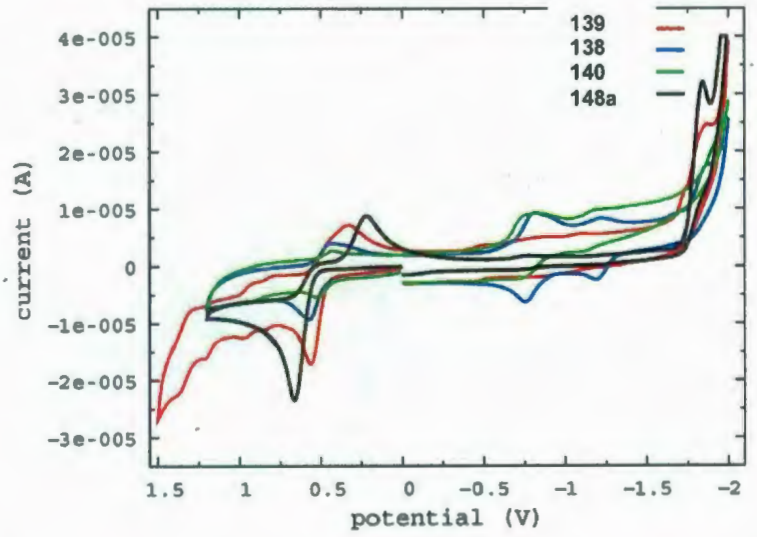

Figure 2.8: Cyclic voltammograms of compounds **148a** and **138-140** as recorded in CHCl3-MeCN (4:1, v/v) at rt; Bu_4NBF_4 (0.1 M) as the supporting electrolyte, glassy carbon as the working electrode, Pt wire as the counter electrode, and Ag/AgCl as the reference, scan rate 100 mV/s.

Table 2.1: Electrochemical redox data for compounds **148a** and **138-140.**

Compd	Reduction (V)		Oxidation (V)	
	*E*pc	*E*pa	*E*pa	*E*pc
148a	–1.84	–	0.66	0.22
138	–0.82, –1.22	–0.76, –1.19	0.57	0.43
139	–1.87	–	0.56, 1.00, 1.22	0.33
140	–0.84	–0.70	0.53	0.43

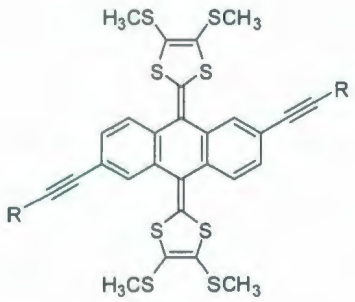

158-160

Entry	R	Yield (%)
158		74
159	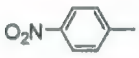	53
160	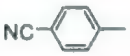	50
150	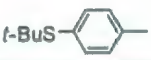	59

Figure 2.9: Structures of compounds **150**, **158-160**.

Redox properties of D/A disubstituted TTFAQs **150**, and **158-160** were investigated by cyclic voltammetry, and the results are summarized in Figure 2.10 and Table 2.2. For comparison purposes, the cyclic voltammogram of compound **148a** was first measured as

reference. From Figure 2.10, it can be seen that the TTFAQ core gives rise to a quasi-reversible redox wave pair in the positive potential region with $E_{1/2}^{ox}$ 484 mV vs. Ag/AgCl, which is ascribed to a simultaneous two-electron oxidation process. The *t*-butylthiol group of **150** is expected to be somewhat electron-donating by resonance effect; therefore, it should lead to an E_{pa} value lower than that of the **158**, if the resonance effect is predominant. Experimentally, considering the dramatic conformational change from the ground state to the dicationic oxidation state at the central TTFAQ unit upon two-electron oxidation, it is rationalized that other factors such as the energy costs to flatten the saddle-like TTFAQ core and to reorganize the solvation shells around the molecule may come into play, in addition to the electronic effects. In addition, the inductive effect of the thiol group may also play an important role here. As a result, **150** shows a larger oxidation potential than **158**, although **150** is more electron rich. It is also notable that the redox wave pair of compound **150** in the positive potential region is irreversible and shows the widest separation of the E_{pa} and E_{pc} values (*ca.* 297 mV) among the four TTFAQ derivatives. This observation implies that the sizes of the substitutents flanking the 2,6-diethynylated TTFAQ core have a significant impact on electrochemical redox properties.

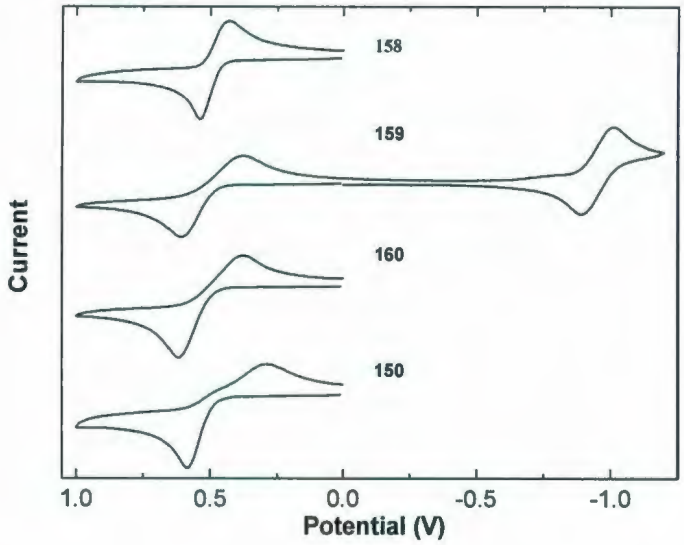

Figure 2.10: Comparison of cyclic voltammograms for **150, 158-160**. Data were recorded in *o*-dichlorobenzene/CH_3CN (4:1, v/v) at room temperature. Bu_4NBF_4 (0.1 M) as the supporting electrolyte, glassy carbon as the working electrode, and Pt wire as the counter electrode. Potentials are give in volts vs. Ag/AgCl reference electrode. Scan rate = 100 mV/s.

Table 2.2: Summary of electrochemical data for compounds **150, 158-160**.

Entry	Oxidation		Reduction	
	E_{pa} (V)	E_{pc} (V)	E_{pa} (V)	E_{pc} (V)
158	0.583	0.430	–	-1.802, -1.951
159	0.608	0.374	-0.891	-1.011, -1.546, -1.954
160	0.619	0.376	–	-1.690, -1.810
150	0.585	0.288	–	-1.785, -1.934

UV-Vis spectra of compounds **150, 158-160** were measured in $CHCl_3$ at room temperature and detailed data are given in Figure 2.11. From Figure 2.11, it can be clearly seen that TTFAQ derivative **150** shows no dramatic changes in the low energy absorption region in comparison to reference **158**, indicating that the *t*-BuS groups have little electronic effects on the TTFAQ unit even though they are connected through direct π-conjugation.

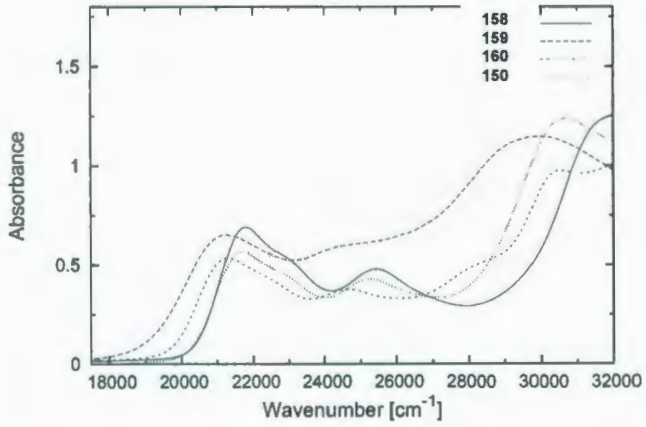

Figure 2.11: UV-Vis spectra of compounds 150, 158-160 measured in $CHCl_3$.

Fluorescence spectra of compounds **150, 158-160** are given in Figure 2.12. Reference compound **158** emits as a single peak at 503 nm. Interestingly, the major emission band of **150** shows little shift relative to **158**, which is indicative of weak electronic interactions between the *t*-BuS groups and the TTFAQ unit. This is in line with what has been observed in its absorption spectrum. A prominent shoulder band at 611 nm is also discernible in the fluorescence spectrum of **158**. The origin of this shoulder emission is not clear yet, however, the participation of the *t*-BuS group in π-conjugation is believed to be a reason for it.

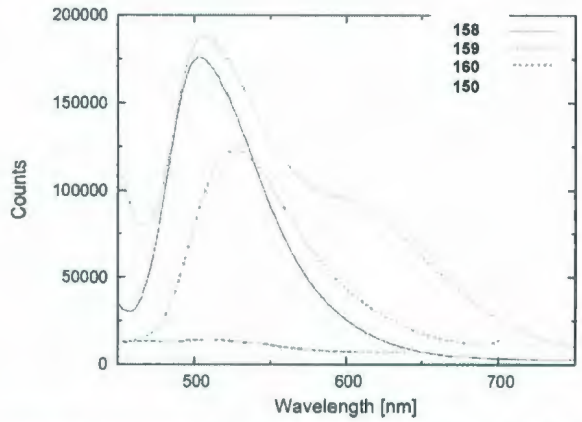

Figure 2.12: Fluorescence spectra of compounds **150**, **158-160** measured in degassed $CHCl_3$.

2.3 Experimental

General procedures and methods

Chemicals and reagents were purchased from commercial suppliers and used without further purification. THF was distilled from sodium/benzophenone. Et_3N and toluene were distilled from LiH. Catalysts, $Pd(PPh_3)_4$ and $Pd(PPh_3)_2Cl_2$, were prepared from $PdCl_2$ according to standard procedures. All reactions were performed in standard, dry glassware under an inert atmosphere of N_2 unless otherwise noted. Evaporation and concentration was done at H_2O-aspirator pressure. Flash column chromatography was carried out with silica gel 60 (230-400 mesh) from VWR international. Thin-layer chromatography (TLC) was carried out with silica gel 60 F254 covered on plastic sheets and visualized by UV light or $KMnO_4$ stain. Melting points (mp) were measured with a Fisher-Johns melting point apparatus and are uncorrected. ^1H and ^{13}C NMR spectra were measured on the Bruker AVANCE 500 MHz spectrometer. Chemical shifts are reported in ppm downfield from the signal of the internal reference $SiMe_4$. Coupling constants (*J*)

are given in Hz. Infrared spectra (IR) were recorded on a Bruker Tensor 27 spectrometer. UV-Vis spectra were recorded on an Agilent 8453 UV-Vis or a Cary 6000i UV-Vis-NIR spectrophotometer. Fluorescence spectra were measured in $CHCl_3$ at ambient temperature using a Quantamaster 10000 fluorometer. APCI mass spectra were measured on an Agilent 1100 series LCMSD spectrometer, and high-resolution MALDI-TOF mass spectra on an Applied Biosystems Voyager instrument with dithranol as the matrix.

2,6-Diiodoanthracene-9,10-dione (143). In a 100 mL round-bottomed flask, 2,6-diaminoanthraquinone (357 mg, 1.498 mmol) was dissolved in 5 mL of concentrated H_2SO_4 (by ultrasound). Solid $NaNO_2$ (414 mg, 6.000 mmol) was added in very small amounts at 0 °C to this flask. After the mixture was stirred for 5 h, a small amount ice was added to this mixture, and then KI (1990 mg, 12.042 mmol) was dissolved in 2 mL of water was also added dropwise to this mixture. The mixture was stirred at rt overnight. 10% $Na_2S_2O_3$ solution was added to this mixture to destroy excess I_2. The aqueous mixture containing a solid was extracted with dichloromethane. The combined organic layers were washed by brine and dried over magnesium sulfate. Finally, the solvent was removed in vacuo. The compound was separated via flash column chromatography (eluent: dichloromethane/hexanes, 1/1) to give the desired product **143** (311 mg, 0.676 mmol, 45%) as a yellow solid. ^{1}H NMR (500 MHz, $CDCl_3$): δ 8.65 (2H, s), 8.18 (2H, d, J = 8.0 Hz), 7.99 (2H, d, J = 8.0 Hz). ^{13}C NMR (125 MHz, $CDCl_3$): δ 181.58, 143.39, 136.37, 133.84, 132.12, 128.76, 102.70. IR (cm^{-1}): 3058, 2110, 1673, 1571, 1313, 1289, 1163, 950, 925, 842, 801, 726, 708. GC-MS: *m/z* calculated for $C_{14}H_6I_2O_2$ 459.85, found 460.00. Mp: 274-275 °C.

2-Iodoanthracene-9,10-dione (144). In a 250 mL round-bottomed flask, 2-aminoanthraquinone (2000 mg, 8.959 mmol) was dissolved in 20 mL of concentrated H_2SO_4 (by ultrasound). Solid $NaNO_2$ (920 mg, 13.333 mmol) was added in a very small amount at 0 °C to this flask. After the mixture was stirred for 5 h, a small amount ice was added to this mixture, and then KI (4480 mg, 26.988 mmol) dissolved in 10 mL of water was also added dropwise to this mixture. The mixture was stirred at rt overnight. 10% $Na_2S_2O_3$ solution was added to this mixture to destroy I_2. The aqueous mixture was extracted with dichloromethane. The combined organic layers were washed with brine, dried over magnesium sulfate. Finally, the solvent was removed in vacuo. The residue was purified by flash column chromatography (eluent: dichloromethane/hexanes, 1/3) to give the desired product **144** (1777 mg, 5.319 mmol, 59%) as a yellow solid. ^{1}H NMR (500 MHz, $CDCl_3$): δ 8.66 (1H, s), 8.32-8.30 (2H, m), 8.17 (1H, d, J = 8.5 Hz), 8.01 (1H, d, J = 8.5 Hz), 7.84-7.82 (2H, m). ^{13}C NMR (125 MHz, $CDCl_3$): δ 182.64, 181.94, 136.36, 136.26, 134.60, 134.52, 134.07, 133.34, 133.08, 132.59, 127.49, 127.44, 127.35, 127.29. IR (cm^{-1}): 3079, 1674, 1569, 1325, 1290, 1162, 971, 951, 927, 848, 706. GC-MS: *m/z* calculated for $C_{14}H_7IO_7$ 334.11, found 334.00. Mp: 173-174.5 °C.

2,6-Bis((trimethylsilyl)ethynyl)anthracene-9,10-dione (145). In a 100 mL round-bottomed flask, **143** (100 mg, 0.217 mmol), CuI (10 mg, 0.053 mmol) and $PdCl_2(PPh_3)_2$ (20 mg, 0.017 mmol) were dissolved in dry 20 mL of THF and Et_3N (2:1). After complete degassing with freeze-pump-thaw cycles, TMSA (0.18 mL, 1.300 mmol) was added to this mixture. This mixture was allowed to be stirred at rt overnight. After solvent was got rid of in vacuo, this compound was redissolved in dichloromethane again,

washed by 1 M HCl, brine, and dried over magnesium sulfate. After the solvent was removed in vacuo, the crude product was purified with flash chromatography (eluent: dichloromethane/hexanes, 1/4) to give the desired product **145** (57 mg, 0.142 mmol, 64%) as a pale yellow solid. ^{1}H NMR (500 MHz, $CDCl_3$): δ 8.36 (2H, s), 8.26 (2H, d, J = 8.0 Hz), 7.84 (2H, d, J = 8.0 Hz), 0.30 (18H, s).

2-((Trimethylsilyl)ethynyl)anthracene-9,10-dione (146). In a 50 mL round-bottomed flask, **144** (100 mg, 0.299 mmol), CuI (10 mg, 0.053 mmol) and $Pd(PPh_3)_4$ (20 mg, 0.017 mmol) were dissolved in dry 20 mL of THF and Et_3N (1:1). After complete degassing with freeze-pump-thaw cycles, TMSA (0.21 mL, 1.500 mmol) was added to this mixture. This mixture was allowed to be stirred at rt overnight. After solvent was rid of in vacuo, this compound was redissolved in dichloromethane again, washed by 1 M HCl, brine, and dried over magnesium sulfate. After the solvent was removed in vacuo, the crude product was purified with flash column chromatography (eluent: dichloromethane/hexanes, 1/4) to give the desired product **146** (80 mg, 0.263 mmol, 86%) as a pale yellow solid. ^{1}H NMR (500 MHz, $CDCl_3$): δ 8.37 (1H, s), 8.33-8.31 (2H, m), 8.26 (1H, d, J = 8.5 Hz), 7.84-7.80 (3H, m), 0.29 (9H, s).

(9,10-Bis(4,5-bis(methylthio)-1,3-dithiol-2-ylideene)-9,10-dihydroanthracene-2,6-diyl)bis(ethyne-2,1-diyl)bis(trimethylsilane) (148a). In a 100 mL round-bottomed flask, *n*-butyllithium (2.54 mL, 1.38 M, 3.505 mmol) was added dropwise to the solution containing **147** (959 mg, 3.151 mmol) in dry THF (50 mL) at -78 °C. After this solution was stirred for 30 min, **145** (504 mg, 1.260 mmol) was also added to this solution

dropwise at -78 °C, and then this mixture was allowed to warm to rt and be stirred overnight. After the solvent was removed in vacuo, this compound was redissolved in dichloromethane, washed by 1 M HCl, brine, and then dried over magnesium sulfate. After the solvent was removed in vacuo, this crude product was purified by flash column chromatography (eluent: dichloromethane/hexanes, 1/4) to afford the desired product **148a** (807 mg, 1.066 mmol, 85%) as a yellow solid. ^{1}H NMR (500 MHz, $CDCl_3$): δ 7.60 (2H, s), 7.47 (4H, d, J = 8.5 Hz), 7.40 (4H, d, J = 8.5 Hz), 2.41 (6H, s), 2.40 (6H, s), 0.27 (18H, s).

2,2'-(2,6-Diethynylanthracene-9,10-diylideene)bis(4,5-bis(methylthio)-1,3-dithiole) (148b). In a 100 mL round-bottomed flask, K_2CO_3 (3.0 mg) was added to the solution containing **148a** (880 mg, 1.162 mmol) in a mixture of wet THF and MeOH (v/v, 1:1). After this solution was stirred for 30 min, the solvent was removed in vacuo. This residue was redissolved in dichloromethane, washed by 1 M HCl, brine, and then dried over magnesium sulfate. After the solvent was removed in vacuo, this crude product was purified by flash column chromatography (eluent: dichloromethane/hexanes, 1/4) to afford the desired product **148b** (640 mg, 1.044 mmol, 90%) as a yellow solid. ^{1}H NMR (500 MHz, $CDCl_3$): δ 7.66 (2H, s), 7.52 (2H, d, J = 8.0 Hz), 7.44 (2H, d, J = 1.0 Hz), 3.14 (2H, s), 2.41 (6H, s), 2.39 (6H, s), 0.01 (18H, s).

((9,10-Bis(4,5-bis(methylthio)-1,3-dithiol-2-ylideene)-9,10-dihydroanthracen-2-yl)ethynyl)trimethylsilane (149a). In a 100 mL round-bottomed flask, butyllithium (0.60 mL, 2.5 M, 1.500 mmol) was added dropwise to the solution containing **147** (460

mg, 1.511 mmol) in dry 50 mL of THF at -78 °C. After this solution was stirred for 30 min, **146** (160 mg, 0.526 mmol) was also added to this solution dropwise at -78 °C, and then this mixture was allowed to warm up to rt and be stirred overnight. After the solvent was removed in vacuo, this compound was redissolved in dichloromethane, washed by 1 M HCl, brine, and then dried over magnesium sulfate. After the solvent was removed in vacuo, this crude product was purified by flash column chromatography (eluent: dichloromethane/hexanes, 1/4) to afford the desired product **149a** (190 mg, 0.287 mmol, 55%) as a yellow solid. ^{1}H NMR (500 MHz, $CDCl_3$): δ 7.61 (1H, s), 7.56-7.53 (2H, m), 7.49 (1H, d, J = 8.0 Hz), 7.39 (1H, d, J = 8.0 Hz), 7.32-7.30 (2H, m), 2.41-2.39 (12H, m), 0.27 (9H, s). ^{13}C NMR (125 MHz, $CDCl_3$): δ 134.85, 134.77, 134.66, 134.58, 132.21, 132.08, 130.10, 126.65, 128.60, 126.58, 126.48, 126.12, 125.89, 125.78, 125.61, 125.54, 125.47, 125.43, 123.31, 122.95, 121.17, 105.13, 95.17, 19.42, 19.27, 19.23, 19.21. IR (cm^{-1}): 2954, 2918, 2152, 1530, 1495, 1454, 1419, 1310, 1280, 1247, 1004, 893, 856, 841, 755, 697, 684. HRMS (APCI, +ve): *m/z* calculated for $C_{29}H_{28}S_8Si$ 659.9726, found 660.1131. Mp: 193-195 °C.

2,2'-(2-Ethynylanthracene-9,10-diylideene)bis(4,5-bis(methylthio)-1,3-dithiole) (149b). In a 100 mL round-bottomed flask, **149a** (200 mg, 0.303 mmol) was added to 30 mL of wet THF and MeOH (1:1). TBAF (1.0 M, 0.21 mL, 0.210 mmol) was also added to this solution. This mixture was stirred at rt for 1 h, and then the solvent was rid of in vacuo. This compound was redissolved in dichloromethane, washed by 1 M HCl, brine, and dried over magnesium sulfate. Finally, this compound was purified by flash column chromatography (eluent: CH_2Cl_2/hexanes, 3/17) to afford the desired product as a yellow

solid **149b** (140 mg, 0.238 mmol, 80%). ^{1}H NMR (500 MHz, $CDCl_3$): δ 7.66 (1H, s), 7.57-7.55 (2H, m), 7.52 (1H, d, J = 9.0 Hz), 7.43 (1H, d, J = 9.0 Hz), 7.33-7.31 (2H, m), 3.13 (1H, s), 2.41-2.39 (12H, m).

2,2'-(9,10-Bis(4,5-bis(methylthio)-1,3-dithiol-2-ylideene)-9,10-dihydroanthracene-2,6-diyl)bis(ethyne-2,1-diyl)dianthracene-9,10-dione (138). In a 100 mL round-bottomed flask, **148b** (500 mg, 0.816 mmol) and **144** (700 mg, 2.095 mmol) were dissolved in 30 mL of dry THF and Et_3N (2:1). After complete degassing freeze-pump-thaw cycles, $PdCl_2(PPh_3)_2$ (40 mg, 0.057 mmol) and CuI (20 mg, 0.105 mmol) dissolved in 5 mL of dry THF were also added to this mixture. This solution was allowed to warm up to rt and be stirred overnight. After the solvent was removed in vacuo, this compound was redissovled in dichloromethane, washed by 1 M HCl, brine, and dried over magnesium sulfate. After the solvent was removed in vacuo, the crude compound was purified by flash column chromatography (eluent: dichloromethane/hexanes, 2/1) to give the desired product **138** (420 mg, 0.410 mmol, 50%) as a black powder. ^{1}H NMR (500 MHz, $CDCl_3$): δ 8.49 (2H, s), 8.36-8.32 (6H, m), 7.96 (2H, d, J = 8.0 Hz), 7.84-7.82 (4H, m), 7.75 (2H, s), 7.62 (2H, d, J = 8.5 Hz), 7.55 (2H, d, J = 8.0 Hz), 2.44 (6H, s), 2.43 (6H, s). ^{13}C NMR (125 MHz, $CDCl_3$): δ 182.82, 182.62, 136.76, 135.38, 134.91, 134.49, 134.36, 134.28, 133.81, 133.71, 133.64, 132.57, 130.50, 130.18, 129.73, 128.55, 127.60, 127.54, 127.50, 126.90, 126.12, 125.81, 122.11, 120.43, 94.54, 89.07, 19.48, 19.31. IR (cm^{-1}): 3065, 2919, 2850, 2204, 1674, 1590, 1525, 1490, 1461, 1428, 1399, 1316, 1285, 977, 930, 897, 854, 834, 722, 710. HR-MALDI-

TOF MS(dithranol): *m/z* calculated for $C_{56}H_{33}O_4S_8$ 1024.0066, found 1025.2352. Mp: > 300 °C.

Compound 139. In a 50 mL round-bottomed flask, *n*-butyllithium (0.18 mL, 1.38 M, 0.250 mmol) was added dropwise to the solution containing **147** (76 mg, 0.248 mmol) in dry THF (10 mL) at -78 °C. After this solution was stirred for 30 min, **138** (50 mg, 0.049 mmol) was also added to this solution dropwise at -78 °C, and then this mixture was allowed to warm to rt and be stirred overnight. After the solvent was removed in vacuo, this compound was redissolved in $CHCl_3$, washed by 1 M HCl, brine, and then dried over magnesium sulfate. Finally, this crude product was purified by flash column chromatography (eluent: pure $CHCl_3$) to afford the desired product **139** (76 mg, 0.044 mmol, 90%) as an orange solid. ^{1}H NMR (500 MHz, $CDCl_3$): δ 7.73 (4H, s), 7.57 (8H, d, J = 8.5 Hz), 7.52-7.49 (4H, m), 7.34-7.32 (4H, m), 2.42-2.40 (36H, m). ^{13}C NMR (125 MHz, $CDCl_3$): δ 134.99, 134.81, 134.67, 134.65, 133.32, 132.30, 132.27, 129.74, 128.39, 126.61, 126.52, 126.30, 126.04, 125.62, 125.52, 123.34, 122.95, 122.54, 121.37, 121.18, 19.39, 19.22. IR (cm^{-1}): 2916, 2849, 1720, 1670, 1598, 1528, 1493, 1453, 1417, 1310, 1284, 967, 892, 833, 754. HR-MALDI-TOF MS(dithranol): *m/z* calculated for $C_{76}H_{57}S_{24}$ 1735.7679, found 1736.5644 (MALDI, positive). Mp: > 300 °C.

2,6-Bis((9,10-bis(4,5-bis(methylthio)-1,3-dithiol-2-ylideene)-9,10-dihydroanthracen-2-yl)ethynyl)anthracene-9,10-dione (140). In a 100 mL round-bottomed flask, **149b** (78 mg, 0.132 mmol) and **143** (15 mg, 0.033 mmol) were dissolved in 30 mL of dry THF and Et_3N (1:1). After complete degassing freeze-pump-thaw cycles,

$Pd(PPh_3)_4$ (40 mg, 0.035 mmol) and CuI (20 mg, 0.105 mmol) dissolved in 5 mL of dry THF were also added to this mixture. This solution was allowed to warm to rt and be stirred overnight. After the solvent was removed in vacuo, this compound was redissovled in dichloromethane, washed by 1 M HCl, brine, and dried over magnesium sulfate. After the solvent was removed in vacuo, the crude compound was purified by flash column chromatography (eluent: dichloromethane/hexanes, 1/1) to give the desired product **140** (35 mg, 0.025 mmol, 76%) as a brown powder. ^{1}H NMR (500 MHz, $CDCl_3$): δ 8.48 (s, 2 H), 8.35 (2H, d, J = 8.0 Hz), 7.96 (2H, d, J = 8.0 Hz), 7.74 (2H, s), 7.60-7.58 (6H, m), 7.53 (2H, d, J = 8.0 Hz), 7.35-7.32 (4H, m), 2.43 (6H, s), 2.42 (6H, s), 2.412 (6H, s), 2.406 (6H, s). Meaningful ^{13}C NMR spectrum could not be obtained due to low solubility. IR (cm^{-1}): 3473, 2918, 2850, 2205, 1723, 1673, 1591, 1528, 1494, 1454, 1411, 1329, 1304, 1283, 1266, 1246, 969, 922, 892, 874, 836, 755, 741, 712, 697. HR-MALDI-TOF MS(dithranol): *m/z* calculated for $C_{66}H_{45}O_2S_{16}$ 1379.8873, found 1382.6318. Mp: > 250 °C.

2-Chloro-2-methylpropane (152). To 75 mL of **151** was added 165 mL of concentrated HCl. The mixture was shaken for 15 min. The organic layer was separated, washed by water, $NaHCO_3$, brine, and dried over $MgSO_4$. Then it was distilled to collect the fraction **152** at 50-52 °C. ^{1}H NMR (500 MHz, $CDCl_3$): δ 1.63 (9H, s).

(4-Bromophenyl)(*tert*-butyl)sulfane (154). Compound **153** (500 mg, 2.644 mmol) was dissolved in 2 mL of **152**. $AlCl_3$ (18 mg, 0.136 mmol) was added over 5 min under nitrogen atmosphere. The mixture was allowed to be stirred for 5 h. Water was added.

The mixture was extracted by hexanes. The combined organic layer was washed by brine, dried over magnesium sulfate, and evaporated in vacuo to afford a colorless liquid **154** (560 mg, 2.286 mmol, 86%). ^{1}H NMR (500 MHz, $CDCl_3$): δ 7.47 (2H, d, J = 8.0 Hz), 7.39 (2H, d, J = 8.0 Hz), 1.28 (9H, s).

4-(*Tert*-butylthio)benzaldehyde (155). *n*-Butyllithium (0.82 mL, 2.5 M, 2.100 mmol) was added dropwise under a nitrogen atmosphere to a mixture of **154** (500 mg, 2.041 mmol) in 15 mL of dry THF at -78 °C. The reaction was stirred at -78 °C for 15 min. Then dry DMF (2 mL) was added in one portion and stirring was maintained at rt for 30 min. The clear reaction minture was poured into water and extracted with hexane. The extract was washed by brine, and dried over magnesium sulfate, and concentrated in vacuo. The crude product was purified with flash column chromatography (eluent: dichloromethane/hexanes, 1/1) to give the desired product **155** (270 mg, 1.481 mmol, 73%) as a pale-yellow liquid. ^{1}H NMR (500 MHz, $CDCl_3$): δ 10.04 (1H, s), 7.84 (2H, d, J = 8.0 Hz), 7.69 (2H, d, J = 8.0 Hz), 1.35 (9H, s).

***Tert*-butyl(4-ethynylphenyl)sulfane (156)**. Compound **155** (260 mg, 1.426 mmol) and $PPh_3.CHBr_3$ (1500 mg, 2.913 mmol) were added to 20 mL of dry THF. ^{t}BuOK (340 mg, 3.030 mmol) was also added. The color of reaction mixture quickly turned into brown. After stirring for 15 min, another portion of ^{t}BuOK (840 mg, 7.486 mmol) was added and stirred for 20 min. The solution was quenched with brine and extracted with ethyl acetate, worked up and dried over magnesium sulfate. The solution was filtered through a silica plug. The crude compound was separated by flash column

chromatography (eluent: hexanes/ethyl acetate, 5/1) to afforded a brown oil **156** (160 mg, 0.897 mmol, 63%). ^{1}H NMR (500 MHz, $CDCl_3$): δ 7.49 (2H, d, J = 7.5 Hz), 7.45 (2H, d, J = 7.5 Hz), 3.14 (1H, s), 1.29 (9H, s).

2,6-Bis((4-(*tert*-butylthio)phenyl)ethynyl)anthracene-9,10-dione (157). In a 100 mL round-bottomed flask, **156** (300 mg, 1.683 mmol) and **145** (200 mg, 0.435 mmol) were dissolved in 20 mL of dry THF. After complete degassing freeze-pump-thaw cycles, CuI (20 mg, 0.105 mmol) and $PdCl_2(PPh_3)_2$ (40 mg, 0.057 mmol) dissolved in 5 mL of dry THF were added to this mixture. Then the mixture was allowed to warm up and be stirred at rt for 48 h. After the solvent was removed in vacuo, this compound was dissolved in dichloromethane again, washed by 1 M HCl, brine, and dried over magnesium sulfate. This crude product was separated by flash column chromatography (eluent: dichloromethane/hexanes, 1/3) to give the desired product **157** (130 mg, 0.232 mmol, 54%) as a yellow solid. ^{1}H NMR (500 MHz, $CDCl_3$): δ 8.46 (2H, s), 8.34 (2H, d, J = 7.5 Hz), 7.93 (2H, d, J = 7.5 Hz), 7.56-7.54 (8H, m), 1.33 (18H, s).

Compound 150. To a solution of **145** (50 mg, 0.164 mmol) in THF (10 mL) at -78 °C was added *n*-BuLi (0.064 mL, 2.5 M, 0.160 mmol). After stirring for 30 min, compound **157** (20 mg, 0.036 mmol) was added. The mixture was warmed up to rt and stirred overnight. After the reaction was complete, the mixture was evaporated *in vacuo* and the residue was diluted with CH_2Cl_2. The organic solution was washed with aq. HCl (10%), brine, and dried over $MgSO_4$. Evaporation *in vacuo* afforded the crude product, which was purified through silica column chromatography using an eluent of 25% CH_2Cl_2 in

hexanes, yielding **150** as a yellow solid (24 mg, 0.026 mmol, 59%). Mp: 258 °C (dec.); IR (neat) 3443, 2957, 2919, 2860, 2361, 1528, 1492, 1458 cm^{-1}; ^{1}H NMR (500 MHz, CDCl3) δ 7.68 (2H, s), 7.55 (2H, d, J = 9.0 Hz), 7.53 (8H, s), 7.47 (2H, d, J = 8.5 Hz), 2.42 (12H, s), 1.31 (18H, s); ^{13}C NMR (125 MHz, $CDCl_3$): 137.4, 134.8, 134.7, 133.6, 133.3, 131.8, 129.8, 128.3, 126.8, 126.0, 125.7, 123.7, 122.4, 121.2, 91.0, 89.8, 46.7, 31.1, 19.4, 19.3; MALDI-TOF MS (dithranol): *m/z* calculated for $C_{48}H_{44}S_{10}$ 940.0650, found 941.4941.

Chapter 3

Thiophene Functionalized π-Extended Tetrathiafulvalenes

3.1 Introduction

In Chapters 1 and 2, a wide range of quinodimethane based π-extended TTF derivatives and their use as π electron donors were discussed. To develop novel π-extended TTF derivatives with a more pronounced gain of aromaticity and planarity during the oxidation processes, chemists have designed some TTF analogues with a greater distance between the two dithole rings than that in TTFAQs.

In 2004, the Martín group prepared compounds **161-163** (Figure 3.1),[86] in which bianthracene was fused with two dithiole termini. These three compounds have a broad UV-Vis absorption band at 431 nm for **161**, 436 nm for **162**, and 450 nm for **163**, respectively. The trend for the absorption band shift toward higher wavelength is due to the electron-donating effect of the substituents attached to the dithiole rings (SCH_3, SCH_2CH_2S). Compared with related compounds **164** (428 nm), **165** (434 nm) and **166** (446 nm),[86] the bathochromic shifts are small in spite of the larger intramolecular distances between the conjugated bianthracenes in **161-163**, suggesting that electronic interactions in the ground state through the two anthracene units are rather weak.

Compounds **161-163** all gave rise to an electrochemically irreversible oxidation waves, indicating that dications probably formed new compounds at higher voltage. (**161**: E_{ap} = +0.74 V; **162**: E_{ap} = +0.81 V; **163**: E_{ap} = +0.82 V). The reduction wave,

corresponding to the reversion of the new products to the neutral molecules, was observed at negative values (**161**: E_{cp} = -0.25 V; **162**: E_{cp} = -0.11 V; **163**: E_{cp} = -0.09 V). From UV-Vis and CV data, the three compounds exhibit large redox potentials for oxidation in comparison to parent TTF (E_{ap} = +0.40 V). This is likely due to the large distance separating the two dithiole rings, leading to the two dithioles to be nearly independent. Although these experiments did not yield the anticipated results, more spatially extented conjugated TTF derivatives still present a novel class of ex-TTF for fundamental and application studies.

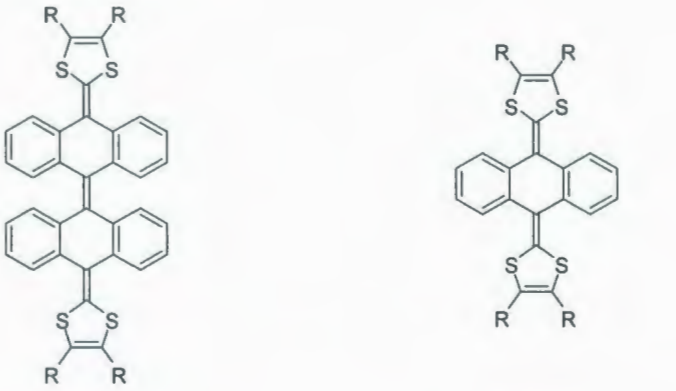

161 R = H
162 R = SMe
163 R = SCH_2CH_2S

164 R = H
165 R = SMe
166 R = SCH_2CH_2S

Figure 3.1: Structures of compounds **161-166**.

Sulfur-rich π-conjugated molecules constitute important building blocks in current research on molecular electronics. Thiophene is the essential repeat unit for a class of well-known conducting polymers, poly/oligothiophenes,[87-89] while TTF and its derivatives are excellent organic electron donors which may be exploited in systems ranging from charge-transfer complexes, nonlinear optical materials, organic transistors, to molecular switches and sensors.[90-93] There exists an extensive literature devoted to the

design and synthesis of π-conjugated molecular systems based on oligothiophenes and TTF derivatives as semiconducting materials. Integration of these structural components into a single molecular entity is expected to give rise to molecular assemblies with increased dimensionality and improved donor ability. Furthermore, rigid films where intimate solid-state packing may minimize the on-site Coulombic repulsion in the di- or poly-cationic states and enhance stability of the corresponding cation radicals or dications.

In 1993, the Kato group prepared thiophene functionalized π-extended TTFs **167** and **168** (Figure 3.2).[94] These two compounds were found to be good electron donors based on voltammeric analysis. Compound **167** showed a reversible two-electron oxidation wave at $E_{1/2}^{ox}$ = +0.02 V, while **168** underwent one reversible and one irreversible single-electron oxidation at $E_{1/2}^{ox}$ = + 0.04 V and $E_{1/2}^{ox}$ = +0.23 V respectively.

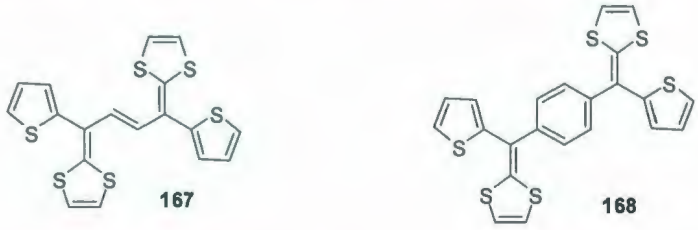

Figure 3.2: Structures of compounds **167-168**.

Also in 1993, Roncali *et al.* demonstrated extended TTFs **169-173** (Figure 3.3)[95] possessed several similar electrochemical characteristics: (1) Two reversible one-electron oxidation waves at E_{pa} +0.5-+0.7 V, followed by a third one-electron oxidation wave +0.8-+1.0 V. The authors concluded that the insertion of the terthienyl group led to a significant decrease of oxidation potentials, compared with the electrochemical properties of the parent dibenzo-TTF (+0.72 and +1.06 V). (2) The smaller difference between the

first and the second oxidation steps (120 mV for **172** instead of 340 mV for dibenzo-TTF) indicated a significant reduction of the on-site Coulombic repulsion between positive charges in the dication state.

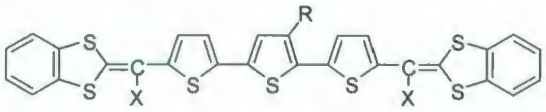

	X	R
169	H	H
170	H	Me
171	Me	Me
172	H	$(CH_2)_7Me$
173	H	$(CH_2CH_2O)_2Me$

Figure 3.3: Structures of compounds **169-173**.

Table 3.1: Cyclic voltammetric and UV-Vis absorption data for **169-173.**

Entry	$E1_{1/2}$/V	$E2_{1/2}$/V	$E3_{pa}$/V	$E2_{1/2}$-$E1_{1/2}$/V	λ_{max}/nm
169	0.50	0.69	0.92	190	417
170	0.46	0.64	0.82	181	444
171	0.45	0.61	1.00	160	440
172	0.50	0.62	0.82	120	450
173	0.52	0.66	0.82	140	438

In 1996, Frère *et al.* developed a new class of linearly π-extended TTFs in which the conjugated spacer consisted of two thiophene units separated by one, two or three double bonds **174** (a-c), **175** (a-c) and **176** (a-c) (Figure 3.4).[96] Their electronic absorptions were dependent on the length of the conjugated spacer and the nature of the substituents on the 1,3-dithiole ring. Both λ_{max} and ΔE (the Homo-Lumo gap) exhibited a marked

dependence on the nature of the R group. Replacing the electron-withdrawing CO_2Me group by electron-donating substituents such as SMe and *n*-propyl resulted in a redshift of λ_{max} and a narrowing of ΔE. As expected, an increase in the number of conjugated double bonds led to a redshift of λ_{max} with a reduction of the HOMO-LUMO gap (ΔE). The electrochemical properties also relied on the nature of R and the π-conjugated bridge. The compounds with electron-donating groups were better electron donors than those bearing electron-withdrawing substituents (R = CO_2Me, SMe, nC_3H_7). The longer conjugation length also led to a decrease in the oxidation potential. The effect was however not so significant.

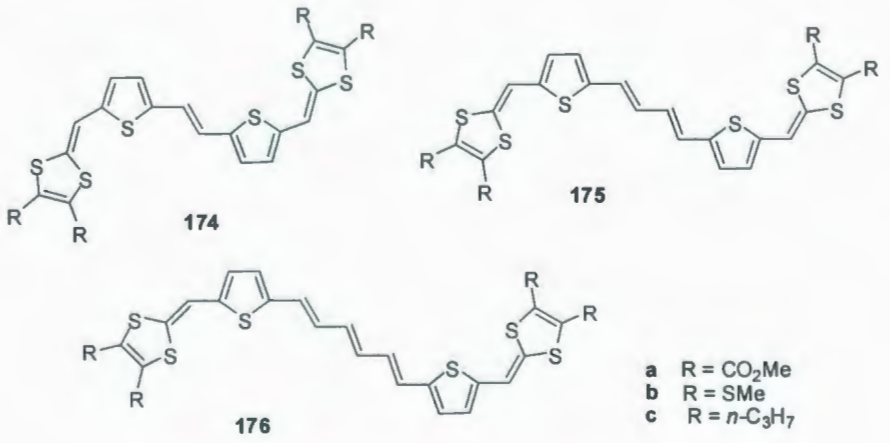

Figure 3.4: Structures of compounds **174-176**.

Table 3.2: Electronic absorption data for **174 (a-c)**, **175 (a-c)**, **176 (a-c)** measured in CH_2Cl_2.

compd	λ_{max} (nm)	ΔE(eV)
174a	468	2.34
174b	484	2.25
174c	493	2.17
175a	476	2.27
175b	489	2.20
175c	502	2.14
176a	486	2.24
176b	501	2.16
176c	512	2.09

Frère *et al.* also designed a new series of linearly π-extended TTFs containing thiophene **177 (a-c)**, thienothiophene **178 (a-c)** and dithienothiophene **179 (a-c)** units (Figure 3.5).[97] From Table 3.3, the results of these compounds were consistent with the conclusions of the work described in the previous paragraph. The optical and electrochemical properties were strongly dependent on both the nature of the substituents on the 1,3-dithiole ring and the length of the conjugated spacer (Table 3.3). UV-Vis spectral data for compounds with electron-donating substituents led to a redshift compared to compounds with electron-withdrawing groups. The elongation of the spacer also caused a redshift. All these compounds showed two reversible one-electron oxidation processes corresponding to the successive formation of cation radical (E_1) and

dication (E_2). Compounds incorporating the most electron-withdrawing CO_2Me substituent exhibited the most positive E_1 and E_2 values and also higher ΔE than those compounds with electron-donating groups. The elongation of the conjugated spacer with an aromatic core will be accompanied by two competitive effects: (1) decreasing the intramolecular Coulombic repulsion favoring access to the dication; (2) increasing the energy in sacrificing the aromatic character of the spacer. In comparison to T-TTF, the first effect is in agreement with the reduction of ΔE for TT-TTF and DTT-TTF, whereas the strongest aromatic character of the spacer explains the increase of ΔE for DTT-TTF compared with TT-TTF despite a much longer conjugation length.

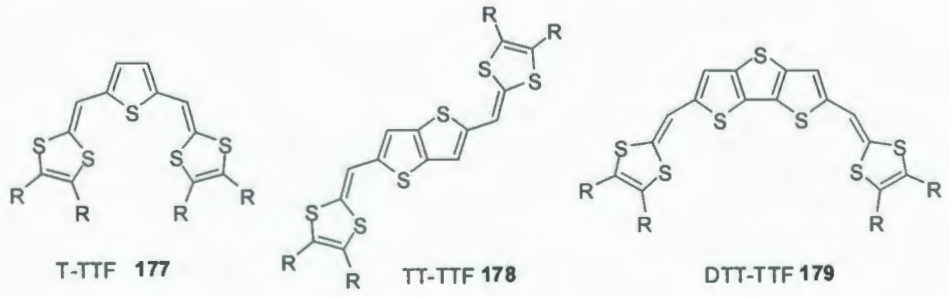

T-TTF **177**

a R = CO_2Me
b R = SMe

TT-TTF **178**

a R = CO_2Me
b R = SMe
c R = SPent

DTT-TTF **179**

a R = CO_2Me
b R = SMe

Figure 3.5: Structures of compounds **177**, **178** and **179**.

Table 3.3: Spectroscopic and electrochemical data for linearly extended TTFs **177-179**.

	λ_{max}/nm	E^o_1/V	E^o_2/V	$\Delta E/mV = E^o_2 - E^o_1$
T-TTFa	412-434	0.68	0.89	210
TT-TTFa	420-447	0.70	0.88	181
DTT-TTFa	431-457	0.69	0.88	190
T-TTFb	434-454	0.46	0.61	150
TT-TTFb	438-465	0.50	0.59	90
TT-TTFc	439-466	0.49	0.59	100
DTT-TTFb	447-475	0.47	0.58	110

Based on the results of the above studies, two new exTTF-thiophene hybrids **180** and **181** were designed (Figure 3.6). It was expected that these compounds may show a better donor properties as well as enhanced solid state packing properties compared to their parent TTF.

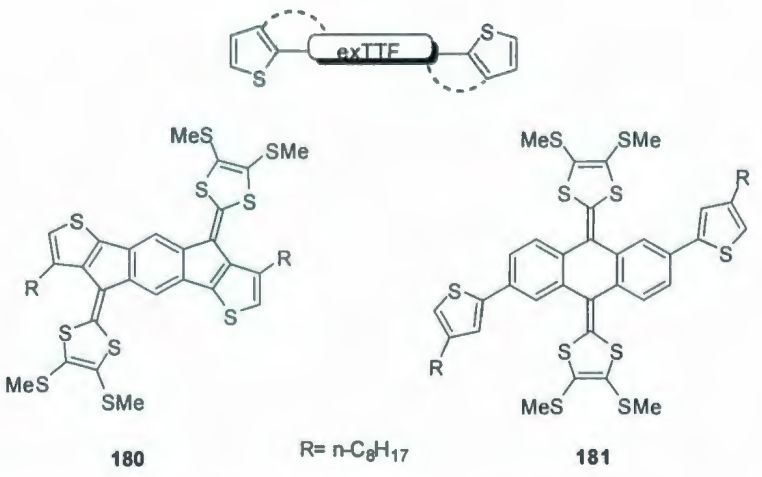

Figure 3.6: Structures of compounds **180** and **181**.

3.2 Results and Discussion

3.2.1 Synthesis

The synthesis of ex-TTF-thiophene triads **180** and **181** is outlined in Scheme 3.1. The synthesis of precursor **191** followed the synthetic route reported by Ng and co-workers.[98,99] From a typical bromination reaction, in which NBS and compound **182** were heated at 60-70 °C in AcOH, compound **182** was converted to monobromination product by strictly controlling the amounts of compound **182** and NBS (compound/NBS, 1/1 mol/mol). Then the bromo group was replaced by TMS. After lithiation of **184** at the 5-position, tributyltin chloride was added slowly to afford thienylstannane **185**. Stille coupling between thiophene **185** and diiodoarene **186**,[101] which gave compound **187** in 77% yield. Removal of the TMS groups in **187** by TFA yielded compound **188**, which was then subjected to saponification and chlorination to form acyl chloride **190**. Compound **190** underwent a two-fold intramolecular Friedel-Crafts cyclization to form the desired ketone **191**. With **191** in hand, a Horner-Wittig reaction was executed to furnish exTTF-thiophene hybrid **180** in 57% yield. 2,6-Diiodoanthraquinone **143** and thienylstanane **185** were subjected to a Stille coupling under the catalysis of Pd(0), affording ketone **192**, which is a key precursor to compound **181**. Upon a Horner-Wittig reaction with the phosphonate ylide generated *in situ* from compound **147**,[100] ketone **192** was converted into exTTF thiophene **193** in a high yield of 95%. Treatment of **193** with TFA removed the TMS groups, giving the desired product **181**. The presence of *n*-octyl groups on the thiophene units during the synthesis of **180** and **181** was essential as they conferred satisfactory solubility to the intermediates and the products.

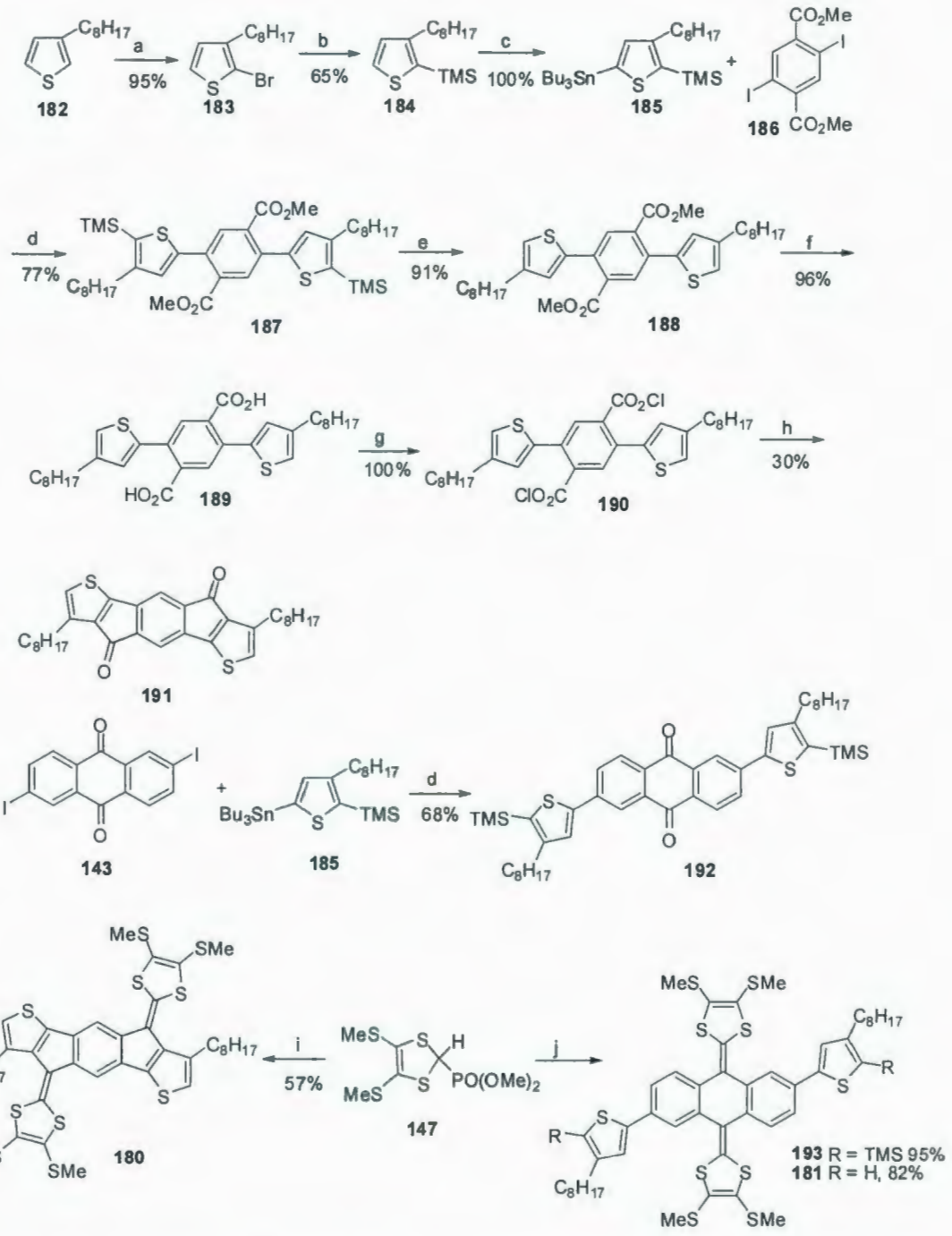

Scheme 3.1: Synthesis of **180** and **181**. (a) NBS, AcOH, 70 °C 1 h; (b) (i) *n*-BuLi, THF, -78 °C, 40 min; (ii) TMSCl, -78 °C, 1 h; (iii) rt, 1 h; (c) (i) *n*-BuLi, THF, 0 °C; (ii) Bu_3SnCl, 0 °C; (d) $Pd(PPh_3)_4$, PPh_3, DMF, 100 °C, 12 h; (e) TFA, CH_2Cl_2, 0 °C; (f)

NaOH, EtOH/H_2O, reflux; (g) ClCOCOCl, CH_2Cl_2, rt, overnight; (h) $AlCl_3$, CH_2Cl_2, 0 °C to rt; (i) *n*-BuLi, -78 °C, 30 min; (ii) then **191** at -78 °C, to rt, overnight; (j) *n*-BuLi, -78° C, 30 min; (ii) then **192** at -78 °C, to rt, overnight.

Diiodoarene **186** was prepared following the synthetic route reported by Zhou[101] and co-workers (Scheme 3.2). From the starting material *p*-xylene, iodonation compound **194** led to disubsituted iodo products. Oxidation of compound **195** by $KMnO_4$ in the presence of pyridine afforded monoacid **196**. Since carbonyl is electron-withdrawing, it was difficult for another methyl group at the *para* position to be oxidized. A stronger base KOH was therefore used instead of pyridine in the second step of oxidation. After oxidation, esterification of acid **197** in MeOH gave diiodoarene **186**.

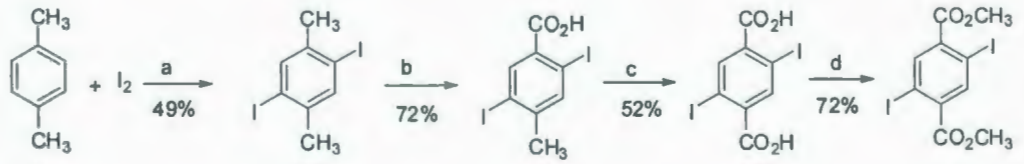

194 **195** **196** **197** **186**

Scheme 3.2: Synthesis of **186**. Reagents and conditions: (a) H_5IO_6, H_2O, AcOH, H_2SO_4, reflux overnight; (b) $KMnO_4$, pyridine/H_2O, reflux 6 h; (c) $KMnO_4$, 10% KOH, reflux overnight; (d) CH_3OH, H_2SO_4, reflux overnight.

3.2.2 Electronic and electrochemical properties of thiophene functionalized π-extended tetrathiafulvalenes 180 and 181

Molecular structures of compounds **180** and **181** were characterized by IR, NMR, and MS analyses, while their electrochemical redox properties were investigated by cyclic voltammetry (CV) and differential pulse voltammetry (DPV) techniques. Figure 3.7

illustrates the voltammograms measured in $CHCl_3/CH_3CN$ (4/1, v/v) at room temperature. In Figure 3.7A, a prominent pair of redox waves (E_{pa}^1 = +0.76 V, E_{pc}^1 = +0.26 V, vs. Ag/AgCl) is clearly seen, which can be attributed to a simultaneous two-electron transfer at the central TTFAQ unit, leading to the formation of dication of **181**. The nature of this redox wave pair is quasi-reversible, which is in line with the typical redox behavior of TTFAQ. [102] In addition to this redox couple, two weak current peaks (E_{pa}^2 = +1.07 V, E_{pc}^2 = +1.01 V) are discernible in the CV of **181**. The DPV of **181** (Figure 3.7B) shows the presence of a significant oxidation peak at +0.63 V followed up by two weak peaks at +0.88 and +1.01 V in the course of anodic scan. The two oxidation processes at relatively higher voltages can be explained by that the formed $[\mathbf{181}]^{2+}$, to some extent, yielded electrochemical byproducts which were subject to further oxidation. In the cyclic voltammogram of **180** (Figure 3.7C), there are three anodic waves observable at +0.93, +1.15, and +1.33 V, along with a barely noticeable cathodic wave at -0.98 V. The first oxidation presumably leads to the formation of dication of **180**. However, in notable contrast to the CV of **181**, the redox pattern displayed by **180** is completely irreversible. The irreversibility is likely due to an EC mechanism (a chemical reaction (*c*) that may follow an electron transfer (*e*) step), which results in decomposition of $[\mathbf{180}]^{2+}$ at high voltage. The DPV of **180** shows three oxidation peaks when scanned anodically from 0 to +1.5 V. This result agrees with its CV data, suggesting the formation of multiple electrochemical products in anodic scan. Compared with compound **181**, compound **180** has a higher first oxidation potential, indicating that **180** is a weaker electron donor than **181**. For both compounds **181** and **180**, no indication of the occurrence of electropolymerization was observed from repetitive CV scan experiments.

The inability of **181** and **180** to undergo electropolymerization can be rationalized as follows: the exTTF units play a dominant role in the oxidation processes, such that the thienyl moieties are not able to form suitable radical cations for electropolymerization.[103]

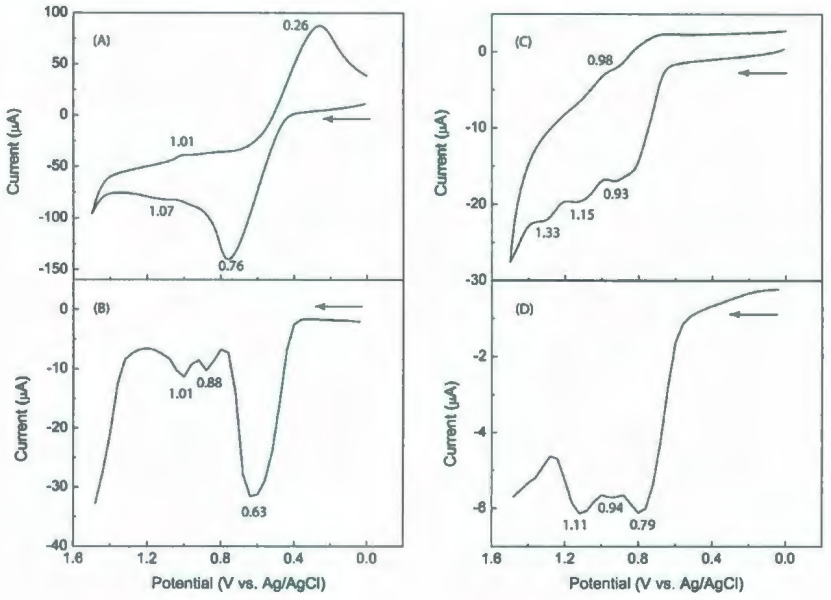

Figure 3.7: (A) Cyclic voltammogram of **181**. (B) Differential pulse voltammogram of **181**. (C) Cyclic voltammogram of **180**. (D) Differential pulse voltammogram of **180**. CV experimental conditions: electrolyte: Bu_4NPF_6 (0.1 M); working: glassy carbon; counter: Pt; reference: Ag/AgCl; scan rate: 100 mV/s. DPV experimental conditions: step: 4 mV; pulse width: 250 mV; period: 200 ms.

To investigate the electronic properties of **181** and **180** in neutral and oxidized forms, oxidative UV-Vis titration and spectroelectrochemistry measurements were conducted on their $CHCl_3$ solutions (see Figure 3.8). In Figure 3.8A, compound **181** shows three UV-Vis absorption bands at 453, 390, and 317 nm in the neutral state. Upon titration with an oxidant, $PhI(OAc)_2/CF_3SO_3H$ (note that one molar equivalent of the oxidant theoretically consumes two moles of electrons),[104] up to 3.0 molar equivalents, the absorption peak at

453 nm is observed to steadily decrease in intensity, while the other two peaks show rather insignificant change. An isosbestic point can be clearly seen at 419 nm. Similar UV-Vis spectroscopic changes were observed (see Figure 3.8C) when compound **181** was subjected to controlled-potential oxidation in a 1 mm quartz cuvette. These results indicate that a two-species equilibrium, presumably between **181** and $[\mathbf{181}]^{2+}$, is formed during the oxidation. Compound **180** shows absorption bands at 475, 357, and 301 nm in its UV-Vis profile (see Figure 3.8B). Upon addition of oxidant up to 2.0 equivalents, the peak at 475 nm decreases considerably. In the meantime, an absorption tail from *ca.* 550 to 750 nm increases appreciably, the origin of which is assigned to $[\mathbf{180}]^{2+}$. There are two isosbestic points at 538 and 441 nm observable in titration of oxidant from 0 to 1.0 molar equivalent, and these two isosbestic points drift slightly when the amount of oxidant is further increased. More significant drift of isosbestic points can be seen in the spectroelectrochemical measurements when the applied voltage is greater than +1.0 V (Figure 3.8D). The drift of isosbestic points is also accompanied by decreasing absorption tail from 550 to 750 nm. This result substantiates the EC mechanism again.

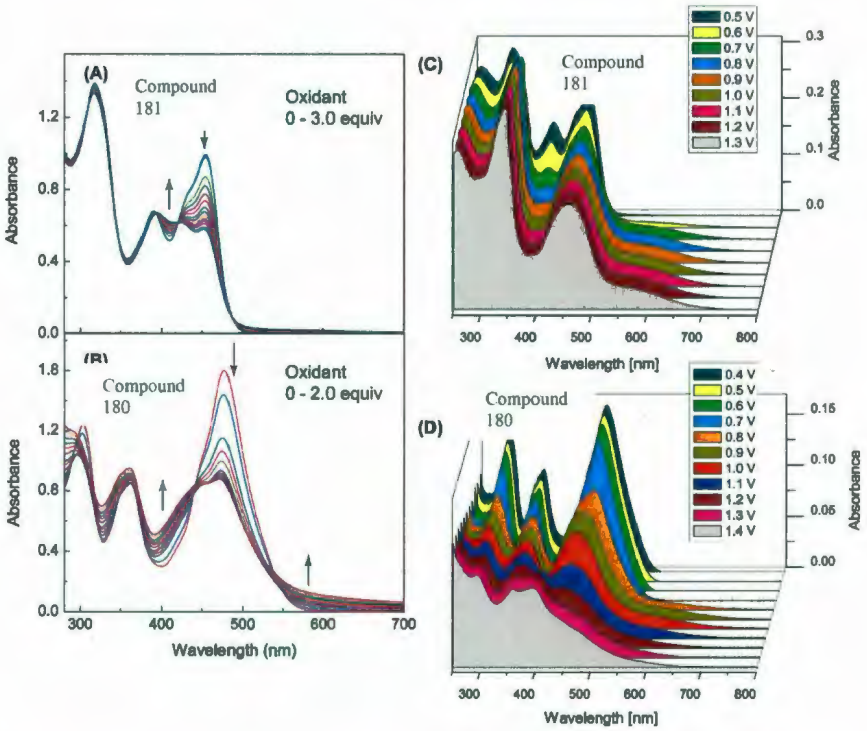

Figure 3.8: UV-Vis spectroscopic changes accompanying: (A) Oxidative titration of **181**. (B) Oxidative titration of **180**. (C) Controlled-potential oxidation of **181**. (D) Controlled-potential oxidation of **180**. Experimental conditions of spectroelectrochemistry: electrolyte: Bu_4NPF_6 (0.1 M); working: Pt mesh; counter: Pt wire; reference: Ag/AgCl.

3.3 Experimental

General procedures and methods

Chemicals and reagents were purchased from commercial suppliers and used without further purification. THF was distilled from sodium/benzophenone. Et_3N and toluene were distilled from LiH. Catalysts, $Pd(PPh_3)_4$ and $Pd(PPh_3)_2Cl_2$, were prepared from $PdCl_2$ according to standard procedures. All reactions were performed in standard, dry glassware under an inert atmosphere of N_2 unless otherwise noted. Evaporation and concentration were done at H_2O-aspirator pressure. Flash column chromatography was

carried out with silica gel 60 (230-400 mesh) from VWR international. Thin-layer chromatography (TLC) was carried out with silica gel 60 F254 covered on plastic sheets and visualized by UV light or $KMnO_4$ stain. Melting points (mp) were measured with a Fisher-Johns melting point apparatus and are uncorrected. ^1H and ^{13}C NMR spectra were measured on the Bruker AVANCE 500 MHz spectrometer. Chemical shifts are reported in ppm downfield from the signal of the internal reference $SiMe_4$. Coupling constants (J) are given in Hz. Infrared spectra (IR) were recorded on a Bruker Tensor 27 spectrometer. UV-vis spectra were recorded on an Agilent 8453 UV-Vis or a Cary 6000i UV-Vis-NIR spectrophotometer. APCI mass spectra were measured on an Agilent 1100 series LCMSD spectrometer, and high-resolution MALDI-TOF mass spectra on an Applied Biosystems Voyager instrument with dithranol as the matrix.

2-Bromo-3-octylthiophene (183). In a 50 mL round-bottomed flask, **182** (400 mg, 2.037 mmol) and NBS (360 mg, 2.022 mmol) were dissolved in AcOH (10 mL). This mixture was allowed to be heated and stirred at 60-70 °C for 1 h under nitrogen atmosphere. After reaction was completed, water and diethyl ether was added into the solvent. The collected organic solvent was washed by brine, and dried over magnesium sulfate. After the solvent was removed in vacuo, the crude product was purified with flash column chromatography (eluent: hexanes) to give the desired product **183** (530 mg, 1.926 mmol, 95%) as a colorless liquid. ^1H NMR (500 MHz, $CDCl_3$): δ 7.19 (1H, d, J = 6.0 Hz), 6.80 (1H, d, J = 6.0 Hz), 2.57 (2H, t, J = 7.5 Hz), 1.58-1.54 (2H, m), 1.31-1.30 (2H, m), 1.29-1.27 (8H, m), 0.90 (3H, t, J = 6.5 Hz).

Trimethyl(3-octyl-2-thienyl)silane (184). In a 100 mL round-bottomed flask, *n*-BuLi (0.90 mL, 2.5 M, 2.250 mmol) in hexanes was added dropwise to a completely degassed solution of **183** (500 mg, 1.817 mmol) in dry THF (10 mL) at -78 °C. The mixture was stirred for 40 min at this temperature, and TMSCl (601 mg, 5.535 mmol) was added dropwise at -78 °C. The resulting mixture was stirred for 1 h at this temperature, then warmed up to rt and stirred for another 1 h. After removal of the solvent in vacuo, the residue was redissolved in Et_2O. The collected organic solution was washed by brine, and dried over magnesium sulfate. After the solvent was removed in vacuo, the crude product was purified with flash column chromatography (eluent: hexanes) to give the desired product **184** (330 mg, 1.164 mmol, 65%) as a colorless liquid. ^{1}H NMR (500 MHz, $CDCl_3$): δ 7.45 (1H, d, J = 5.0 Hz), 7.05 (1H, d, J = 5.0 Hz), 2.68 (2H, t, J = 7.5 Hz), 1.61-1.58 (2H, m), 1.36-1.30 (2H, m), 1.29-1.27 (8H, m), 0.92 (3H, t, J = 7.0 Hz), 0.33 (9H, s).

Trimethyl(3-octyl-5-(tributylstannyl)-2-thienyl)silane (185). *n*-BuLi (0.70 mL, 2.5 M, 1.750 mmol) was added dropwise to a solution of **184** (330 mg, 1.164 mmol) in 20 mL of dry THF at 0 °C. This solution was stirred for 20 min at this temperature and warmed up to rt over 30 min. The mixture was cooled to 0 °C, and tributyltin chloride (567 mg, 1.743 mmol) was added dropwise. The resulting mixture was stirred at 0 °C for 10 min, warmed up to rt over 30 min, poured into water, and extracted with diethyl ether. The collected organic solution was washed by brine, dried over magnesium sulphate, and concentrated in vacuo to give the crude product **185** as a yellow liquid (960 mg, 1.722 mmol, 100%). This crude product was used for next step without further purification. ^{1}H

NMR (500 MHz, $CDCl_3$): δ 7.08 (1H, s), 2.62 (2H, J = 7.5 Hz), 1.61-1.58 (8H, m), 1.36-1.31 (14H, m), 1.29-1.27 (8H, m), 0.90 (12H, m), 0.34 (9H, s).

Dimethyl 2,5-bis(4-octyl-5-(trimethylsilyl)-2-thienyl)terephthalate (187). In a 100 mL round-bottomed flask, **185** (2600 mg, 4.663 mmol) and **186** (670 mg, 1.502 mmol) were added to dry DMF (30 mL). After this solution was completely degassed, $Pd(PPh_3)_4$ (50 mg, 0.043 mmol) and PPh_3 (30 mg, 0.114 mmol) were added to this solution. This mixture was allowed to be heated to 100 °C overnight. After quenching with brine, this mixture was extracted with ethyl acetate. The combined organic layers was then washed with 10% aqueous KF and filtered through of a pad of Celite. This filtrate was washed by brine, and dried over magnesium sulfate. After the solvent was removed in vacuo, the crude product was purified with flash column chromatography (eluent: CH_2Cl_2/hexanes, 1/7) to give the desired product **187** (840 mg, 1.155 mmol, 77%) as a yellow solid. ^1H NMR (500 MHz, $CDCl_3$): δ 7.76 (2H, s), 7.02 (2H, s), 3.78 (6H, s), 2.64 (4H, t, J = 7.5 Hz), 1.61-1.58 (4H, m), 1.37-1.29 (20H, m), 0.90 (6H, t, J = 7.0 Hz), 0.36 (18H, s).

Dimethyl 2,5-bis(4-octylthiophen-2-yl)terephthalate (188). To a solution of **187** (680 mg, 0.935 mmol) in dry CH_2Cl_2 (20 mL) was added dropwise trifluoroacetic acid (296 mg, 2.596 mmol) at 0 °C. This mixture was stirred for 1 h at 0 °C, washed with brine, and dried over magnesium sulphate. After the solvent was removed in vacuo, the crude product was purified with flash column chromatography (eluent: CH_2Cl_2/hexanes, 1/1) to give the desired product **188** (500 mg, 0.859 mmol, 91%) as a yellow liquid. ^1H

NMR (500 MHz, $CDCl_3$): δ 7.77 (2H, s), 6.96 (2H, s), 6.93 (2H, s), 3.77 (6H, s), 2.62 (4H, t, J = 7.5 Hz), 1.64-1.60 (4H, m), 1.36-1.28 (20H, m), 0.90 (6H, t, J = 6.5 Hz).

2,5-Bis(4-octylthiophen-2-yl)terephthalic acid (189). A mixture of **188** (470 mg, 0.806 mmol) and sodium hydroxide (216 mg, 5.400 mmol) in 27 mL of ethanol and 3 mL of water was refluxed overnight. The solvent was evaporated in vacuo to about half of its original volume. Water was added, and the resulting aqueous layer was treated with HCl to form a solid product **189** (430 mg, 0.775 mmol, 96%). ^{1}H NMR (500 MHz, $CDCl_3$): δ 7.82 (2H, s), 7.18 (2H, s), 2.67 (4H, t, J = 7.5 Hz), 1.71-1.65 (4H, m), 1.40-1.31 (20H, m), 0.91 (6H, t, J = 7.5 Hz).

Compound 190. A solution of **189** (400 mg, 0.721 mmol) and oxalyl chloride (927 mg, 7.222 mmol) in dry 30 mL of CH_2Cl_2 and several drops DMF was stirred for 12 h at rt. The solvent was removed in vacuo to obtain the crude bis(acid chloride) **190** (430 mg, 0.727 mmol, over 100%), which was used for the next step without further purification.

Compound 191. A solution of **190** (430 mg, 0.727 mmol) in 30 mL of dry CH_2Cl_2 was added to a suspension of anhydrous $AlCl_3$ (216 mg, 1.620 mmol) in 10 mL of dry CH_2Cl_2 at 0 °C. The resulting mixture was stirred at this temperature for 20 min, and then at rt for 3 h. The reaction mixture was poured into ice water and 1 M hydrochloric acid and extracted with CH_2Cl_2, washed with brine, and dried over magnesium sulphate. After the solvent was removed in vacuo, the crude product was purified with flash column chromatography (eluent: CH_2Cl_2/hexanes, 1/1) to give the desired product **191** (110 mg,

0.213 mmol, 30%) as a dark-blue solid. ^{1}H NMR (500 MHz, $CDCl_3$): δ 7.19 (2H, s), 6.80 (2H, s), 2.74 (4H, t, J = 7.5 Hz), 1.68-1.65 (4H, m), 1.35-1.27 (20H, m), 0.89 (6H, t, J = 7.0 Hz).

Compound 180. In a 100 mL round-bottomed flask, *n*-butyllithium (0.37 mL, 2.5 M 0.920 mmol) was added dropwise to a solution containing **147** (280 mg, 0.920 mmol) in 30 mL of dry THF at -78 °C. After this solution was stirred for 30 min, **191** (120 mg, 0.230 mmol) was added to this solution dropwise at -78 °C, and then this mixture was allowed to warm up to rt and be stirred overnight. After the solvent was removed in vacuo, this compound was redissolved in dichloromethane, washed by 1 M HCl, brine, and then dried over magnesium sulfate. After the solvent was removed in vacuo, the crude product was purified by flash column chromatography (eluent: dichloromethane/hexanes, 1/1) to afford the desired product **180** (110 mg, 0.126 mmol, 57%) as an orange solid. ^{1}H NMR (500 MHz, $CDCl_3$): δ 7.70 (2H, s), 6.84 (2H, s), 3.09 (4H, t, J = 8.0 Hz), 2.57 (6H, s), 2.52 (6H, s), 1.70-1.67 (4H, m), 1.43-1.40 (4H, m), 1.35-1.25 (16H, m), 0.89 (6H, t, J = 6.0 Hz). ^{13}C NMR (125 MHz, $CDCl_3$): δ 143.23, 140.30, 137.19, 137.11, 136.59, 131.89, 129.58, 127.88, 122.24, 120.78, 113.90, 32.77, 32.12, 32.10, 31.77, 29.90, 29.75, 29.61, 29.56, 22.89, 19.68, 19.44, 14.31. IR (cm^{-1}): 2941, 2878, 1560, 1507, 1473, 1336. CI-MS (+ve): *m/z* calculated for $C_{42}H_{50}S_{10}$ 874.1120, found 875.1230 $[M+H]^+$. Mp: 158-160 °C.

2,6-Bis(4-octyl-5-(trimethylsilyl)thiophen-2-yl)anthracene-9,10-dione (192). In a 100 mL round-bottomed flask, **143** (100 mg, 0.217 mmol) and **185** (490 mg, 0.879 mmol)

were added to a DMF (30 mL). After this solution was completely degassed, $Pd(PPh_3)_4$ (50 mg, 0.043 mmol) and PPh_3 (30 mg, 0.114 mmol) were added to this solution. This mixture was allowed to be heated to 80 °C for 8 h. After quenching with brine, this mixture was extracted with ethyl acetate. The combined organic layers was then washed with 10% aqueous KF and filtered through of a pad of Celite. This filtrate was washed by brine, and dried over magnesium sulfate. After the solvent was removed in vacuo, the crude product was purified with flash column chromatography (eluent: CH_2Cl_2/hexanes, 1/4) to give the desired product **192** (110 mg, 0.148 mmol, 68%) as an orange solid. ^1H NMR (500 MHz, $CDCl_3$): δ 8.50 (2H, s), 8.31 (2H, d, J = 8.5 Hz), 7.97 (2H, d, J = 8.5 Hz), 7.53 (2H, s), 2.70 (4H, t, J = 8.0 Hz), 1.68-1.65 (4H, m), 1.42-1.25 (20H, m), 0.91 (6H, t, J = 3.5 Hz), 0.40 (18H, s). ^{13}C NMR (125 MHz, $CDCl_3$): δ 180.57, 152.16, 145.68, 140.22, 136.55, 134.33, 131.86, 130.33, 128.95, 128.35, 123.62, 32.04, 31.93, 31.72, 29.91, 29.67, 29.41, 22.83, 14.26, 0.46. IR (cm^{-1}): 2955, 2923, 2852, 1667, 1591, 1374, 1295, 1248, 1047, 1013, 910, 840, 756, 711. HR-EIMS (+ve): *m/z* calculated for $C_{44}H_{60}O_2S_2Si_2$ 740.3573, found 740.3595. Mp: 119-120 °C.

Compound 193. In a 100 mL round-bottomed flask, *n*-butyllithium (0.60 mL, 2.5 M, 1.500 mmol) was added dropwise to a solution containing **147** (300 mg, 0.986 mmol) in dry THF (30 mL) at -78 °C. After this solution was stirred for 30 min, **192** (180 mg, 0.240 mmol) was added to this solution dropwise at -78 °C, and then this mixture was warmed up to rt and stirred overnight. After the solvent was removed in vacuo, this compound was redissolved in dichloromethane, washed by brine, and then dried over magnesium sulfate. After the solvent was removed in vacuo, the crude product was

purified by flash column chromatography (eluent: dichloromethane/hexanes, 1/4) to afford the desired product **193** (250 mg, 0.228 mmol, 95%) as an orange sticky liquid. ^{1}H NMR (500 MHz, $CDCl_3$): δ 7.79 (2H, s), 7.54 (4H, s), 7.30 (2H, s), 2.69 (4H, t, J = 7.5 Hz), 2.41 (12H, d), 1.66-1.63 (4H, m), 1.41-1.26 (20H, m), 0.91 (6H, t, J = 6.5 Hz), 0.38 (18H, s). ^{13}C NMR (125 MHz, $CDCl_3$): δ 151.79, 147.73, 135.18, 133.45, 133.34, 132.67, 131.60, 126.91, 126.09, 125.98, 125.96, 123.67, 123.39, 122.70, 32.06, 31.97, 31.79, 29.91, 29.71, 29.43, 22.84, 19.26, 19.24, 14.27, 0.59. IR (cm^{-1}): 2952, 2922, 2852, 1527, 1495, 1466, 1428, 1403, 1248, 838, 774. CI-MS (+ve): *m/z* calculated for $C_{54}H_{72}S_{10}Si_2$ 1096.2380, found 1097.1987.

Compound 181. To a solution of **193** (70 mg, 0.064 mmol) in dry CH_2Cl_2 (20 mL) was added dropwise trifluoroacetic acid (31 mg, 0.272 mmol) at 0 °C. This mixture was stirred for 1 h at 0 °C, washed with brine, and dried over magnesium sulphate. After the solvent was removed in vacuo, the crude product was purified with flash column chromatography (eluent: CH_2Cl_2/hexanes, 1/1) to give the desired product **181** (50 mg, 0.052 mmol, 82%) as a yellow viscous solid. ^{1}H NMR (500 MHz, $CDCl_3$): δ 7.77 (2H, s), 7.55 (2H, d, J = 8.0 Hz), 7.53 (2H, d, J = 8.1 Hz), 7.21 (2H, s), 6.90 (2H, s), 2.64 (4H, t, J = 7.7 Hz), 2.41 (6H, s), 2.40 (6H, s), 1.67-1.63 (4H, m), 1.37-1.25 (20H, m), 0.89 (6H, t, J = 6.8 Hz). ^{13}C NMR (125 MHz, $CDCl_3$): δ 144.66, 143.67, 135.22, 133.48, 132.83, 131.71, 126.16, 126.05, 124.89, 123.48, 123.48, 123.36, 122.64, 119.96, 32.07, 30.81, 30.62, 29.63, 29.53, 29.45, 22.84, 19.31, 19.27, 14.28. IR (cm^{-1}): 2921, 2851, 2360, 2342, 1637, 1617, 1558, 1530, 825, 667. HR-EIMS (+ve): *m/z* calculated for $C_{48}H_{56}S_{10}$ 952.1589, found 952.1589 $[M]^+$.

1,4-Diiodo-2,5-dimethylbenzene (195). The mixture of p-xylene (5166 mg, 48.658 mmol), H_5IO_6 (4500 mg, 19.742 mM), iodide (9500 mg, 37.430 mmol), water (10 mL), H_2SO_4 (3 mL) and acetic acid (92 mL) were stirred and heated to 80°C for 4 h. Water (125 mL) was added and the flask was cooled in ice water to promote the crystallization of the product. The white solid was collected and recrystallized from acetone/H_2O to give white crystals (8500 mg, 23.743 mmol). ^{1}H NMR (500 MHz, $CDCl_3$): δ 7.65 (2H, s), 2.34 (6H, s).

2,5-Diiodo-4-methylbenzoic acid (196). A (6750 mg, 18.855 mmol) and $KMnO_4$ (17750 mg, 112.320 mmol) were dissolved in the mixture of pyridine (75 mL) and water (25 mL). The mixture was refluxed for 6 h and then filtered while it was still hot. The brown MnO_2 solid was rinsed with a hot 5% KOH solution, and the filtrate was dried in vacuo. The residue was then redissolved in water, filtered, cooled, and acidified with HCl in an ice-water bath. The white solid was collected and recrystallized from acetone/H_2O to give white crystals (5300 mg, 13.662 mmol). ^{1}H NMR (500 MHz, $CDCl_3$): δ 8.31 (1H, s), 8.01 (1H, s), 2.46(3H, s).

2,5-Diiodoterephthalic acid (197). To a mixture of A (1000 mg, 2.578 mmol) in 10% KOH (50 mL) was added $KMnO_4$ (1630 mg, 10.320 mmol). This mixture was stirred and refluxed overnight. The hot mixture was filtered, and the brown soid MnO_2 was rinsed with hot 5% KOH solution. The filtrate was evaporated to its half of its original volumn in vacuo and then was acidified with 18% HCl. A light pink solid was

collected and recrystallized from acetone/H_2O to give white needle crystals (560 mg, 1.340 mmol). ^{1}H NMR (500 MHz, $CDCl_3$): δ 8.37 (2H, s).

Dimethyl 2,5-diiodoterephthalate (186). In a 100 mL round-bottomed flask, A (1840 mg, 4.402 mmol) and H_2SO_4 (1 mL) in 30 mL MeOH were stirred and refluxed overnight. After the solvent was removed in vacuo, this compound was redissolved in dichloromethane, saturated brine, and then dried over magnesium sulfate. After the solvent was removed in vacuo, this crude product was purified by flash chromatography (eluent: dichloromethane: hexane, 1:4) to afford the desired product (1420 mg, 3.184 mmol) as a white solid. ^{1}H NMR (500 MHz, $CDCl_3$): δ 8.33 (2H, s), 3.96 (6H, s).

Chapter 4

Phenylboronic Acid Functionalized TTFAQ as an Electrochemical Sensor for Saccharides

4.1 Introduction

Saccharides play significant roles in biological processes, ranging from protein targeting, cell recognition, production of metabolic energy, to disease diagnosis and management.[105,106] The development of an ideal saccharide sensor has been a long-term goal for researchers, and there have been numerous reports of saccharide sensors. Continuation of this study resides in the fact that there are many parameters to be met together, such as selectivity, linear range and response time, as well as other critical parameters; although in some cases they receive less attention in spite of their great importance. For example, reproducibility and reversibility of signal, reproducibility of sensor fabrication, biocompatibility, operational lifetimes at body temperature, and storage stability of the sensor. So far, there is still a lack of effective and reliable saccharide sensors.

A number of approaches toward the development of saccharide sensors that employ different transduction mechanisms and recognition units for saccharides have been described. Generally, the designed architecture of saccharide biosensors contains three essential components: the linkage group, the appropriate three-dimensional scaffold that provides the appropriated positioning and orientation of the relevant functional groups; readout unit; and receptor, in which proper functional groups afford strong interactions

with sacchrides in aqueous media, have been extensively explored. Boronic acid, since the discovery of its ability to rapidly and reversibly form cyclic ester with *cis* 1,2- or 1,3-diols through covalent interactions in aqueous media, have been extensively explored as saccharide receptors.[106-111] Another advantage of boronic acids as saccharide receptors lies in the possibility to achieve selectivity for a range of saccharides. Among various signal transduction mechanisms for saccharide recognition, such as circular dichroism,[112] absorption,[113] redox property,[114] and fluorescence,[115] two mechanisms have been employed most frequently to design saccharide sensors: photoinduced electron-transfer (PET)[116] and thermal or photoinduced charge-transfer mechanism.[117] Saccharide sensors based on the PET mechanism contain three components: a fluorophore, an amine (donor), and a boronic group (receptor). The interaction of a boronic acid and neighbouring amine is strengthened on saccharide binding. The strength of this boronic acid-amine interaction modulates the PET from the amine to the fluorophore. Sensors show increased fluorescence at neutral pH through suppression of the PET from nitrogen to the fluorophore on saccharide binding at neutral pH, a direct result of the stronger boron-nitrogen interaction. Intramolecular charge transfer (ICT) is another important mechanism for saccharide sensing. The wavelength or oxidation potential of sensors are sensitive to binding with different saccharides. In recent years, boronic acid based electrochemical sensors have emerged as an appealing alternative to the conventionally used enzymatic electrochemical sensors for saccharides.[118] Molecular components with excellent redox reversibility and stability, such as ferrocene[119] and polyanilines,[120] have been widely employed as readout units. In 1995, the Shinkai group[119] devised compound **198** as a saccharide sensor (Figure 4.1). Once this compound was bound to some

saccharides, redox potential change was detectable by differential pulse voltammetry (DPV). Shinkai demonstrated that compounds **198** exhibited chiral selectivity for certain linear saccharides. In 2002, the James group[120] synthesized an electrochemical saccharide sensor with two boronic acid units (receptor), one ferrocene unit (read-out unit) and a hexamethylene linker unit (D-glucose selectivity) (Figure 4.2). DPV data showed that the stability constants of diboronic acid sensor **199** with D-glucose and D-galactose were enhanced to a greater degree than its monoboronic counterpart **200**.

(+) **198** (-) **198**

Figure 4.1: Structure of compound **198**.

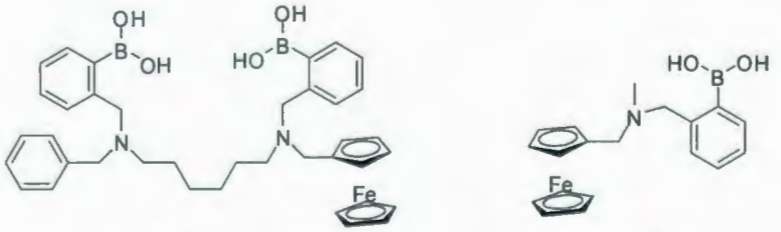

199 **200**

Figure 4.2: Structures of compounds **199-200**.

Tetrathiafulvalene (TTF) and π-extended TTF analogues (exTTFs) are well known organic electronic materials owing to their redox activities and the ability to form electrically conductive charge-transfer complexes.[121,122] In the field of molecular sensors, TTF based saccharide sensors functionalized with boronic acid groups are not well developed. Recently, the Zhu group devised a TTF-anthracence-boronic acid triad system

(Figure 4.3), in which the TTF unit was employed instead of amine as the electron-donor to modulate photoinduced electron transfer (PET). As such, fluorescence sensing function towards saccharides was attained.[61]

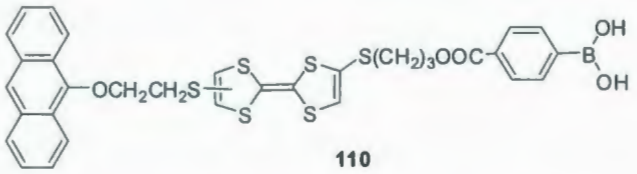

110

Figure 4.3: Structure of compound **110**.

However, boronic acid based electrochemical sensors for saccharides using TTF as the electrochemical reporter still remain unexplored. Molecular assemblies involving diphenylboronic acids and a central exTTF unit have been recently developed by the Zhao group. These compounds are intended to be prototypes for testing the viability of saccharide sensing and recognition by exTTF based sensors. The proposed mechanism for this type of electrochemical sensors is depicted in Scheme 4.1. The anthraquinodimethane-type exTTF (TTFAQ) was chosen as the electrochemical reporter, in view of its strong electron donating ability and redox activity of this type of molecules.[121] Basically, the binding of boronic acid groups with the diols of saccharides under aqueous conditions is expected to alter the oxidation potential of the central exTTF donor unit, which in turn gives rise to detectable electrochemical readouts via potentiometric or voltammoletric techniques. The incorporation of two boronic acid groups was intended to deliver a two-fold benefit: (1) to increase affinity for saccharides, and (2) to afford enhanced selectivity for particular saccharides through chelate complexation.

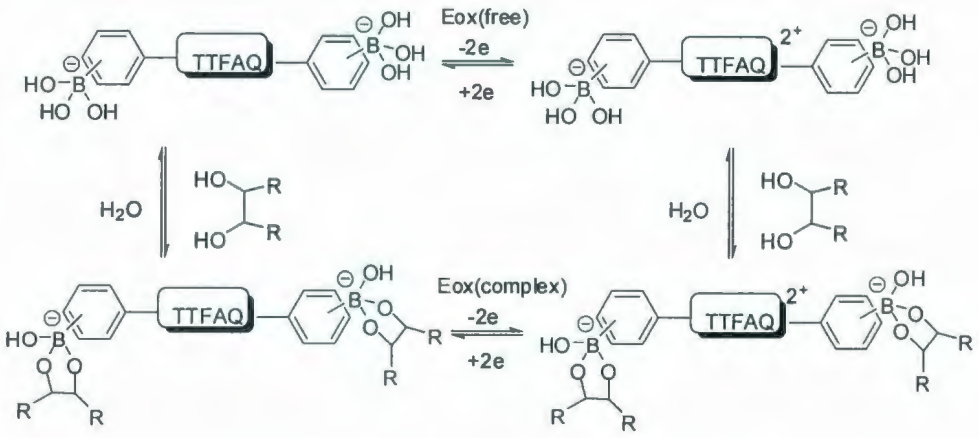

Scheme 4.1: Proposed working principle for saccharide sensing and recognition with a diboronic acid functionalized TTFAQ.

4.2 Results and disscusion

4.2.1 Synthesis

The coupling of boronic acid to TTFAQ was accomplished by using Cu-catalyzed alkyne-azide cycloaddition (CuAAC), the flagship reaction of the click chemistry developed by Sharpless and co-workers.[123-126] The click reaction has the potential to efficiently and modularly connect azides and any electrophore bearing a terminal alkyne. The detailed synthetic route is described in Scheme 4.2. A 2,6-dialkynylated TTFAQ building block **148b** was expected to react with azido-appended pinacol boronate **205**,[127] which was previously developed by the James group, under the catalysis of CuI in THF to afford diboronate ester functionalized TTFAQ **206**. Compound 2-bromotoluene **201** was converted to the boronic acid by lithiation with BuLi and boronation with $B(OMe)_3$. After boronic acid **202** was obtained, pinacol protection and bromination of this acid gave boronate ester **204**. After substitution of the bromo group with azido, a copper-catalyzed

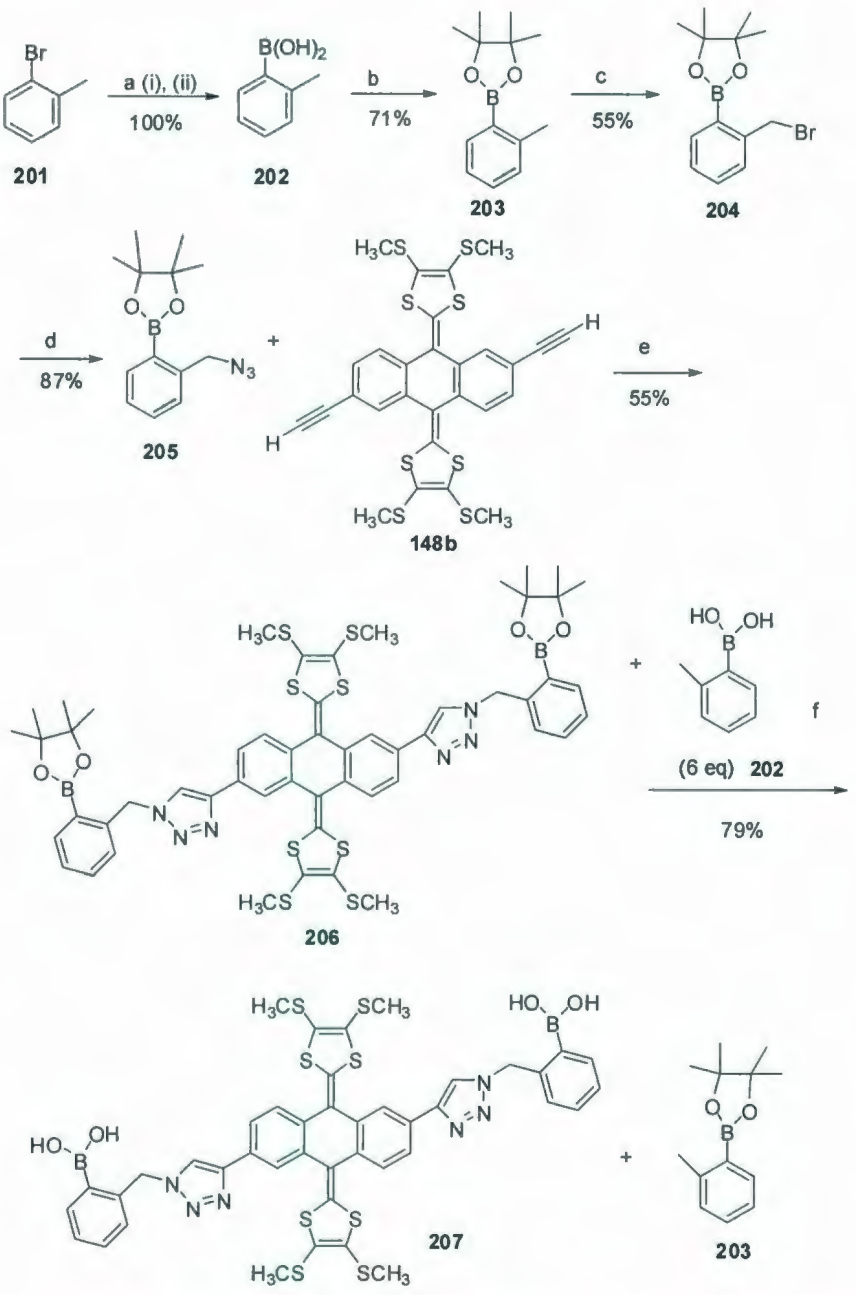

Scheme 4.2: Synthesis of **207**. Reagents and conditions: (a) (i) *n*-BuLi, THF, -78 °C, 30 min; (ii) $B(OMe)_3$, -78 °C, 30 min, rt, HCl; (b) pinacol, toluene, reflux, 2 h; (c) NBS, benzoyl peroxide, CH_3CN, 90 °C 5 h; (d) NaN_3, acetone, reflux, 24 h; (e) CuI, THF, 65 °C, 24 h; (f) dioxane, 100 °C, 24 h.

azide-alkyne cycloaddition occurred to afford pinacol ester **206**. The initial trial of the reaction at room temperature was unsuccessful, due to very slow reaction rate. Increasing the reaction temperature to 65 °C and the amount of CuI to 0.89 molar equivalent relative to **148b** greatly accelerated the reaction, giving compound **206** in 55% yield. Boronate ester **206** was then subjected to an ester exchange reaction with excess *o*-toluneboronic acid (6 equivalents) in dioxane at 100 °C to form the desired product, TTFAQ-diboronic acid **207**, in 79% yield. The byproduct pinacol *o*-toluneboronic ester was recovered as a useful precursor to starting material **202**. TTFAQ-diboronic acid **207** appears as a dark brown solid, showing good solubility only in DMSO. The structure and purity of compound **207** was verified by NMR, IR, and MS analysis.

4.2.2 Electrochemical sensing properties of phenylboronic acid functionalized TTFAQ 207 toward various saccharides

To test the sensor function of **207** towards saccharides, four different saccharide species, including glucose, fructose, ribose, and rinose, were titrated respectively into a solution of **207** in DMSO/H_2O (3:2, v/v). A buffer system (KCl 0.08 M, KH_2PO_4 0.022 M, Na_2HPO4 0.022 M) was added to the solution of **207** to keep pH at *ca.* 8.75 as well as to function as the electrolytes for voltammetric experiments. The binding of saccharide molecules to **207** was monitored by differential pulse voltammetry (DPV), and the detailed titration voltammograms are given in Figure 4.4. The reason for choosing DMSO/H_2O as the solvent system for the titration experiments is because of the insolubility of compound **207** in pure H_2O. With the assistance of DMSO as a co-solvent, compound **207** could be solubilized to form a viscous and slightly turbid solution (*ca.*

2.56 mM). The DP voltammogram of **207** (see Figure 4.4A) before titration with saccharides showed rather weak current signals, likely as a result of high viscosity and limited solubility.

In gradual addition of **207** with fructose, the solution became less viscous and more transparent, indicating much improved solubility of **207** in DMSO/H_2O upon binding with fructose. This observation is consistent with the steadily increased current intensity in DP voltammogram. There are two oxidation peaks observable in the voltammogram of **207**. The first oxidation peak (E^{ox1}) shifted from +0.36 to +0.42 V and the second oxidation peak (E^{ox2}) from +0.62 to +0.68 V during the titration of **207** with fructose from 0.5 to 100 molar equivalents. Also of note is that the first oxidation peak increased significantly, gradually becoming stronger in intensity than the second oxidation peak when the addition of fructose was greater than 8 equivalents. The substantial current responses shown in the DP voltammogram attest to the viability of using **207** as an electrochemical sensor to detect fructose.

The titration experiment of **207** with ribose gives a similar pattern of DP voltammograms (see Figure 4.4B); however, the degree of current variation in response to ribose titration appears to be less significant in comparison to the titration of fructose. This result suggests that the binding of **207** with ribose is relatively weaker than with fructose. The voltammograms of **207** upon titration with rinose and glucose under the same conditions showed no appreciable voltammetric changes (see Figure 4.4C and D), thus indicating very weak binding between compound **207** and these two saccharide species.

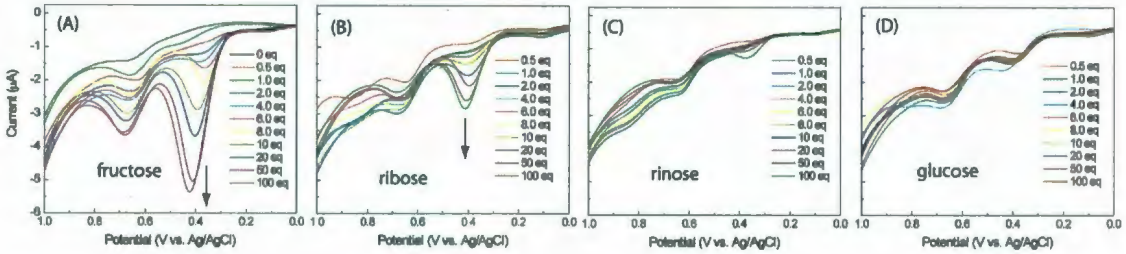

Figure 4.4 Differential pulse voltammograms of **207** (2.56 mM) obtained during titration with various saccharides at pH 8.75 in DMSO/H_2O (3:2, v/v). Electrolytes: KCl (2.08 M), KH_2PO_4 (0.022 M), Na_2HPO_4 (0.022 M); Working electrode: glassy carbon; Counter: Pt wire; Reference: Ag/Agcl; Scan rate: 20 mV/s; Pulse width: 50 mV; Step: 4 mV; Pulse period: 200 ms.

In summary, this work has demonstrated that phenylboronic acid and TTFAQ moieties can be efficiently tethered together via the CuAAC (click) protocol. TTFAQ-dibronic acid **207** was found to give different voltammetric responses to the four saccharides tested. This result substantiates the viability of developing effective saccharide sensors using TTFAQ-boronic acid as a platform.

4.3 Experimental

General procedures and methods

Chemicals and reagents were purchased from commercial suppliers and used without further purification. THF was distilled from sodium/benzophenone. Et_3N and toluene were distilled from LiH. Catalysts, $Pd(PPh_3)_4$ and $Pd(PPh_3)_2Cl_2$, were prepared from $PdCl_2$ according to standard procedures. All reactions were performed in standard, dry glassware under an inert atmosphere of N_2 unless otherwise noted. Evaporation and

concentration was done at H_2O-aspirator pressure. Flash column chromatography was carried out with silica gel 60 (230-400 mesh) from VWR International. Thin-layer chromatography (TLC) was carried out with silica gel 60 F254 covered on plastic sheets and visualized by UV light or $KMnO_4$ stain. Melting points (mp) were measured with a Fisher-Johns melting point apparatus and are uncorrected. ^1H and ^{13}C NMR spectra were measured on the Bruker AVANCE 500 MHz spectrometer. Chemical shifts are reported in ppm downfield from the signal of the internal reference $SiMe_4$. Coupling constants (*J*) are given in Hz. Infrared spectra (IR) were recorded on a Bruker Tensor 27 spectrometer. APCI mass spectra were measured on an Agilent 1100 series LCMSD spectrometer, and high-resolution MALDI-TOF mass spectra on an Applied Biosystems Voyager instrument with dithranol as the matrix.

***o*-Tolylboronic acid (202).** *n*-BuLi (10.32 mL, 2.5 M, 25.800 mmol) was added dropwise to a solution of **201** (4400 mg, 25.726 mmol) in THF (60 mL) at -78 °C, resulting in a white suspension. The reaction mixture was stirred for 30 min at -78 °C, then $B(OMe)_3$ (6701 mg, 64.489 mmol) was added. The resulting mixture was stirred at -78 °C for a further 30 min and then allowed to warm up to rt. The reaction mixture was acidified with 10% aq. HCl solution and extracted with Et_2O. The organic layer was then dried over magnesium sulfate and concentrated under vacuum to afford an off-white crystalline solid **202** (3560 mg, 26.184 mmol, 100%) that was used without further purification.

4,4,5,5-Tetramethyl-2-*o*-tolyl-1,3,2-dioxaborolane (203). In a 250 mL round-bottomed flask, **202** (3560 mg, 26.184 mmol) and pinacol (3720 mg, 31.477 mmol) were dissolved in 150 mL of toluene. The mixture was refluxed for 2 h under Dean-Stark conditions. The mixture was allowed to cool to rt and the solvent was removed in vacuo. The residue was dissolved in CH_2Cl_2 again, washed by brine, and dried by magnesium sulfate. After the solvent was removed in vacuo, the desired product **203** (4060 mg, 18.624 mmol, 71%) was obtained as a colourless oil. ^{1}H NMR (500 MHz, $CDCl_3$): δ 7.77 (1H, d, J = 7.0 Hz), 7.31 (1H, t, J = 7.0 Hz), 7.17 (2H, d, J = 7.0 Hz), 2.54 (3H, s), 1.35 (12H, s).

2-(2-(Bromomethyl)phenyl)-4,4,5,5-tetramethyl-1,3,2-dioxaborolane (204). In a 250 mL round-bottomed flask, compound **203** (4060 mg, 18.624 mmol), NBS (4970 mg, 27.893 mmol), and benzoyl peroxide (50 mg, 0.206 mmol) were heated at 90 °C in MeCN for 5 h. After cooled to rt, the solvent was removed in vacuo. The residue was redissolved in CH_2Cl_2, washed by brine, and dried over magnesium sulfate. After the solvent was removed in vacuo, the crude product was purified over flash column chromatography (eluent: CH_2Cl_2/hexanes, 1/9) to give the desired product **204** (3020 mg, 10.203 mmol, 55%) as a white solid. ^{1}H NMR (500 MHz, $CDCl_3$): δ 7.82 (1H, d, J = 7.5 Hz), 7.41-7.39 (2H, m), 7.28-7.27 (1H, m), 4.92 (2H, s), 1.37 (12H, s).

2-(2-(Azidomethyl)phenyl)-4,4,5,5-tetramethyl-1,3,2-dioxaborolane (205). Compound **204** (1040 mg, 3.502 mmol) and sodium azide (270 mg, 4.153 mmol) were dissolved in 100 mL of acetone and refluxed for 24 h. After the solvent was removed in vacuo, the residue was redissolved in CH_2Cl_2, washed with brine, and dried over

magnesium sulfate. After the solvent was removed in vacuo, the desired product **205** (790 mg, 3.049 mmol, 87%) was used in the next step without further purification. ^{1}H NMR (500 MHz, $CDCl_3$): δ 7.89 (1H, d, J = 7.5 Hz), 7.46 (1H, t, J = 7.5 Hz), 7.35-7.32 (2H, m), 4.66 (2H, s), 1.36 (12H, s).

Compound (206). In a 100 mL round-bottomed flask, compound **205** (230 mg, 0.888 mmol), **148b** (180 mg, 0.294 mmol), and CuI (50 mg, 0.263 mmol) were heated to 65 °C in 60 mL of THF for 24 h. After cooled to rt, the solvent was removed in vacuo. The residue was redissolved in CH_2Cl_2, washed by brine, and dried over magnesium sulfate. After the solvent was removed in vacuo, the crude product was purified with flash column chromatography (eluent: ethyl acetate/hexanes, 2/8) to give the desired product **206** (180 mg, 0.159 mmol, 55%) as an orange solid. ^{1}H NMR (500 MHz, $CDCl_3$): δ 7.92 (2H, d, J = 8.3 Hz), 7.81 (2H, s, triazole-H), 7.76 (2H, dd, J = 8.0Hz, 1.60 Hz,), 7.57 (2H, d, J = 8.3 Hz), 7.45 (2H, t, J = 7.7 Hz), 7.36 (2H, t, J = 7.1 Hz), 7.29 (2H, d, J = 7.7 Hz), 5.92 (4H, s, CH_2), 2.38 (6H, s, SCH_3), 2.34 (6H, s, SCH_3), 1.39 (24H, s, pinacol ester CH_3). ^{13}C NMR (125 MHz, $CDCl_3$): δ140.9, 136.7, 135.0, 134.1, 131.9, 131.6, 129.3, 129.0, 127.9, 126.5, 125.9, 125.4, 123.5, 123.3, 122.5, 120.0 (two sp^2 carbon signals not observed due to coincidental overlap), 84.3, 53.5, 25.0, 19.2, 19.1. IR (cm^{-1}): 2976, 2921, 1601, 1532, 1495, 1454, 1382, 1348, 1143, 1069, 1045. HR-MALDI-TOF MS (dithranol): *m/z* calted for $C_{54}H_{56}B_2N_6O_4S_8$ 1130.2315, found 1130.2339. Mp: 138-140 °C.

Compound 207. In a 100 mL round-bottomed flask, compound **206** (270 mg, 0.239 mmol), **202** (200 mg, 1.471 mmol) were heated to 100 °C in a mixture of dioxane (12

mL) and HCl (4 mL, 5 M) for 24 h. After cooled to rt, the solvent was removed in vacuo. The residue was washed by pure ethyl acetate, acetonitrile and then diethyl ether. The product **207** was obtained as a brown solid (180 mg, 0.186 mmol, 79%). ^{1}H NMR (500 MHz, $CDCl_3$): δ 8.59 (2H, s), 8.05 (2H, s), 7.83 (2H, d, J = 9.6 Hz), 7.66 (2H, d, J = 6.4 Hz), 7.63 (2H, d, J = 8.3 Hz), 7.37 (2H, t, J = 7.4 Hz), 7.31 (2H, t, J = 7.1 Hz), 7.11 (2H, d, J = 7.7 Hz), 5.87 (4H, s, CH_2), 2.42 (6H, s, SCH_3), 2.37 (6H, s, SCH_3) ($B(OH)_2$ signal not observed due to rapid proton exchange) ^{13}C NMR (125 MHz, $CDCl_3$): δ 146.42, 140.21, 135.21, 135.15, 129.93, 128.68, 128.55, 128.01, 127.81, 126.58, 126.53, 124.47, 124.34, 123.96, 122.73, 122.69, 122.44, 122.19, 53.61, 19.77, 19.66. IR (cm^{-1}): 3386, 2919, 1599, 1530, 1492, 1444, 1366, 1075, 762, 706. HR-MALDI-TOF MS (dithranol): *m/z* calculated for $C_{42}H_{36}B_2N_6O_4S_8$ 966.0750, found 966.0751. Mp: 230-232 °C.

Chapter 5

Design of TTFAQ-based Electrochemical Sensors for Transition Metal Ions

5.1 Introduction

The swift and efficient detection of toxic metal cations, such as Cu^{2+}, Ag^{+}, Hg^{2+}, Pb^{2+}, Zn^{2+}, *etc.*, in analytical and environmental fields is a challenging task and has attracted considerable attention. A molecular system containing a signal reporter and a host unit capable of cation, anion, and neutral molecules binding can be employed as a chemical sensor. Many reports[128-134] concerning electrochemical sensing and recognition of specific guests have employed ferrocene, TTF and other metallocenes as redox-active moieties, while TTFAQs as electrochemical reporters in this type of sensors have been less studied, although TTFAQs possess strong electron-donating ability and very rich redox and electronic characteristics.

Generally, sensing for a specific guest can be achieved by carefully designing the host unit and the signal report unit. According to the published literatures,[128-131] organic functional groups containing heteroatoms such as amino and carboxyl groups can strongly interact with transition metal cations. In the resulting Lewis acid-base complexes, the electronic nature of the organic groups (ligands) are usually considerably altered. Upon this consideration, we studied two new TTFAQ-cored D/A ensembles (**208** and **209** in figure 5.1), in which the terminal functionalities are either amino or carboxylic ester groups. These two TTFAQ derivatives not only add new members to the TTFAQ-

cored D/A triad family as described in previous chapters, but may serve useful redox-active ligands for detection of transition metal ions.

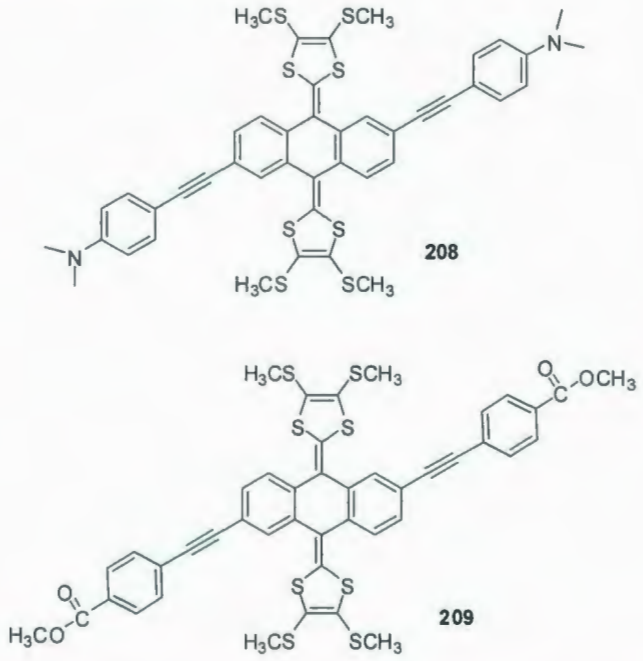

Figure 5.1: TTFAQ-cored D/A ensembles **208** and **209.**

In 2007, the Song group proposed a molecular structure as electrochemical sensors for toxic metal ions. In their design, ferrocene was employed as the signal reporter and thiourea group as the host unit. The electrochemical properties were measured in acetonitrile. The addition of Ni^{2+}, Cu^{2+}, Hg^{2+}, Pb^{2+} and Co^{2+} to the solutions of compounds **210** and **213**[128] led to significant positive shifts of the redox potential of Fc/Fc^{+}. All these complexes displayed quasi-reversible patterns. However, only in the presence of Ni^{2+}, Cu^{2+} and Hg^{2+}, large anodic shifts were observed ($\Delta E > 100$ mV), indicating good selectivity for these cations.

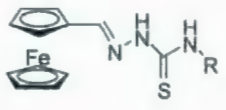

210 R = p-$CH_3OC_6H_4$
211 R = m-$CH_3OC_6H_4$
212 R = $CH_3OC_6H_4$
213 R = 1-naphthalene

Figure 5.2: Ferrocenylthiosemicarbazone metal cation sensor **210-213**.

In 2000, the Fu group employed ferrocene unit as redox-active center and dioxopolyamines as receptor unit to prepare chemosensors for cations. A series of novel ferrocene macrocyclic dioxopolyamines **214-217**[129] were synthesized, and their coordination behaviour with some cations and electrochemical properties of these complexes were systematically studied by CV and UV-Vis analyses. Coordination of compounds **214-217** with Ni^{2+}, Cu^{2+} and Co^{2+} ions were confirmed by IR, UV-Vis spectra, and fast atom bombardment mass spectrometry (FAB-MS). Their IR spectra showed changes in stretching vibrations of both C=O (i.e. from ca. 1660 to ca.1600 cm^{-1}) and N-H (disappeared in the complexes) in amide. FAB MS also showed the molecular ion peaks of the metal complexes MH_2L. The increase in absorbance at λ_{max} of complexes can be clearly seen by addition of metal ions to the solutions of the ligands. In CV, the coordination of the ligands with transition metal ions (Cu^{2+}, Ni^{2+} and Co^{2+}) causes the redox peak potential of Fc/Fc^+ to more anodic positions.

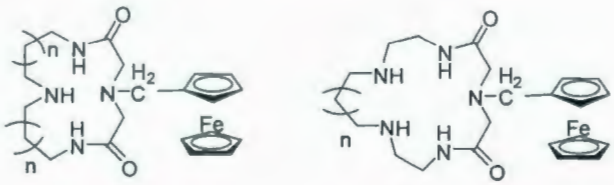

214 n = 0
215 n = 1

216 n = 0
217 n = 1

Figure 5.3: Ferrocene macrocyclic dioxopolyamines **214-217**.

Other than ferrocene moiety, TTF is also a widely used electroactive building unit. In Jørgensen's review,[52] a set of planar TTF derivatives **218-224** was employed as redox-active units in cation sensors. The CV showed two oxidation peaks in their acetonitrile solution. With the addition of metal ions, such as Li^+, Na^+, K^+, and Ag^+, up to 250 equivalents to their solution, various anodic shifts of their first oxidation potentials were observed, while the second potentials remained unchanged due to the expulsion of the cation after the first oxidation. Compound **221** seems to have the highest affinity (+80 mV) for Na^+, while compound **222** gives the highest selectivity (+60 mV) for K^+. The largest positive shift (+170 mV) for **223** was observed when Ag^+ was added. Compound **224** also has high sensitivity (+90 mV) to Ag^+.

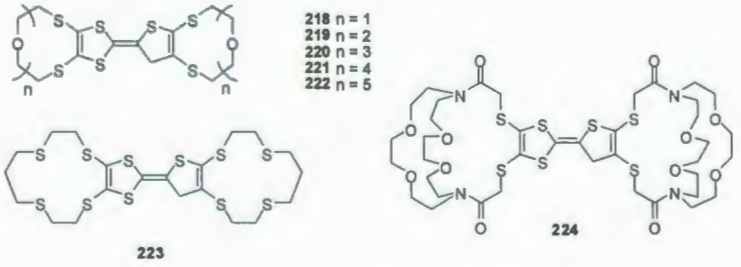

Figure 5.4: Planar TTFs **218-224** as electrochemical sensors.

Based on previous reports on the electrochemical sensors for cations, two compounds **208** and **209** in Figure 5.1 were designed and synthesized in this project, and their properties were investigated by CV and UV-Vis methods.

5.2 Results and discussion

5.2.1 Synthesis

The synthesis of triad **208** started from a cheap and efficient method[135] for selective para-iodination of aniline **225** (Scheme 5.1). This method overcomes the shortcomings of previous routes,[136] avoiding harsh, costly, environmentally hazardous reaction conditions (such as heavy metal, strong oxidants, or strong acid or base conditions). In this reaction, besides the aromatic amine, the only reagent used is molecular iodine dissolved in a mixture of pyridine/dioxane (1:1). The reaction temperature was 0 °C. After this precursor was made, cross-coupling with **148b** through Sonogashira coupling was performed. The Sonogashira reaction did not work under general reaction conditions, THF/Et_3N (v/v, 1:1). After modifying the solvent system (using piperidine solvent instead of THF/ Et_3N), this reaction was improved with a satisfactory yield of 55%.

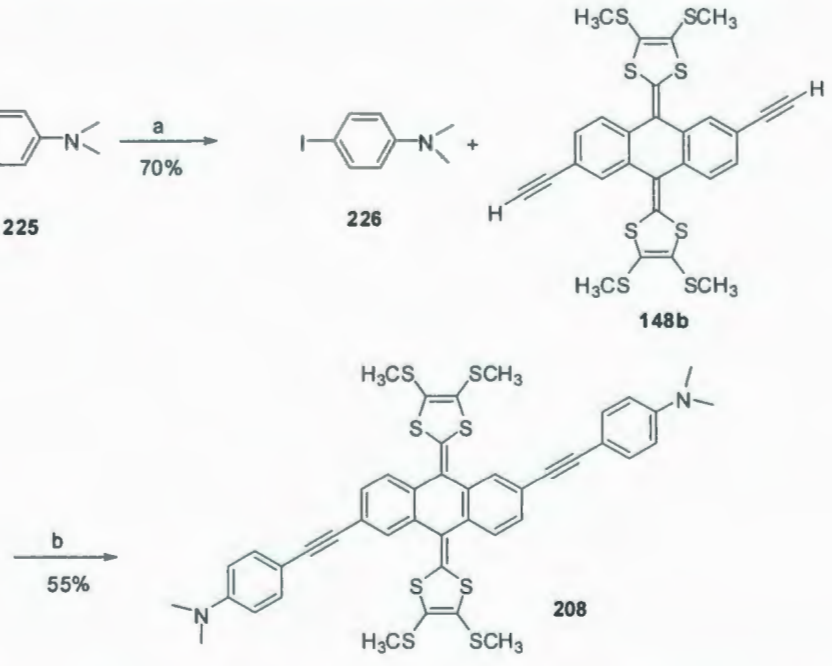

Scheme 5.1: Synthesis of **208**. Reagents and conditions: (a) I_2, pyridine/dioxane (1:1), 0 °C for 1 h, then rt for 1 h; (b) $Pd(PPh_3)_4$, CuI, piperidine, -78 °C to rt, overnight.

The synthesis of triad **209** began with iodination of compound **227** (Scheme 5.2) via a Sandmeyer-type reaction. The next step was Fisher esterification of acid **228** in the presence of MeOH and several drops of sulfuric acid as catalyst. For the Sonogashira reaction between **148b** and **229**, solvent system was pure Et_3N instead of THF/ Et_3N, the yield was moderate, 33%.

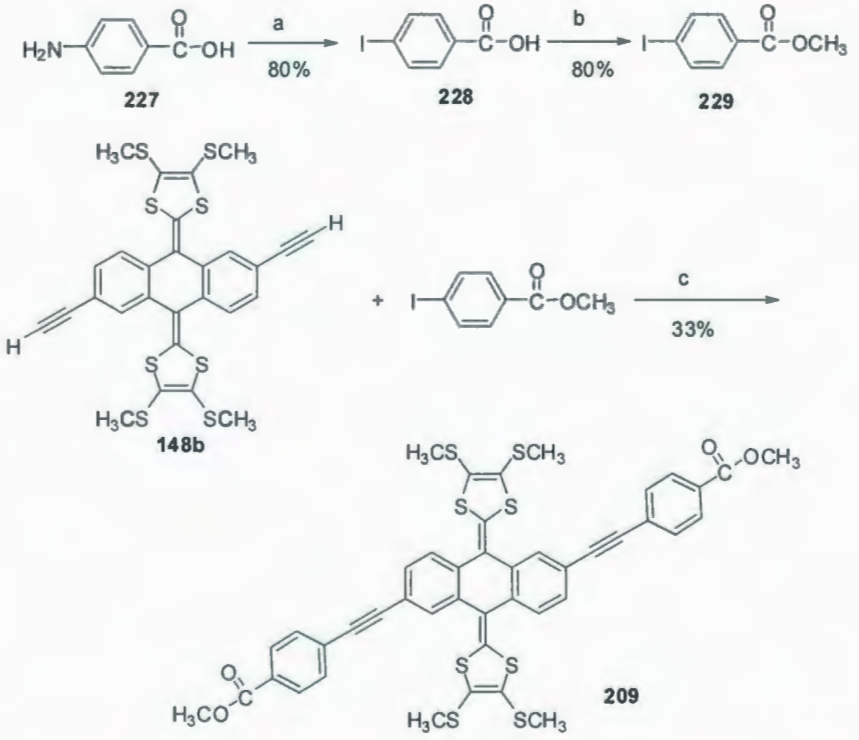

Scheme 5.2: Synthesis of **209**. Reagents and conditions: (a) (i) H_2SO_4, KNO_2, 0 °C, 5 h; (ii) KI, 0 °C to rt, overnight; (b) CH_3OH, reflux, overnight; (c) $Pd(PPh_3)_4$, CuI, Et_3N, -78 °C to rt, overnight.

5.2.2 Electronic and electrochemical properties of 208 and 209

The electronic properties of the two TTFAQ derivatives (**208** and **209**) were investigated by UV-Vis absorption spectroscopy. Figure 5.5 shows the absorption spectra of **208** and **209** measured in $CHCl_3$, and detailed spectral data are summarized in Table 5.1.

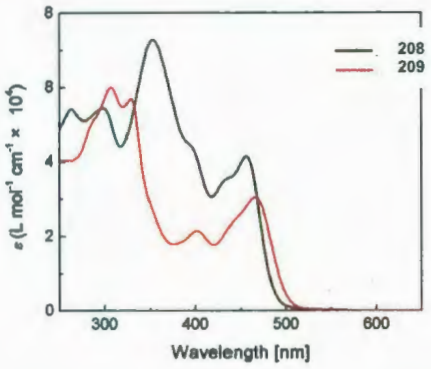

Figure 5.5: UV-Vis absorption spectra of compounds **208** and **209** measured in $CHCl_3$ at room temperature.

Table 5.1: UV-Vis spectroscopic and electrochemical data of **208** and **209**.

Entry	λ_{max} (nm)	ε (L mol^{-1} cm^{-1})	E_{pa} (V)	E_{pc} (V)
208	453	4.1×10^4	+0.56	–
	391 (sh)	4.5×10^4	+0.92	
	350	7.2×10^4		
	295	5.4×10^4		
	259	5.3×10^4		
209	460	2.9×10^4	+0.61	+0.47
	396	2.1×10^4		
	325	5.6×10^4		
	305	6.0×10^4		

305	6.0×10^4

From UV-Vis spectral analysis, the lowest-energy absorption band of compound **208** is blueshifted by 7 nm relative to that of **209**. This observation indicates a narrower HOMO-LUMO gap in **209** as a result of the electron push-pull effect. Furthermore, the amino (donor) attached TTFAQ **208** shows molar extinction coefficients that are considerably greater than those of carboxylic ester (acceptor) endcapped TTFAQ **209**. To further probe the D/A-substituent effects on the electronic spectroscopic behavior, the UV-Vis data of **208** and **209** were compared with analogous substituted TTFAQs **138-139, 150,** and **158-159** (Figure 5.6).

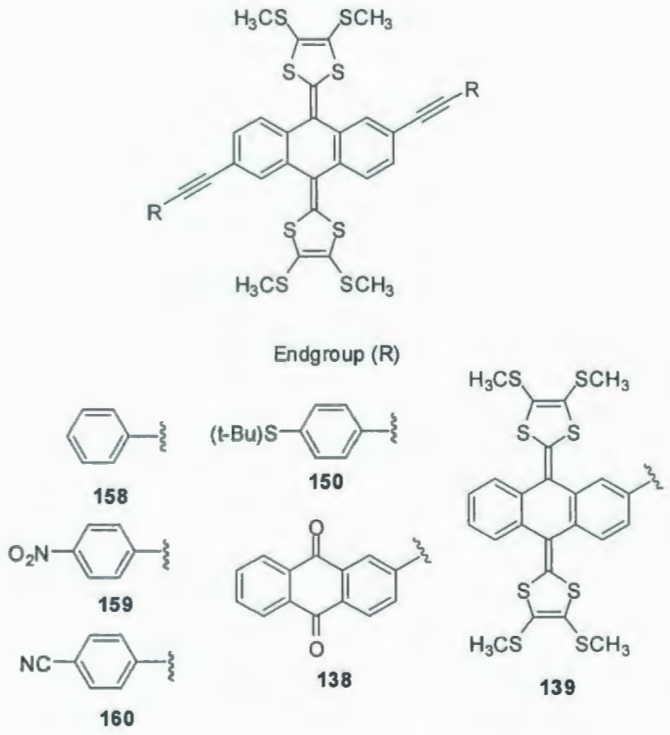

Figure 5.6: TTFAQ-cored D/A ensembles **138-139, 150,** and **158-160**.

Table 5.2. Substituent effects on the UV-Vis absorption behavior of **208** and **209**.

Entry	Subsitituent	λ_{max} (nm)	ε (L mol^{-1} cm^{-1})	$\Delta\lambda_{max}$ (nm)	σ_{para}
158	H	458	2.7×10^4	0	0
159	NO_2	470	2.2×10^4	+12	+0.81
160	CN	470	1.9×10^4	+12	+0.70
150	S(t-Bu)	461	2.6×10^4	+3	–
208	NMe_2	453	4.1×10^4	-5	-0.83
209	$COOCH_3$	460	2.9×10^4	+2	+0.45

From Table 5.2, a clear trend can be established that the lowest-energy absorption peak (λ_{max}) that corresponds to HOMO to LUMO transition energy is redshifted as the substituent increases with acceptor strength. Conversely, the electron-donating substituent causes a blueshift of the λ_{max} value in comparison to the unsubstituted TTFAQ **158**. Of note is that the λ_{max} of **150** is noticeably redshifted by 3 nm relative to **158**. This result indicates that the S(*t*-Bu) group in **150** should be deemed as weakly electron-withdrawing as a result of its inductive effect which prevails over the resonance (electron-donating) effect.

stark contrast to other TTFAQ analogues, wherein oxidation of the TTFAQ moiety usually gives rise to a quasi-reversible redox wave pair. A possible explanation for the irreversibility could be that swift chemical reaction(s) took place after the oxidation of the amino groups.

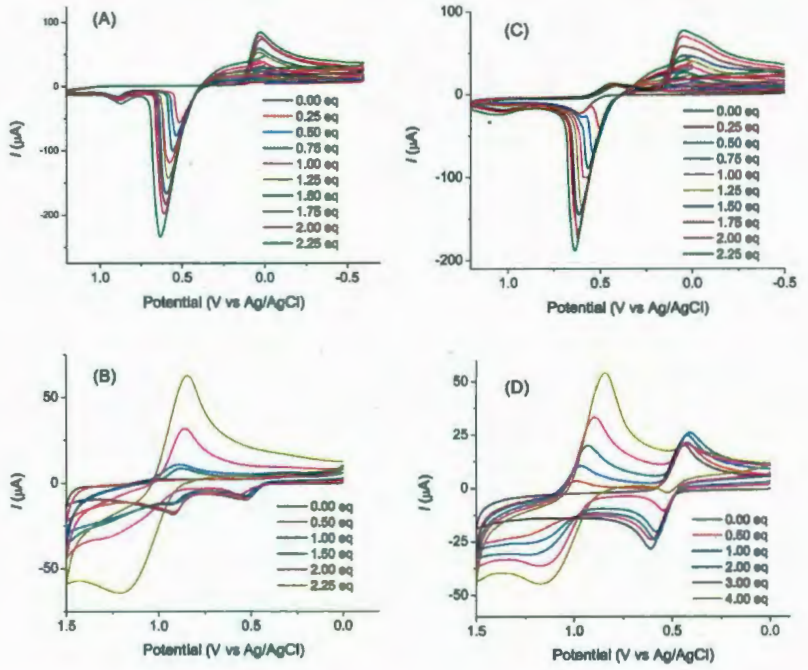

Figure 5.7: Cyclic voltammetric titrations of TTFAQ triads **208** and **209** with AgOTf and $Cu(OTf)_2$. (A) **208** (1.0 μM) and AgOTf; (B) **208** (1.0 μM) and $Cu(OTf)_2$; (C) **209** (1.0 μM) and AgOTf; (D) **209** (1.0 μM) and $Cu(OTf)_2$; (. Electrolyte: Bu_4NBF_4 (0.1 M); solvent: CH_2Cl_2/CH_3CN (4:1); working electrode: glassy carbon; counter electrode: Pt; reference electrode: Ag/AgCl.

In the cyclic voltammogram of **209**, a quasi-reversible wave pair is discernible at E_{pa} = +0.61 and E_{pc} = +0.47 V respectively, which is characteristic of TTFAQ. The anodic potential is higher than that of **208**, which testifies to the electron-withdrawing effect of the carboxylic ester groups.

solvent: CH_2Cl_2/CH_3CN (4:1); working electrode: glassy carbon; counter electrode: Pt; reference electrode: Ag/AgCl.

In the cyclic voltammogram of **209**, a quasi-reversible wave pair is discernible at E_{pa} = +0.61 and E_{pc} = +0.47 V respectively, which is characteristic of TTFAQ. The anodic potential is higher than that of **208**, which testifies to the electron-withdrawing effect of the carboxylic ester groups.

Conceivably, the amino groups and carboxyl groups of **208** and **209** could function as ligands to coordinate with transition metal ions. If such complexation occurs, the electronic nature of the substituent should be considerably altered. In principle, the resulting complexes should show more electron-deficient TTFAQ core in comparison to their neutral states, hence exhibiting anodically shifted oxidation potentials. In the experiments, aliquots of AgOTf or $Cu(OTf)_2$ were titrated to the solution of TTFAQ derivatives **208** and **209**. The titration processes were monitored by cyclic voltammetry.

Surprisingly, the results (shown in Figure 5.7) appear to be more complex than our expectation. The addition of Cu^{2+} to **208** and **209** showed interesting electrochemical properties. The increasing addition of Cu^{2+} to **208** considerably reduced the current intensity of the second anodic peak. The second anodic peak is likely due to oxidation of the amino group. The result indicates that the amino groups are the active binding sites for complexation with Cu^{2+} cation. The addition of Cu^{2+} to **209** also reduced appreciably the current intensity of the anodic peak of central TTFAQ core. This result suggests that **209** coordinates with Cu^{2+} cation to form complexes, leading to significant changes of the redox behavior of central TTFAQ core in **209**. Besides, with increasing addition, the

anodic peak of Cu^{2+} (1.16 V) moved apparently towards the anodic peaks of central TTFAQ core (+0.74 V of **208** and +0.61 V of **209**). The reasons causing this phenomenon are currently unclear.

The addition of Ag^{+} to **208** and **209** did not cause any significant changes of the redox features of the TTFAQ core, which just slightly shifted positively. However, the anodic peak at +0.58 V due to Ag^{+} showed apparent anodic shift with increasing addition, moving towards the redox potential of the central TTFAQ.

In conclusion, two new D/A-substituted TTFAQ derivatives **208** and **209** were prepared and added to the family of TTFAQ-cored D/A triads. Availability of these compounds has allowed for a systematic examination of the D/A substitution effects on the electronic spectroscopic properties of TTFAQ through acetylenic conjugation. As a general trend, electron-withdrawing substitution tends to cause a redshift of electronic absorption, whereas electron-donating group leads to a blueshift. The electrochemical properties of TTFAQ derivatives **208** and **209** were investigated, the potential of using **208** and **209** as redox active ligands to recognize transition metal ions were surveyed. The decrease of current intensity of **208** and **209** with the increasing addition of Cu^{2+} demonstrates that **208** and **209** have good selectivity to Cu^{2+} cation, indicating that these two compounds probably can be employed as electrochemical sensors for Cu^{2+}. In order to substantiate the viability of these two compounds as electrochemical sensors for transition metals, more titrations of **208** and **209** with other transition metal cations, such as Pb^{2+}, Cd^{2+}, Hg^{2+}, Zn^{2+}, etc, are worthwhile to undertake in the future work.

5.3 Experimental

General procedures and methods

Chemicals and reagents were purchased from commercial suppliers and used without further purification. THF was distilled from sodium/benzophenone. Et_3N and toluene were distilled from LiH. Catalysts, Pd $(PPh_3)_4$ and Pd $(PPh_3)_2Cl_2$, were prepared from $PdCl_2$ according to standard procedures. All reactions were performed in standard, dry glassware under an inert atmosphere of N_2 unless otherwise noted. Evaporation and concentration was done at H_2O-aspirator pressure. Flash column chromatography was carried out through silica gel 60 (230-400 mesh) from VWR international. Thin-layer chromatography (TLC) was carried out on silica gel 60 F254 covered plastic sheets and visualized by UV light or $KMnO_4$ stain. Melting points (mp) were measured with a Fisher-Johns melting point apparatus and are uncorrected. ^1H and ^{13}C NMR spectra were measured on the Bruker AVANCE 500 MHz spectrometer. Chemical shifts are reported in ppm downfield from the signal of the internal reference $SiMe_4$. Coupling constants (*J*) are given in Hz. Infrared spectra (IR) were recorded on a Bruker Tensor 27 spectrometer. UV-vis spectra were recorded on an Agilent 8453 UV-Vis or a Cary 6000i UV-Vis-NIR spectrophotometer. Fluorescence spectra were measured in $CHCl_3$ at ambient temperature using a Quantamaster 10000 fluorometer. APCI mass spectra were measured on an Agilent 1100 series LCMSD spectrometer, and high-resolution MALDI-TOF mass spectra on an Applied Biosystems Voyager instrument with dithranol as the matrix.

4-Iodo-*N*,*N*-dimethylaniline (226). In a 100 mL round-bottomed flask, **225** (500 mg, 4.126 mmol) was added in 30 mL of pyridine/dioxane (1:1) at 0 °C. Iodine (3140 mg, 12.371 mmol) was added in one portion. After 1 h, the ice bath was removed and the

reaction was further stirred for 1 h at rt. 10% Na_2SO_3 solution was added to this mixture to destroy excess I_2 until the brown color disappeared. After the solvent was removed in vacuo, the residue was redissovled in dichloromethane, washed by brine, and dried over magnesium sulfate. After the solvent was removed in vacuo, the crude compound was purified by flash column chromatography (eluent: dichloromethane/hexanes, 2/8) to give the desired product **226** as a white powder (720 mg, 2.914 mmol, 70%). ^{1}H NMR (500 MHz, $CDCl_3$): δ 7.48 (2H, d, J = 8.9 Hz), 6.51(2H, d, J = 8.9 Hz), 2.92 (6H, s).

4,4'-(9,10-Bis(4,5-bis(methylthio)-1,3-dithiol-2-ylideene)-9,10-dihydroanthracene-2,6-diyl)bis(ethyne-2,1-diyl)bis(*N*,*N*-dimethylaniline) (208). In a 100 mL round-bottomed flask, **148b** (120 mg, 0.196 mmol), **226** (240 mg, 0.971 mmol), Pd $(PPh_3)_4$ (30 mg, 0.026 mmol) and CuI (20 mg, 0.105 mmol) were added in 30 mL of piperidine. After complete degassing with freeze-pump-thaw cycles, this solution was allowed to warm up to rt and stirred overnight. After the solvent was removed in vacuo, the compound was redissovled in dichloromethane, washed by 1 M HCl, brine, and dried over magnesium sulfate. After the solvent was removed in vacuo, the crude compound was purified by flash column chromatography (eluent: dichloromethane/hexanes, 1/1) to give the desired product **208** (90 mg, 0.106 mmol, 55%) as an orange powder. ^{1}H NMR (500 MHz, $CDCl_3$): δ 7.64 (4H, s), 7.51 (2H, d, J = 7.9 Hz), 7.46-7.41 (6H, m), 6.69 (4H, d, J = 7.9 Hz), 3.00 (12H, s), 2.41 (12H, s);. ^{13}C NMR ($CDCl_3$): δ 150.23, 150.15, 132.88, 132.69, 132.38, 132.27, 129.65, 129.51, 128.50, 126.45, 125.91, 112.31, 111.96, 111.75, 111.20, 77.35, 76.96, 40.23, 19.31, 18.94. IR (cm^{-1}): 2917, 2852, 2197, 1730, 1609, 1593, 1524, 1492, 1366, 1227, 1197, 1139, 834, 810. HR-MOLDI-TOF MS: *m/z* calculated for $C_{44}H_{38}N_2S_8$ 850.0801, found 850.0869. Mp: 250-252 °C.

4-Iodobenzoic acid (228). In a 250 mL round-bottomed flask, **227** (1000 mg, 7.292 mmol) was dissolved in 20 mL of concentrated H_2SO_4. The solid $NaNO_2$ (2000 mg, 28.986 mmol) was added in a very small amount at 0 °C to this flask. After the mixture was stirred for 5 h at 0 °C, a small amount of ice was added to this mixture, and then KI (9680 mg, 58.313 mmol) dissolved in 10 mL of H_2O was added dropwisely to this mixture. The mixture was stirred at rt overnight. 10% Na_2SO_3 solution was added to this mixture to destroy excess I_2 until the brown color disappeared. The resulting solid was extracted by EtOAc. The combined organic layers were washed by brine, and dried with magnesium sulfate. Finally, the solvent was removed in vacuo. The compound was separated via flash column chromatograghy (eluent: EtOAc/hexanes, 1/4) to afford the desired product **228** as an orange solid (1450 mg, 5.846 mmol, 80%). ^{1}H NMR (500 MHz, $CDCl_3$): δ 7.94 (2H, d, J = 8.4 Hz), 7.81(2H, d, J = 8.4 Hz).

Methyl 4-iodobenzoate (229). In a 100 mL round-bottomed flask, **228** (440 mg, 1.774 mmol) and several drops of H_2SO_4 were added in 30 mL of methanol. This solution was refluxed overnight. After the solvent was removed in vacuo, the residue was redissolved in EtOAc. The solution was washed with brine, and dried with magnesium sulfate. After the solvent was removed in vacuo, the crude product was purified with flash column chromatography (eluent: EtOAc/hexanes, 1/1) as a white solid (370 mg, 1.412 mmol, 80%). ^{1}H NMR (500 MHz, $CDCl_3$): δ 7.81(2H, d, J = 8.4 Hz), 7.75 (2H, d, J = 8.4 Hz), 3.91 (3H, s).

Dimethyl 4,4'-(9,10-bis(4,5-bis(methylthio)-1,3-dithiol-2-ylideene)-9,10-dihydroanthracene-2,6-diyl)bis(ethyne-2,1-diyl)dibenzoate (209). In a 100 mL round-bottomed flask, **148b** (90 mg, 0.147 mmol), **229** (120 mg, 0.458 mmol), $Pd(PPh_3)_4$ (30 mg, 0.026 mmol) and CuI (20 mg, 0.105 mmol) were dissolved in 20 mL of dry Et_3N. After complete degassing with freeze-pump-thaw cycles, this solution was allowed to warm up to rt and be stirred overnight. After the solvent was removed in vacuo, this compound was redissovled in EtOAc, washed by 1 M HCl, brine, and dried over magnesium sulfate. After the solvent was removed in vacuo, the crude compound was purified by flash column chromatography (eluent: EtOAc/hexanes, 1/1) to give the desired product **209** as an orange powder (43 mg, 0.049 mmol, 33%). ^1H NMR (500 MHz, $CDCl_3$): δ 8.04 (4H, d, J = 8.4 Hz), 7.69 (2H, d, J = 1.3 Hz), 7.63 (4H, d, J = 8.4 Hz), 7.55 (2H, d, J = 8.4 Hz), 7.48 (2H, dd, J = 8.0, 1.5 Hz), 3.94 (6H, s), 2.42 (12H, s). ^{13}C NMR ($CDCl_3$): δ 166.93, 135.15, 135.02, 133.93, 132.01, 129.95, 128.28, 127.13, 126.22, 125.93, 122.54, 121.09, 92.74, 89.86, 52.65, 19.82. IR (cm^{-1}): 2948, 2920, 2205, 1723, 1604, 1526, 1491, 1461, 1433, 1402, 1275, 1172, 1106, 768. HR-MALDI-TOF MS: *m/z* calculated for $C_{44}H_{32}O_4S_8$ 880.0066, found 880.0057. Mp: 135-136 °C.

Chapter 6

Crown Ether-Annulated TTFAQ as a Fluorescent Sensor

6.1 Introduction

In the previous chapters, electrochemical sensors for different guests employed TTFs and TTFAQs as signal reporters have been explored. In all these cases, TTFs or TTFAQs played a dominating role as critical components in these molecular systems. It was reported respectively by Becher and Jørgensen that macrocycles incorporating the TTF unit into crown ethers showed well electrochemical recognition of various metal cations.[52, 54] While in this project, TTFAQ acted as an auxiliary moiety in the designed molecular system, not as a signal reporter anymore.

Among various signal transduction mechanisms, two mechanisms have frequently been employed to design effective cation sensors: photoinduced electron-transfer mechanism (PET) and internal charge-transfer mechanism (ICT). One of the most useful report-unit for optical readouts is fluorescence. Fluorescence spectroscopy is more sensitive than absorbance spectroscopy in general. Typical fluorescent PET sensors are composed of three major components: a fluorophore, an electron-donating group and a receptor. In 1977, the Sousa group synthesized molecules **230** and **231** containing a naphthalene (fluorophore), a crown ether (receptor) and electron-donating groups methylene (Figure 6.1).[137] These compounds were observed to show the fluorescence changes upon the binding of alkali metal ions. Since then, numerous reports[138-141] relating

to this type of fluorescent sensors have emerged. Generally, in these studies, crown, azacrown ethers or cryptands were employed as receptors. The electro-donating groups are mostly nitrogeneous groups since nitrogen atom has a lone pair of electrons. Fluorescence of the excited aromatic compounds was quenched by intramolecular electron donor groups, such as amine. After addition of metal ions, the amine is bound to the metal cations and unable to donate its lone-pair electrons to quench the exited state of the fluorophores. As such, then fluorescence of the fluorophore is retained. This has been a widely accepted mechanism for the design of fluorescence chemosensors.

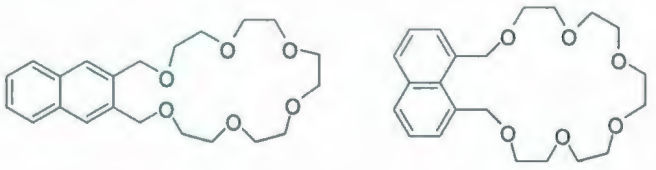

230 **231**

Figure 6.1: Structures of **230** and **231**.

TTF and its derivatives are strong electron donors, and synthetic routes to crown ether annulated TTF have been well developed by the Obsubo group.[53] The Zhu group synthesized a fluoroscence sensor **109**[60] (Figure 6.2), in which a TTF unit replaced traditional nitrogeneous group as electron donor. It was anticipated that the fluorescence of compound **109** would be enhanced with the addition of sodium cations. But the fluorescence only increased slightly. Since it has been reported that both intermolecular and intromolecular photoinduced electron transfer could occur efficiently between C_{60} and TTF derivatives,[142] C_{60} was therefore employed as input. The fluorescence of compound **109** showed slight enhancement after interation with C_{60}. However, the fluorescence of compound **109** was greatly enhanced in the presence of both Na^+ and C_{60}.

These results indicated that if C_{60} and Na^+ are regarded as two input signals, and the fluorescence of dyad **109** as output signal, the fluorescence modulation of dyad **109** gives a performance of an "AND" logic gate.[143]

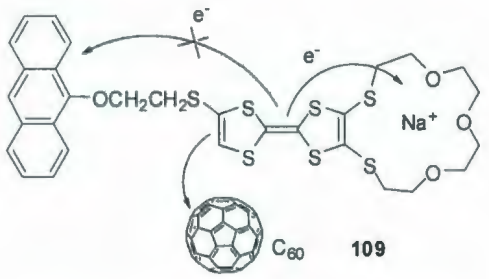

Figure 6.2: Structure of sensor **109**.

In 2006, the Zuo group devised and synthesized a novel dual functional sensor **232**[144] (Figure 6.3) for Li^+ and $^1O_2$. No significant change in fluorescence intensity was observed with the addition of 1 equiv of Li^+. With the addition of singlet oxygen ($^1O_2$) from H_2O_2/NaOCl solution in situ, the fluorescence was increased by 1.4 fold. The increase resulted from the oxidation of the TTF unit so that PET from TTF to anthracene group was suppressed. After the addition of 1 equiv of Li^+ to the above system, fluorescence intensity was two times of that induced by singlet oxygen alone. This is likely due to further restriction of PET since the oxidation potential of the receptor was raised by cation addition. These results substantiate that compound **232** is not only a probe for $^1O_2$, but also a good sensor for Li^+. Furthermore, the presence of $^1O_2$ triggered the detection of Li^+ cation.

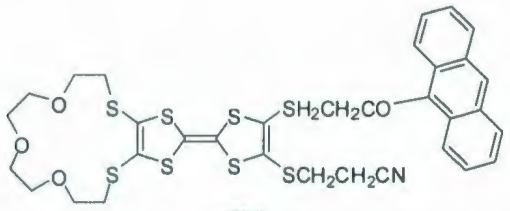

232

Figure 6.3: Dual functional sensor **232** for Li^+ and $^1O_2$.

TTF employed as an electron donor in many cases could efficiently quench fluorescence emission of the fluorophore, and the boronic acid group as a receptor can form cyclic esters with saccharides reversibly. In this light, the Zhu group designed a sensor system (compound **110**) composed of TTF as an electron-donating group and boronic acid as the host unit for saccharide sensing (Figure 6.4). The weak fluorescence of compound **110** was observed due to quenching by PET from TTF unit to excited anthracene moiety. A fivefold fluorescence enhancement was obtained with the increase of fructose concentration up to 50 mM. Since the boronate is a stronger electron acceptor than relating boronic acid, the PET occurred strongly between TTF units and the boronates, and fluorescence emission of anthrancene was recovered.

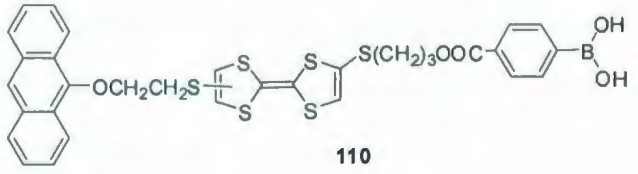

110

Figure 6.4: Structure of sensor **110**.

In this chapter, the applicability of TTFAQ as an electron-donating group in fluorescent sensors was investigated. Compound **233** (Figure 6.5) was devised as an efficient metal cation sensor, since TTFAQ has a better electron-donating ability than

TTFs. Similar crown ether annulated TTFAQ **234** (Figure 6.6) was reported by Bryce and co-workers[145] to have a highly curved crown-π molecular framework. It was anticipated that once two symmetric highly curved crown rings were annulated on both sides of TTFAQ, it would form a "claw-like" conformation with somewhat cylindrical cavity. If the size of this cavity is suitable to accommodate some cations, it would strengthen the affinity for binding metal cations via a synergic action with the crown ether ring (Figure 6.7). In light of this consideration, compound **233** was synthesized as a new class of chemosensor for metal cations.

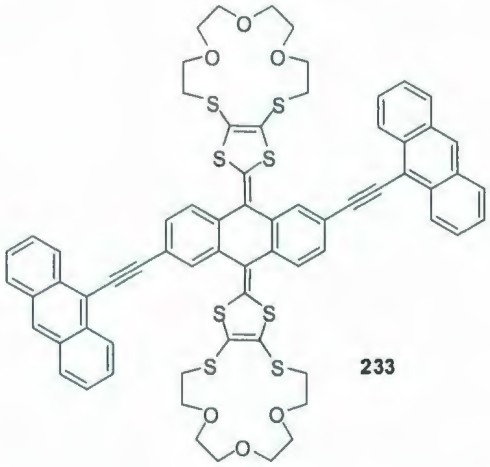

233

Figure 6.5: Structure of compound **233**.

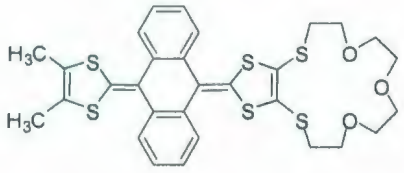

234

Figure 6.6: Structure of compound **234**.

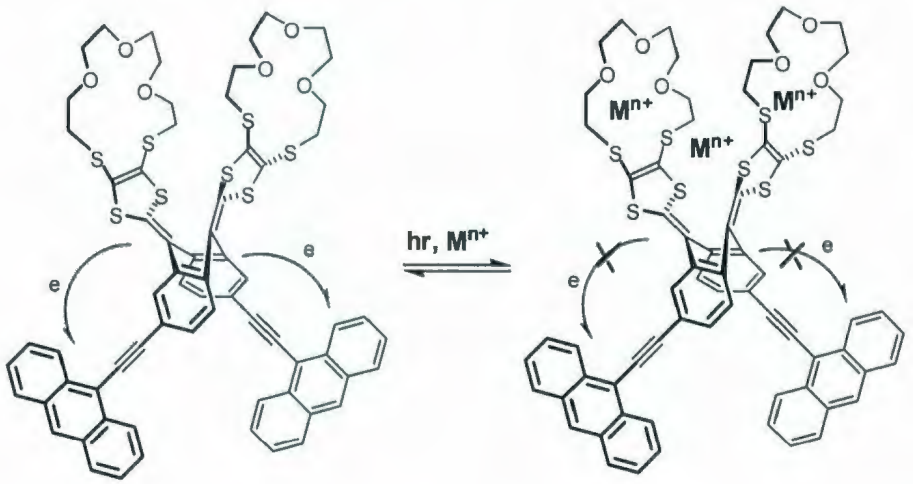

Figure 6.7: Proposed mechanism of metal cation sensing by compound **233**.

6.2 Results and discussion

6.2.1 Synthesis

Crown ether annulated TTFs was first synthesized by Otsubo and Ogura in 1985[53] and their metal-binding characteristics were investigated by the Becher group.[54] This thione was also first prepared by the Otsubo group, but its yield was very low, only 14%.[53] Based on the Otsubo group's experience and the other references, we designed a new synthetic route to make this compound in a better yield (Scheme 6.1). In this scheme, the synthesis started from available salt **7** which was prepared through the routes described in Scheme 1.6. Once dibenzoyl ester **236** was attained, dithiolate **237** was easily generated under treatment with sodium in ethanol. Reaction of dithiolate with diiodo tetraethylene glycol **238** was carried out by high-dilution conditions. In most cases, a series of mono-, di-, tri-, tetra-, and even pentamers was attained.[54] The distribution of the products could be affected by the use of high dilution techniques and variations in solvent. After this intermediate thione **239** was made, the following steps followed the Bryce group's

methodology[145] to prepare Horner-Wittig reagent, phosphonium salt **243**. Following the detailed procedure concerning Horner-Wittig in Chapter 2, reaction between **243** and **145** afforded this crown ether annulated TTFAQ **244**. After desilylated with K_2CO_3 to afford free terminal alkynes **245**, this terminal alkyne was cross-coupled with 2 equiv of 9-iodoanthraquinone **246** through Sonogashira reaction to give the final product **233** as an orange powder in an acceptable yield of 33%.

The precursors diiodo glycols **238** and 9-iodoanthraquinone **246** were prepared through the routes depicted in Scheme 6.1. The starting material **247** was lithiated by *n*-butyl lithium at rt first, then iodination by adding molecule iodine in the solution and stirring overnight. The condition of this reaction is very mild, and the desired product **246** was attained in a high yield of 80%. Tetraethylene glycol **248** was converted to tosyl product **249** by reaction with tosyl chloride in Et_3N at rt overnight. The next step was easily handled by refluxing **249** with sodium iodide in acetone for 8 h. The desired product **238** was used in the next step without further purification.

The molecular structure of compound **233** was unambiguously characterized by NMR, IR, and MS analyses, while its solid-state structure was clearly unveiled by X-ray single-crystal crystallography.

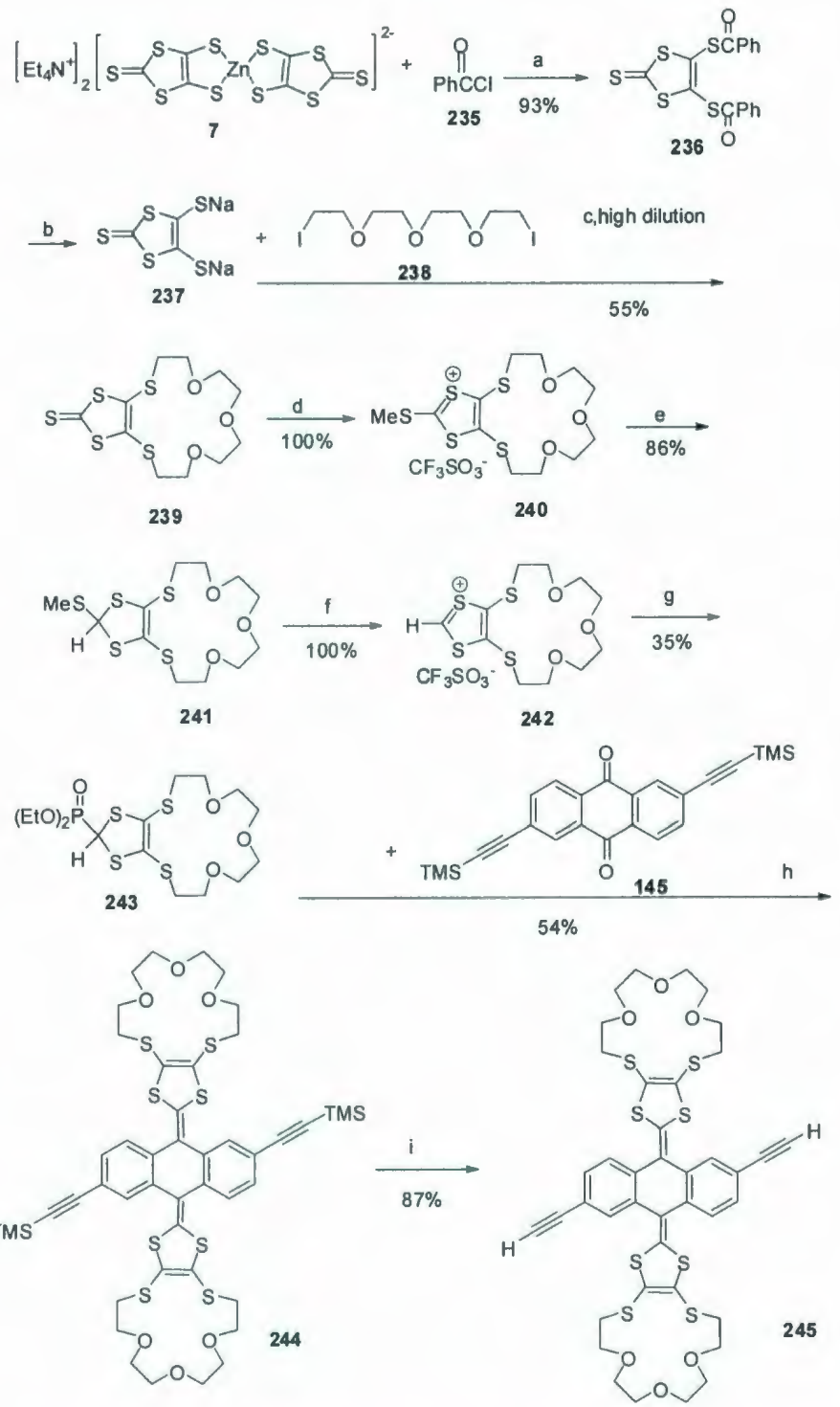

Scheme 6.1: Synthesis of **233**, **238** and **246**. Reagents and conditions: (a) acetone, rt, 4 h, (b) Na, EtOH, rt, 5 h; (c) EtOH/THF (1:1), rt, 2 d; (d) $MeSO_3CF_3$, CH_2Cl_2, rt;

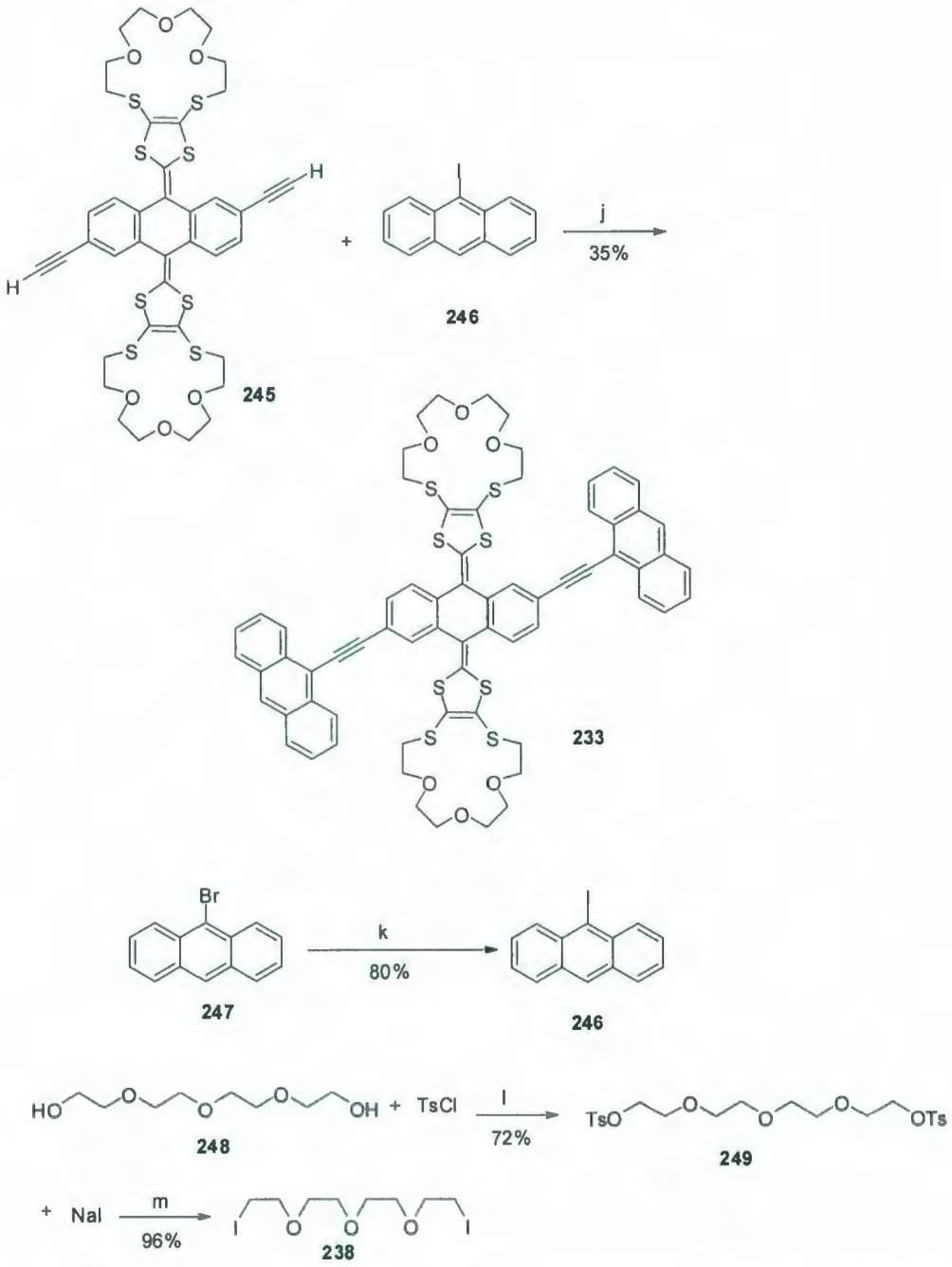

(e) $NaBH_3CN$, EtOH, 0 °C; (f) CF_3SO_3H, MeCN, rt; (g) $P(OEt)_3$, MeCN, rt, 3 h; (h) *n*-BuLi,, THF, -78 °C to rt, overnight; (i) K_2CO_3, THF/MeOH(wet), (1:1); (j) piperidine, $Pd(PPh_3)_4$, CuI; (k) Et_2O, *n*-BuLi, I_2, rt, overnight; (l) Et_3N, rt, overnight; (m) acetone, reflux 8 h.

6.2.2 X-ray crystal structure of TTFAQ-anthracence derivative 233

In Figure 6.8, an X-ray crystallographic study of compound **233** showed a motif of saddle-shaped TTFAQ core with two "claw-like" crown ether rings. Its particular structure can be elucidated by the following data: the anthraquinone moiety is observed to be bent downwards along the C(5)-C(12) axis, hence the two benzene rings forming a dihedral angle of ca. 148°. While the two dithiole rings bend upwards ca. 33° from the plane of C(4)C(6)C(13)C(11), leading to a saddle-shaped TTFAQ core. Both dithiole rings in **233** are folded inward along S(1)-S(2) and S(5)-S(6) by ca. 15°. The two crown rings are bent further inward along S(3)-S(4) and S(7)-S(8) by ca. 106°, reversing the direction of two crown rings and resulting in these two crown ether rings opposite to each other. Besides, two crown rings are enhanced the U-bend by folding inward along the vectors O(1)-O(3) and O(4)-O(6) by ca. 39°. So the two crown ether groups curl up inwardly with a close edge-to-edge distance ca. 4 Å from C(56) to C(65), C(57) to C(64) and C(58) to C(63)), forming a cylindrical inner cavity which has a distance of 10.8 Å between two opposite atoms S(3)-S(8) and S(4)-S(7). Overall, the crystal structure of **233** shows a consistent conformation similar to other crown-annulated TTFAQ derivatives.[145]

The two anthracence units show a rather small twist angle with respect to the two benzene rings of TTFAQ. The near co-planar orientation likely results from a significant conjugation effect. The packing motif of **233** in the solid state displayed intimate face-to-face p-stacking in a distance of ca. 3.4 Å. The intimate and ordered packing hence allows for the formation of hollow channels as revealed in Figure 6.9C.

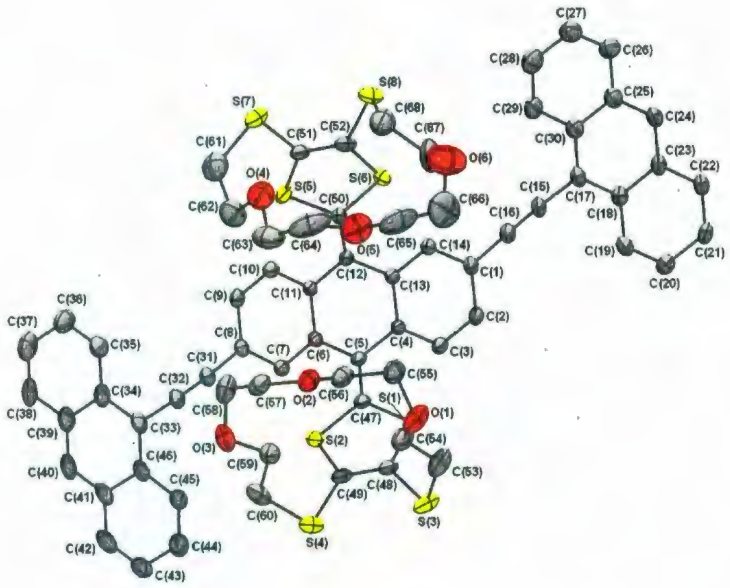

Figure 6.8: Single crystal structure of **233**.

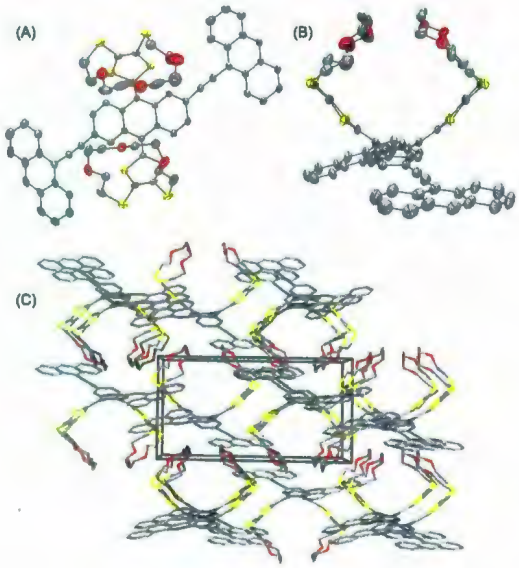

Figure 6.9: ORTEP presentations of compound **233** (50% ellipsoid probability). (A) Front view; (B) side view; (C) crystal packing viewed down the b-axis.

6.2.3 The electronic and electrochemical properties of TTFAQ-anthracence derivative 233

The electronic properties of TTFAQ-anthracence derivative **233** were investigated by UV-Vis absorption and fluorescence spectroscopy. As can be seen from Figure 6.10A, the UV-Vis absorption spectrum of **233** shows three relatively broad low-energy bands at 472, 423, and 393 nm, which are ascribed to the $\pi \rightarrow \pi^*$ transitions at the central TTFAQ core by comparison to the UV-Vis data of other TTFAQ derivatives (see Chapter 5). In the high-energy region, a shoulder at 315 nm and an intense sharp band at 264 nm are absorptions due to the anthracence moieties. The fluorescence spectrum of **233** exhibits a similar spectral pattern to its absorption profile (see Figure 6.10B). The sharp emission band peaking at 428 nm and the shoulder at 455 nm are assigned to the 0-0 and 0-1 bands of anthracence, while the broad, featureless hump centering at 532 nm stems from the emission of the TTFAQ core.

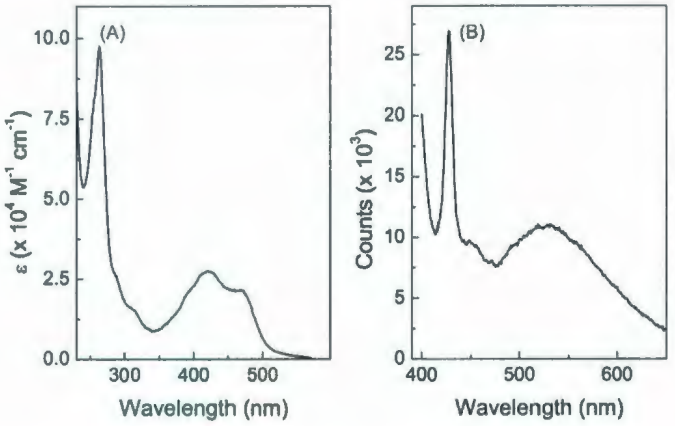

Figure 6.10: (A) UV-vis and (B) fluorescence spectra of compound **233** measured in degassed THF at room temperature.

To assess the metal cation sensing function of compound **233**, fluorescence titration experiments were carried out in THF using $Ba(OTf)_2$, $Mg(OTf)_2$, LiOTf, and AgOTf as the titrant respectively. There are two reasons for choosing the four metal cations. The first reason is that O-containing crown ethers have a strong affinity for binding hard ions (alkali and alkaline earth metals), whereas crown thioethers for soft transition metals or group Ib and IIb metal ions.[146] The mixed O, S-crown ethers are expected to be more selective towards heavy soft metal ions.[147] The other reason is that we want to substantiate the postulation of "claw-like" cavity effect on metal cation binding. Considering the distances between two atoms which have a lone pair of electrons (O and S) in crown ring fall into the range of 4.0 Å to 6.5 Å, and claw-like cylindrical cavity has a distance of ca. 10.8 Å from two opposite S atoms. So three hard metal cations Li^+, Mg^{2+}, and Ba^{2+} with a diameter of 1.20 Å , 1.30 Å and 2.70 Å respectively (Pauling radius for metal ions), and soft metal ions Ag^+ with a diameter of 2.52 Å were picked up for titration. The small cations can fit inside the crown ether ring, while the large cations would fit better in the cavity of **233** upon metal binding. The detailed titration results are given in Figure 6.11.

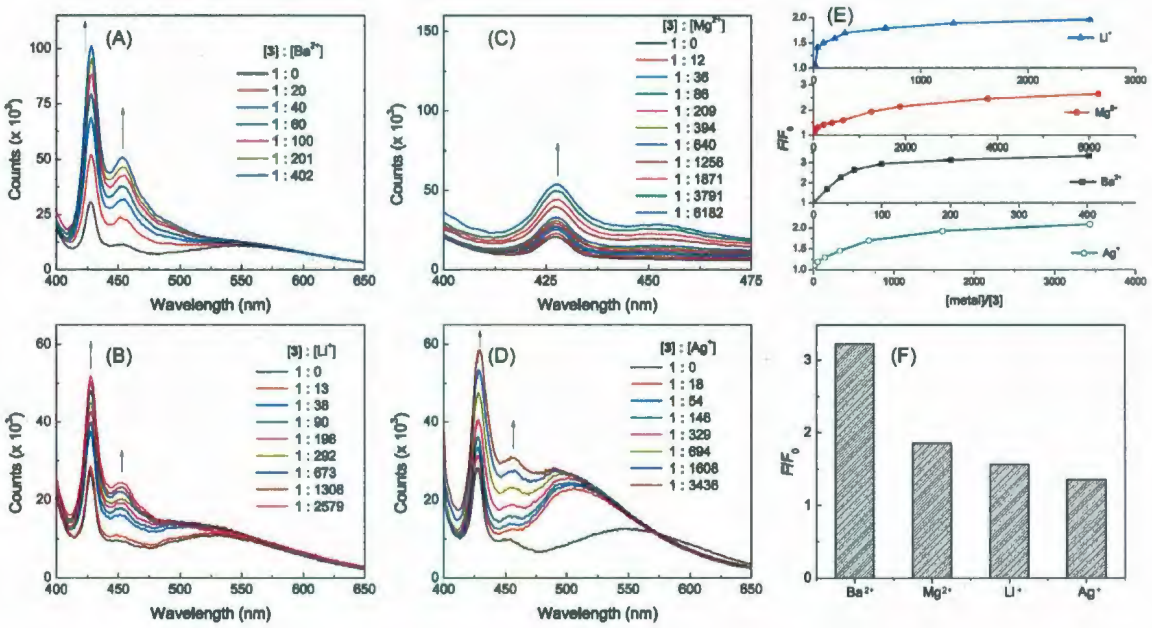

Figure 6.11: Fluorescence speactra monitoring the titration of compound **233**(10^{-6} M) with various metal cations in THF. (A) with [Ba^{2+}]; (B) with [Li^{+}]; (C) with [Mg^{2+}]; (D) with [Ag^{+}]; (E) Plots of F/F_0 (at 428 nm) vs [metal]/[**233**]; (F) Comparison of fluorescence enhancement upon titration of **233** with various metal ions (ca. 200 molar equivalents).

Upon titration of **233** with [Ba^{2+}] (Figure 6.11A), the two bands at 428 and 455 nm that are characteristic emissions of anthracence showed a steady increasing trend. The emission band at 532 nm remained nearly unchanged. This observation is in line with the turn-on sensing mechanism proposed in Figure 6.7. Apparently, the binding of [Ba^{2+}] with the biscrown-annulated TTFAQ receptor has resulted in reduced electron density over the TTFAQ unit, which in turn attenuated the efficiency of PET form TTFAQ donor to the two anthracence moieties. Similar fluorescence enhancement was observed in the titration of **233** with [Li^{+}]. However, the amounts of metal ions to staturate the fluorescence enhancement appeared to be dramatically different for [Ba^{2+}] and [Li^{+}]. As

illustrated in Figure 6.11E, saturation was reached by adding ca. 200 molar equivalents of [Ba^{2+}], whereas for [Li^{+}] more than 2000 equivalents were needed.

The titration of **3** with [Mg^{2+}] (see Figure 6.11C) led to a consistent trend of enhancement of the two anthracence emission bands, which took nearly 6000 molar equivalents of [Mg^{2+}] to arrive at saturation (Figure 6.11E). The low-energy emission band due to the TTFAQ core, however, displayed somewhat erratic and random variations with increasing [Mg^{2+}]. This obseravation suggests that Mg^{2+} might have multiple binding motifs with the biscrown-TTFAQ units, while the details await further investigation.

In addition to alkali and alkaline earth metal ions, sensor **233** was also tested with a soft transition metal ion [Ag^{+}]. As shown in Figure 6.11D, with increasing addition of [Ag^{+}] to **233**, the intensities of two anthracence emission bands increased steadily, and saturation was attained when more than 3000 molar equivalents of [Ag^{+}] were titrated (Figure 6.11E). Of particular note is the emission of TTFAQ core at 532 nm was not only significantly enhanced in intensity, but also notably blueshifted by ca. 30 nm during the process of titration. Such spectral variation can be rationalized by that soft [Ag^{+}] would be preferrably bound to soft ligands (i.e., S atoms of TTFAQ) rather than hard ligands (O atms of crown ether). As such, the binding of [Ag^{+}] with **233** should resulted in pronounced and direct electron-withdrawing effect on the dithiole rings of TTFAQ, causing substantially modulated emission behavior of the TTFAQ units. Figure 6.11F compares the sensitivity of sensor **233** towards various metal cations. Upon addition of ca. 200 molar equivalents of metal cations, the order of fluorescence enhancement at 428 nm (F/F_0) is found to be: Ba^{2+} (3.22) > Mg^{2+} (1.85) > Li^{+} (1.56) > Ag^{+} (1.35). This trend

indicates that sensor **233** is more selective toward hard metal ions with large diameter such as Ba^{2+}. The discriminative sensing behavior is likely originated from a complementarity of metal ions and the binding pocket of **233** in terms of size and electrostatic affinity.

To evaluate the stability constant of complex between **233** and metal ions, fluorescence titration data were subjected to a global analysis of equilibrium using the software package *SPECFIT*. The analysis provides stability constants are listed in Table 6.1. Both 1:1 and 1:2 binding stoichiometry were determined. For 1:1 complexation, Ba^{2+} and Li^{+} have stability constants of the same order of magnitude, while the stability constant (β_{11}) for Ag^{+} is greater than the other two by approximately one order of magnitude. For 1:2 complexation, Ba^{2+} shows the largest cummulative stability constant (β_{12}) among the other metal ions, which is congruous with the highest selectivity for Ba^{2+} shown in Figure 6.11F.

Table 6.1: Binding constants of **233** for various metal ions in THF.

Metal ion	$\log\beta_{11}$ (M^{-1})	$\log\beta_{12}$ (M^{-2})
Ba^{2+}	4.51±0.42	8.76±0.45
Li^{+}	4.25±0.12	6.48±0.26
Ag^{+}	5.42±0.17	7.83±0.18

In conclusion, a new type of fluorescence chemosensor (compound **233**) based on a biscrown-annulated TTFAQ receptor and two anthrancence fluorophores has been designed and synthesized. The solid-state structure of sensor **233** was elucidated by X-ray single crystallographic analysis, showing an unqiue claw-like structure along the biscrwon-TTFAQ backbone. Compound **233** was found to show sensing behaviour toward various metal ions via a fluorescence turn-on mechanism, with a unique high

sensitivity and selectivity for Ba^{2+}. Our study substantiates the applicability of biscrown-annulated TTFAQ as a sensitive donor and effective metal cation receptor in the design and synthesis of fluorophore-based chemosensors.

6.3 Experimental

General procedures and methods

Chemicals and reagents were purchased from commercial suppliers and used without further purification. THF was distilled from sodium/benzophenone. Et_3N and toluene were distilled from LiH. Catalysts, $Pd(PPh_3)_4$ and $Pd(PPh_3)_2Cl_2$, were prepared from $PdCl_2$ according to standard procedures. All reactions were performed in standard, dry glassware under an inert atmosphere of N_2 unless otherwise noted. Evaporation and concentration was done at H_2O-aspirator pressure. Flash column chromatography was carried out through silica gel 60 (230-400 mesh) from VWR international. Thin-layer chromatography (TLC) was carried out on silica gel 60 F254 covered plastic sheets and visualized by UV light or $KMnO_4$ stain. Melting points (mp) were measured with a Fisher-Johns melting point apparatus and are uncorrected. ^1H and ^{13}C NMR spectra were measured on the Bruker AVANCE 500 MHz spectrometer. Chemical shifts are reported in ppm downfield from the signal of the internal reference $SiMe_4$. Coupling constants (*J*) are given in Hz. Infrared spectra (IR) were recorded on a Bruker Tensor 27 spectrometer. UV-Vis spectra were recorded on an Agilent 8453 UV-Vis or a Cary 6000i UV-Vis-NIR spectrophotometer. Fluorescence spectra were measured in $CHCl_3$ at ambient temperature using a Quantamaster 10000 fluorometer. APCI mass spectra were measured on an

Agilent 1100 series LCMSD spectrometer, and high-resolution MALDI-TOF mass spectra on an Applied Biosystems Voyager instrument with dithranol as the matrix.

S,s'-2-thioxo-1,3-dithiole-4,5-diyl dibenzothioate (236). In a 100 mL round-bottomed flask, compound **7** (300 mg, 0.418 mmol) was dissolved in 30 mL of acetone. Compound **235** (242 mg, 1.722 mmol) was added to this flask under nitrogen atmosphere. This mixture was allowed to be stirred for 4 h at rt. After removal of the solvent in vacuo, this mixture was redissolved in dichloromethane again, washed by brine, and dried over magnesium sulfate. After the solvent was removed in vacuo, this residue was purified by flash column chromatograph (eluent: dichloromethane/hexanes, 1/4) to give the desired product **236** (160 mg, 0.394 mmol, 100%) as a yellow powder. ^{1}H NMR (500 MHz, $CDCl_3$): δ 7.97 (2H, d, J = 7.5 Hz), 7.66 (1H, t, J = 6.5 Hz), 7.52 (2H, t, J = 8.0 Hz).

5,6,8,9,11,12,14,15-Octahydro-[1,3]dithiolo[4,5-k][1,4,7,10,13]trioxadithiacyclopentadecine-2-thione (239). Sodium (460 mg, 20.000 mmol) in small pieces was dissolved in 30 mL of dry ethanol, and the solution was allowed to cool. Powder **236** (4000 mg, 9.838 mmol) was added to this solution and stired for a half hour. Then this solution was sucked to a syringe. A solution of **238** (4140 mg, 10.002 mmol) in 30 mL of ethanol was sucked into another syringe. These two syringes were added slowly to a 250 mL bottle containing THF (90 mL) and EtOH (30 mL). After 2 days stirring, solvent was removed in vacuo and redissolved in EtOAc. This solution was washed with brine, and dried over magnesium sulfate. After the solvent was

removed in vacuo, the residue was purified with flash column chromatograph (eluent: EtOAc/hexanes, 1/1) to give the desired product as a yellow solid **239** (1930 mg, 5.413 mmol, 55%). ^{1}H NMR (500 MHz, $CDCl_3$): δ 3.08 (4H, t, J = 6.0 Hz), 3.69 (8H, dd, J = 15.3 Hz, J = 5.0 Hz), 3.82 (4H, t, J = 6.0 Hz). ^{13}C NMR (125 MHz, $CDCl_3$): δ 211.38, 136.90, 71.62, 71.06, 70.13, 36.87. IR (cm^{-1}): 3474, 2944, 2877, 1720, 1466, 1292, 1254, 1123, 1071, 976, 892. GC-MS: *m/z* calculated for $C_{11}H_{16}O_3S_5$ 355.97, found 356.00. Mp: 68-70 °C.

2-(Methylthio)-5,6,8,9,11,12,14,15-octahydro-[1,3]dithiolo[4,5-k][1,4,7,10,13]trioxadithiacyclopentadecin-1-ium trifluoromethanesulfonate (240). Into a solution of **239** (1300 mg, 3.646 mmol) in dichloromethane (30 mL) was added methyl triflate (620 mg, 3.780 mmol). This solution was stirred at rt for 5 h to give a dark brown solution. This solution was partially evaporated in vaccuo (to leave ca. 5 mL) and 30 mL of diethyl ether was added and the mixture was stirred for 30 min. The solvent was decanted off and the residual oil dried in vacuo to afford **240** as a brown oil (2020 mg, over 100%) of high purity suitable for use in the next step without further purification. ^{1}H NMR (500 MHz, $CDCl_3$): δ 3.90 (4H, t, J = 5.0 Hz), 3.64 (4H, t, J = 4.0 Hz), 3.52 (4H, t, J = 4.3 Hz), 3.39 (4H, t, J = 5.5 Hz), 3.24 (3H, s).

2-(Methylthio)-5,6,8,9,11,12,14,15-octahydro-[1,3]dithiolo[4,5-k][1,4,7,10,13]trioxadithiacyclopentadecine (241). Into an ice cooled solution of **240** (5540 mg, 10.640 mmol) in 50 mL of ethanol was added sodium cyanoborohyddride portionwise (690 mg, 10.980 mmol) at 0 °C and the mixture was stirred at 0 °C for 1 h.

The solvent was then evaporated in vacuo and the residue was purified by flash column chromatography (eluent: EtOAc/hexanes; 1/1) to give the desired product **241** as a brown oil (3390 mg, 9.098 mmol, 86%). ^{1}H NMR (500 MHz, $CDCl_3$): δ 5.70 (1H, s), 3.75-3.73 (4H, m), 3.64-3.62 (4H, m), 3.24-3.21 (4H, m), 2.77-2.74 (4H, m), 2.27 (3H, s).

5,6,8,9,11,12,14,15-Octahydro-[1,3]dithiolo[4,5-k][1,4,7,10,13]trioxadithiacyclopentadecin-1-ium trifluoromethanesulfonate (242). Into a solution of **241** (1090 mg, 2.925 mmol) in 10 mL of acetonitrile was added triflic acid (3.545, 23.458 mmol) and the mixture was stirred at rt for 10 min to give a deep red-orange solution. This solution was partially evaporated in vacuo (to leave ca. 2 mL) and 30 mL of diethyl ether was added and the mixture was stirred for 30 min. The solvent was decanted off and the residual oil dried in vacuo to afford **242** as a brown oil (1150 mg, 2.423 mmol, 100%). ^{1}H NMR (500 MHz, $CDCl_3$): δ 6.15 (1H, s), 3.92-3.88 (4H, m), 3.53-3.51 (4H, m), 3.43-3.41 (4H, m), 3.33-3.32 (4H, m).

Diethyl 5,6,8,9,11,12,14,15-octahydro-[1,3]dithiolo[4,5-k][1,4,7,10,13]trioxadithiacyclopentadecin-2-ylphosphonate (243). To a stirred suspension of freshly-prepared salt **242** (1150 mg, 2.423 mmol) in 10 mL of dry acetonitrile at rt was added triethylphosphine (497 mg, 2.991 mmol) and the mixture was stirred for 3 h. Then the solvent was evaporated in vacuo and the residue extracted into ethyl acetate. The solution was washed with brine, and dried with magnesium sulfate. After the solvent was removed in vacuo, the residue was purified with flash column chromatography (eluent: EtOAc) to afford the desired product as a pale-pink sticky stuff

(400 mg, 0.865 mmol, 35%). ^{1}H NMR (500 MHz, $CDCl_3$): δ 4.28-4.24 (4H, m), 3.94 (1H, s), 3.80-3.66 (12H, m), 3.17-3.12 (2H, m), 2.97-2.92 (2H, m), 1.38-1.35 (6H, m).

(9,10-Bis(5,6,8,9,11,12,14,15-octahydro-[1,3]dithiolo[4,5-k][1,4,7,10,13]trioxadithiacyclopentadecin-2-ylideene)-9,10-dihydroanthracene-2,6-diyl)bis(ethyne-2,1-diyl)bis(trimethylsilane) (244). To a 100 mL round-bottomed flask, **243** (800 mg, 1.693 mmol) was added in 30 mL of dry THF. *n*-BuLi (0.68 mL, 2.5 M, 1.700 mmol) was added to this solution at -78 °C. After 2 h stirring at -78 °C, **144** (230 mg, 0.575 mmol) was added dropwise to this solution. This solution was allowed to warm up to rt and stirred overnight. The solvent was removed in vacuo and redissolved in EtOAc, washed by brine, and dried over magnesium sulfate. After the solvent was removed in vacuo, the residue was purified by flash column chromatography (eluent: EtOAc/hexanes, 2/1) to afford the desired product **244** as an orange solid (300 mg, 0.294 mmol, 54%). ^{1}H NMR (500 MHz, $CDCl_3$): δ 7.61 (2H, s), 7.46 (2H, d, J = 8.0 Hz), 7.39 (2H, d, J = 8.0 Hz), 3.76-3.73 (8H, m), 3.65-3.62 (8H, m), 3.59-3.57 (8H, m), 3.07-2.94 (8H, m), 0.27 (18H, s). ^{13}C NMR (125 MHz, $CDCl_3$): δ 134.49, 134.38, 132.72, 130.05, 128.27, 127.09, 126.35, 125.24, 121.99, 121.11, 104.83, 95.18, 71.32, 71.22, 70.52, 69.94, 69.86, 35.87, 35.76. IR (cm^{-1}): 3418, 2957, 2927, 2858, 2152, 1715, 1618, 1556, 1528, 1493, 1462, 1396, 1361, 1282, 1249, 1220, 1118, 845. HR-MALDI-MS: *m/z* calculated 1016.1381, found 1016.1394. Mp: 151-152 °C.

2,2'-(2,6-Diethynylanthracene-9,10-diylideene)bis(5,6,8,9,11,12,14,15-octahydro-[1,3]dithiolo[4,5-k][1,4,7,10,13]trioxadithiacyclopentadecine) (245). In a 100 mL

round-bottomed flask, **244** (40 mg, 0.039 mmol) was added to the solution of 20 mL of wet THF and MeOH (1:1). Anhydrous potassium carbonate (50 mg) was also added to this solution. This mixture was stirred at rt for a half hour, and then the solvent was removed in vacuo. This compound was redissolved in EtOAc, washed by 1 M HCl, brine, and dried over magnesium sulfate. Finally, this compound was purified by flash column chromatography (eluent: EtOAc/hexanes, 2/1) to afford the desired product **245** as a yellow solid (30 mg, 0.034 mmol, 87%). ^{1}H NMR (500 MHz, $CDCl_3$): δ 7.66 (2H, s), 7.52 (2H, d, J = 8.5 Hz), 7.43 (2H, d, J = 8.5 Hz), 3.75-3.70 (8H, m), 3.64-3.56 (16H, m), 3.15 (2H, s), 3.05-2.98 (4H, m), 2.97-2.93 (4H, m).

2,2'-(2,6-Bis(anthracen-9-ylethynyl)anthracene-9,10-diylideene)bis(5,6,8,9,11,12,14,15-octahydro-[1,3]dithiolo[4,5-k][1,4,7,10,13]trioxadithiacyclopentadecine) (233). In a 100 mL round-bottomed flask, **245** (100 mg, 0.115 mmol), **246** (150 mg, 0.493 mmol), $Pd(PPh_3)_4$ (30 mg, 0.026 mmol) and CuI (20 mg, 0.105 mmol) were added in 30 mL of piperidine. After complete degassing with freeze-pump-thaw cycles, this solution was allowed to warm up to rt and stirred overnight. After the solvent was removed in vacuo, this compound was redissovled in EtOAc, washed by 1 M HCl, brine, and dried over magnesium sulfate. After the solvent was removed in vacuo, the crude compound was purified by flash column chromatography (eluent: EtOAc/hexanes, 3/1) to give the desired product **233** (50 mg, 0.041 mmol, 35%) as an orange powder. ^{1}H NMR (500 MHz, $CDCl_3$): δ 8.73 (2H, d, J = 8.0 Hz), 8.50 (1H, s), 8.08 (2H, d, J = 8.5 Hz), 8.00 (1H, s), 7.77 (1H, d, J = 8.5 Hz), 7.74 (1H, d, J = 8.5 Hz), 7.67 (2H, t, J = 7.5 Hz), 7.57 (2H, t, J = 7.5 Hz), 3.79-3.77 (8H,

m), 3.66-3.60 (16H, m), 3.08-3.06 (4H, m), 3.03-2.99 (4H, m). ^{13}C NMR (125 MHz, $CDCl_3$): δ 135.29, 135.00, 133.65, 133.10, 131.64, 129.96, 129.17, 128.67, 128.32, 127.24, 127.20, 127.16, 126.16, 126.06, 122.53, 122.02, 117.52, 101.25, 87.82, 71.75, 71.74, 71.03, 71.01, 70.37, 70.34, 36.28, 36.24. IR (cm^{-1}): 2922, 2853, 2190, 1721, 1638, 1620, 1524, 1490, 1464, 1280, 1119, 784. HR-MALDI-MS: *m/z* calculated 1224.1843, found 1224.1881. Mp: 255-256 °C.

9-Iodoanthracene (246). In a 100 mL round-bottomed flask, **247** (1000 mg, 3.889 mmol) was added in 50 mL of anhydrous diethyl ether. To this solution was added *n*-BuLi (2.16 mL, 2.5 M, 5.400 mmol) dropwise at rt. After stirring for 0.5h, I_2 (1700 mg, 6.698 mmol) was added. This mixture was stirred overnight. This solution was washed with 25% (w/w) sodium thiosulfate in water for 5 times. The solution was dried with magnesium sulfate. After the solvent was removed in vacuo, the crude product was purified with flash column chromatography (eluent: hexanes) as a green-yellow solid **246** (940 mg, 3.091 mmol, 80%). ^1H NMR (500 MHz, $CDCl_3$): δ 8.49 (2H, d, J = 8.0 Hz), 8.46 (1H, s), 7.97 (2H, d, J = 8.0 Hz), 7.60 (2H, t, J = 8.0 Hz), 7.52 (2H, t, J = 8.0 Hz).

2,2'-(2,2'-Oxybis(ethane-2,1-diyl)bis(oxy))bis(ethane-2,1-diyl) bis(4-methylbenzenesulfonate) (249). Compound **248** (5000 mg, 25.743 mmol) and TsCl (11000 mg, 57.697 mmol) were added to a round-bottomed flask containing 200 mL of Et_3N. This solution was allowed to be stirred overnight at rt. After Et_3N was removed in vacuo, EtOAc was used to extract the mixture. The extract was washed with brine, and dried over magnesium sulfate. The residue was purified by flash column chromatograph

(eluent: EtOAc/hexanes, 1/1) to give the desired product **249** as a colorless liquid (9330 mg, 18. 563 mmol, 72%). ^{1}H NMR (500 MHz, $CDCl_3$): δ 7.80 (4.0H, d, J = 8.0 Hz), 7.34 (4.0H, d, J = 8.0 Hz), 4.16 (4H, t, J = 5.0 Hz), 3.68 (4H, t, J = 5.0 Hz), 3.57 (8H, s), 2.44 (6H, s).

1-Iodo-2-(2-(2-(2-iodoethoxy)ethoxy)ethoxy)ethane (238). Compound **249** (3380 mg, 6.725 mmol) and NaI (4040 mg, 26.953 mmol) were added to a round-bottomed flask containing acetone (100 mL). The mixture was refluxed for 8 h under nitrogen. After removal of the solvent, this residue was redissolved in dichloromethane, washed by brine, and dried over magnesium sulfate. After the solvent was removed in vacuo, the desired product **240** was obtained as an orange liquid without further purification. (2680 mg, 6.473 mmol, 96%). ^{1}H NMR (500 MHz, $CDCl_3$): δ 3.78 (4H, t, J = 7.0 Hz), 3.67 (8H, s), 3.28 (4H, t, J = 7.0 Hz).

Chapter 7

Conclusions and Future Work

The research work has focused on the synthesis of TTF-based materials with potential applications in electrochemical sensors, fluorescent sensors, and charge-transfer materials. Investigation of their electrochemical and optical properties were conducted mainly by means of spectroscopic and voltammetric techniques. A series of synthetic targets have been designed and successfully synthesized, using Horner-Wittig reaction, Sonogashira reaction, and Stille coupling as the key steps.

In Chapter 2, extended π-conjugated triads **138**, **139** and **140** have been efficiently synthesized. Trimer **139** behaved as an independent unit without significant electronic communications among the TTFAQ units within the molecules, whereas the D/A triads **138** and **140** displayed appreciable electronic interactions among the electroactive groups. Potential applications in the field of intramolecular charge transfer and nonlinear optical materials were envisioned for these new molecular materials. A shortage of these materials is that they only show moderate solubility in organic solvents, such as chloroform and methylene chloride. In the future work, increasing the alkyl length of subsitituted group on 1,3-dithiole rings, using $-SC_5H_{11}$ to replace $-SCH_3$, would be an efficient approach to address this problem.

In Chapter 3, synthetic routes to two compounds **180** and **181** have been successfully developed, and their electrochemical and electronic absorption properties were elucidated by voltammetric techniques in combination with UV-Vis spectroscopic analysis. Efforts towards electropolymerization of these two compounds have not been successful in

repetive CV scan experiments. Although **181** showed a quasi-reversible peak in CV, its first oxidation potential occurred at +0.76 V which is higher than typical TTFAQ derivatives. Nevertheless, the synthetic work has successfully hybridized TTFAQ and thiophene groups in a molecular ensemble. In the future work, bromination of thiophene unit is expected to afford an intermediate, which will likely form corresponding oligomers by a Stille coupling with tributylstannane. This step can be performed repetitively until works satisfied oligomer chain lengths are attained. The resulting oligomers/polymers of TTFAQ-thiophene hybrids may display useful properties for electronic devices.

In Chapter 4, a new TTFAQ-diboronic acid was synthesized as an electrochemical sensor, which showed high selectivity for some saccharides. However, solubility problem in water limits its potential application as a practical saccharide sensor. With the assistance of DMSO as a co-solvent, TTFAQ-diboronic acid could be solubilized to form a viscous and slightly turbid solution. In the DPV data of TTFAQ-boronic acid, rather weak current signals were observed before titration with saccharides. With increasing addition of fructose and ribose to the solution of TTFAQ-boronic acid in DMSO/H_2O, the solution of this product became less viscous and more transparent. In the mean time, a steady increase of current intensity in DPV was also clearly seen. This result indicates that this compound is able to complex with particular saccharides with improved aqueous solubility was improved. In the future work, changing the substitients on 1,3-dithiole ring, which show more affinity for water, could solve the solubility problem and afford more practically useful saccharide sensors.

In Chapter 5, compounds **208** and **209** showed promising electrochemical behaviors, making them suitable candidates as electrochemical sensors for some transition metal ions. In order to validate their applicability, more titration experiments would needed in the future work, with other metal salts, such as Pb^{2+}, Cd^{2+}, Hg^{2+} ions.

The project in Chapter 6 has been completed with surprising success. Single crystal structure of **233** was carefully obtained and analyzed. This compound showed fluorescene sensing function to a number of metal cations: Li^{+}, Mg^{2+}, Ag^{+}, Ba^{2+}. High selectivity for Ba^{2+} was observed. This result substantiates the possible use of this compound as a fluorescent sensor for large alkaline earth metal ions. In the future work, systematic characterizations on the binding motifs and fluorescence sensing mechanisms would be described, so as to offer valuable guidance to the design of selective metal chemosensors based on the TTFAQ framework.

References

1. Wudl, F.; Wobschall, D.; Hufnagel, E. J. *J. Am. Chem. Soc.* **1972**, *94*, 670.
2. Ferraris, J.; Cowan, D. O.; Walatka, V.; Perlstein, J. H. *J. Am. Chem. Soc.* **1973**, *95*, 948.
3. Andrieux, A.; Duroure, C.; Jérome, D.; Bechgaard, K. *J. Phys. Lett.* **1979**, *40*, 381.
4. Bryce, M. R. *Chem. Soc. Rev.* **1991**, *20*, 355.
5. Segura, J. L.; Martín, N. *Angew. Chem. Int. Ed.* **2001**, *40*, 1372.
6. Bendikov. M.; Wudl, F. *Chem. Rev.* **2004**, *104*, 4891.
7. Schukat, G.; Richter, A. M.; Fanghaenel, E. *Sulfur Rep.* **1987**, *7*, 155.
8. Sato, M.; Gonnella, N. C.; Cava, M. P. *J. Org. Chem.* **1979**, *44*, 930.
9. Akiba, K.; Ishikawa, K.; Inamoto, N. *Bull. Soc. Chem. Jpn.* **1978**, *51*, 2674.
10. Ishikawa, K.; Akiba, K.; Inamoto, N. *Tetrahedron Lett.* **1976**, 3695.
11. Imakubo, T.; Lijima, T.; Kobayashi, K.; Kato, R. *Synth. Met.* **2001**, *120*, 899.
12. Simonsen, K. B.; Svenstrup, N.; Lau, J.; Simonsen, O.; Mørk, P.; Kristensen, G. J.; Becher, J. *Synthsis* **1994**, 809.
13. Green, D. C. *J. Org. Chem.* **1979**, *44*, 1476.
14. Jeppesen, J. O.; Becher, J. *Eur. J. Org. Chem.* **2003**, 3245.
15. Bryce, M. R. *J. Mater. Chem.* **2000**, *10*, 589.
16. Aviram, A.; Ratner, M. *Chem. Phys. Lett.* **1974**, *29*, 277.
17. Panetta, C. A.; Baghdadchi, J.; Metzger, R. M. *Mol. Cryst. Liq. Cryst.* **1984**, *107*, 103.

18. DeMiguel, P.; Bryce, M. R.; Goldenberg, L. M.; Beeby, A.; Khodorkovsky, V.; Shapiro, L.; Niemz, A.; Cuello, A. O.; Rotello, V. *J. Mater. Chem.* **1998,** *8*, 71.

19. Scheib, S.; Cava, M. P.; Baldwin, J. W.; Metzger, R. M. *J. Org. Chem.* **1998,** *63*, 1198.

20. Moriarty, R. M.; Tao, A.; Gilardi, R.; Song, Z.; Tuladhar, S. M. *Chem. Commun.* **1998**, 157.

21. Segura, J. L.; Martín, N.; Seoane, C.; Hanack, M. *Tetrahedron Lett.* **1996**, *37*, 2503.

22. (a) Le Paillard, M. P.; Robert, A.; Garrigon-Lagrange, C.; Delhaes, P.; le Maguerès, P.; Quahab, L.; Toupet, L. *Synth. Met.* **1993,** *58*, 223. (b) Le Paillard, M. P.; Robert, A. *Bull. Soc. Chim. Fr.* **1992,** *129*, 205.

23. Goldenberg, L. M.; Becker, J. Y.; Paz-Tal Levi, O.; Khodorkovsky, V. K.; Bryce, M. R.; Petty, M. C. *Chem. Commun.* **1995**, 475.

24. Simonsen, K. B.; Zong, K.; Rogers, R. D.; Cava, M. P.; Becher, J. *J. Org. Chem.* **1997**, *62*, 679.

25. Simonsen, K. B.; Thorup, N.; Cava, M. P.; Becher, J. *Chem. Commun.* **1998**, 901.

26. Prato, M.; Maggini, M.; Giacometti, C.; Scorrano, G.; Sandona, G.; Farnia, G. *Tetrahedron* **1996**, *52*, 5221.

27. Martín, N.; Sánchez, L.; Seoane, C.; Andreu, R.; Garín, J.; Orduna, J. *Tetrahedron Lett.* **1996**, *37*, 5979.

28. Llacay, J.; Mas, M.; Molins, E.; Veciana, J.; Powell, D.; Rovira, C. *Chem. Commun.* **1997**, 659.

29. Bonlle, C.; Rabreau, J. M.; Hudhomme, P.; Cariou, M.; Jubault, M.; Gorgues, A.; Orduna, J.; Gartín, J. *Tetrahedron Lett.* **1997**, *38*, 3909.

30. Llacay, J.; Veciana, J.; Viadal-Gancedo, J.; Boardelande, J. L.; González-Moreno, R.; Rovira, C. *J. Org. Chem.* **1998**, *63*, 5201.

31. (a) Perepichka, D. F.; Bryce, M. R.; Mclnnes, E. J. L.; Zhao, J. P. *Org. Lett.* **2001**, *3*, 1431. (b) Perepichka, D. F.; Bryce, M. P.; Batsanov, A. S.; Mclnnes, E. J. L.; Zhao, J. P.; Farley, R. D. *Chem. Eur. J.* **2002**, *8*, 4656.

32. Andreu, R.; de Lucas, A. I.; Garín, J.; Martín, N.; Orduna, J.; Sánchez, L.; Seoane, C. *Synth. Met.* **1997**, *86*, 1817.

33. González, M.; Segura, J. L.; Seoane, C.; Martín, N.; Garín, J.; Orduna, J.; Alcalá, R.; Villacampa, B.; Hernández, V.; Navarrete, J. T. L. *J. Org. Chem.* **2001**, *66*, 8872.

34. Bryce, M. R.; Green, A.; Moore, A. T.; Perepichka, D. F.; Batsanov, A. S.; Howard, J. A. K.; Ledoux-Rak, I.; González, M.; Martín, N.; Segura, J. L.; Garín, J.; Orduna, J.; Alcalá, R.; Villacampa, B.; *Eur. J. Org. Chem.* **2001**, 1927.

35. González, M.; Martín, N.; Segura, J. L.; Seoane, C.; Gartín, J.; Orduna, J.; Alcalá, R.; Sánchez, C.; Villacampa, B. *Tetrahedron Lett.* **1999**, *40*, 8599.

36. Garín, J.; Orduna, J.; Rupérez, J. I.; Alcalá, R.; Villacampa, B.; Sánchez, C.; Martín, N.; Segura, J. L.; Gonzalez, M. *Tetrahedron Lett.* **1998**, *39*, 3577.

37. Bryce, M. R. Morre, A. J.; *Synth. Met.* **1988**, *25*, 203.

38. Perepichka, D. F.; Bryce, M. R.; Pereoichka, I. F.; Lyubchik, S. B.; Christensen, C. A.; Godbert, N.; Batsanov, A. S.; Levillain, E.; Mclnnes, E. J. L.; Zhao, J. P. *J. Am. Chem. Soc.* **2002**, *124*, 14227.

39. Christensen, C. A.; Bryce, M. R.; Batsanov, A. S.; Becher, J. *Org. Biomol. Chem.* **2003**, *1*, 511.

40. Finn, J.; Bryce, M. R.; Batsanov, A. S.; Howard, J. A. K. *Chem. Commun.* **1999**, 1835.

41. Godbert, N.; batsanov, A. S.; Bryce, M. R.; Howard, J. A. K. *J. Org. Chem.* **2001**, *66*, 713.

42. Christensen, C. A.; Batsanov, A. S.; Bryce, M. R.; Howard, J. A. K. *J. Org. Chem.* **2001**, *66*, 3313.

43. Christensen, C. A.; Batsanov, A. S.; Bryce, M. R. *J. Am. Chem. Soc.* **2006**, *128*, 10484.

44. Christensen, C. A.; Batsanov, A. S.; Bryce, M. R. *J. Org. Chem.* **2007**, *72*, 1301.

45. Martín, N.; Pérez, I.; Sánchez, L.; Seoane, C. *J. Org. Chem.* **1997**, *62*, 870.

46. Pérez, I.; Liu, S. G.; Martín, N.; Echegoyen, L. *J. Org. Chem.* **2000**, *65*, 3796.

47. Díaz, M. C.; Illescas, B. M.; Seoane, C.; Martín, N. *J. Org. Chem.* **2004**, *69*, 4492.

48. Díaz, M. C.; Illescas, B. M.; Martín, N.; Perepichka, I. F.; Bryce, M. R.; Levillain, E.; Viruela, R.; Ortí, E. *Chem. Eur. J.* **2006**, *12*, 2709.

49. Martín, N.; Pérez, I.; Sánchez, L.; Seoane, C.; *J. Org. Chem.* **1997**, *62*, 5690.

50. Herranz, M. A.; Martín, N.; Sánchez, L.; Garín, J.; Orduna, J.; Alcalá, R.; Villacampa, B.; Sánchez, C. *Tetrahedron* **1998**, *54*, 11651.

51. Otero, M.; Herranz, M. A.; Seoane, C.; Martín, N.; Garín, J.; Orduna, J.; Alcalá, R.; Villacampa, B. *Tetrahedron* **2002**, *58*, 7463.

52. Jørgensen, T.; Hansen, T. K.; Becher, J. *Chem. Soc. Rev.* **1994**, 41.

53. Otsubo, T.; Ogura, F. *Bull. Chem. Soc. Jpn.* **1985**, *58*, 1343.

54. Hansen, T. K.; Jørgensen, T.; Stein. P. C.; Becher, J. *J. Org. Chem.* **1992**, *57*, 6403.

55. Nielsen, M. B.; Lomholt, C.; Becher, J. *Chem. Soc. Rev.* **2000**, *29*, 153.

56. Moore, A. J.; Goldenberg, L.; Bryce, M. R.; Petty, M. C.; Monkman, A. P.; Port, S. N. *Adv. Mater.* **1998**, *10*, 395.

57. Liu, H.; Liu, S.; Echegoyen, L. *Chem. Commun.* **1999**, 1493.

58. Nielsen, M. B.; Nielsen, S. B.; Becher, J. *Chem. Commun.* **1998**, 475.

59. Asakawa, M.; Ashton, P. R.; Balzani, V.; Credi, A.; Hamers, C.; Mattersteig, G.; Montalti, M.; Shipway, A. N.; Spencer, N.; Stoddart, J. F.; Tolley, M. S.; Venturi, M.; White, A. J. P.; Williams, D. J. *Angew, Chem. Int. Ed.* **1998**, *37*, 333.

60. Zhang, G. X.; Zhang, D. Q.; Zhou, Y. C.; Zhu, D. B. *J. Org. Chem.* **2006**, *71*, 3970.

61. Wang, Z.; Zhang, D. Q.; Zhu, D. B. *J. Org. Chem.* **2005**, *70*, 5729.

62. Yunoki, S.; Takimiya, K.; Aso, Y.; Otsubu, T. *Tetrahedron Lett.* **1997**, *7*, 1175.

63. Blanchard, P.; Sevnstrup, N.; Becher, J. *Chem. Commun.* **1996**, 615.

64. Bryce, M. R.; Marshallsay, G. J.; Moore, A. J. *J. Org. Chem.* **1992**, *57*, 4859.

65. Formigué, M.; Batail, P. *Chem. Commun.* **1991**, 1370.

66. Lau, J.; Simonsen, O.; Becher, J. *Synthesis* **1995**, 521.

67. Christensen, C. A.; Bryce, M. R. Batsanov, A. S.; Becher, J. *Chem. Commun.* **2000**, 331.

68. Bryce, M. R.; Devonport, W.; Moore, A. J. *Angew. Chem. Int. Ed.* **1994**, *106*, 1862.

69. Bryce, M. R.; de Miguel, P.; Devonport, W. *Chem. Commun.* **1998**, 2565.

70. Andreu, R.; Barberá, J.; Garín, J.; Serrano, J. L.; Sierra, T.; Leriche, P.; Sallé, M.; Riou, A.; Jubault, M.; Gorgues, A. *Synth. Met.* **1997**, *86*, 1869.

71. (a) Schukat, G.; Richter, A. M.; Fanghänel, E. *Sulfer Rep.* **1987**, *7*, 155. (b) Schukat, G.; Fanghänel, E. *Sulfer Rep.* **1993**, *14*, 245. (c) Schukat, G.; Fanghänel, E. *Sulfer Rep.* **1996**, *18*, 1.

72. (a) Yamamoto, T. *Progr. Polym. Sci.* **1992**, *17*, 1153. (b) Yamamoto, T.; Sugiyama, K.; Kushida, T.; Inone, T.; Kanbara, Y. *J. Am. Chem. Soc.* **1996**, *118*, 3930. (c) Yamamoto, T.; Yamada, W.; Tagaki, M.; Kizu, K.; Maruyama, T.; Ooba, N.; Tomaru, S.; Kurihara, T.; Kaino, T.; Kubota, K. *Macromoecules* **1994**, *27*, 6620. (d) Sanechika, K.; Yamamoto, T.; Yamamoto, A. *Bull. Chem. Soc. Jpn.* **1984**, *57*, 752.

73. Huchet, L.; Akoudad, S.; Roncali, J. *Adv. Mater.* **1998**, *10*, 541.

74. (a) Yamada, J.-I.; Akutsu, H.; Nishikawa, H.; Kikuchi, K. *Chem. Rev.* **2004**, *104*, 5057. (b) Nielsen, M. B.; Lomholt, C.; Becher, J. *Chem. Soc. Rev.* **2000**, *29*, 153.

75. Müllen, K.; Frenzel, S. *Synth. Met.* **1996**, *80*, 175-182.

76. Adam, M.; Fanghänel, E.; Müllen, K.; Shen, Y. J.; Wegar, R. *Synth. Met.* **1994**, *66*, 275.

77. Nishikawa, H.; Kawuchi, S.; Misaki, Y.; Yamabe, T. *Chem. Lett.* **1996**, 4344.

78. Iyoda, M.; Fukuda, M.; Yoshida, M.; Sasaki, S. *Chem. Lett.* **1994**, 2369.

79. González, A.; Segura, J. L.; Martín, N. *Tetrahedron Lett.* **2000**, *41*, 3083.

80. Gautier, N.; Sammuel, R.; Sahin, Y.; Levillain, E.; Leroy-Lhez, S.; Hudhomme, P. *Org. Lett.* **2004**, *6*, 1569.

81. Dumur, F.; Gautier, N.; Gallego-Planas, N.; Sahin, Y.; Levillain, E.; Mercier, N.; and Hudhomme, P. *J. Org. Chem.* **2004**, *69*, 2164.

82. Bendikov, M.; Wudl, F.; Perepichka, D. F. *Chem. Rev.* **2004**, *104*, 4891.

83. Atienza, C.; Martín, N.; Wielopolski, M.; Haworth, N.; Clark, T.; Guldi, D. M. *Chem. Commun.* **2006**, 3202.

84. (a) Díaz, M. C.; Illescas, B. M.; Martín, N.; Perepichka, I. F.; Bryce, M. R.; Levillain, E.; Viruela, R.; Ortí, E. *Chem. Eur. J.* **2006**, *12*, 2709. (b) Perepichka, D. F.; Bryce, M. R.; McInnes, E. J. L.; Zhao, J. P. *Org. Lett.* **2001**, *3*, 1431.

85. Bryce, M. R.; de Miguel, P.; Devonport, W. *Chem. Commun.* **1998**, 2565.

86. Díaz, M. C.; Illescas, B. M.; Martín, N.; Viruela, R.; Viruela, P. M.; Ortí, E.; Brede, O.; Zilbermann, I.; Guldi, D. M. *Chem. Eur. J.* **2004**, *10*, 2067.

87. *Handbook of Oligo- and Polythiophenes*; Fichou, D., Ed.; WILEY-VCH: Weinheim, **1999**.

88. Roncali, J. *Chem. Rev.* **1992**, *92*, 711.

89. Mishra, A.; Ma, C.-Q.; Bäuerle, P. *Chem. Rev.* **2009**, *109*, 1141.

90. *TTF Chemistry: Fundamentals and Applications of Tetrathiafulvalene*; Yamada, J., Sugimoto, T., Eds.; Springer-Verlag: Berlin, **2004**.

91. Yamada, J.; Akutsu, H.; Nishikawa, H.; Kikuchi, K. *Chem. Rev.* **2004**, *104*, 4891.

92. Li, H.; Lambert, C. *Chem. Eur. J.* **2006**, *12*, 1144.

93. Mas-Torrent, M.; Durkut, M.; Hadley, P.; Ribas, X.; Rovira, C. *J. Am. Chem. Soc.* **2004**, *126*, 984.

94. Ohta, A.; Kobayashi, T.; Kato, H. *J. Chem. Soc. Perkin Trans.* 1 **1993**, 905.

95. Roncali, J.; Giffard, M.; Frère, P.; Jubault, M.; Gorgues, A. *Chem. Commun.* **1993**, 689.

96. Benahmed-Gasmi, A.; Frère, P.; Elandaloussi, E.H.; Roncali, J.; Orduna, J.; Garín, J.; Jubault, M.; Riou, A.; Gorgues, A. *Chem. Mater.* **1996**, *8*, 2291.

97. Leriche, P.; Raimundo, J-M.; Turbiez, M.; Mouroche, V.; Allain, M.; Sauvage, F-X.; Roncali, J.; Frère, P.; and Skabara, P. J. *J. Mater.Chem.* **2003**, *13*, 1324.

98. Zhao, C.; Zhang, Y.; Ng, M.-K. *J. Org. Chem.* **2007**, *72*, 6364.

99. Zhao, C.; Chen, X.; Zhang, Y.; Ng, M.-K. *J. Polym. Sci.: Part A: Polym. Chem.* **2008**, *46*, 2680.

100. Shao, M.; Chen, G.; Zhao, Y. *Synlett.* **2008**, 371.

101. Zhou, Q. *J. Am. Chem. Soc.* **1995**, *117*, 12593.

102. Gruhn, N. E.; Macías-Ruvalcaba, N. A.; Evans, D. H. *Langmuir* **2006**, *22*, 10683.

103. Skabara, P. J.; Roberts, D. M.; Serebryakov, I. M.; Pozo-Gonzalo, C. *Chem. Commun.* **2000**, 1005.

104. Bendikov, M.; Wudl, F.; Perepichka, D. F. *Chem. Rev.* **2004**, *104*, 4891.

105. Jelinek, R.; Kolusheva, S. *Chem. Rev.* **2004**, *104*, 5987.

106. Moschou, E. A.; Sharma, B. V.; Deo, S. K.; Daunert, S. J. *Fluorescence* **2004**, *14*, 535.

107. James, T. D. In *Boronic Acids Preparation, Applications in Organic Synthesis and Medicine*; Hall, D., Ed.;Wiley-VCH: Weinheim, **2005**.

108. James, T. D.; Phillips, M. D.; Shinkai, S. *Boronic Acids in Saccharide Recognition*; The Royal Society of Chemistry: Cambridge, **2006**.

109. Mader, H. S.; Wolfbeis, O. S. *Microchim. Acta* **2008**, *162*, 1.

110. (a) Tsukagoshi, K.; Shinkai, S. *J. Org. Chem.* **1991**, *56*, 4089. (b) Sandanayake, K. R. A. S.; James, T. D.; Shinkai, S. *Pure Appl. Chem.* **1996**, *68*, 1207. (c) Sugasaki, A.; Sugiyasu, K.; Ikeda, M.; Takeuchi, M.; Shinkai, S. *J. Am. Chem. Soc.* **2001**, *123*, 10239. (d) Takeuchi, M.; Mizuno, T.; Shinkai, S.; Shirakami, S.; Itoh, T. *Tetrahedron*: *Asymmetry* **2000**, *11*, 3311. (e) Zhao, J.; Fyles, T. M.; James, T. D. *Angew. Chem. Int. Ed.* **2004**, *43*, 3461.

111. (a) Takeuchi, M.; Kijima, H.; Hamachi, I.; Shinkai, S. *Bull. Chem. Soc. Jpn.* **1997**, *70*, 699. (b) Shinmori, H.; Takeuchi, M.; Shinkai, S. *J. Chem. Soc. Perkin Trans. 2* **1998**, 847. (c) Ward, C. J.; Patel, P.; James, T. D. *J. Chem. Soc. Perkin Trans. 1* **2002**, 462. (d) Camara, J. N.; Suri, J. T.; Cappuccio, F. E.; Wessling, R. A.; Singaram, B. *Tetrahedron Lett.* **2002**, *43*, 1139.

112. (a) Ori, A.; Shinkai, S. *J. Chem. Soc., Chem. Commun.* **1995**, 1771. (b) Arimori, S.; Ushiroda, S.; Peter, L. M.; Jenkins, A. T. A.; James, T. D. *Chem. Commun.* **2002**, 2368.

113. (a) James, T. D.; Sandanayake, K. R. A. S.; Shinkai, S. *Ange. Chem. Int. Ed.* **1996**, *35*, 1910. (b) James, T. D.; Linnane, P.; Shinkai, S. *Chem. Commun.* **1996**, 281. Other saccharide sensors operated by multiple hydrogen bonds also have been reported: (c) Davis, A. P.; Wareham, R. S. *Angew. Chem. Int. Ed.* **1999**, *38*, 2978 and further references therein. (d) Fang, J.; Selvi, S.; Liao, J.; Slanina, Z.; Chen, C.; Chou, P. *J. Am. Chem. Soc.* **2004**, *126*, 3559.

114. (a) Nagase, T.; Nakata, E.; Shinkai, S.; Hamachi, I. *Chem. Eur. J.* **2003**, *9*, 3660. (b) Nakata, E.; Nagase, T.; Shinkai, S.; Hamachi, I. *J. Am. Chem. Soc.* **2004**, *126*,

490. (c) Arimori, S.; Consiglio, G. A.; Phillips, M. D.; James, T. D. *Tetrahedron Lett.* **2003**, *44*, 4789. (d) Arimori, S.; Phillips, M. D.; James, T. D. *Tetrahedron Lett.* **2004**, *45*, 1539. (e) Arimori, S.; Bell, M. L.; Oh, C. S.; James, T. D. *Org. Lett.* **2002**, *4*, 4249. (f) Yang, W.; Yan, J.; Fang, H.; Wang, B. *Chem. Commun.* **2003**, 792. (g) Zhao, J.; Davidson, M. G.; Mahon, M. F.; Kociok-knhn, G.; James, T. D. *J. Am. Chem. Soc.* **2004**, *126*, 16179.

115. (a) Gao, X.; Zhang, Y.; Wang, B. *Org. Lett.* **2003**, *5*, 4615. (b) DiCesare, N.; Lakowicz, J. R. *J. Phys. Chem. A* **2001**, 6834. (c) DiCesare, N.; Lakowicz, J. R. *Tetrahedron Lett.* **2002**, *43*, 2615. (d) Yang, W.; Yan, J.; Springsteen, G.; Deeter, S.; Wang, B. *Bioorg. Med. Chem. Lett.* **2003**, *13*, 1019.

116. (a) Moore, A. N. J.; Wayner, D. D. M. *Can. J. Chem.*, **1999**, *77*, 681. (b) Tucker, J. H. R.; Collinson, S. R. *Chem. Soc. Rev.* **2002**, *31*, 147.

117. Arimori, S.; Bosch, L. I.; Ward, C. J.; James, T. D. *Tetrahedron Lett.* **2001**, *42*, 4553.

118. (a) Shoji, E.; Freund, M. S. *J. Am. Chem. Soc.* **2002**, *124*, 12486. (b) Deore, B. A.; Braun, M. D.; Freund, M. S. *Marcromol. Chem. Phys.* **2006**, *207*, 660.

119. Ori, A.; Shinkai, S. *Chem. Commun.* **1995**, 1771.

120. Arimori, S.; Ushiroda, S.; Peter, M. L.; Jenkins, A. T. A.; James, T. D. *Chem. Commun.* **2002**, 2368.

121. Bryce, M. R. *Adv. Mater.* **1999**, *11*, 11.

122. Bendikov, M.; Wudl, F.; Perepichka, D. F. *Chem. Rev.* **2004**, *104*, 4891.

123. Kolb, H. C.; Finn, M. G.; Sharpless, K. B. *Angew. Chem. Int. Ed.* **2001**, *40*, 2004.

124. Wu, P. A.; Feldman, K.; Nugent, A. K.; Hawker, C. J.; Scheel, A.; Voit, B.; J. Pyun, J.; Fréchet, M. J.; Sharpless, K. B.; Fokin, V. *Angew. Chem. Int. Ed.* **2004**, *43*, 3928.

125. Bock, V. D.; Hiemstra, H.; van Maarseveen, J. H. *Eur. J. Org. Chem.* **2006**, 51.

126. Wu, P.; Fokin, V. *Aldrichimica Acta* **2007**, *40*, 7.

127. Scrafton, D. K.; Taylor, J. E.; Mahon, M. F.; Fossey, J. S.; James, T. D. *J. Org. Chem.* **2008**, *73*, 2871.

128. Liu, W.; Li, X.; Li, Z. Y.; Zhang, M. L.; Song, M. P. *Inorg. Chem. Commun.* **2007,** *10*, 1485.

129. Xue, P.; Fu, E.; Wang, G. C.; Gao, C. Q.; Fang, M. H.; Wu, C. T. *J. Organometallic. Chem.* **2000**, *598*, 42.

130. Cui, X. L.; Carapuca, H. M.; Delgado, R.; Drew, M. G. B.; Félix, V. *Dalton Tran.* **2004**, 1743.

131. Saravanakumar, D.; Sengottuvelan, N.; Kandaswamy, M. *Inorg. Chem. Commun.* **2005**, *8*, 386.

132. Collinson, S. R.; Gelbrich, T.; Hursthoouse, M. B.; Tucker, J. H. R. *Chem Commun.* **2001**, 555.

133. Westwood, J.; Coles, S. J.; Collinson, S. R.; Gasser, G.; Green, S. J.; Hursthouose, M. B.; Light, M. E.; Tucker, J. H. R. *Organometallics* **2004**, *23*, 946.

134. Beer, P. D.; Gale, P. A. *Angew. Chem. Int. Ed.* **2001**, *40*, 486.

135. Monnereau, C.; Blart, E.; Odobel, F. *Tetrahedron Lett.* **2005**, *46*, 5421.

136. Smith, M. B.; Guo, L.; Okeyo, S.; Stenzel, J.; Yanella, J.; LaChapelle, E. *Org. Lett.* **2002**, *4*, 2321.

137. Sousa, L. R.; Larson, J. M. *J. Am. Chem. Soc.* **1977**, 307.

138. Silva, A. P.; de Silva, S. A. *Chem. Commun.* **1986**, 1709.

139. Fages, F.; Desvergne, J-P.; Bouas-Laurent, H.; Marsau, P.; Lehn, J-M.; Kotzyba-Hibert, F.; Albrecht-Gary, A-M.; Al-Joubbeh, M. *J. Am. Chem. Soc.* **1989**, *111*, 8672.

140. Konopelski, J. P.; Kotzyba-Hibert, F.; Lehn, J-M.; Desvergne, J-P.; Fagés, F.; Castellan, A.; Bouas-Laurent, H. *Chem. Commun.* **1985**, 433.

141. Huston, M. E.; Haider, K. W.; Czarnik, A. W. *J. Am. Chem. Soc.* **1988**, *110*, 4460.

142. Guidi, D. M.; Prato, M. *Acc. Chem. Res.* **2003**, *33*, 695.

143. de Silva, A. P.; Gunaratne, H. Q. N.; McCoy, C. P. *Nature* **1993**, *42*, 364.

144. Liu, W.; Lu, J.-H.; Ji, Y.; Zuo, J.-L.; You, X.-Z. *Tetrahedron Lett.* **2006**, *47*, 3431.

145. Bryce, M. R.; Batsanov, A. S.; Finn, T.; Hansen, T. K.; Moore, A. J.; Howard, J. A. K.; Kamenjicki, M.; Lednev. I. K.; Asher, S. A. *Eur. J. Org. Chem.* **2001**, 933.

146. Lindoy, L. F. The chemistry of macrocyclic ligand complexes. Cambridge University Press: Cambridge, **1989.**

147. (a) Blake, A. J.; Radek, C.; Schröder, M. *Chem. Commun.* **1992**, 1074; (b) Holdt, H.-J. *Pure Appl. Chem.* **1993**, *65*, 477.

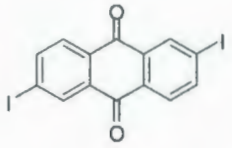

143

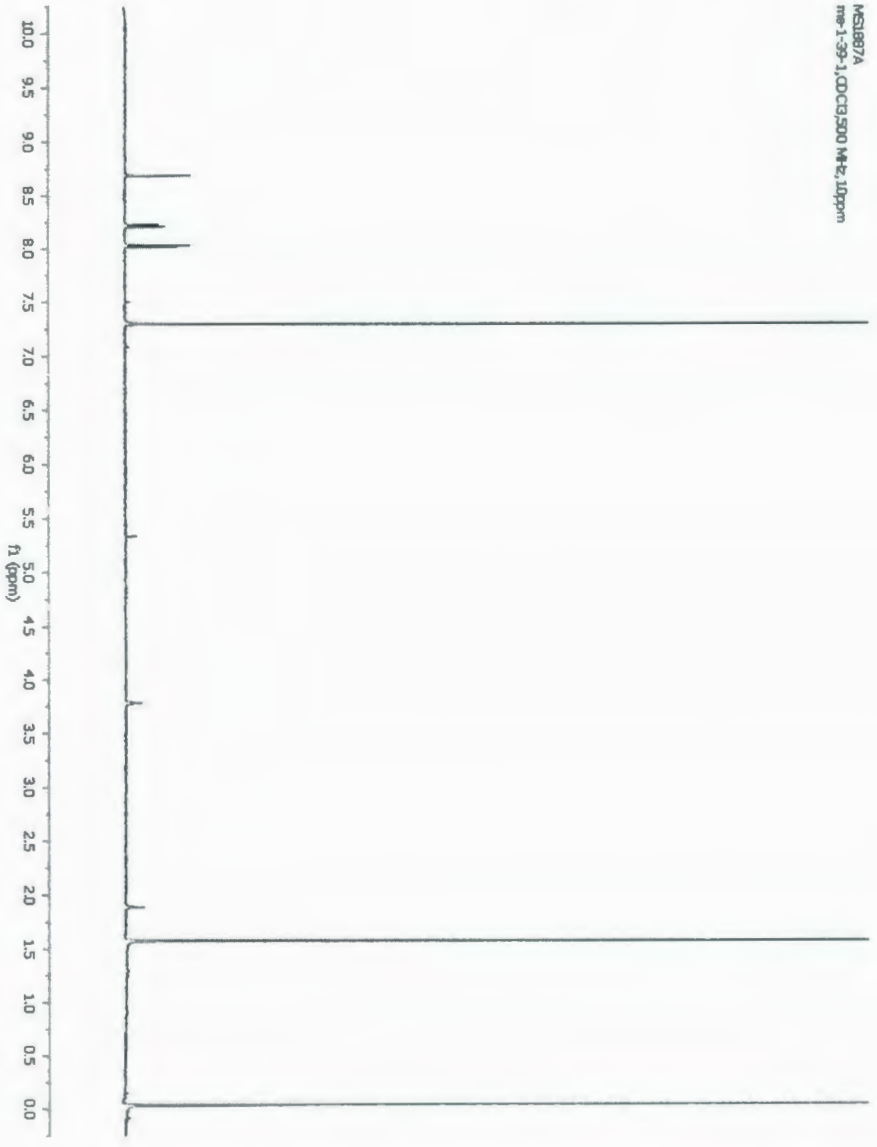

Figure A.1 ^{1}H NMR spectrum for **143**.

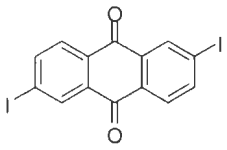

143

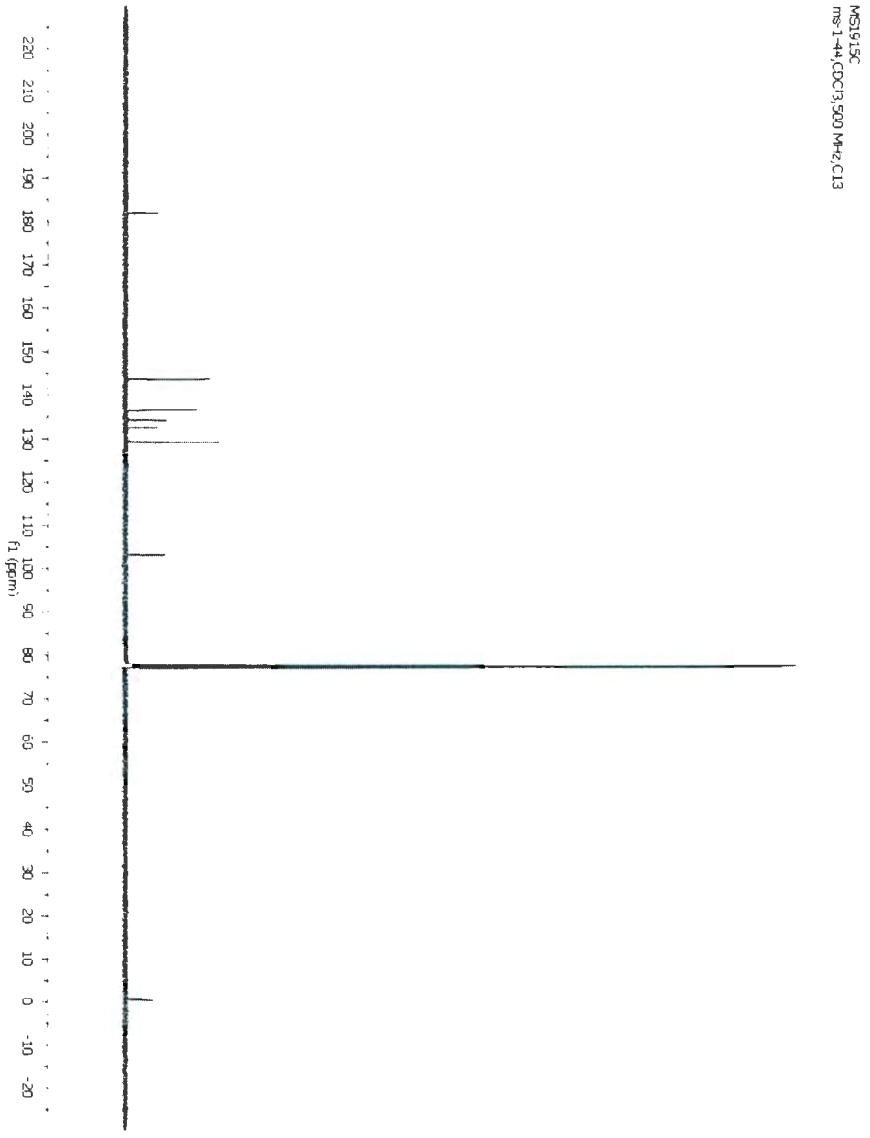

Figure A.2 ^{13}C NMR spectrum for **143**.

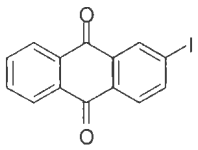

144

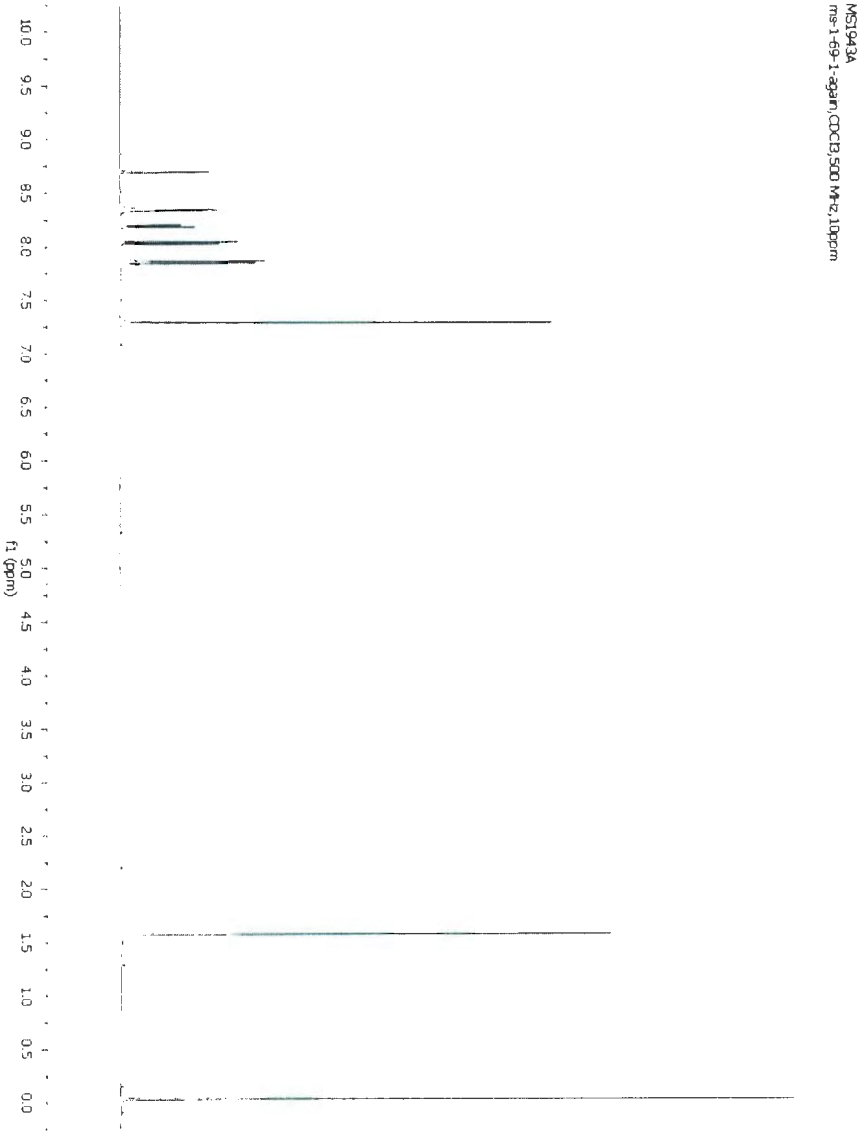

Figure A.3 ^{1}H NMR spectrum for **144**.

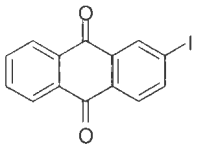

144

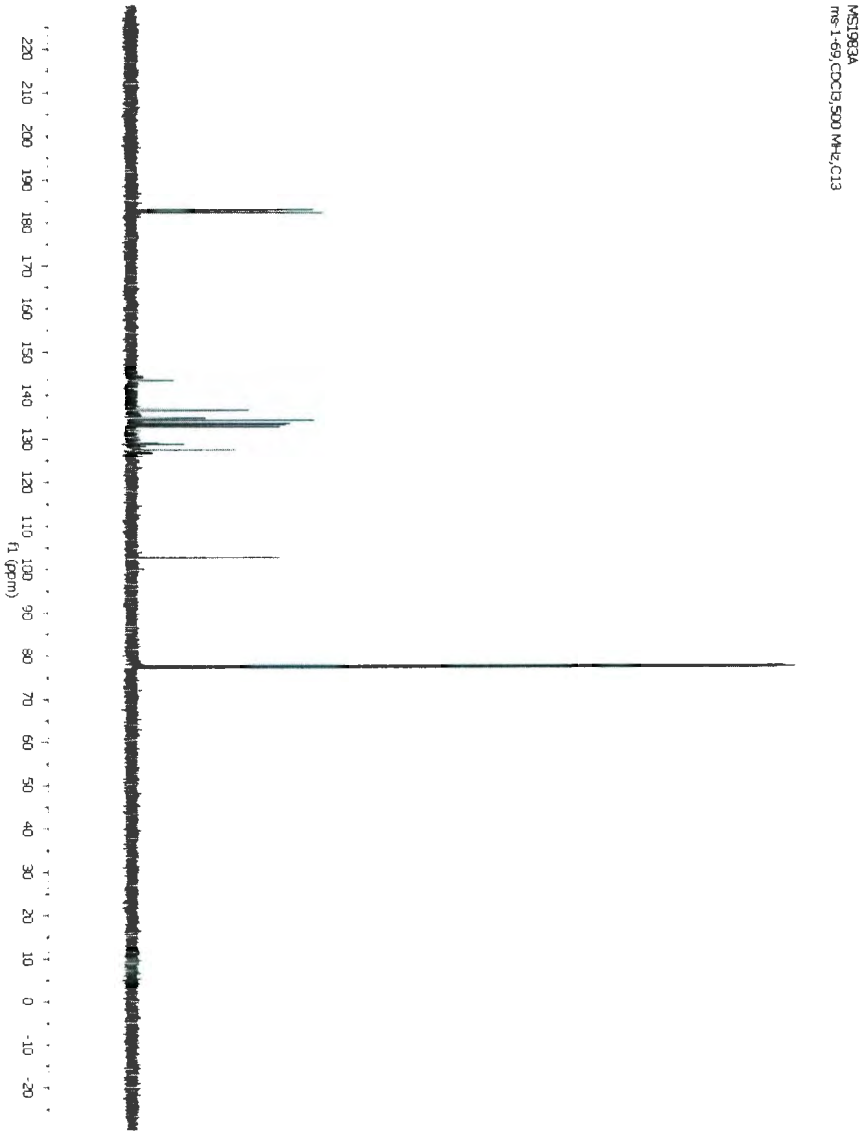

Figure A.4 ^{1}H NMR spectrum for **144**

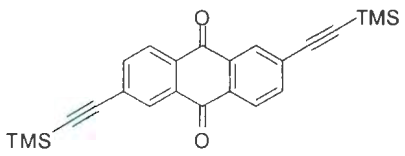

145

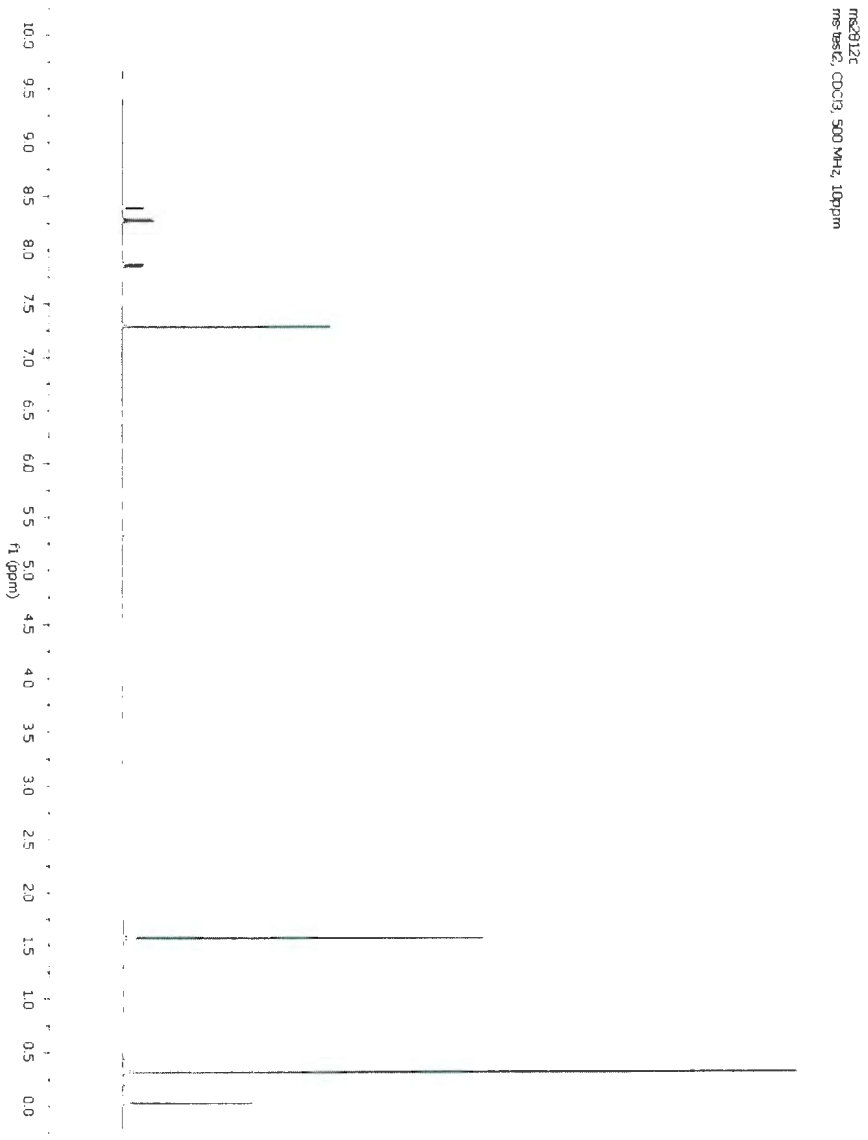

Figure A.5 ^{1}H NMR spectrum for **145**.

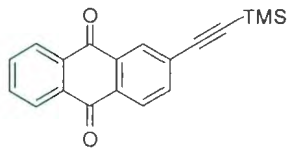

146

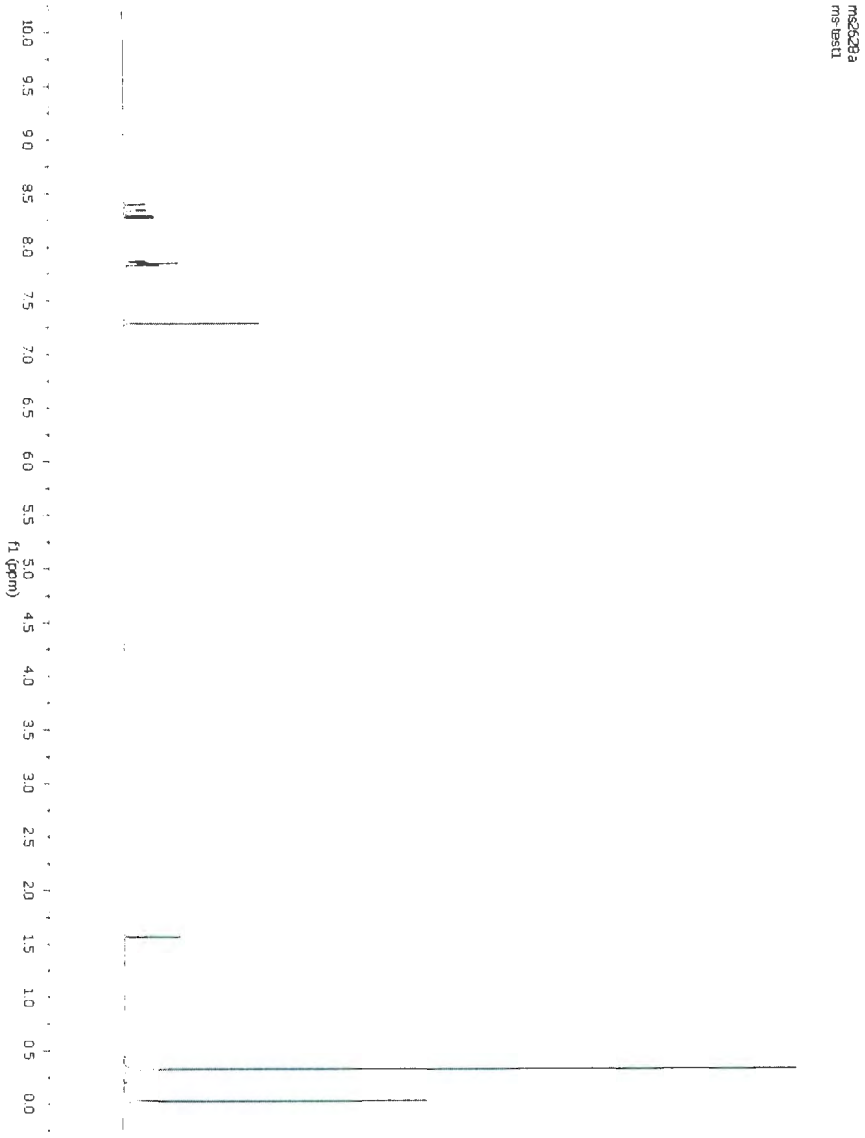

Figure A.6 ^{1}H NMR spectrum for **146**.

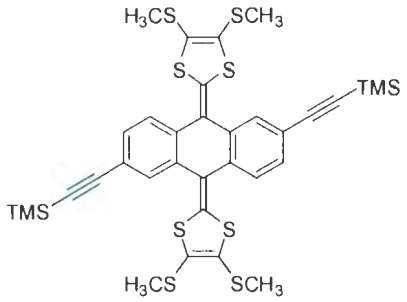

148a

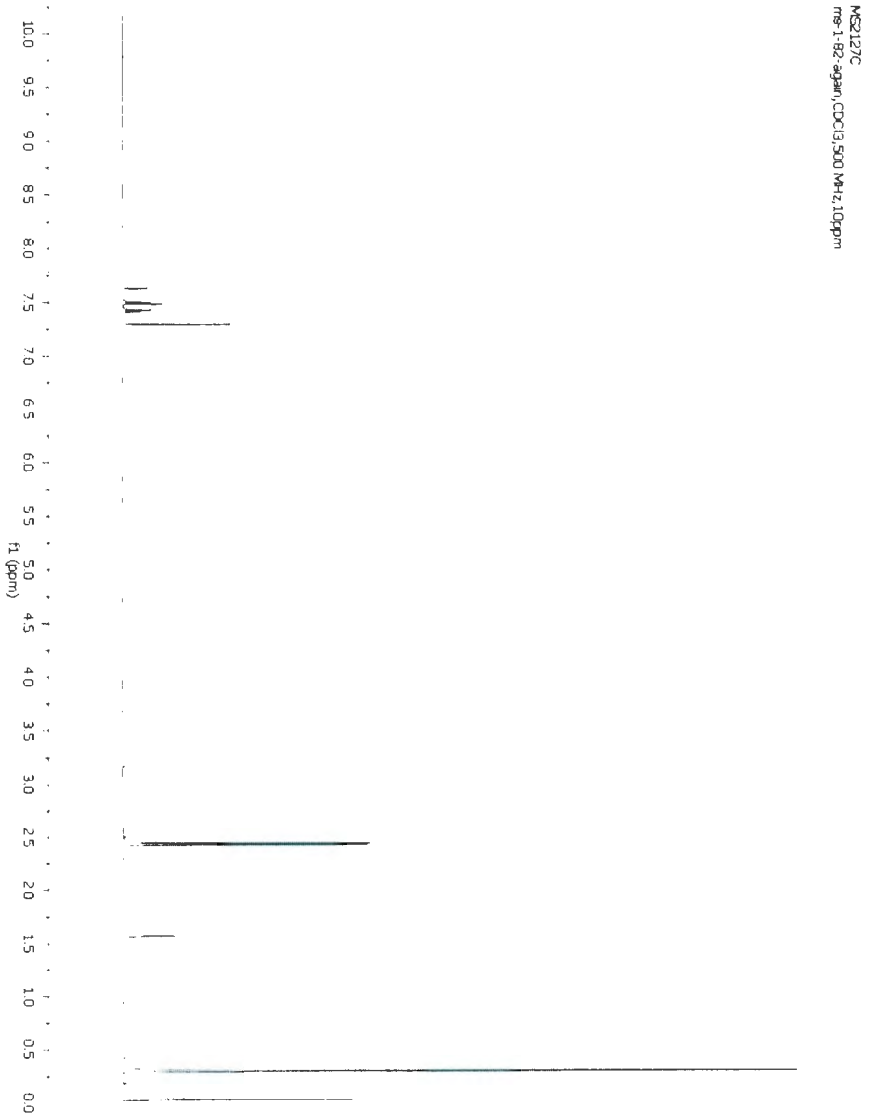

Figure A.7 ^{1}H NMR spectrum for **148a**.

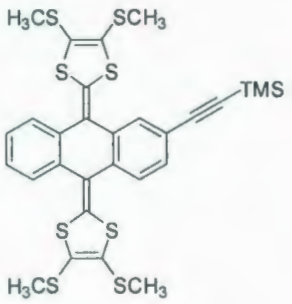

149a

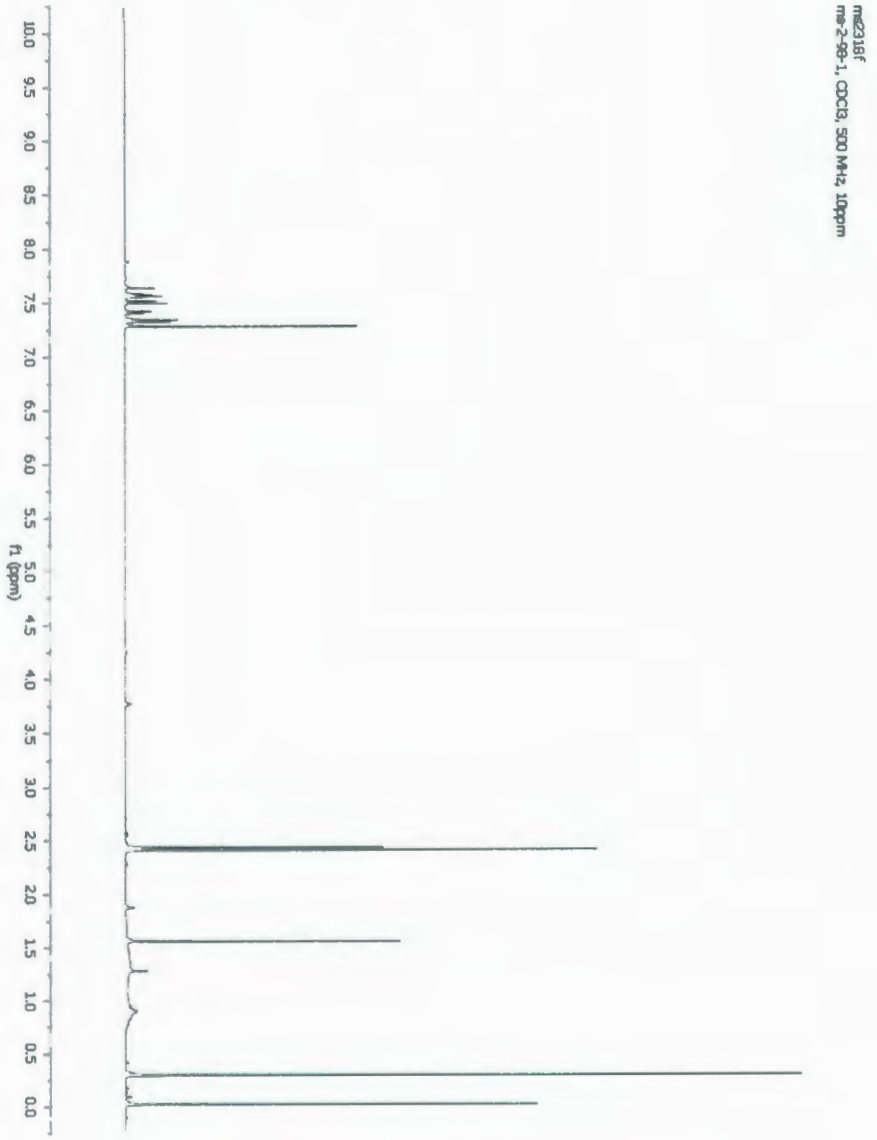

Figure A.8 ^{1}H NMR spectrum for **149a**.

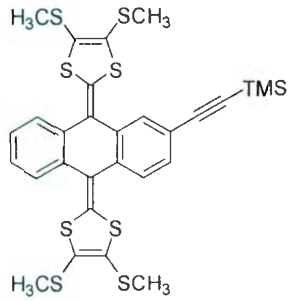

149a

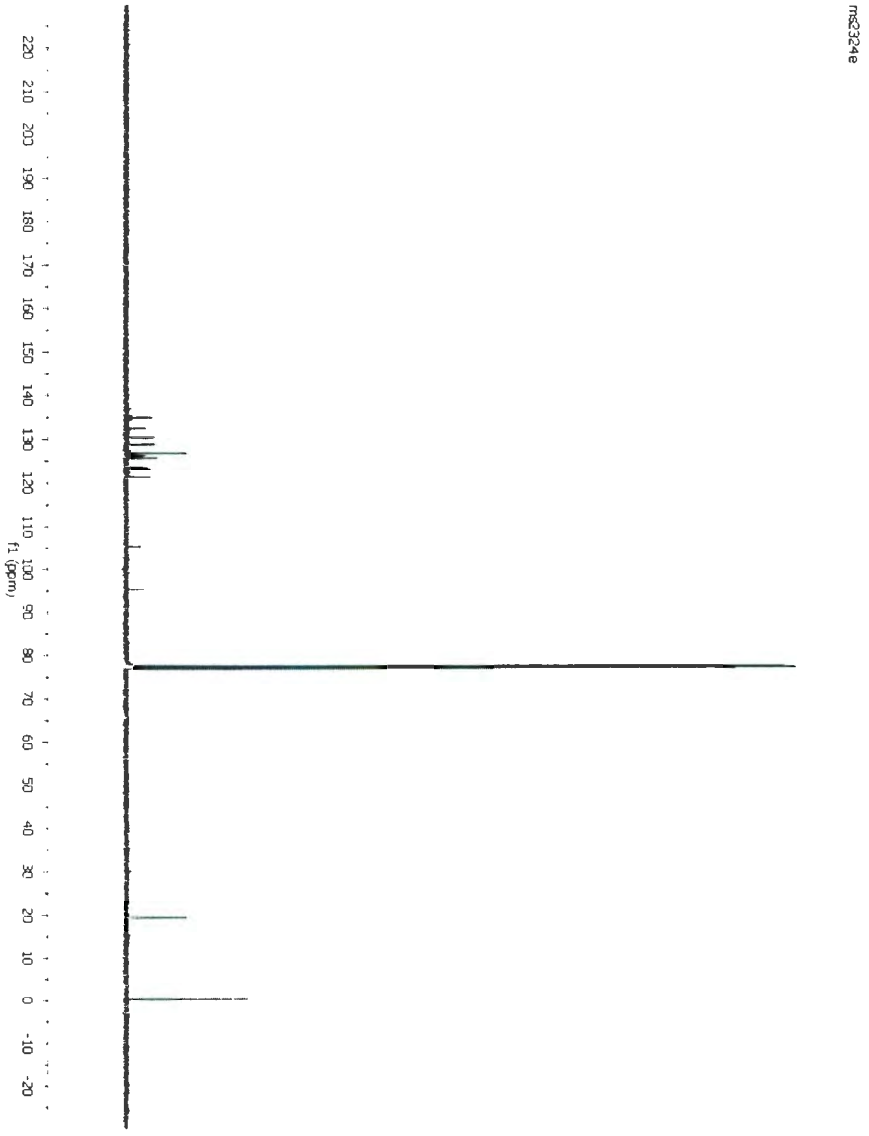

Figure A.9 ^{13}C NMR spectrum for **149a**.

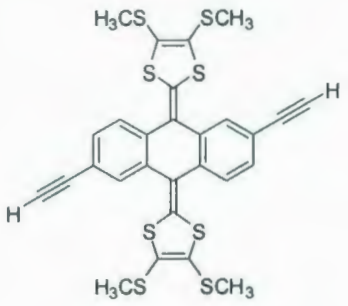

148b

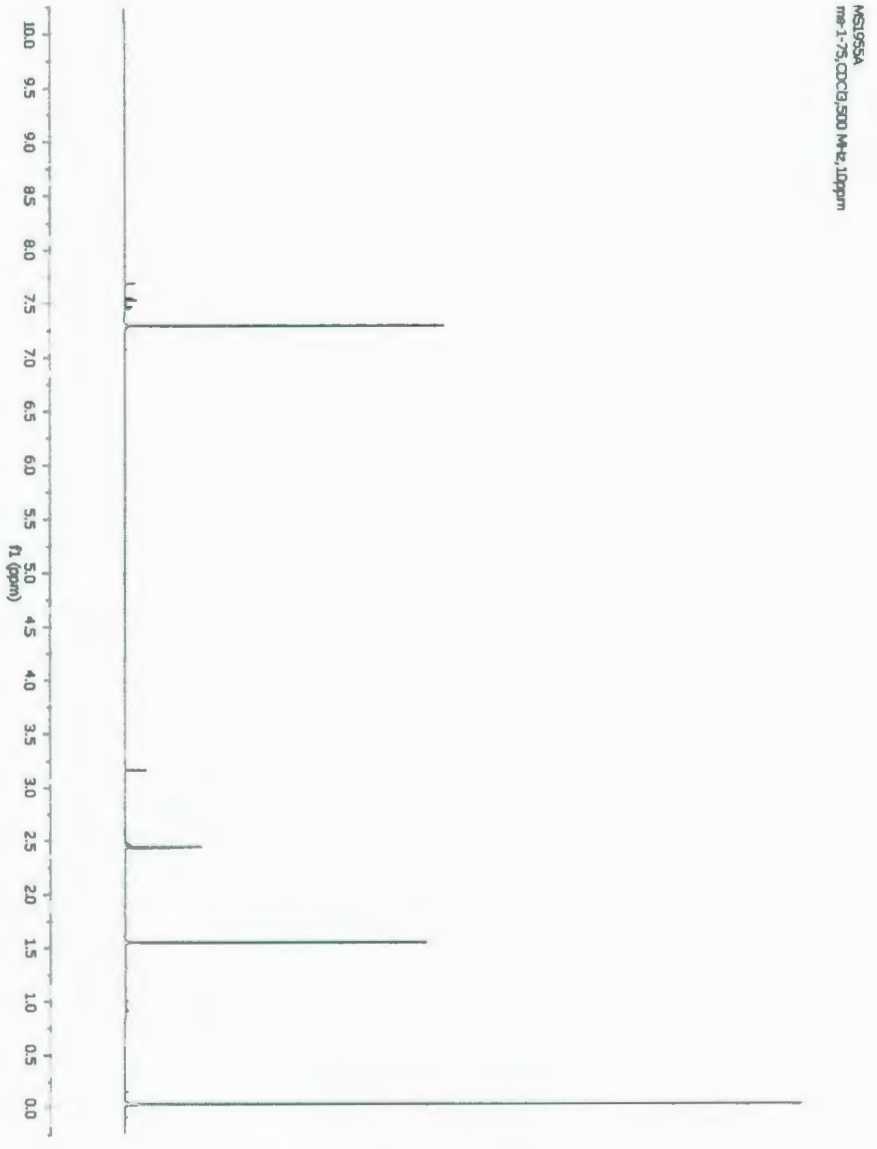

Figure A.10 ^{1}H NMR spectrum for **148b.**

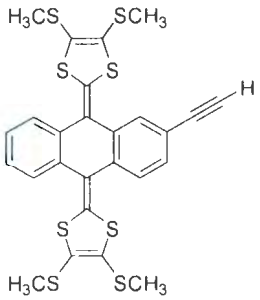

149b

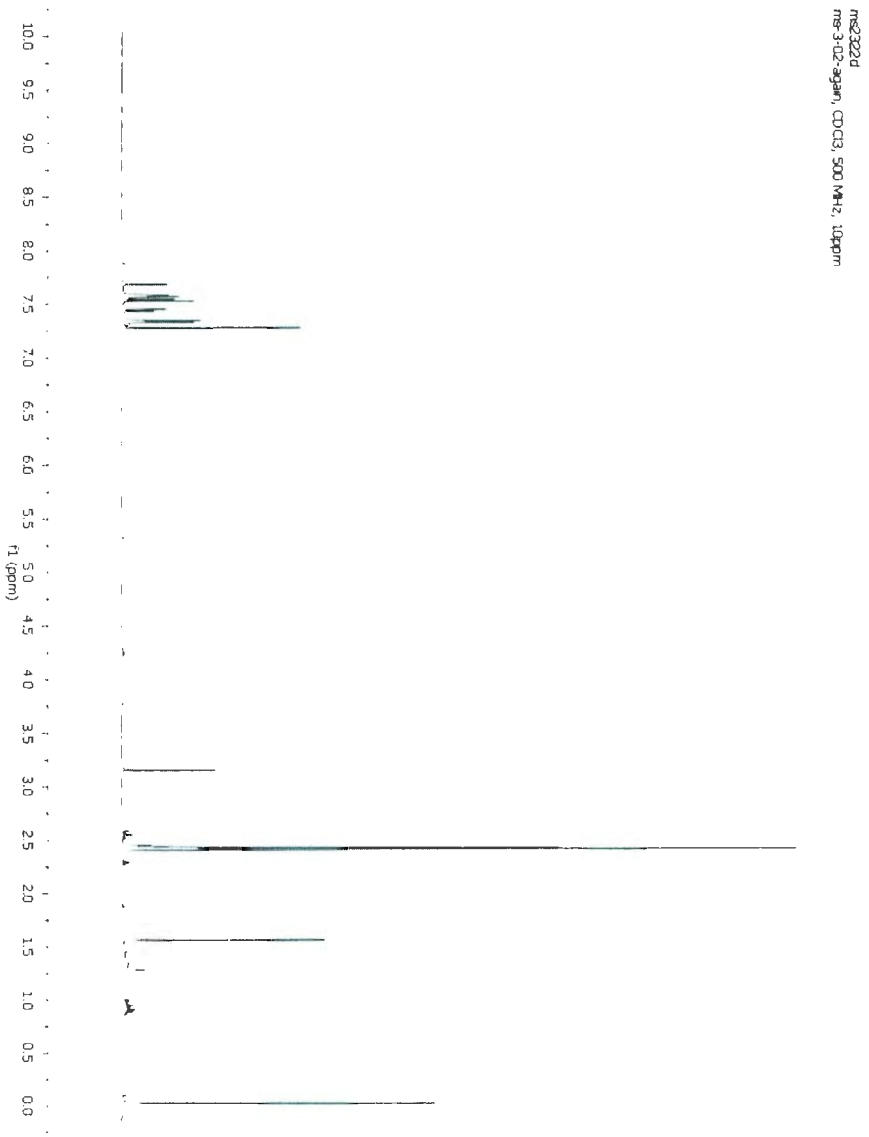

Figure A.11 ^{1}H NMR spectrum for **149b.**

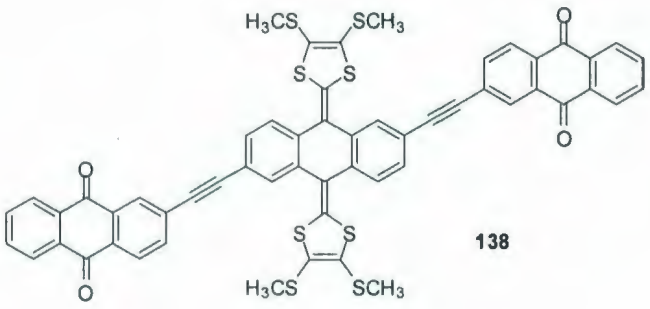

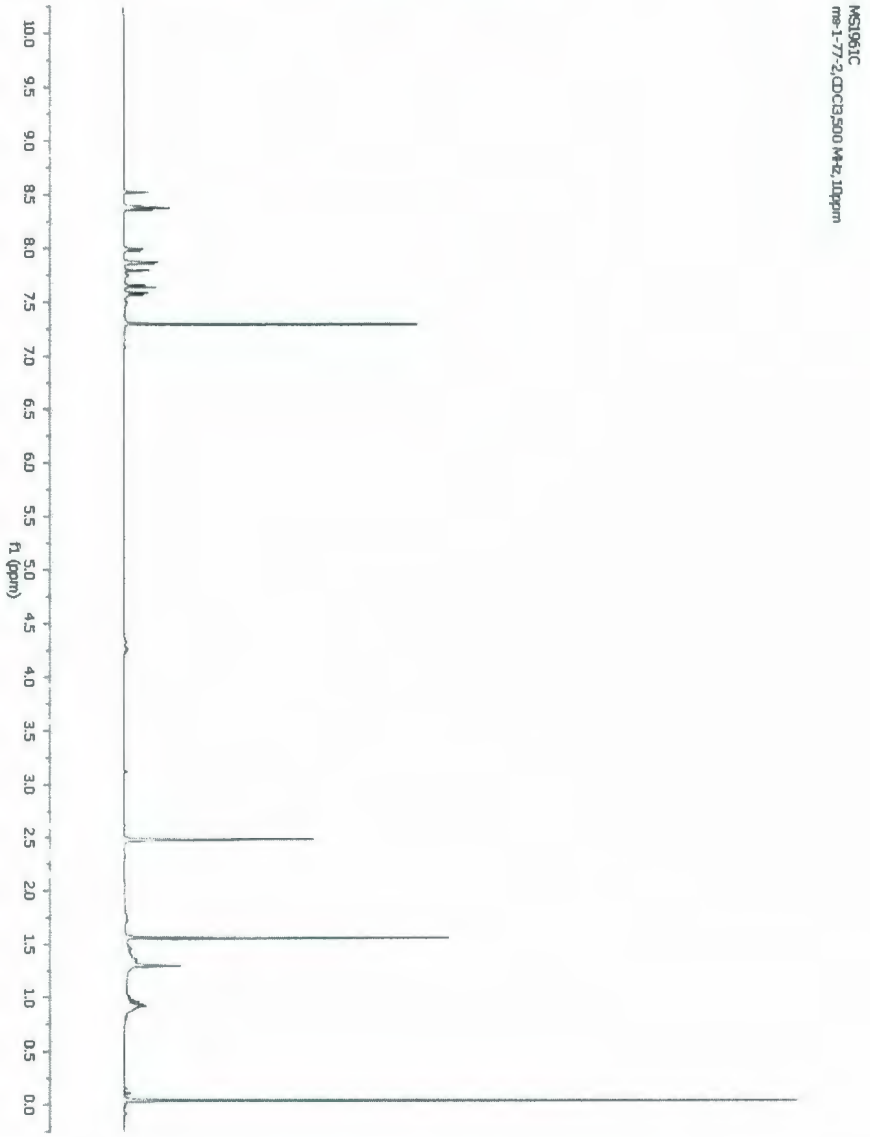

Figure A.12 ^{1}H NMR spectrum for **138.**

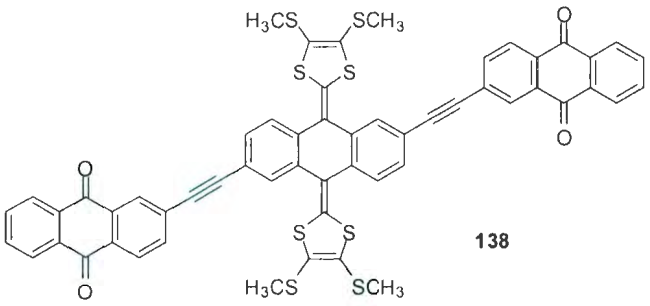

138

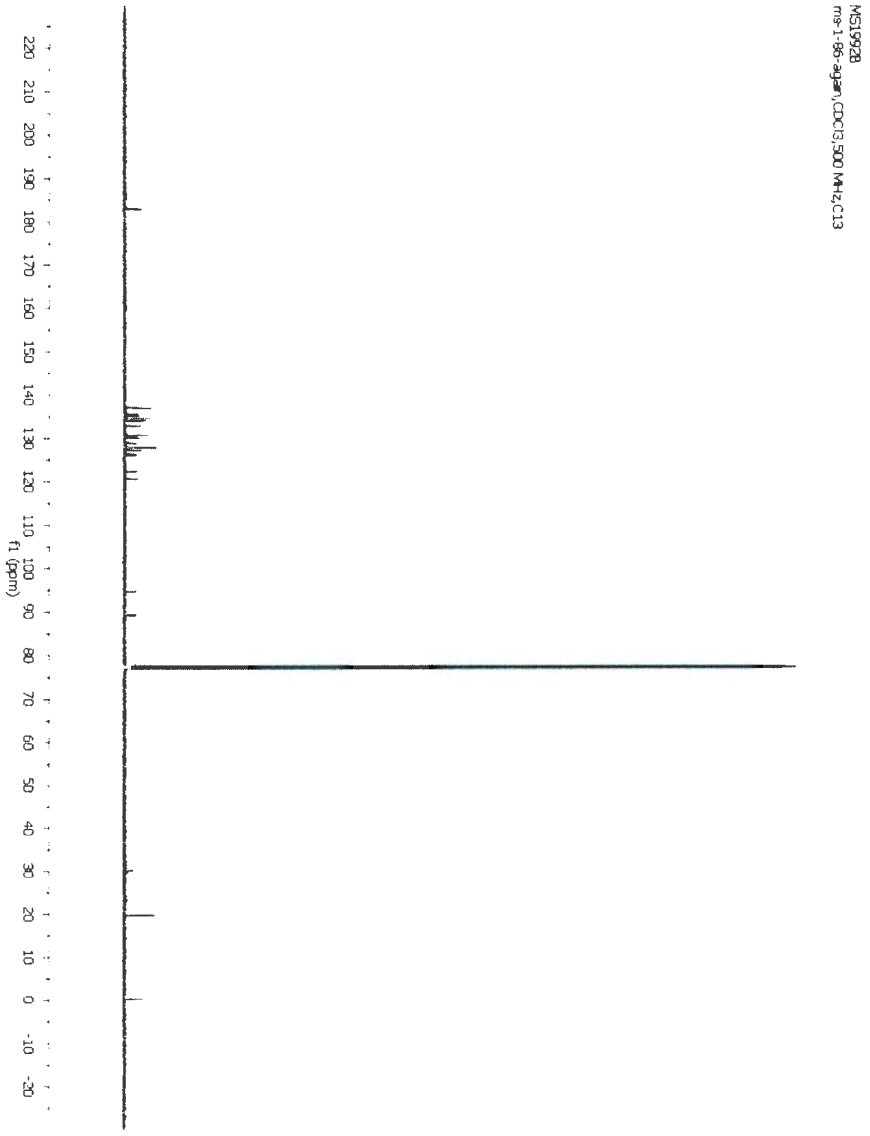

Figure A.13 ^{13}C NMR spectrum for **138.**

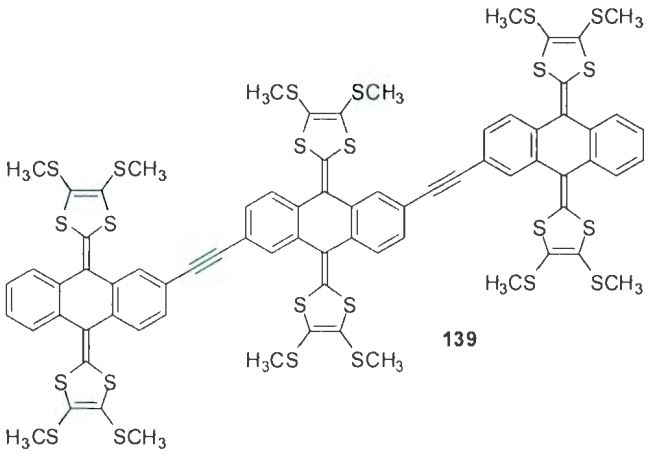

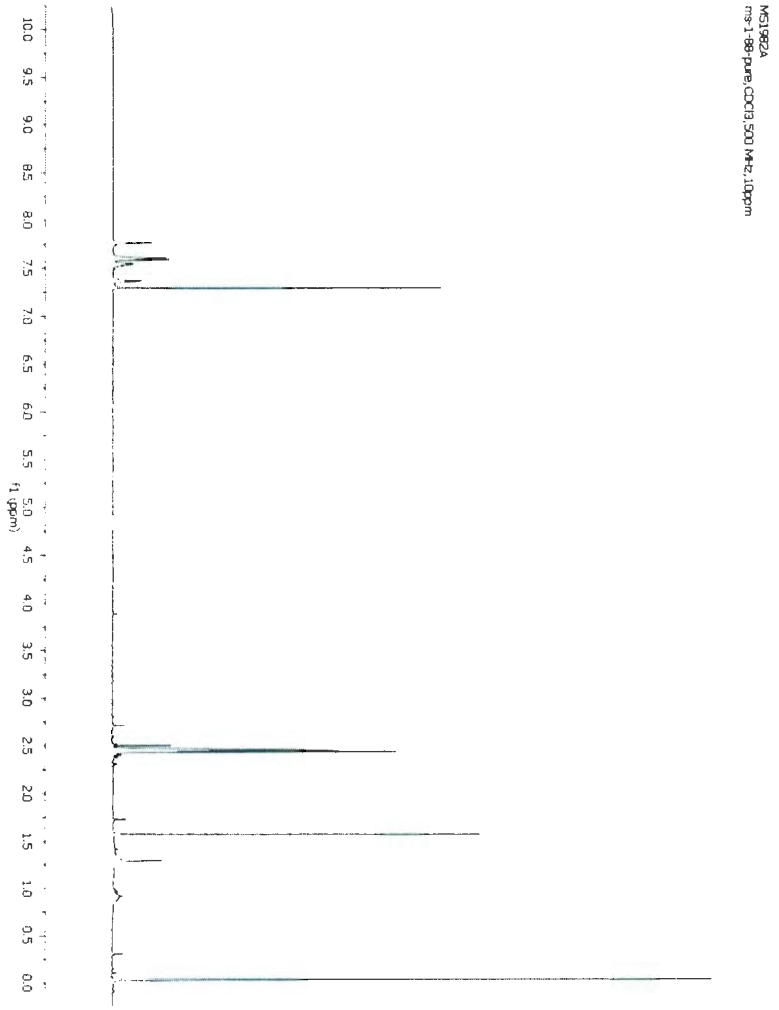

Figure A.14 ^{1}H NMR spectrum for **139.**

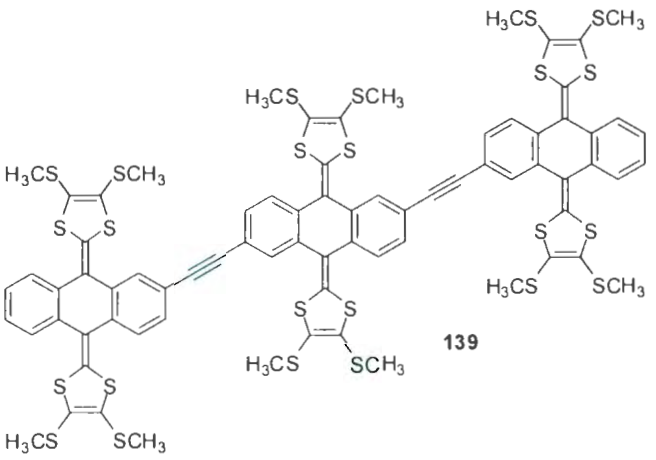

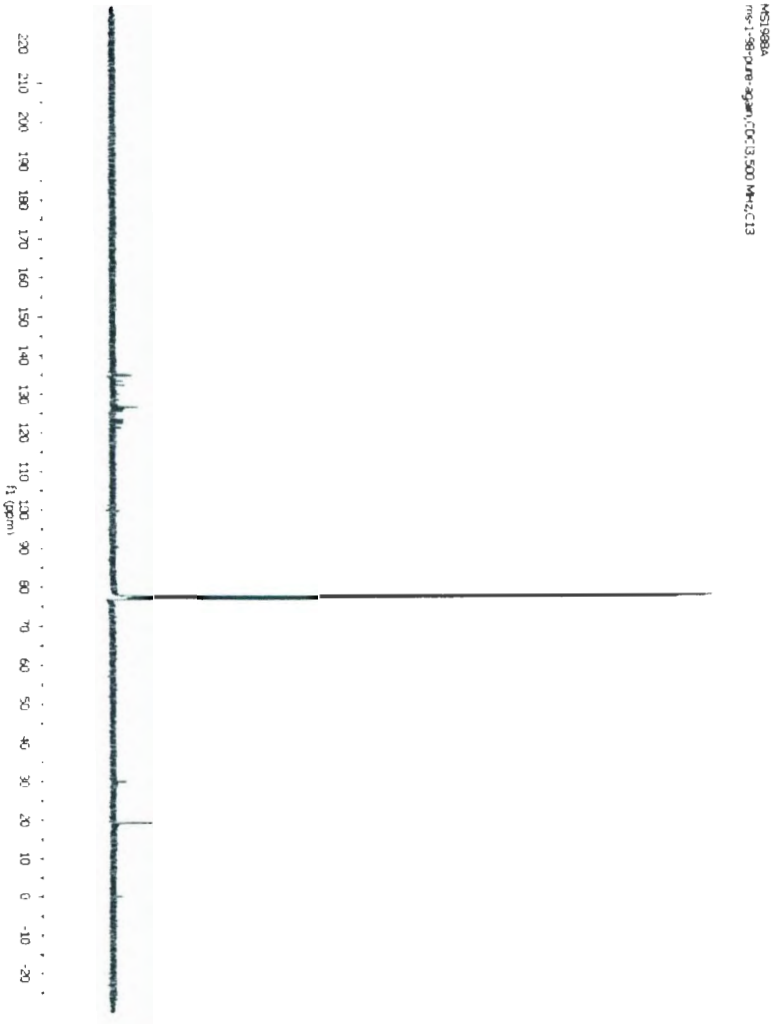

Figure A.15 ^{13}C NMR spectrum for **139.**

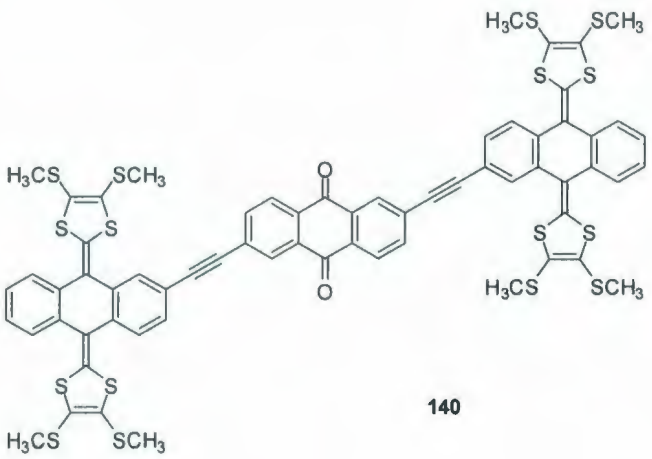

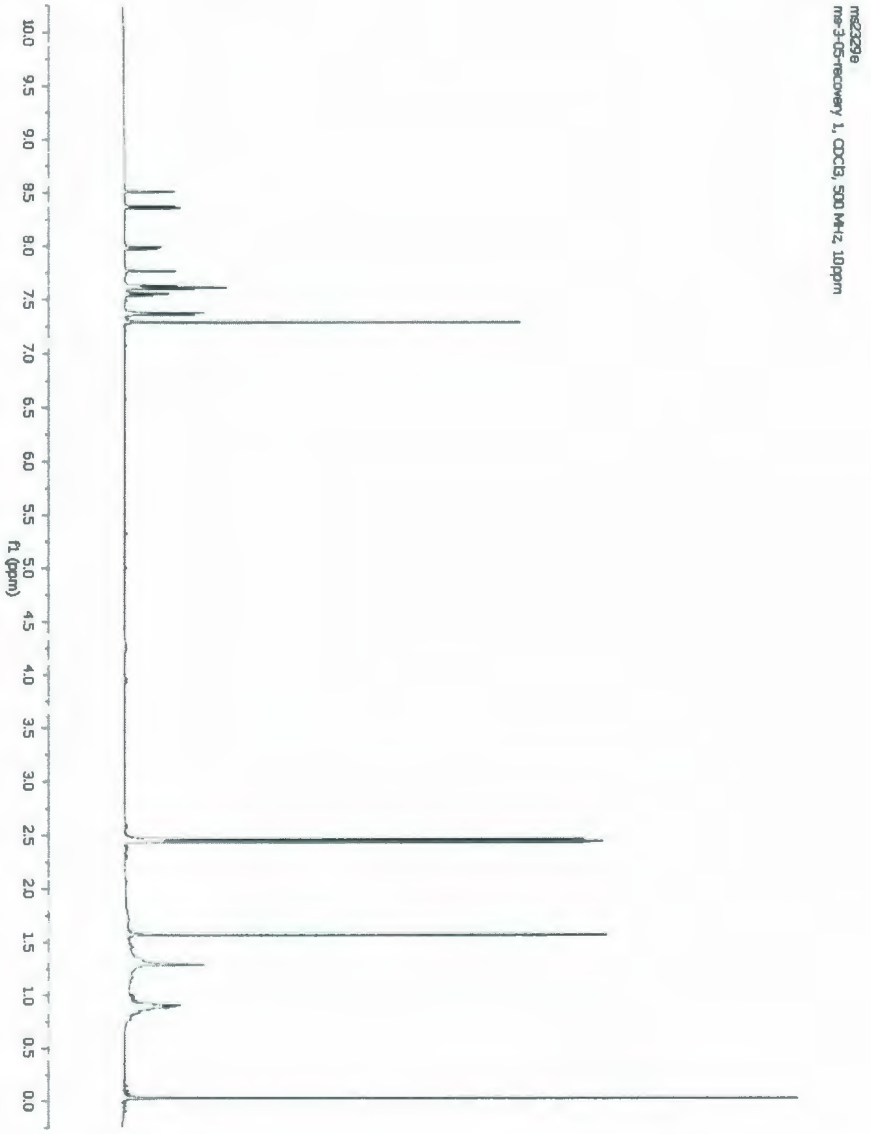

Figure A.15 ^{1}H NMR spectrum for **140.**

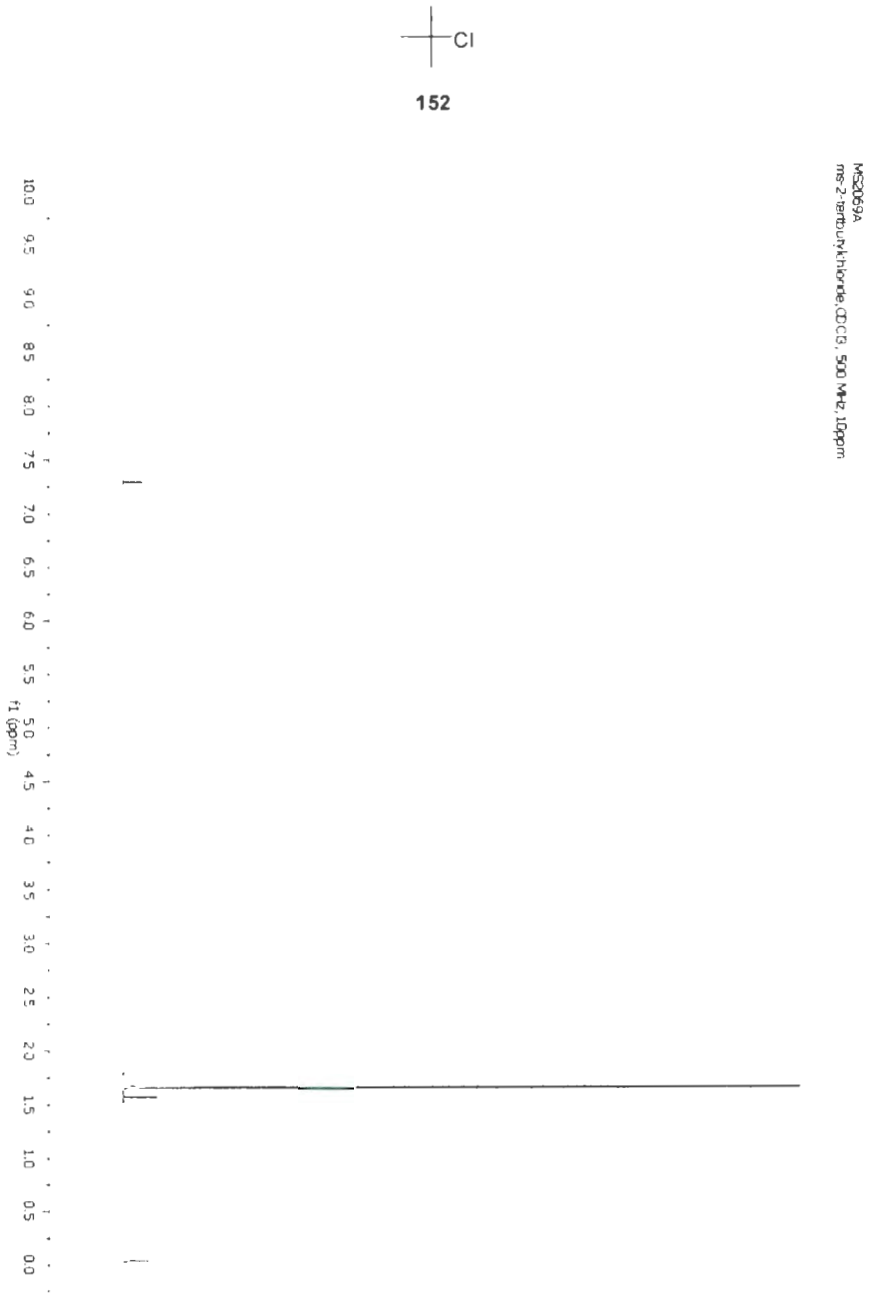

Figure A.16 ^{1}H NMR spectrum for **152.**

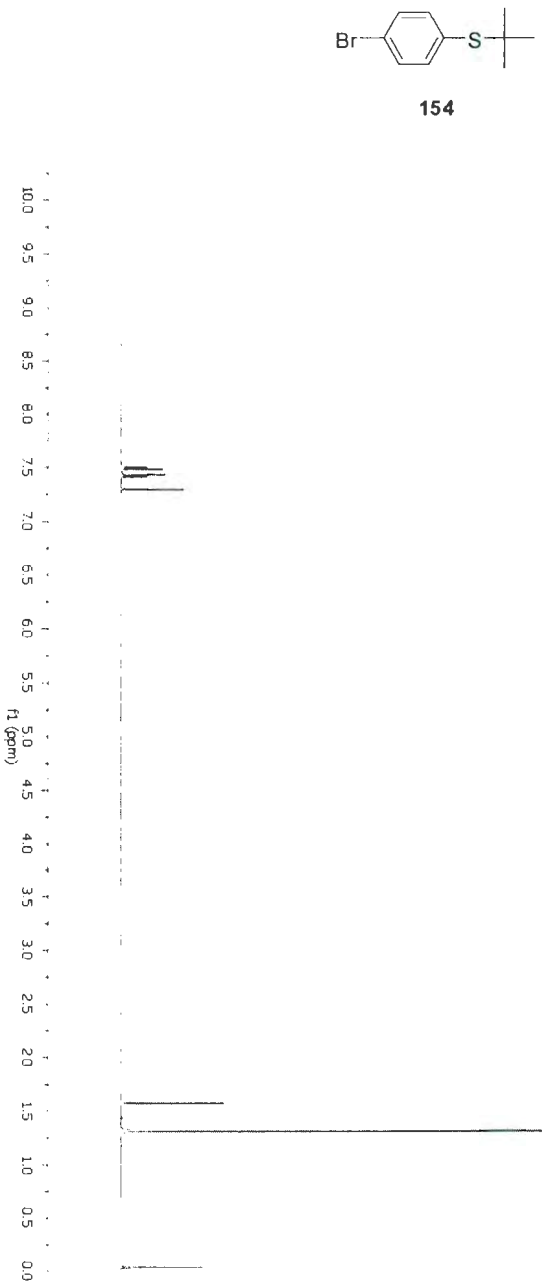

Figure A.17 ^{1}H NMR spectrum for **154.**

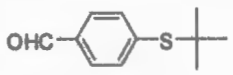

155

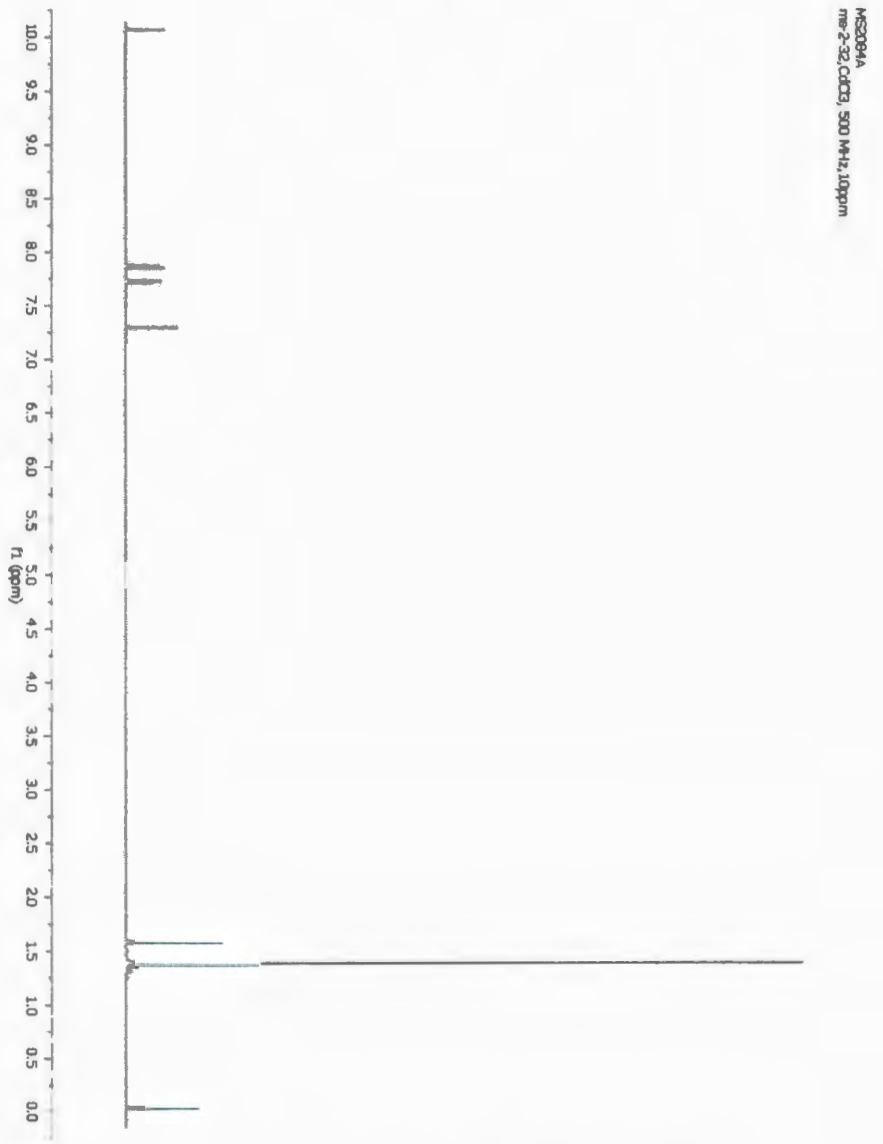

Figure A.18 ^{1}H NMR spectrum for **155.**

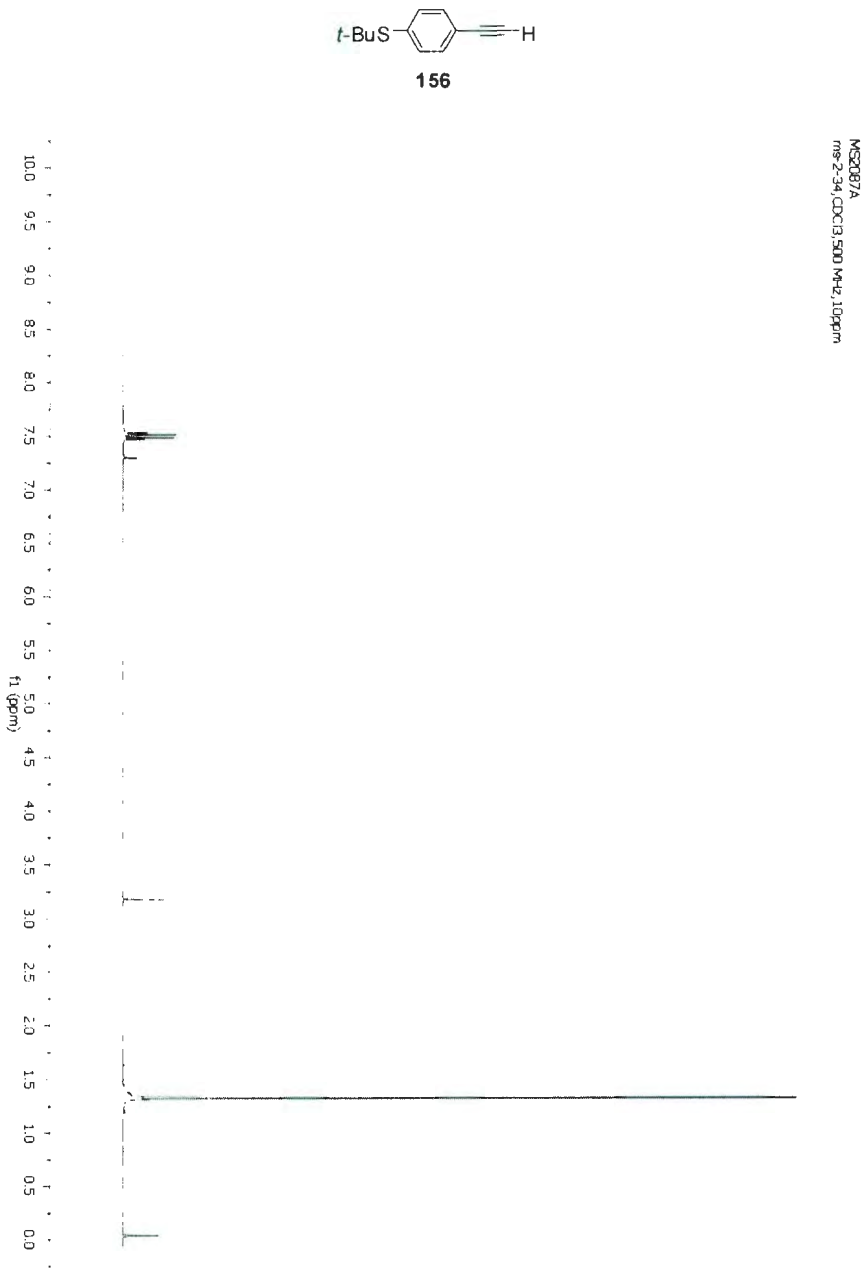

Figure A.19 ^{1}H NMR spectrum for **156.**

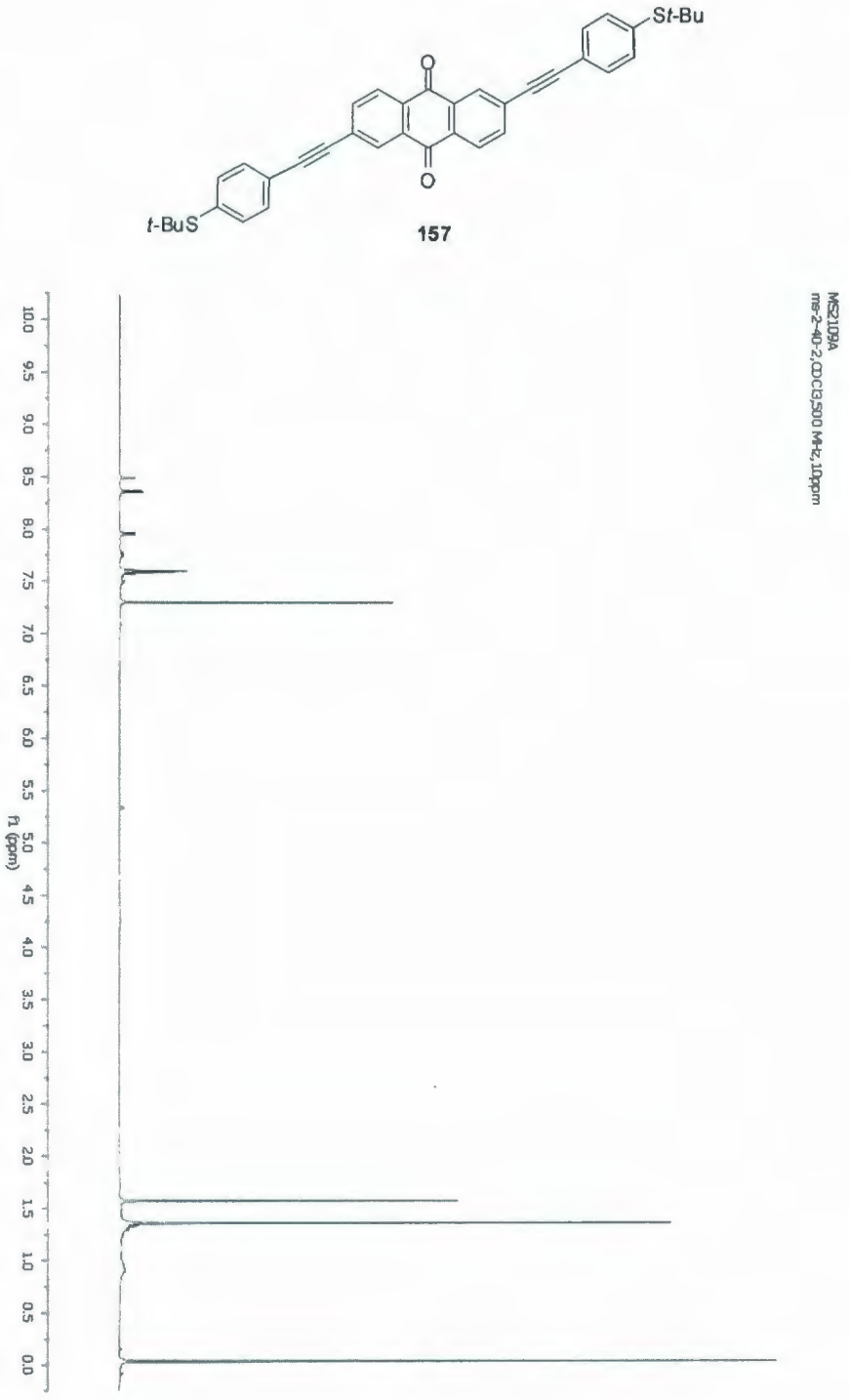

Figure A.20 ^{1}H NMR spectrum for **157.**

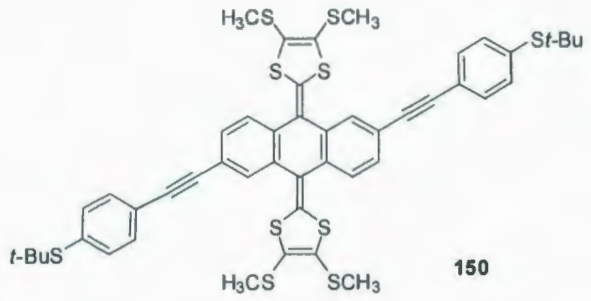

150

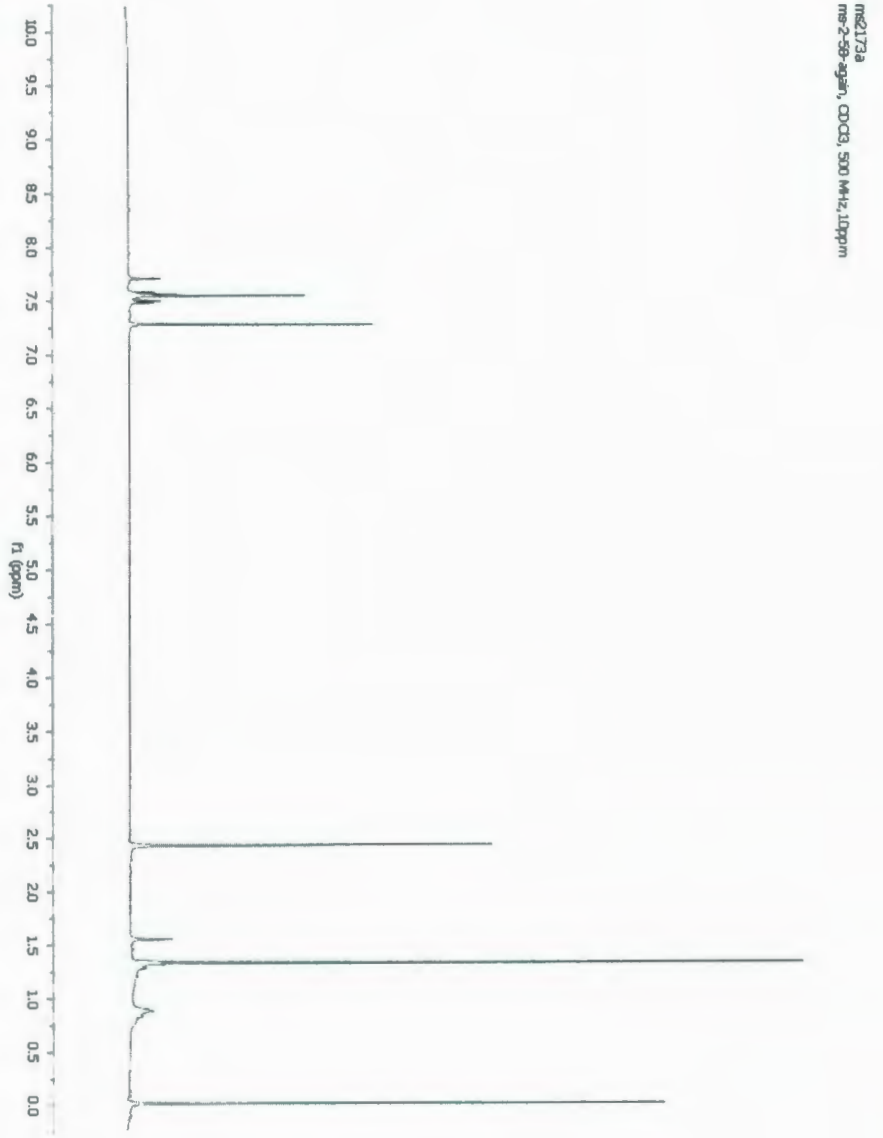

Figure A.21 ^{1}H NMR spectrum for **150.**

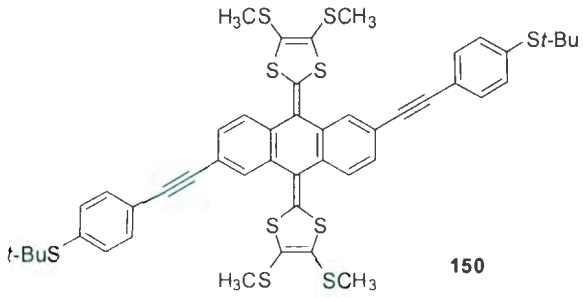

150

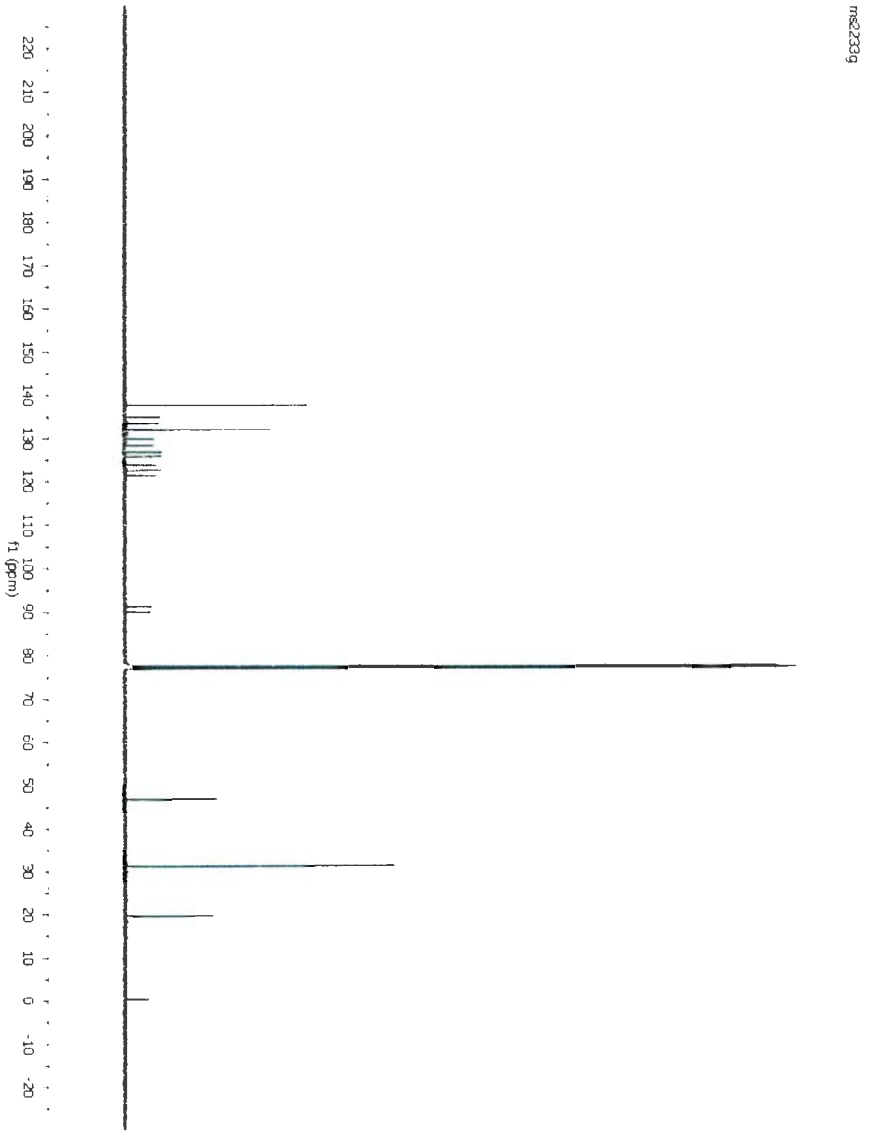

Figure A.22 ^{13}C NMR spectrum for **150.**

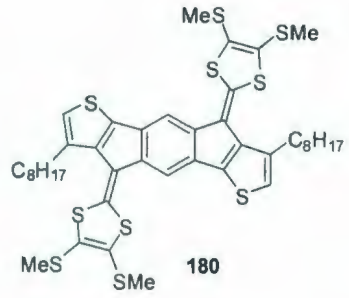

180

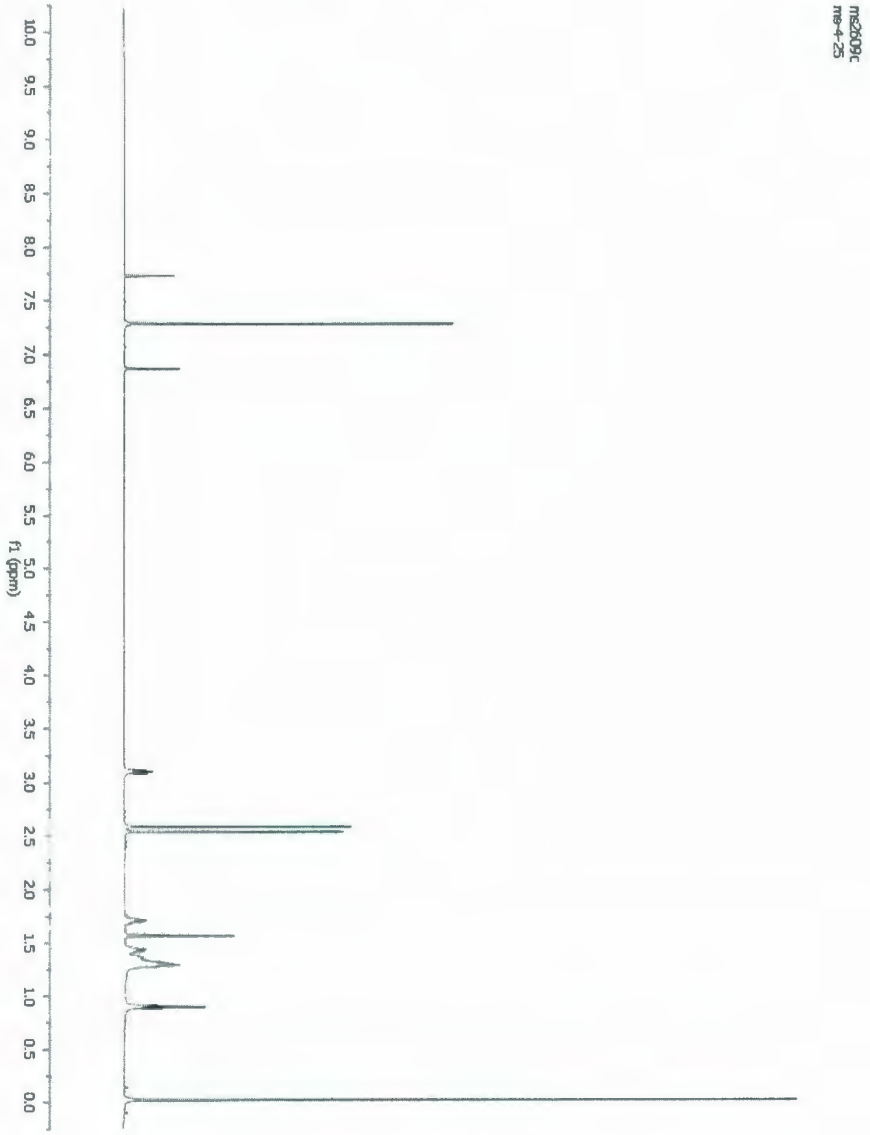

Figure A.23 ^{1}H NMR spectrum for **180.**

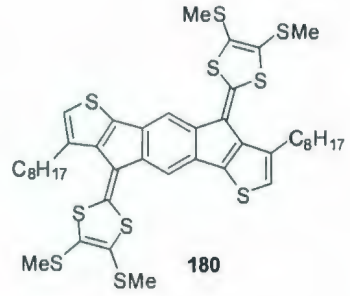

180

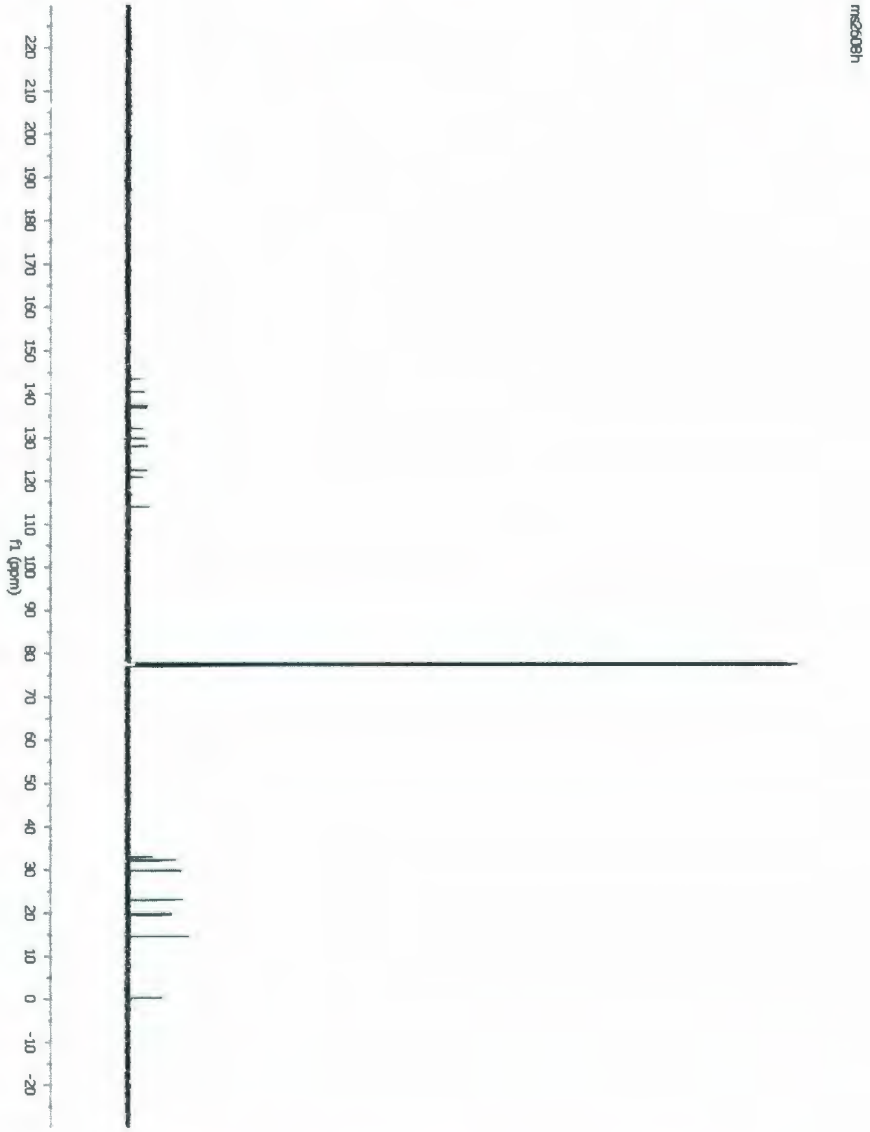

Figure A.24 ^{13}C NMR spectrum for **180.**

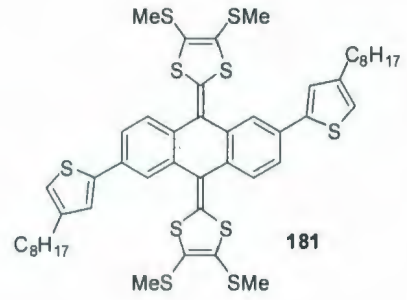

181

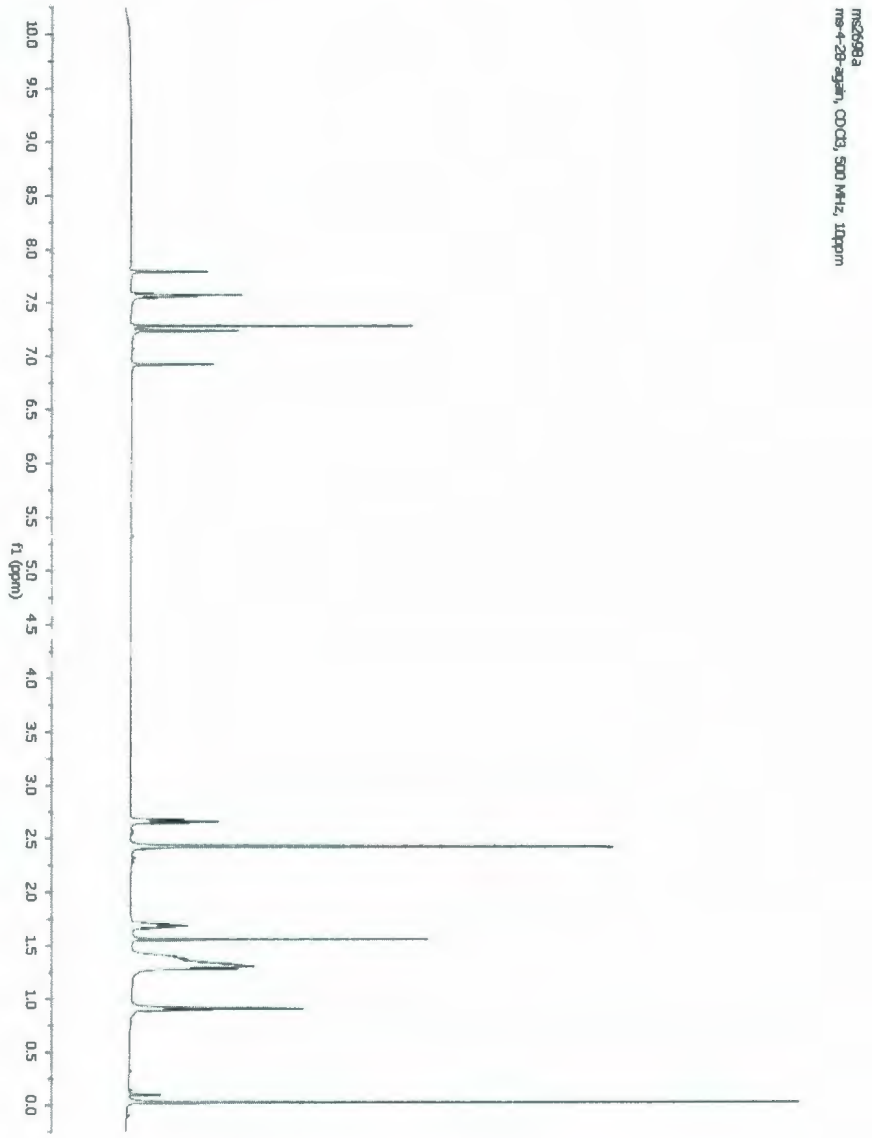

Figure A.25 ^{1}H NMR spectrum for **181.**

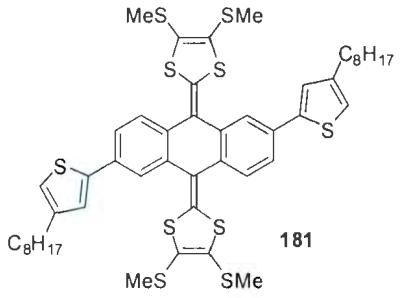

181

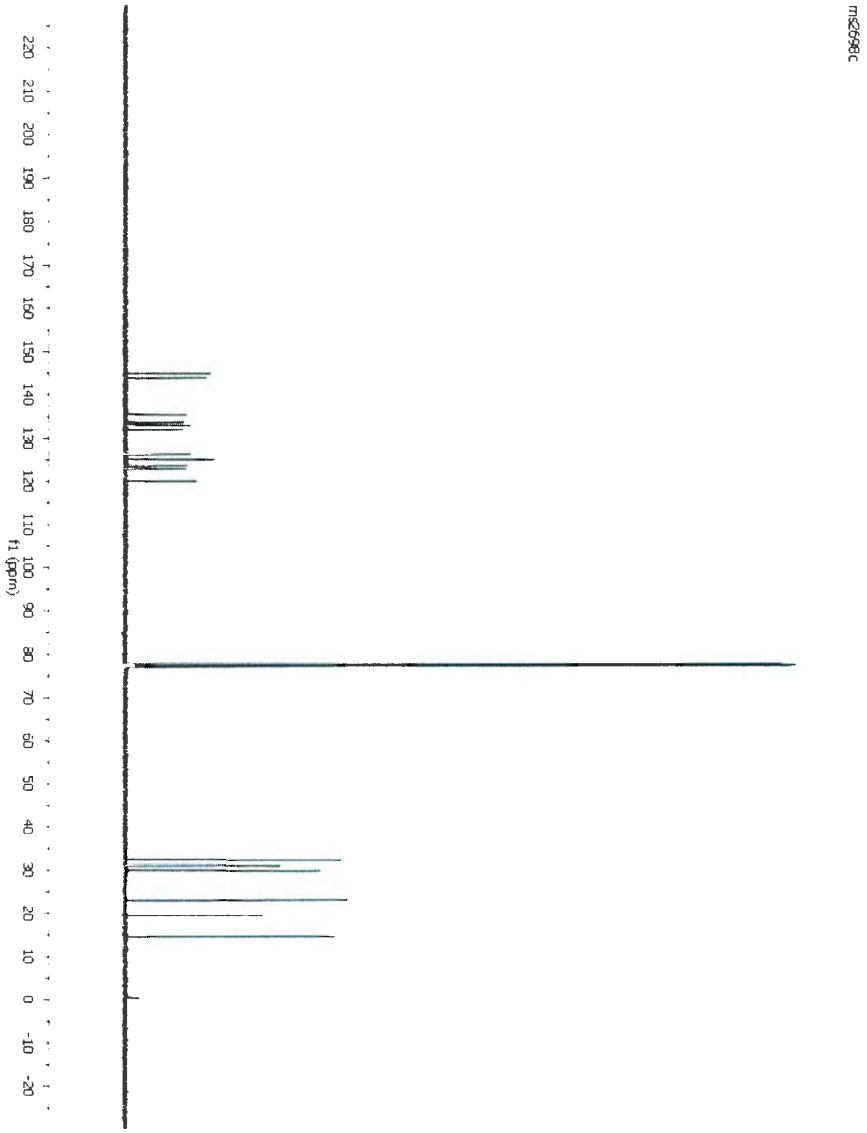

Figure A.26 ^{13}C NMR spectrum for **181.**

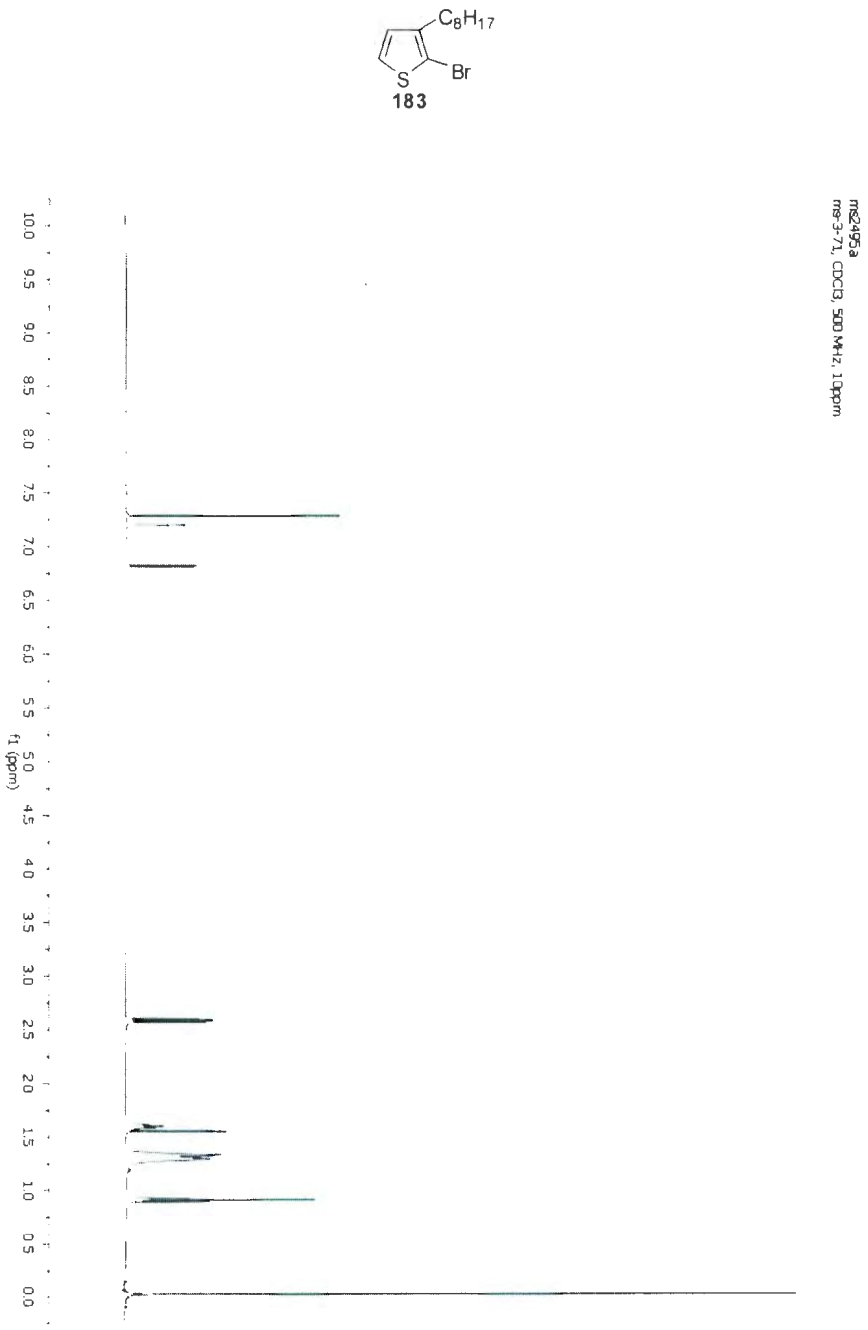

Figure A.27 ^{1}H NMR spectrum for **183.**

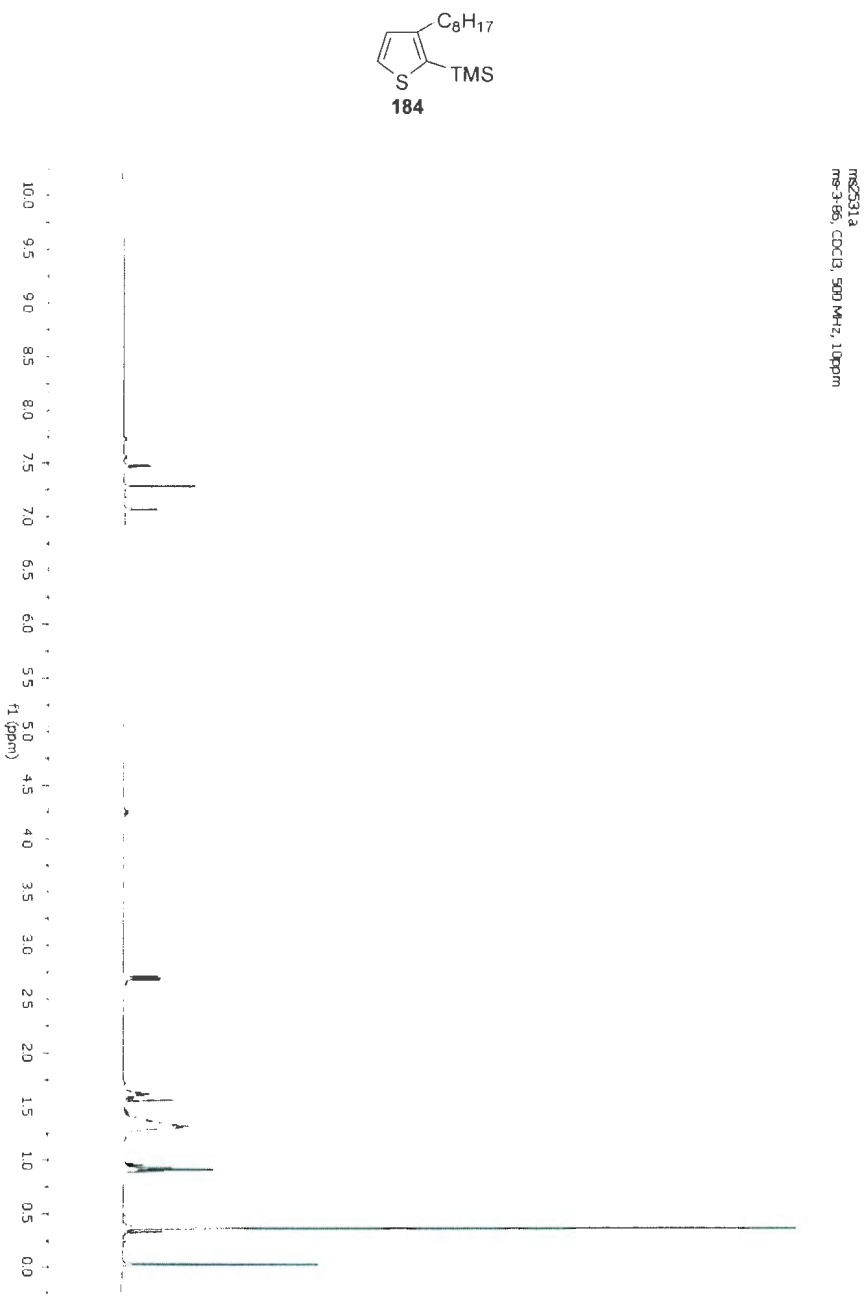

Figure A.28 ^{1}H NMR spectrum for **184.**

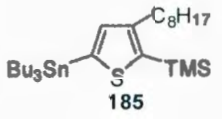

185

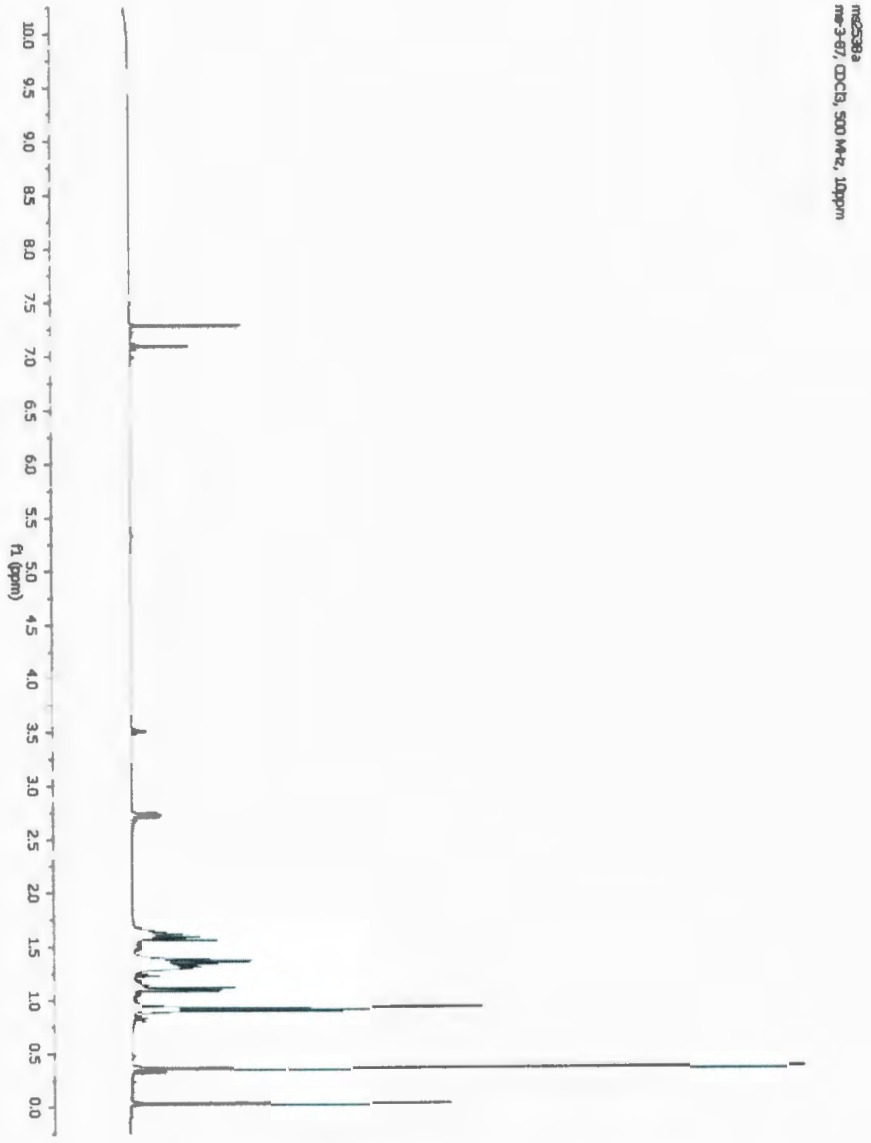

Figure A.29 ^{1}H NMR spectrum for **185.**

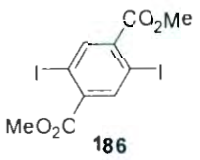

186

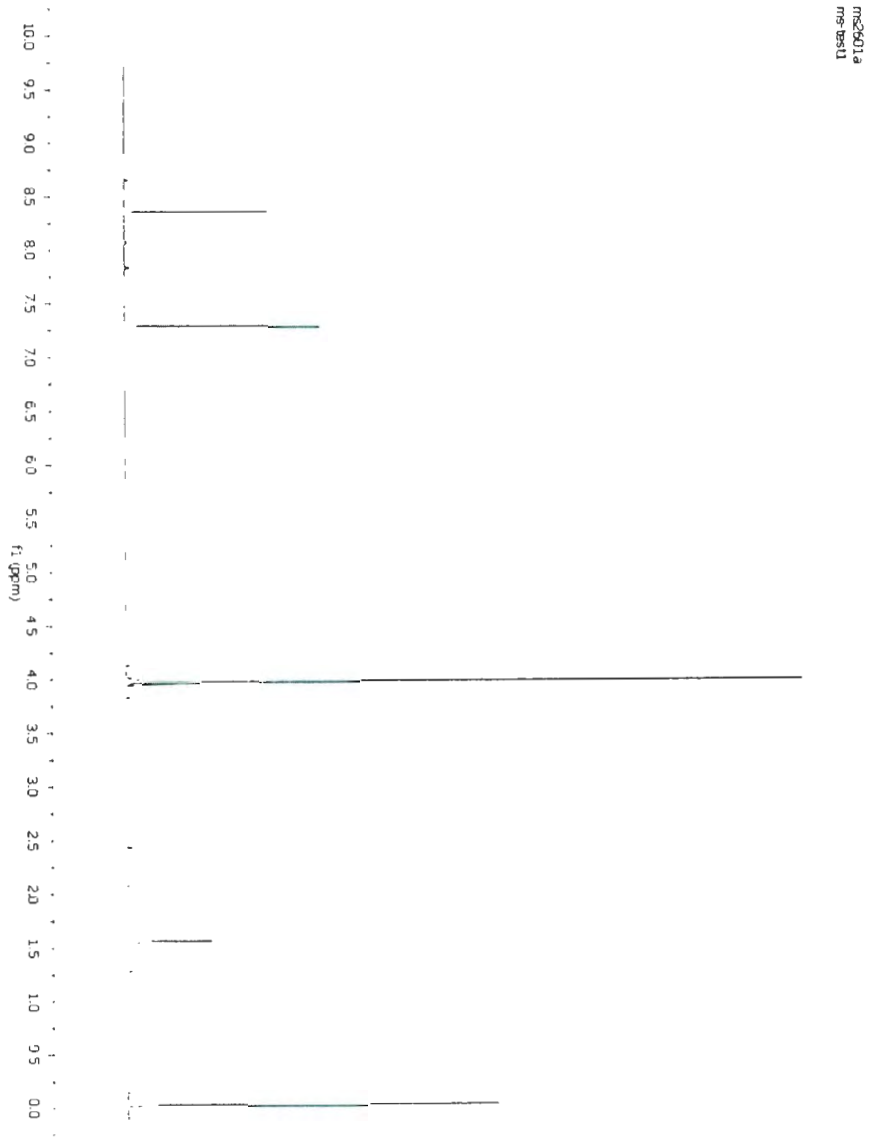

Figure A.30 ^{1}H NMR spectrum for **186.**

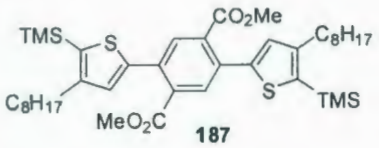

187

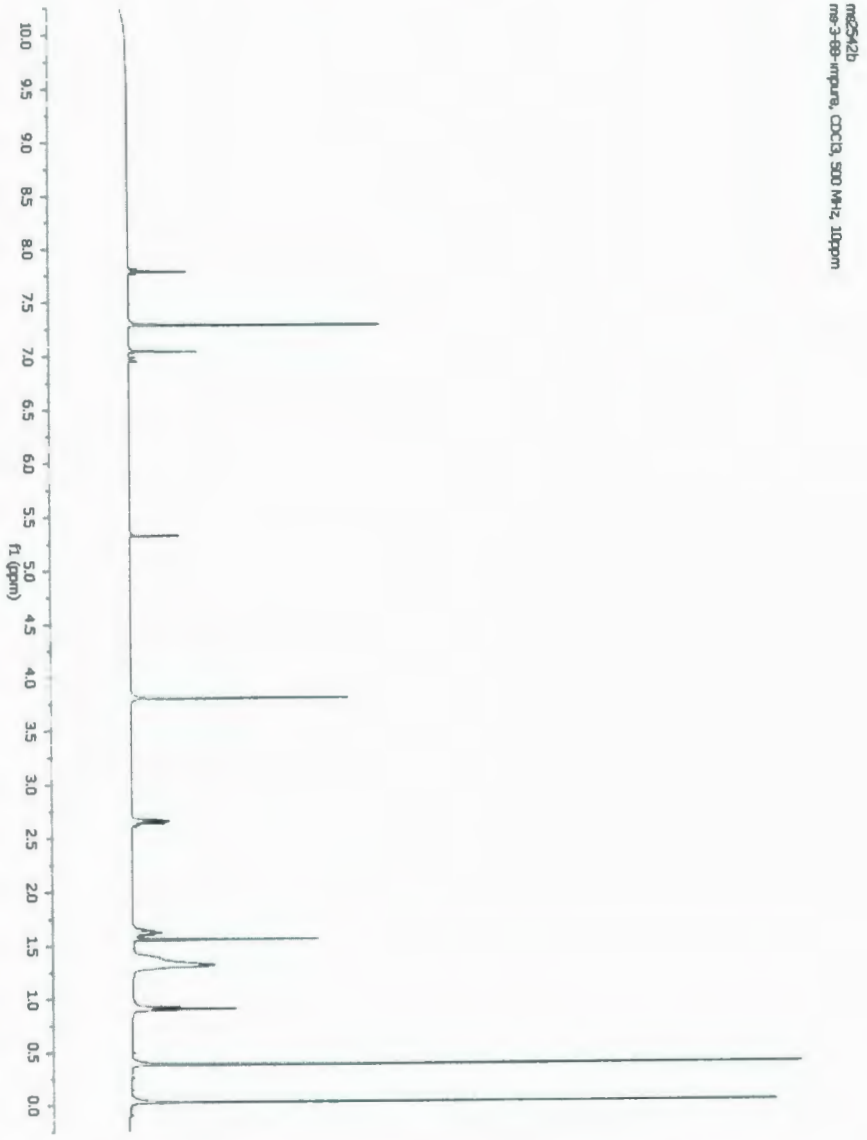

Figure A.31 ^{1}H NMR spectrum for **187.**

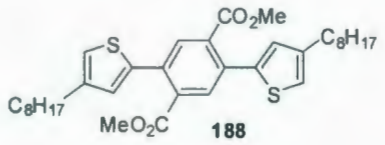

188

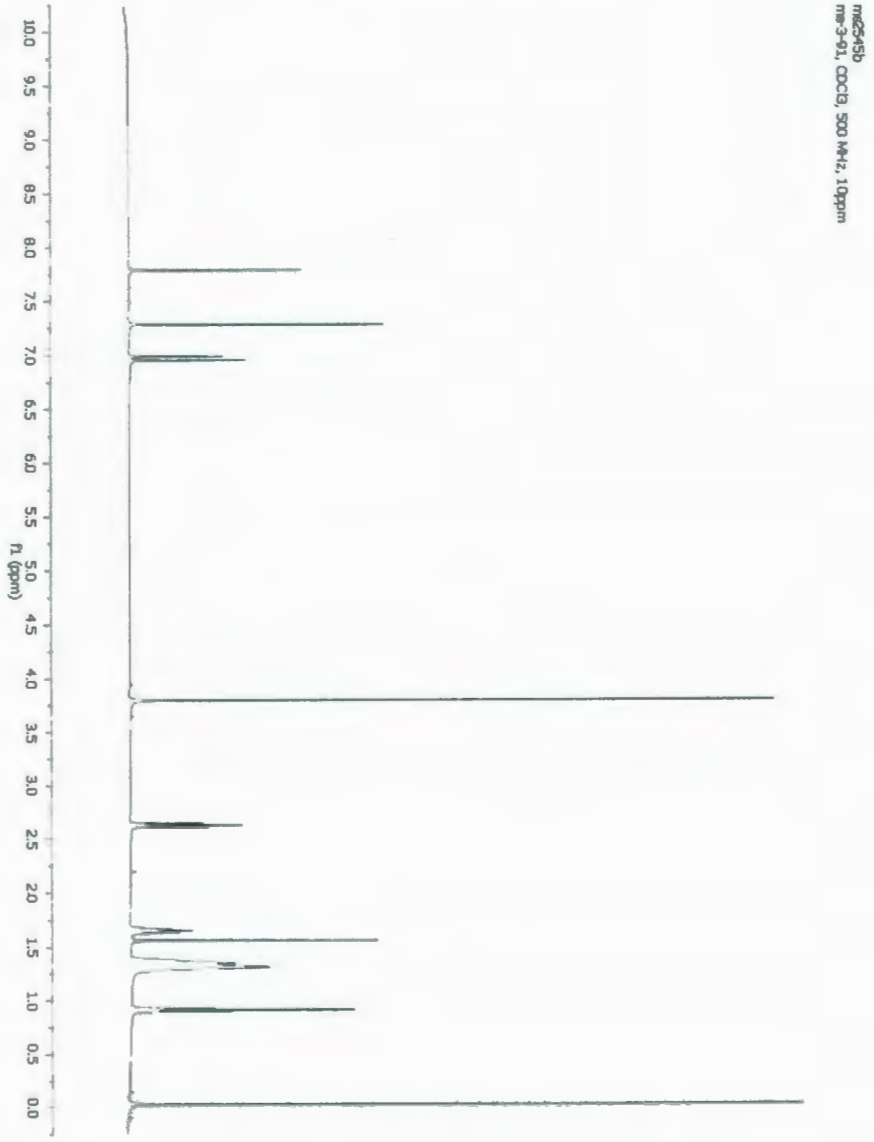

Figure A.32 ^{1}H NMR spectrum for **188.**

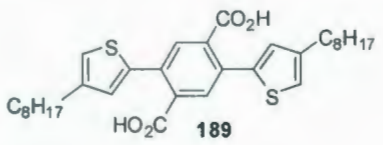

189

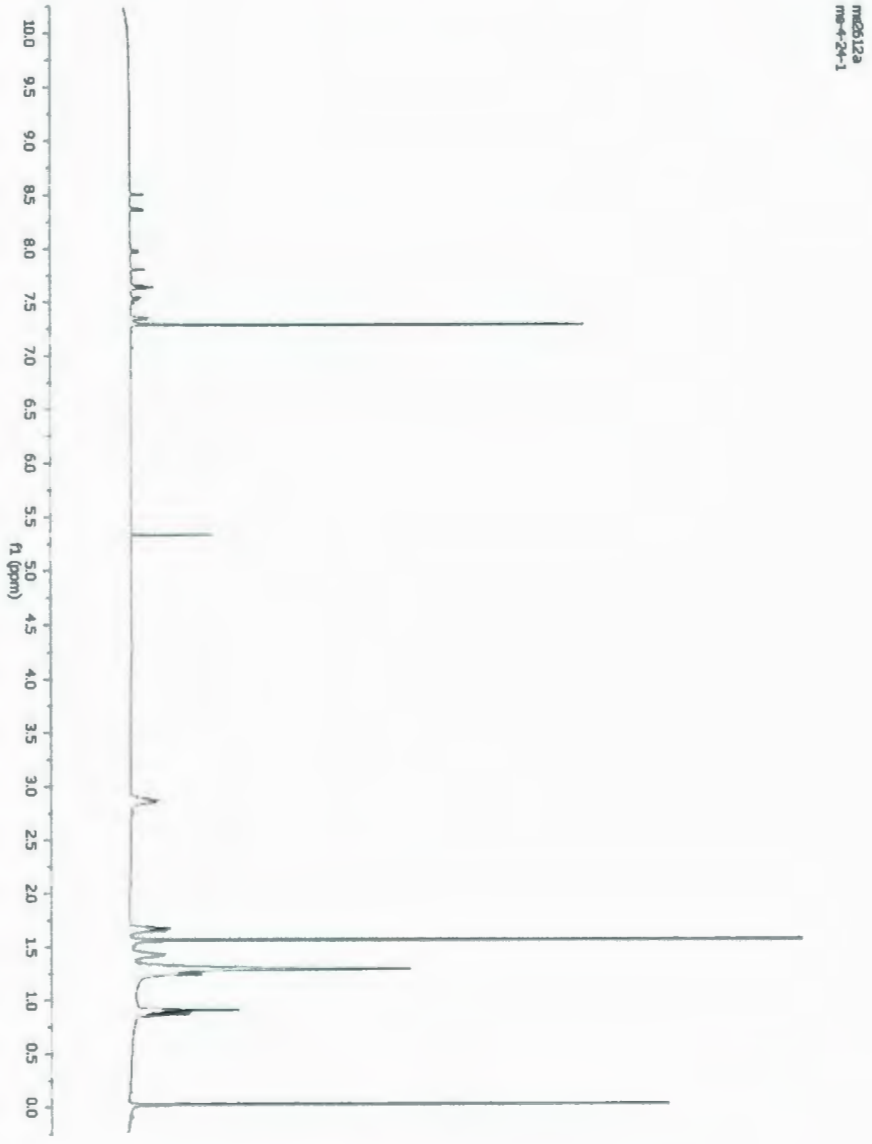

Figure A.33 ^{1}H NMR spectrum for **189.**

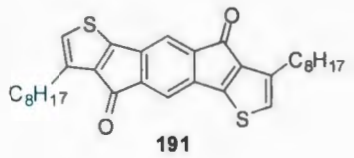

191

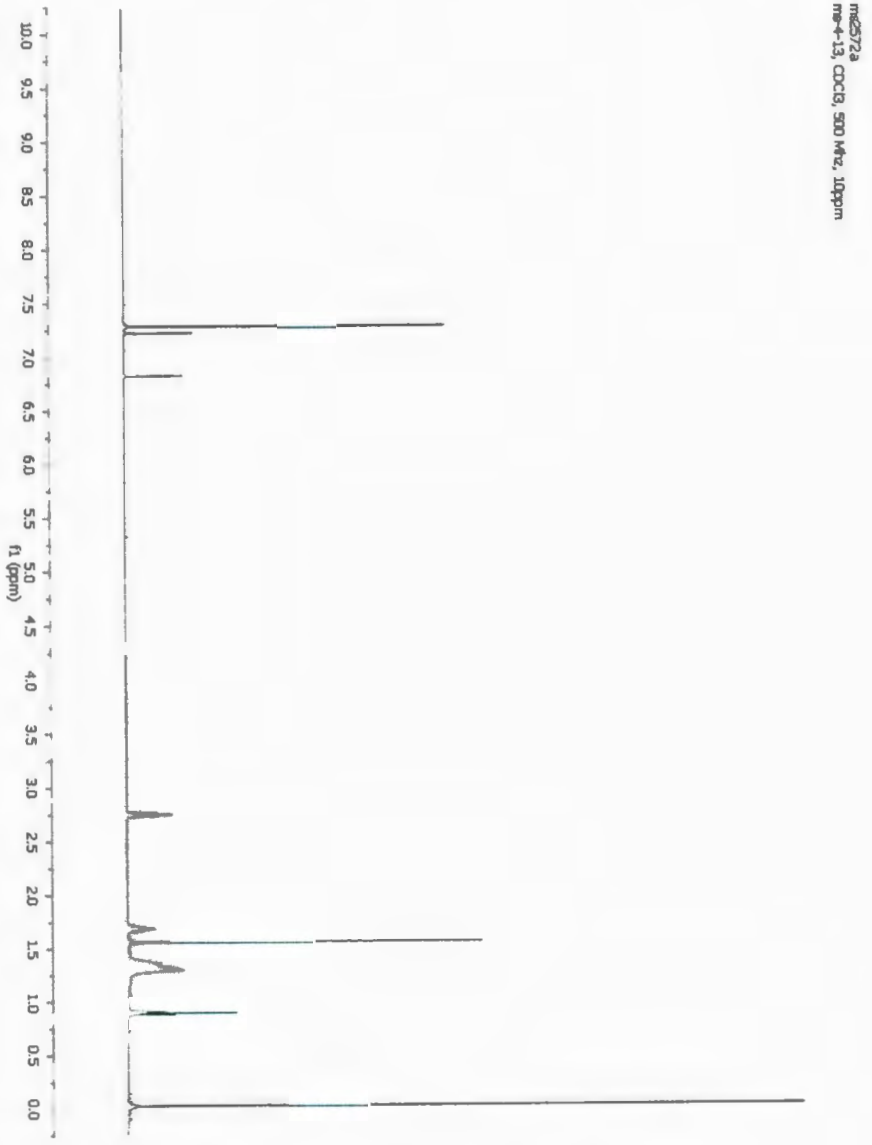

Figure A.34 ^{1}H NMR spectrum for **191.**

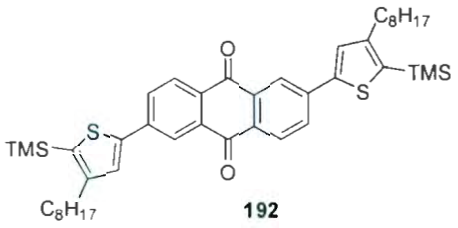

192

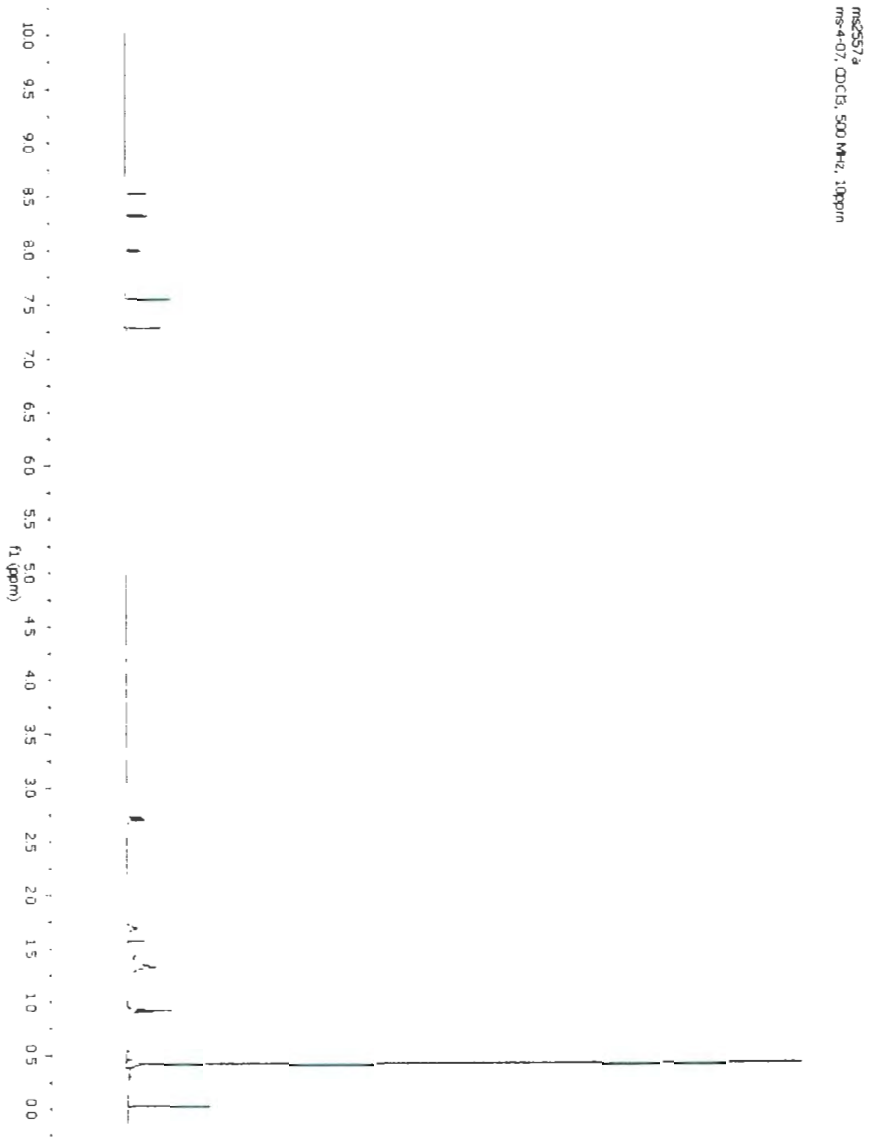

Figure A.35 ^{1}H NMR spectrum for **192.**

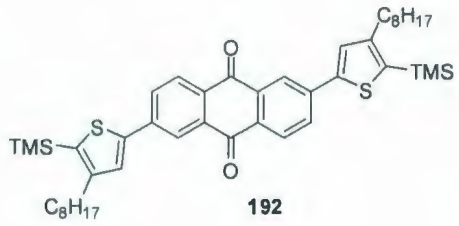

192

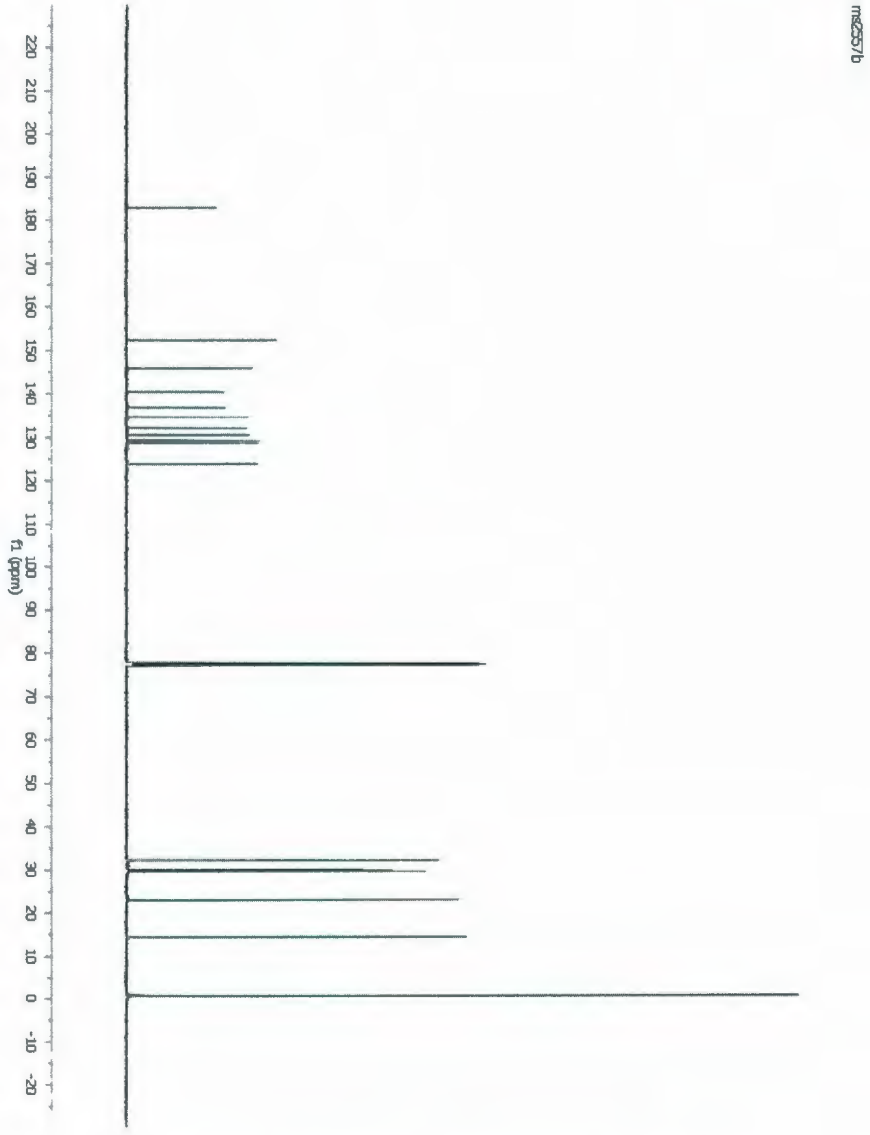

Figure A.36 ^{13}C NMR spectrum for **192.**

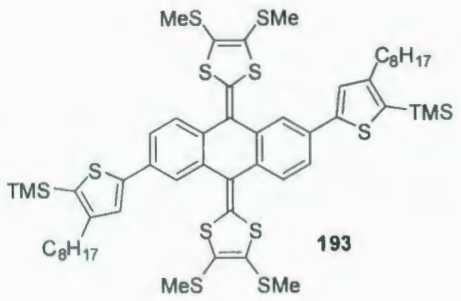

193

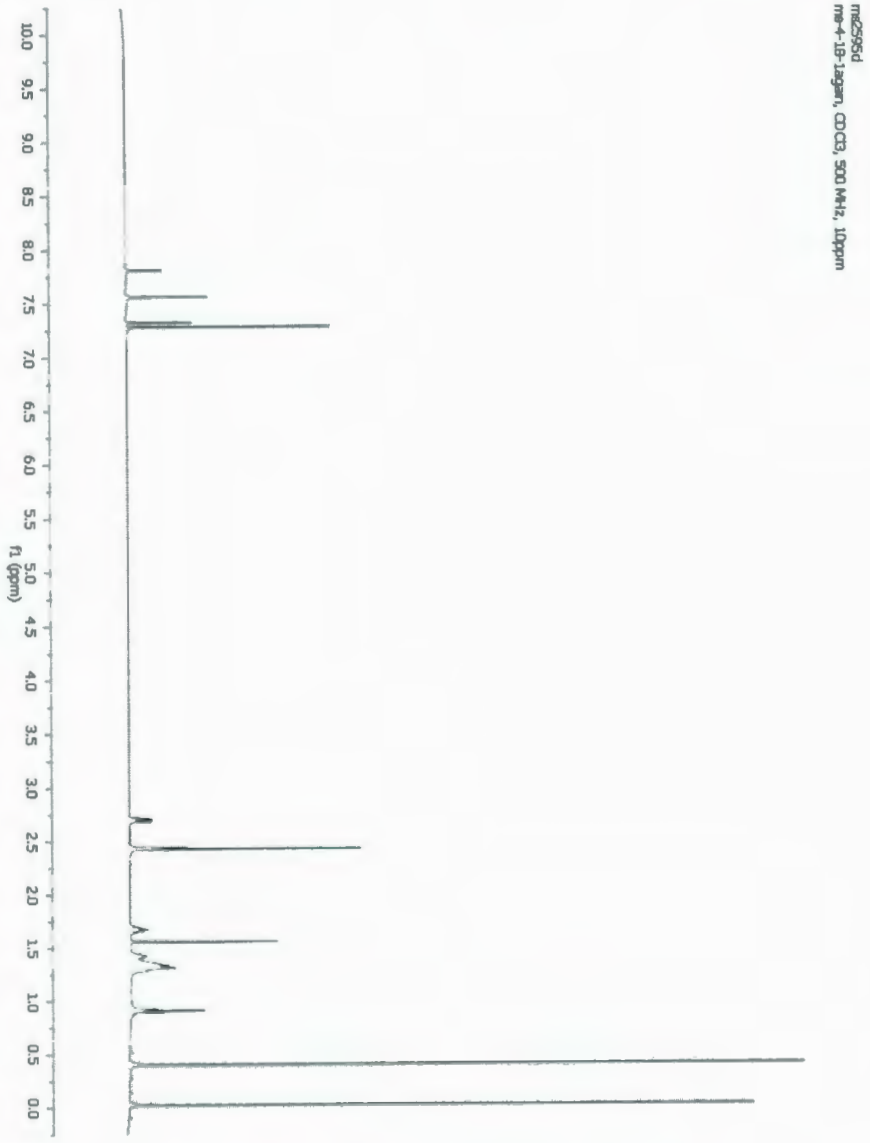

Figure A.37 ^{1}H NMR spectrum for **193.**

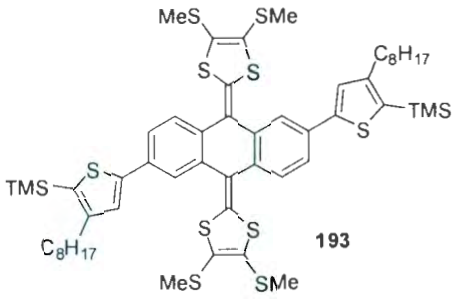

193

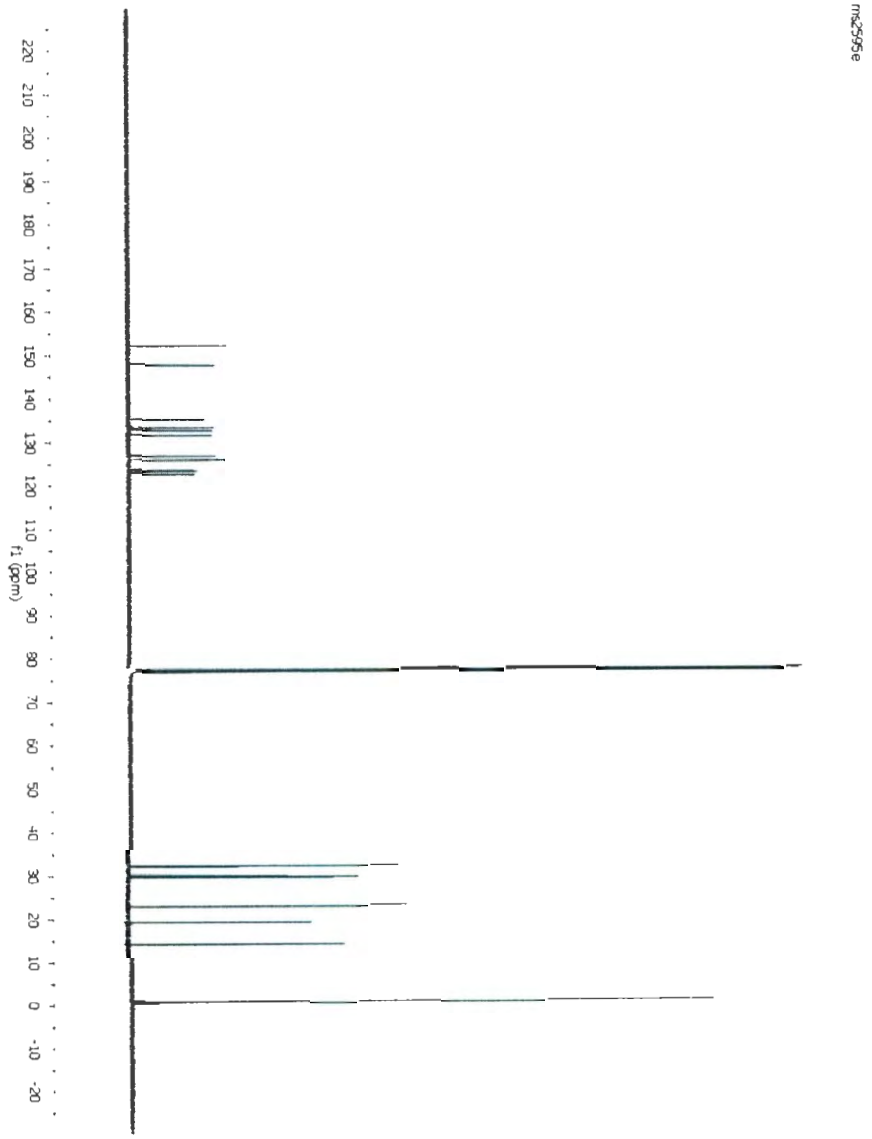

Figure A.38 ^{13}C NMR spectrum for **193.**

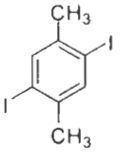

195

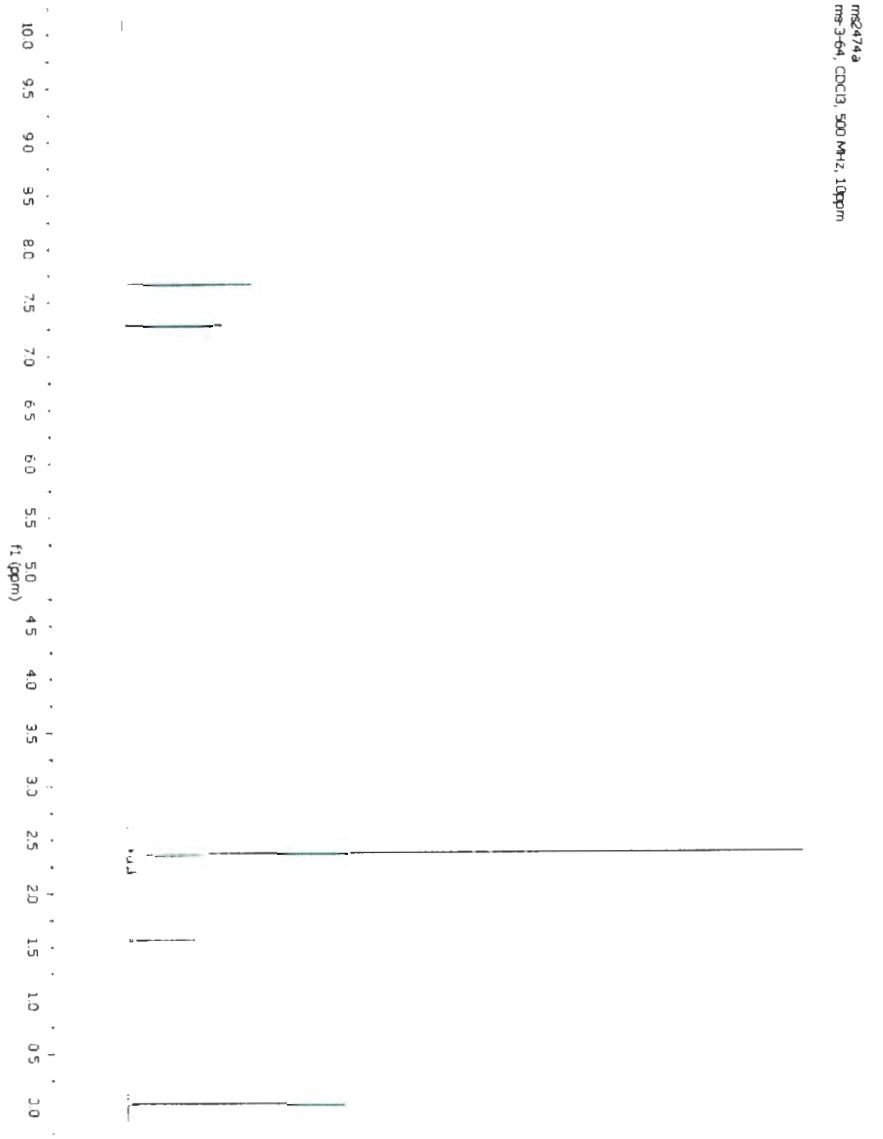

Figure A.39 ^{1}H NMR spectrum for **195.**

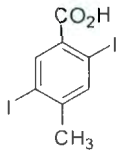

196

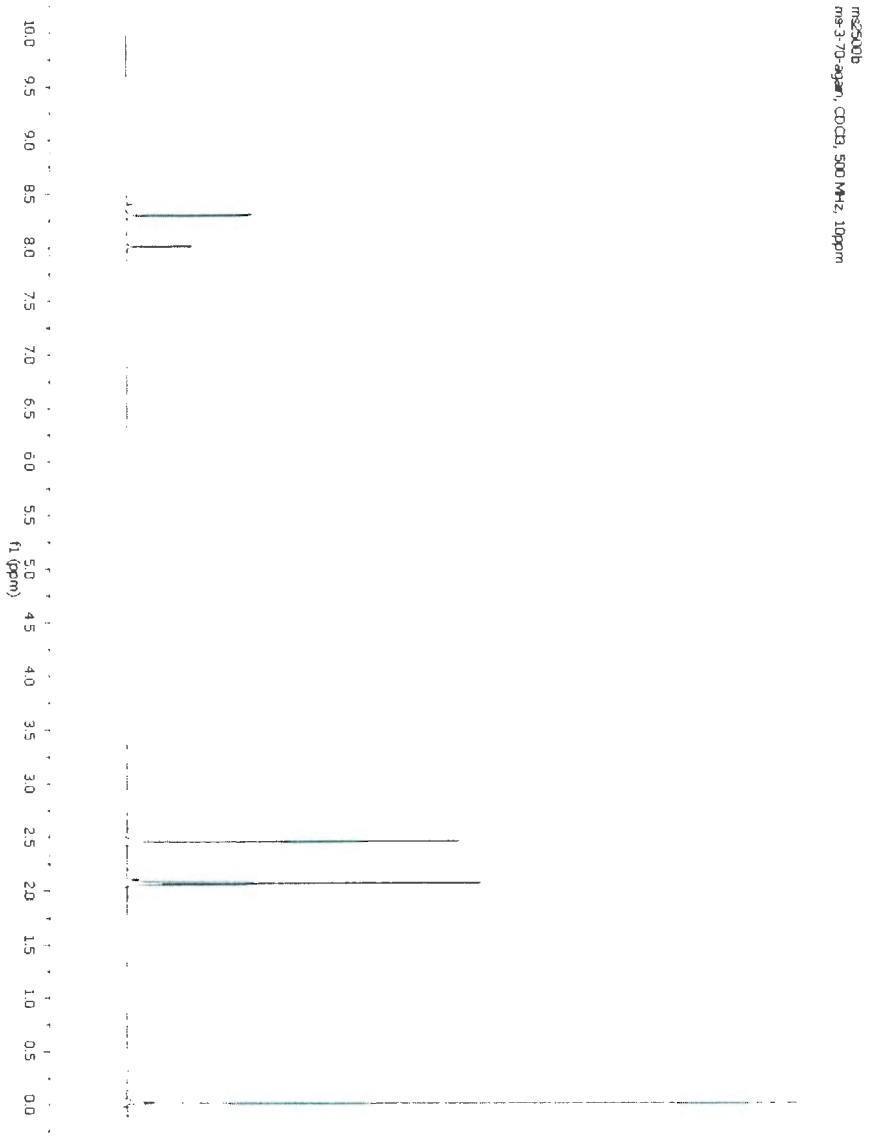

Figure A.40 ^{1}H NMR spectrum for **196.**

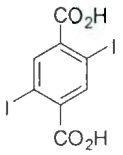

197

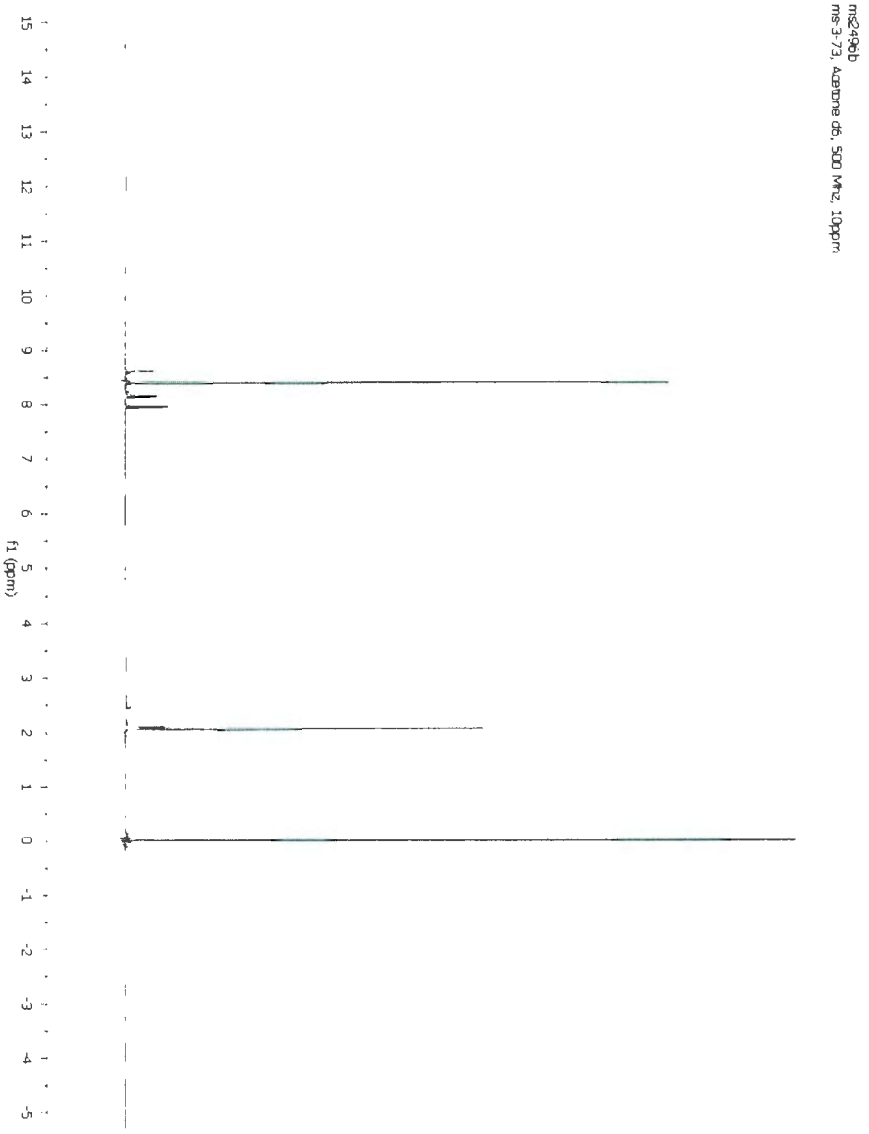

Figure A.41 ^{1}H NMR spectrum for **197.**

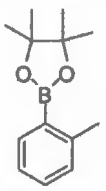

203

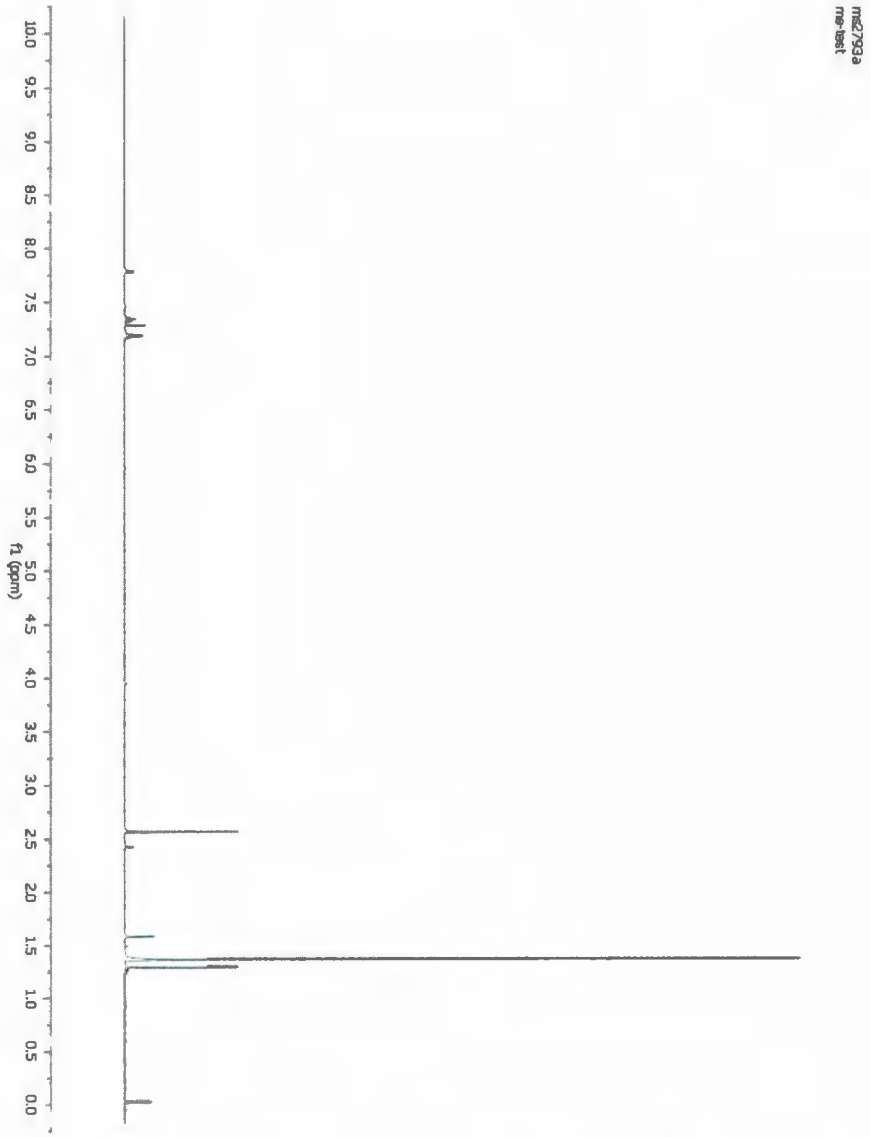

Figure A.42 ^{1}H NMR spectrum for **203.**

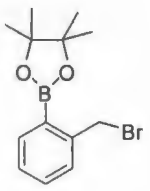

204

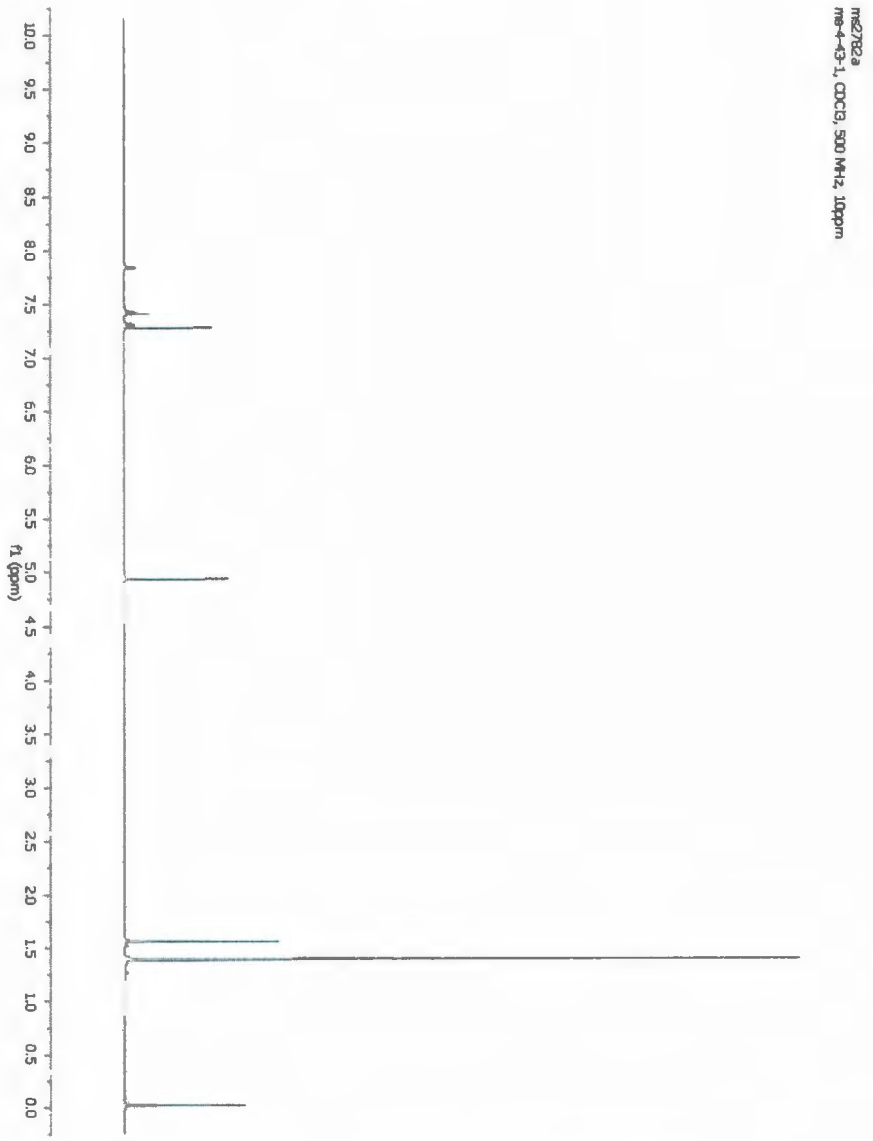

Figure A.43 ^{1}H NMR spectrum for **204.**

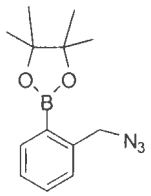

205

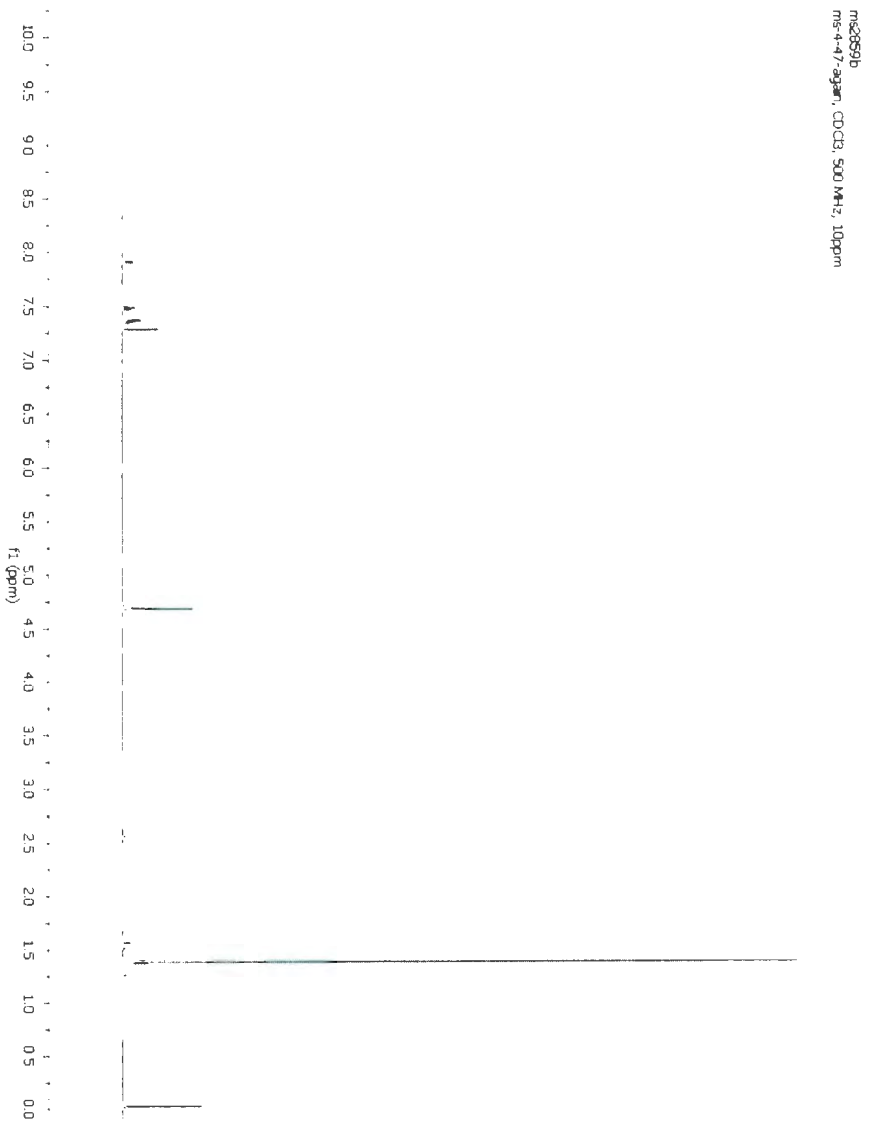

Figure A.44 ^{1}H NMR spectrum for **205.**

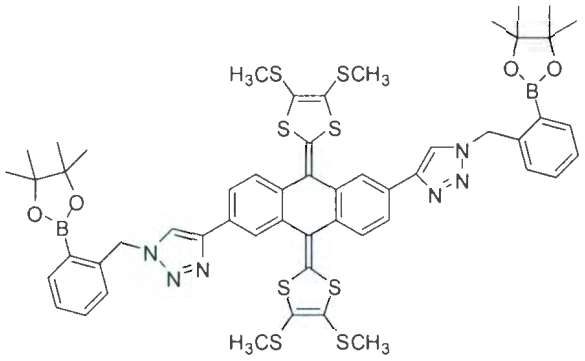

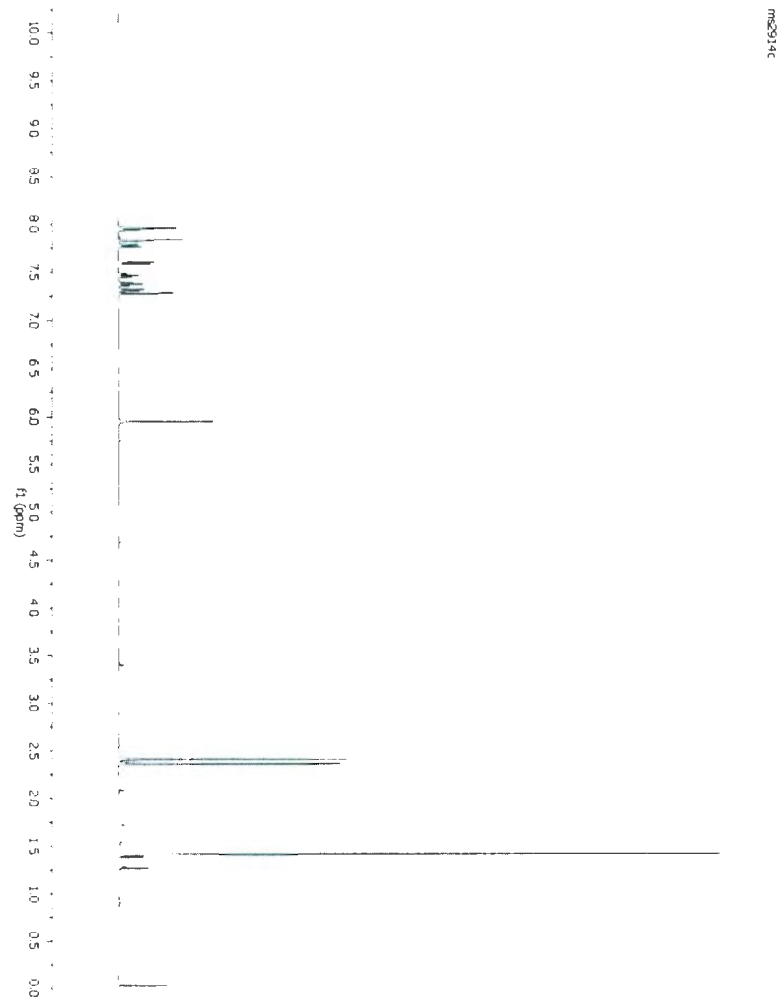

Figure A.45 ^{1}H NMR spectrum for **206.**

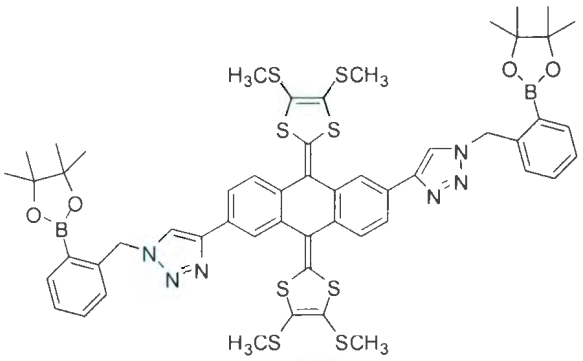

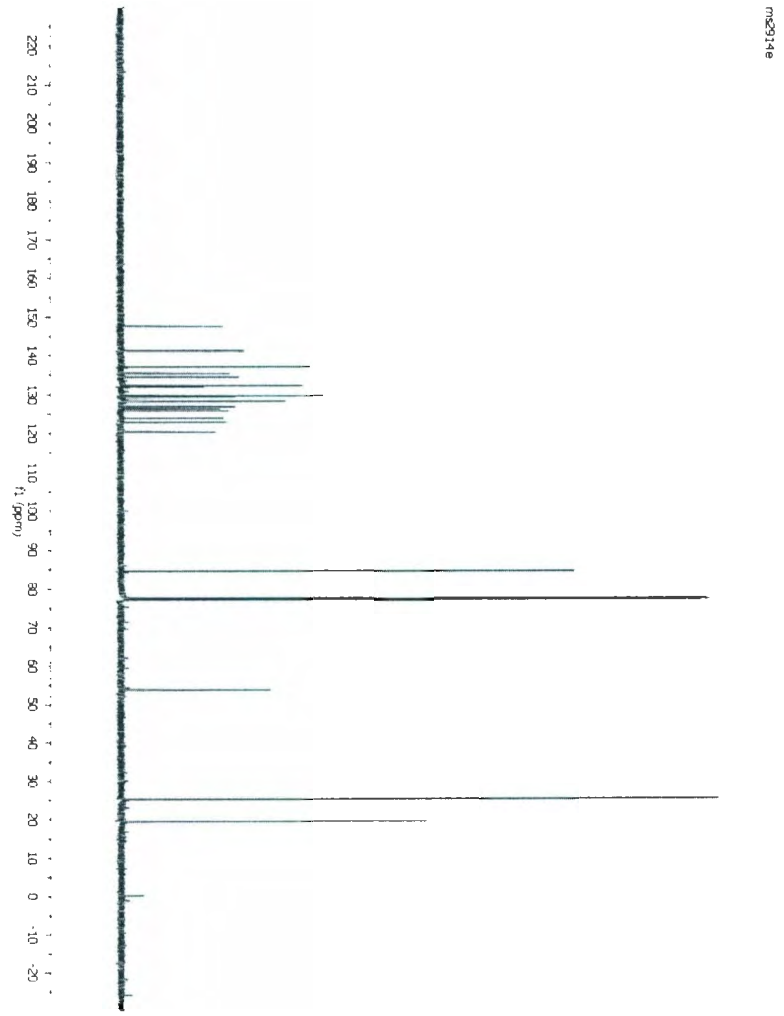

Figure A.46 ^{13}C NMR spectrum for **206.**

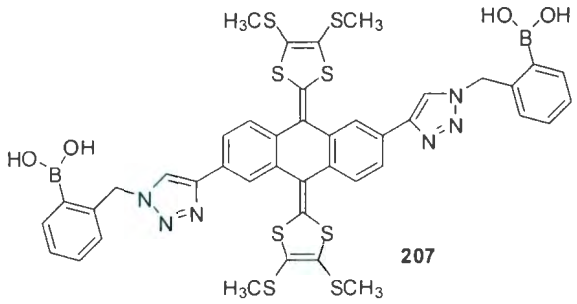

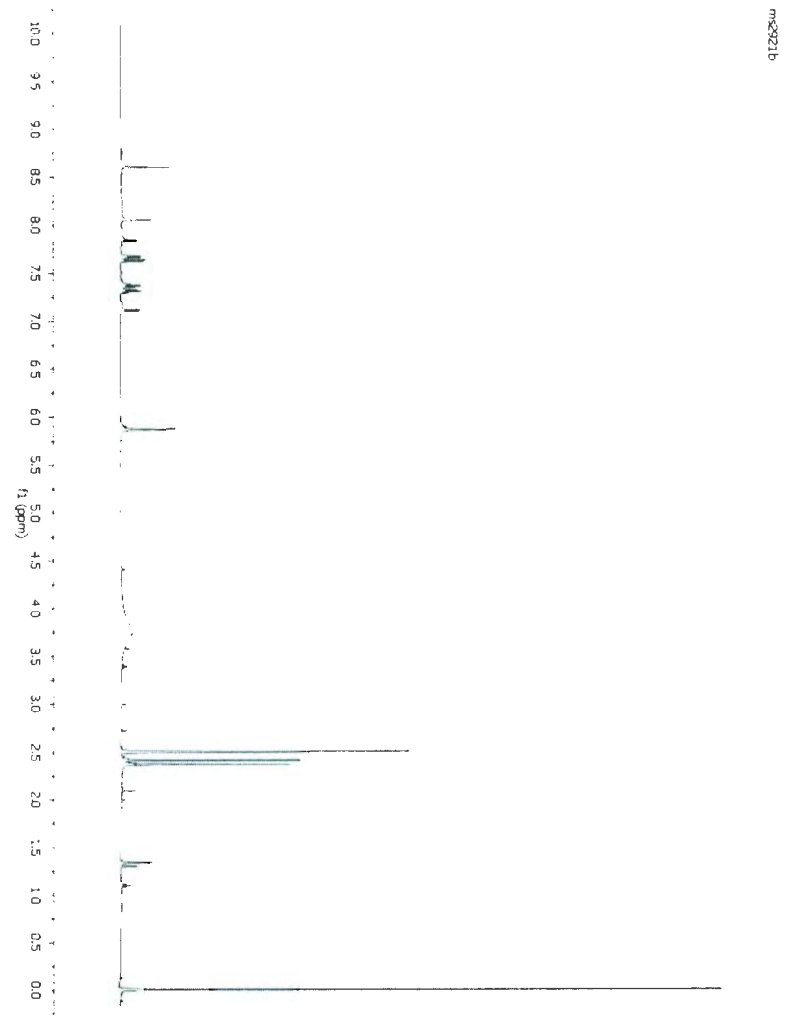

Figure A.47 ^{1}H NMR spectrum for **207.**

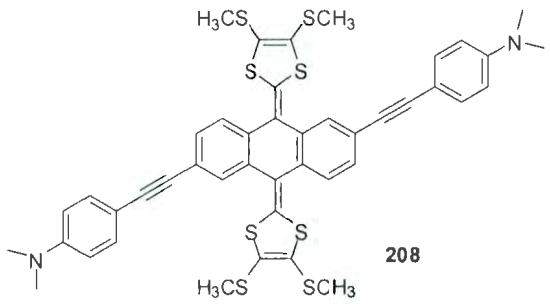

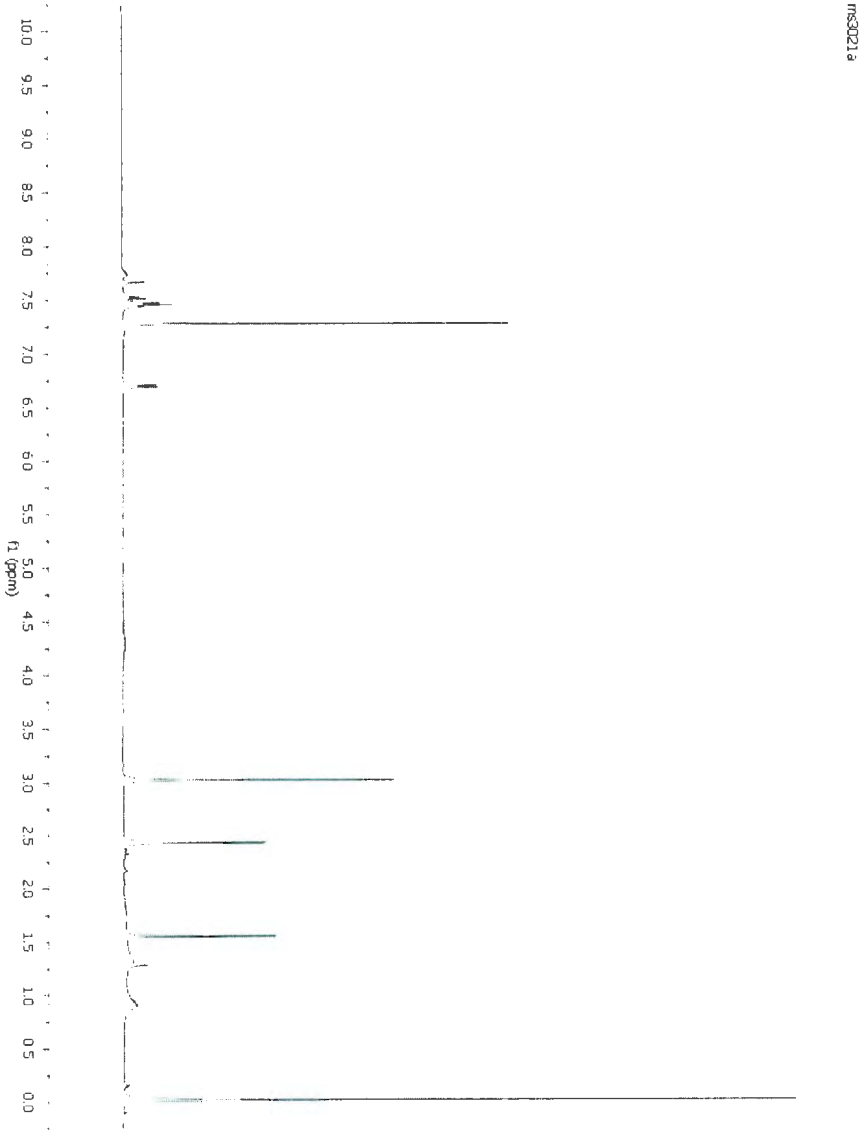

Figure A.48 ^{1}H NMR spectrum for **208.**

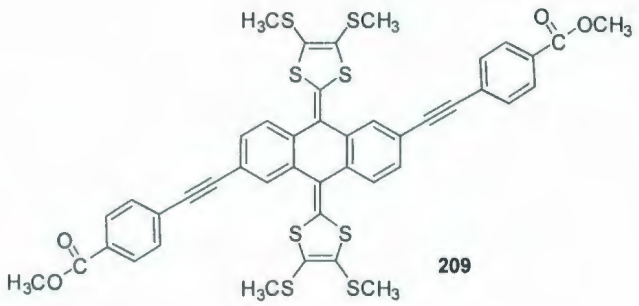

209

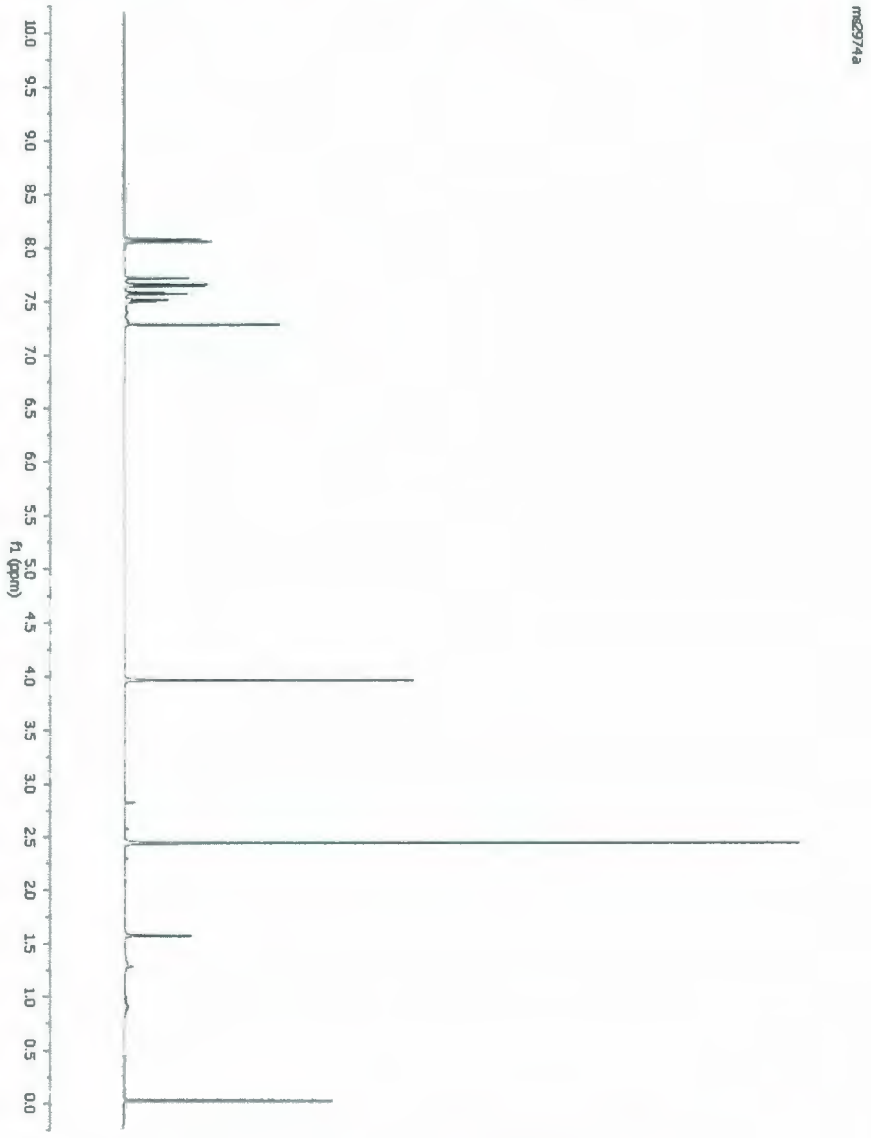

Figure A.49 ^{1}H NMR spectrum for **209.**

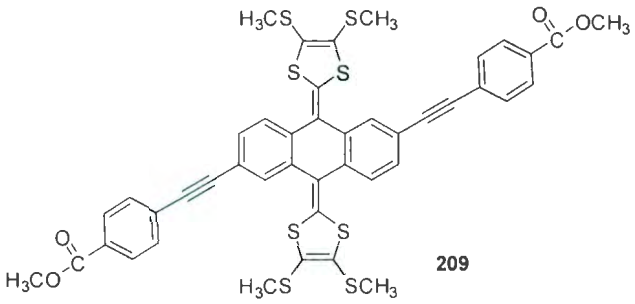

209

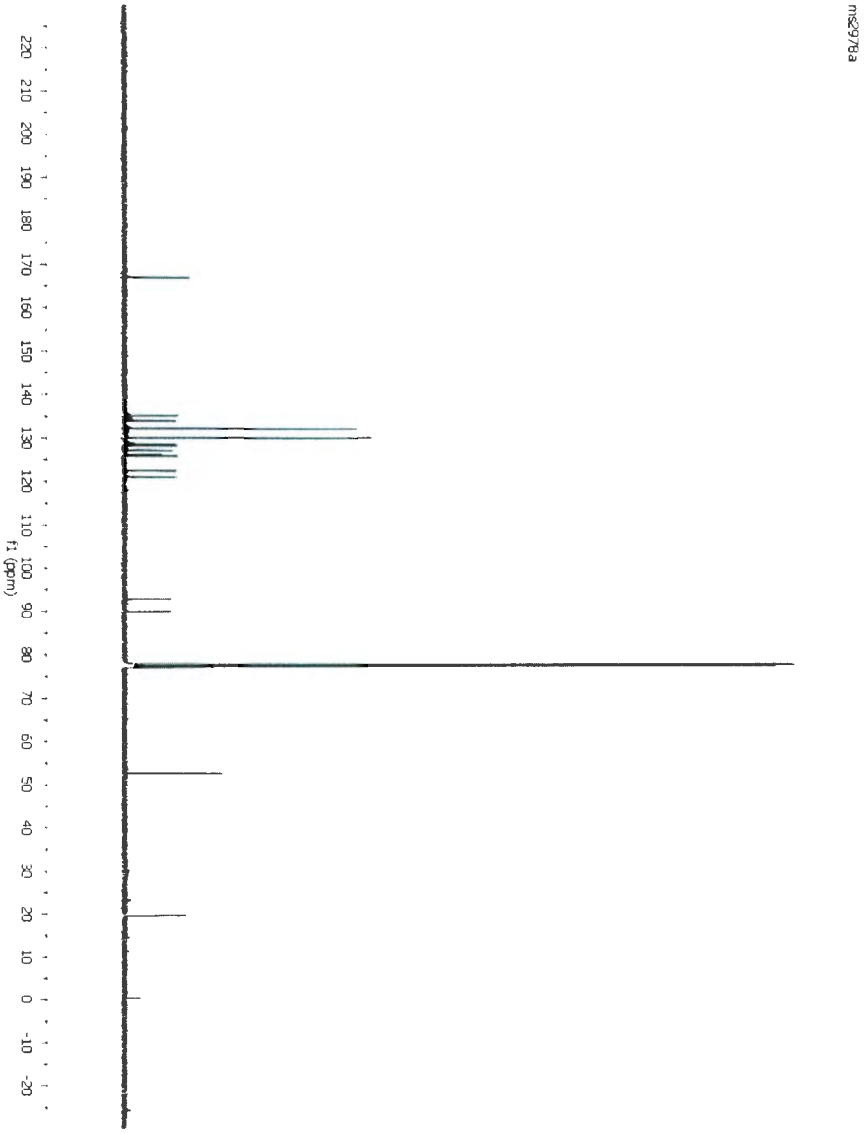

Figure A.50 ^{13}C NMR spectrum for **209.**

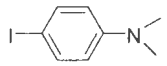

226

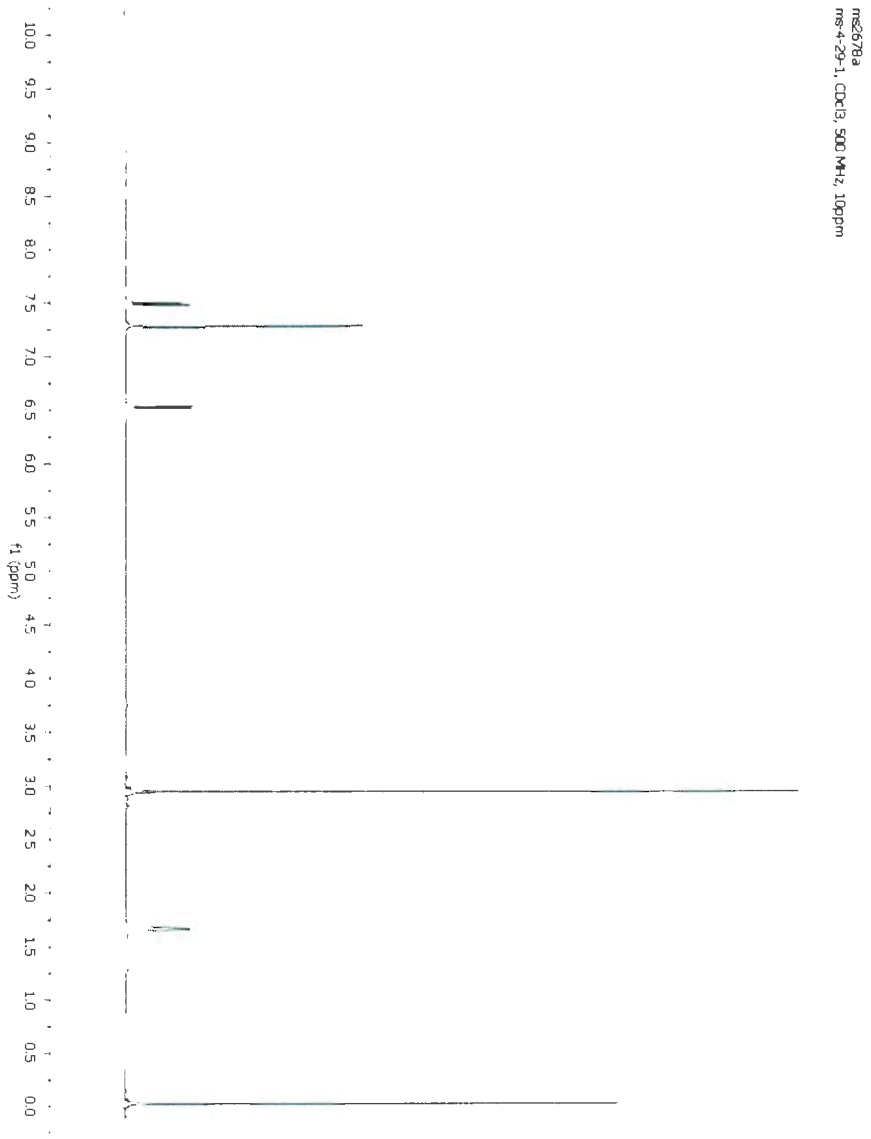

Figure A.51 ^{13}C NMR spectrum for **226.**

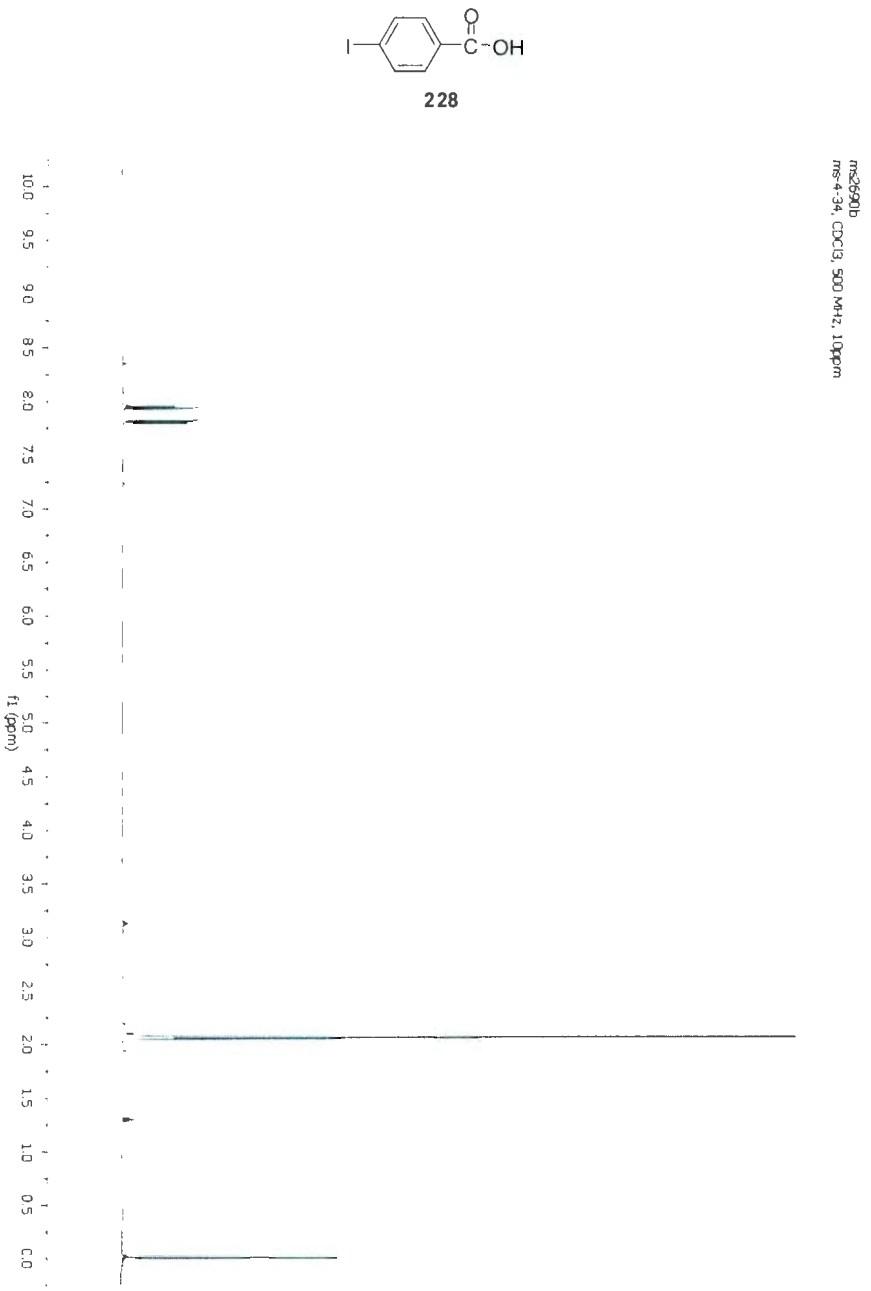

Figure A.52 ^{1}H NMR spectrum for **228.**

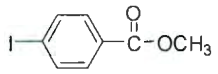

229

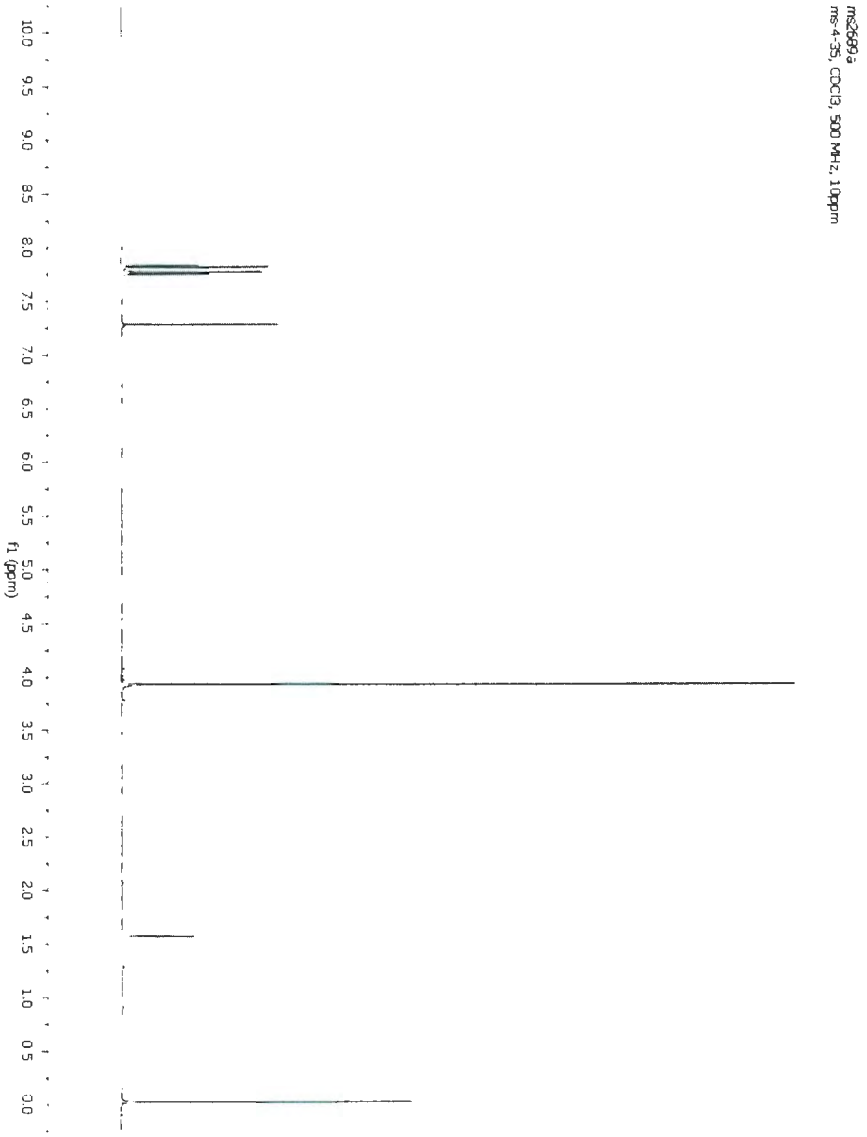

Figure A.53 ^{1}H NMR spectrum for **229.**

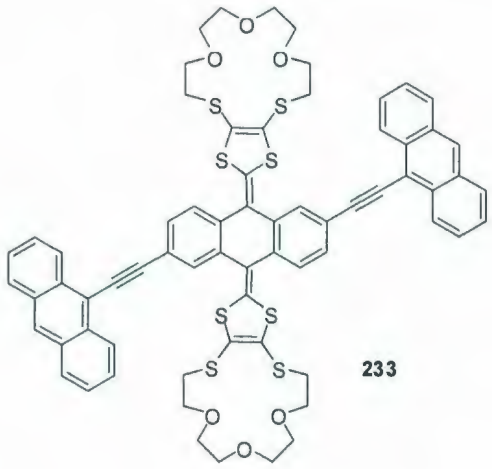

233

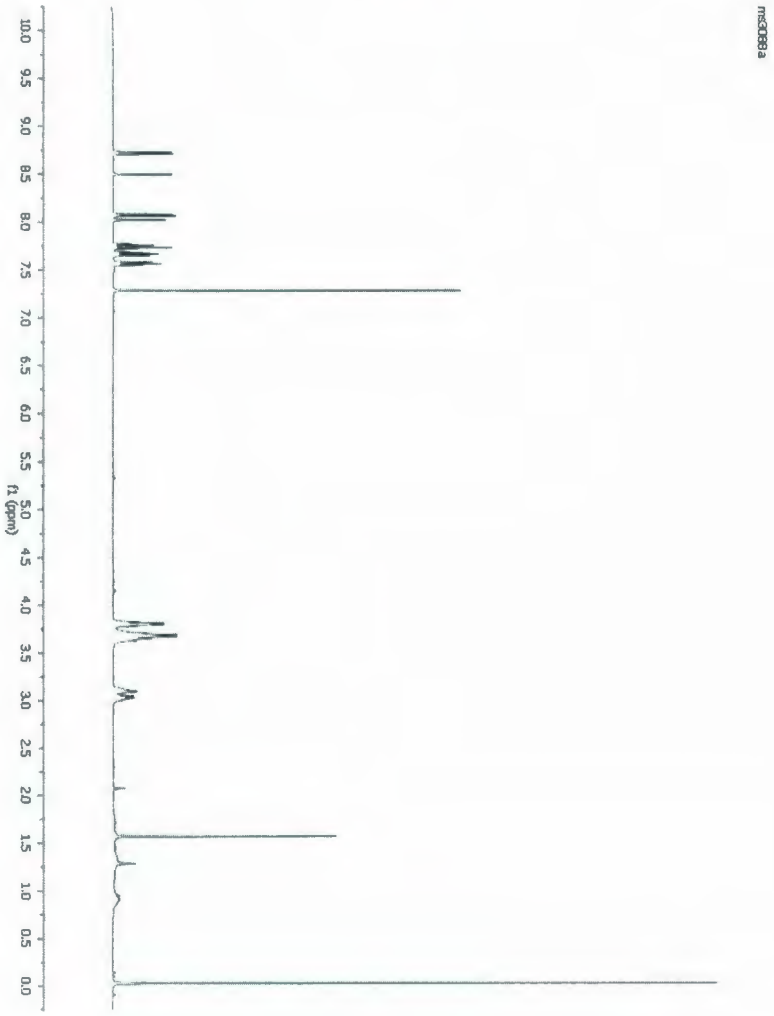

Figure A.54 ^{1}H NMR spectrum for **233.**

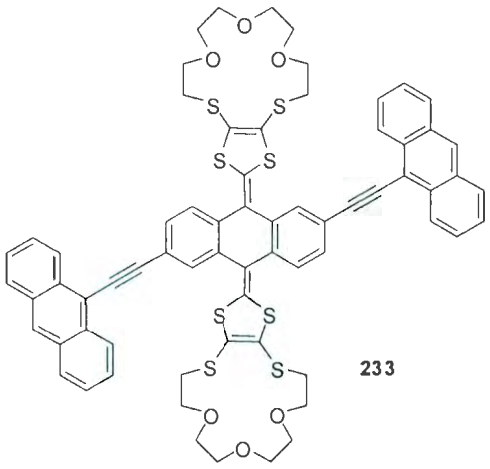

233

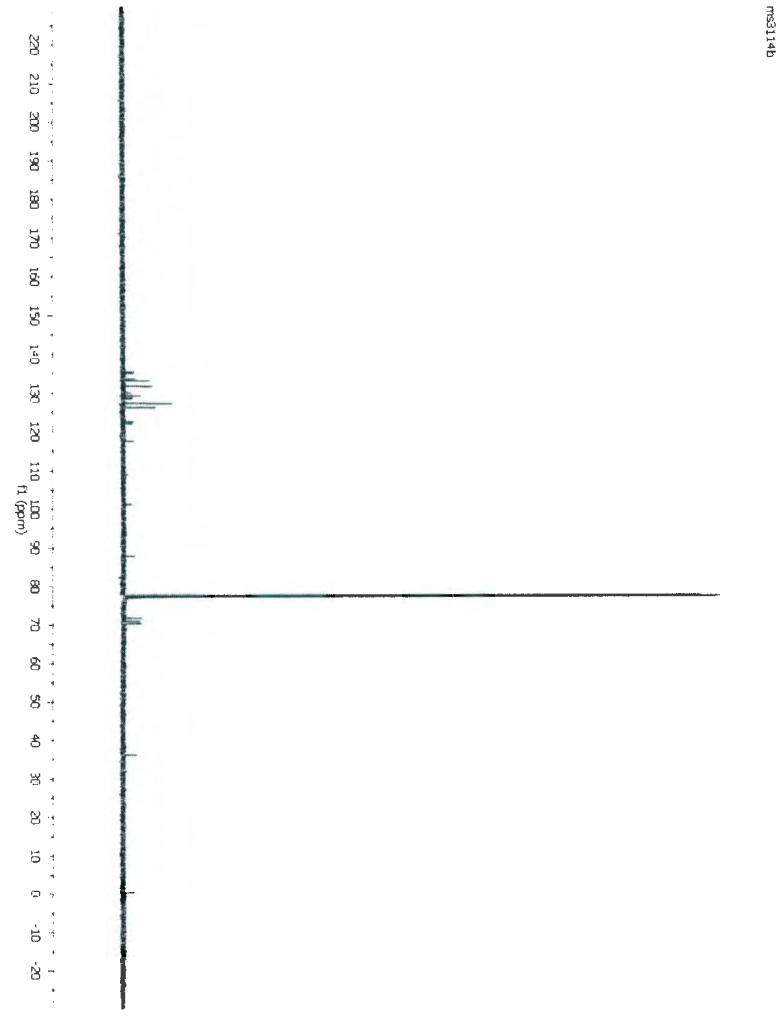

Figure A.55 ^{13}C NMR spectrum for **233.**

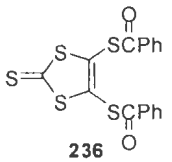

236

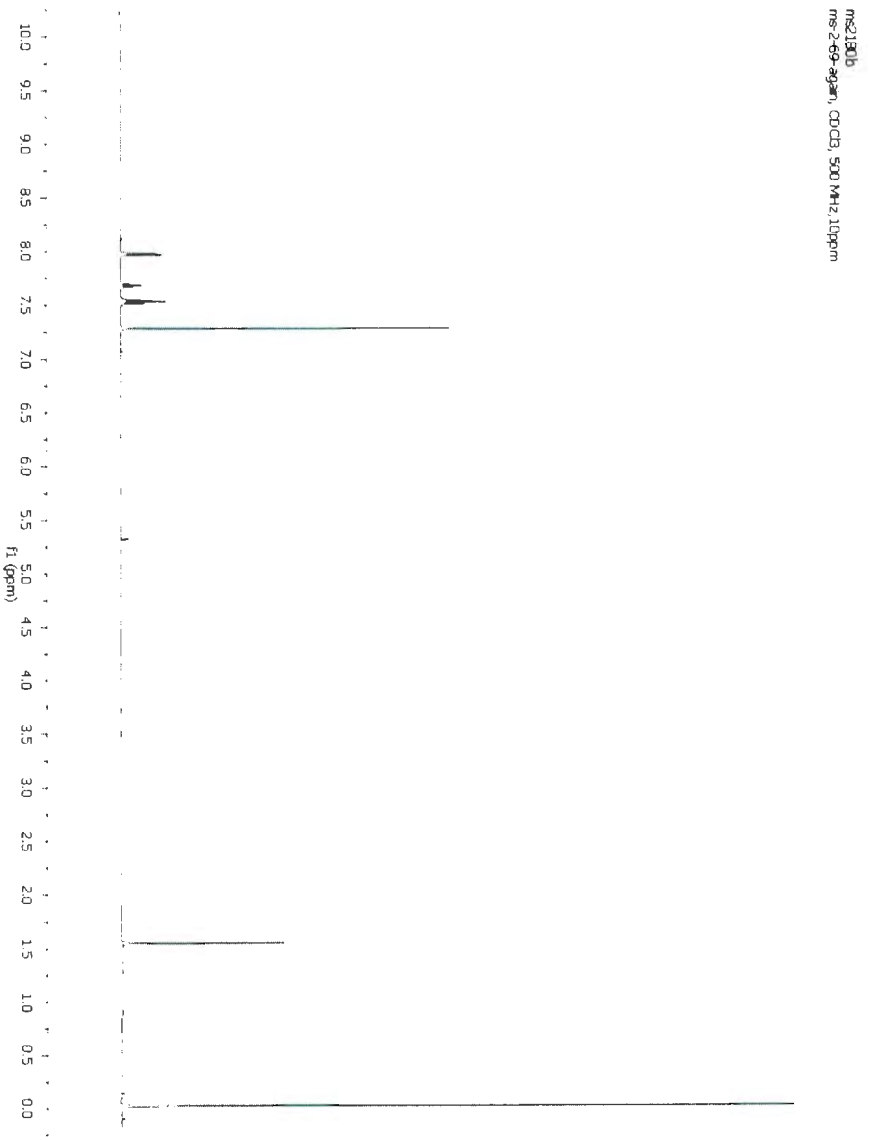

Figure A.56 ^{1}H NMR spectrum for **236.**

238

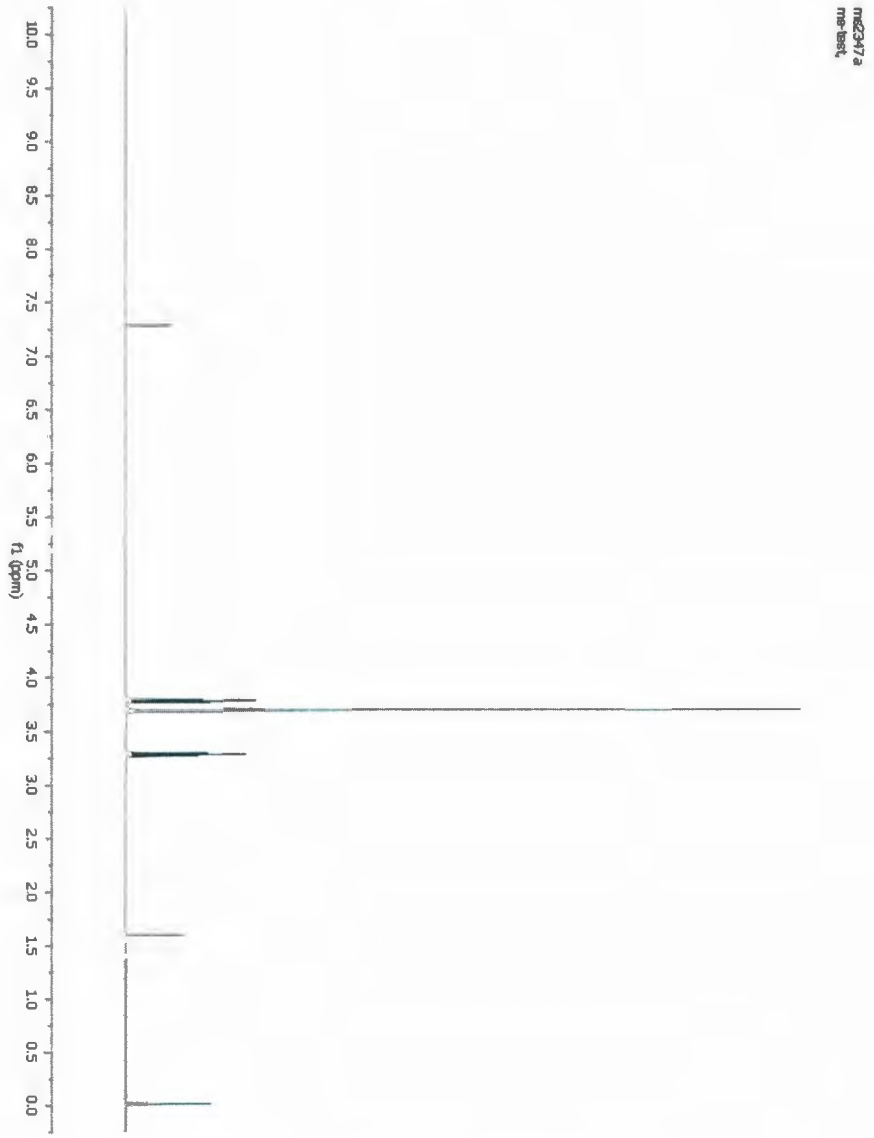

Figure A.57 ^{1}H NMR spectrum for **238.**

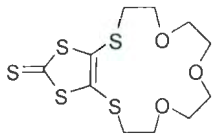

239

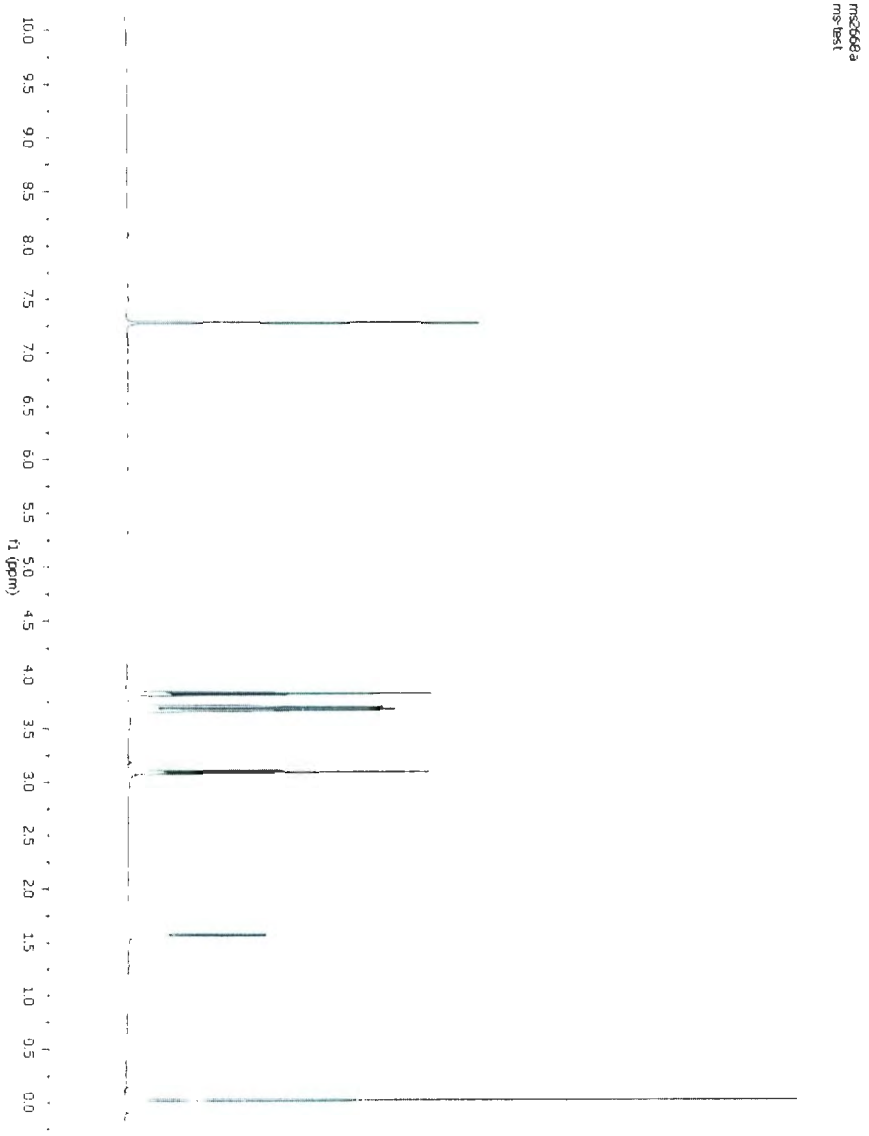

Figure A.58 ^{1}H NMR spectrum for **239.**

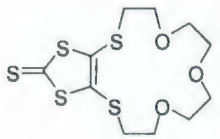

239

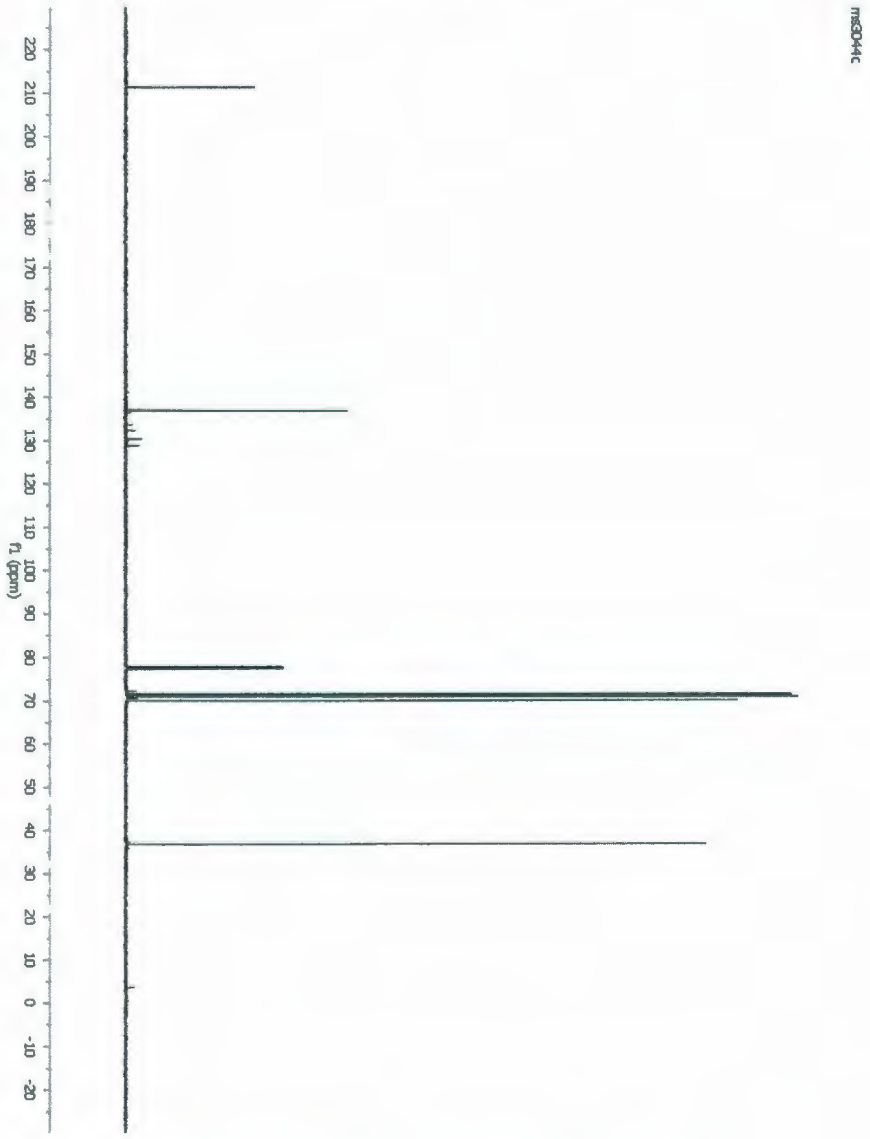

Figure A.59 ^{13}C NMR spectrum for **239.**

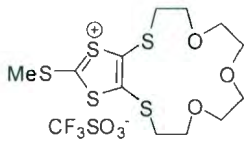

240

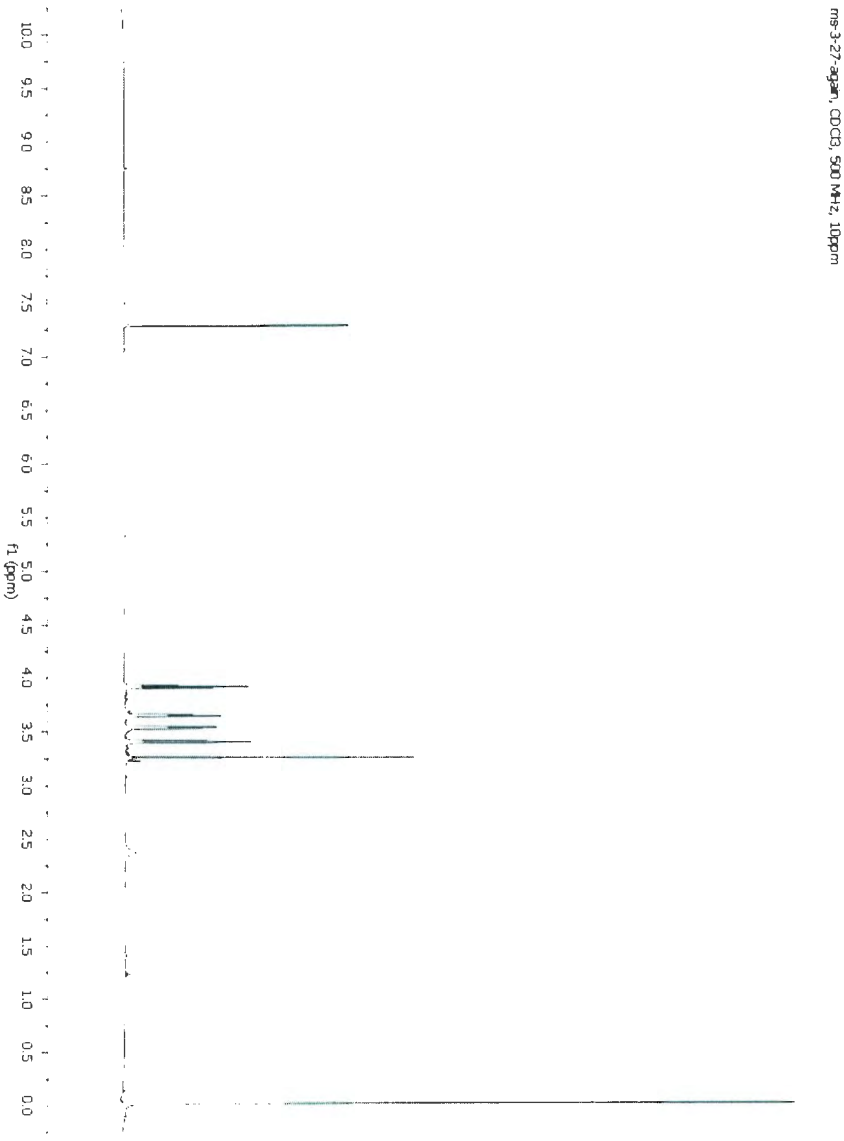

Figure A.60 ^{1}H NMR spectrum for **240.**

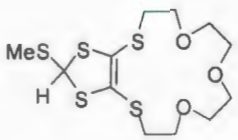

241

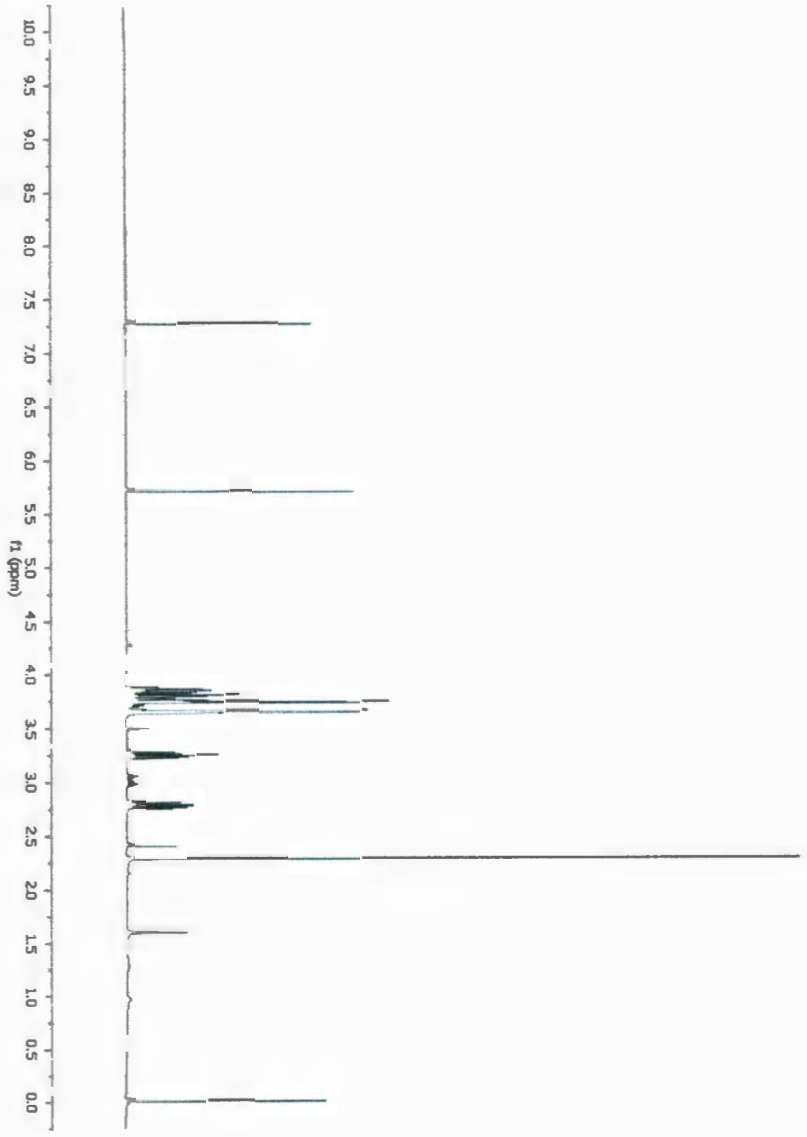

Figure A.61 ^{1}H NMR spectrum for **241.**

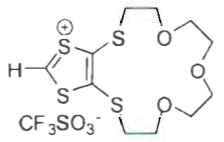

242

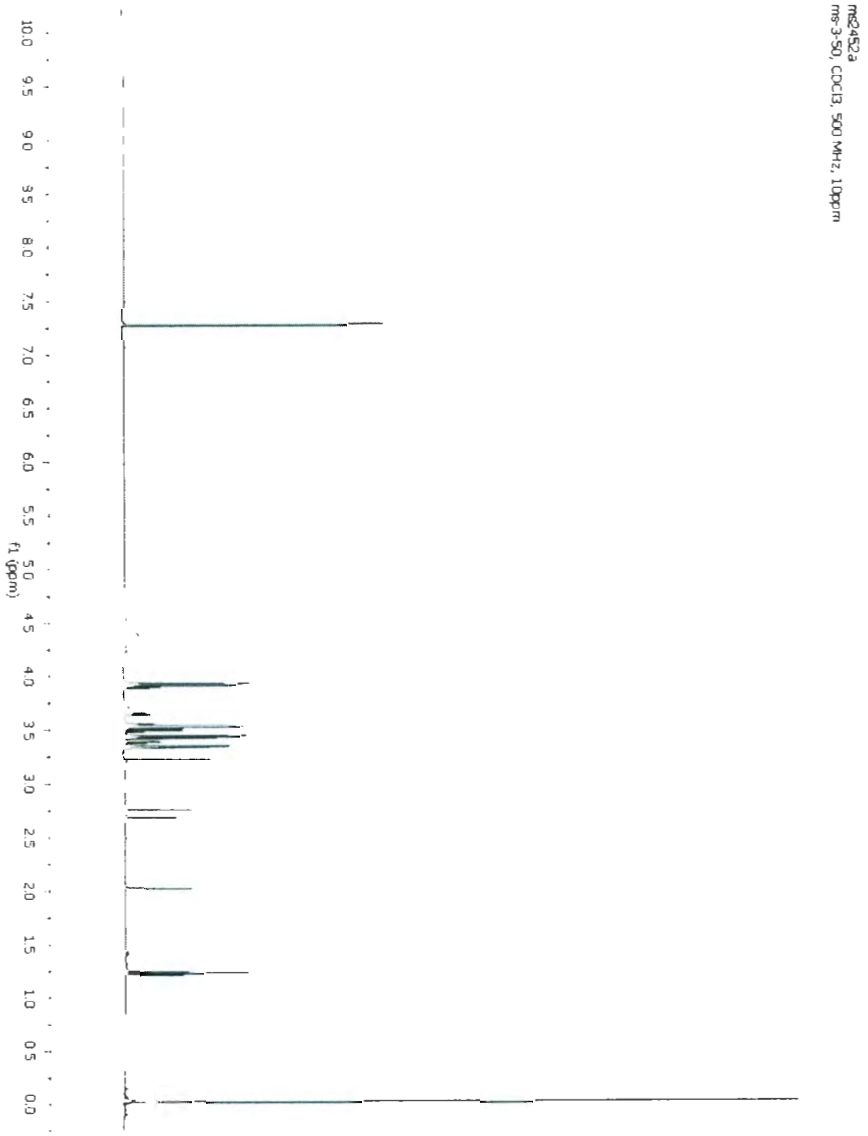

Figure A.62 ^{1}H NMR spectrum for **242.**

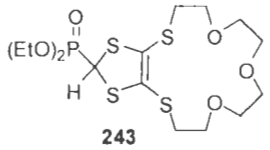

243

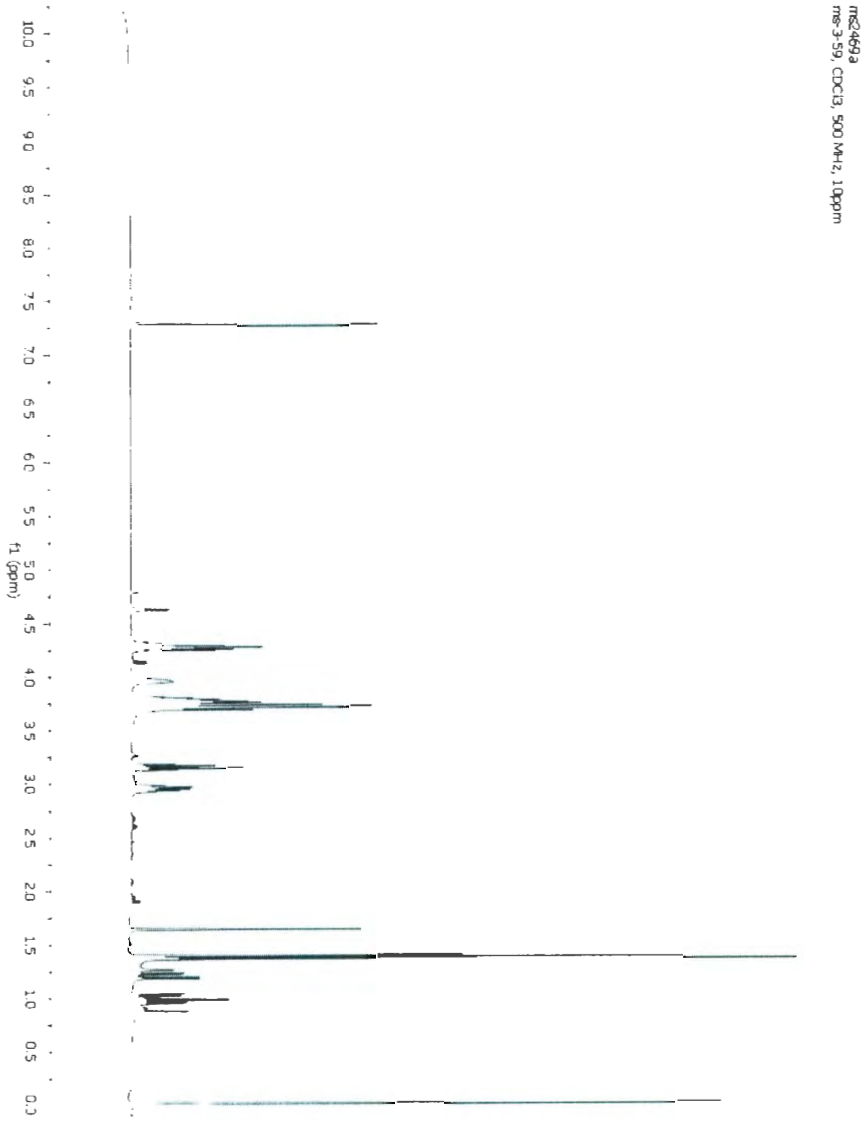

Figure A.63 ^{1}H NMR spectrum for **243.**

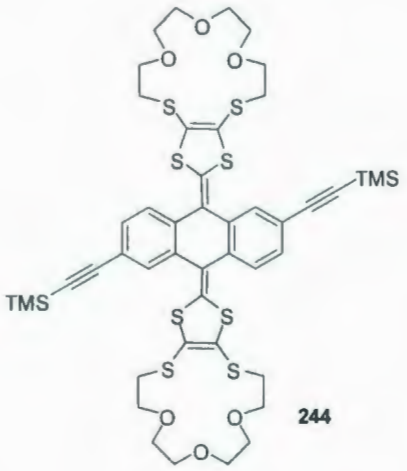

244

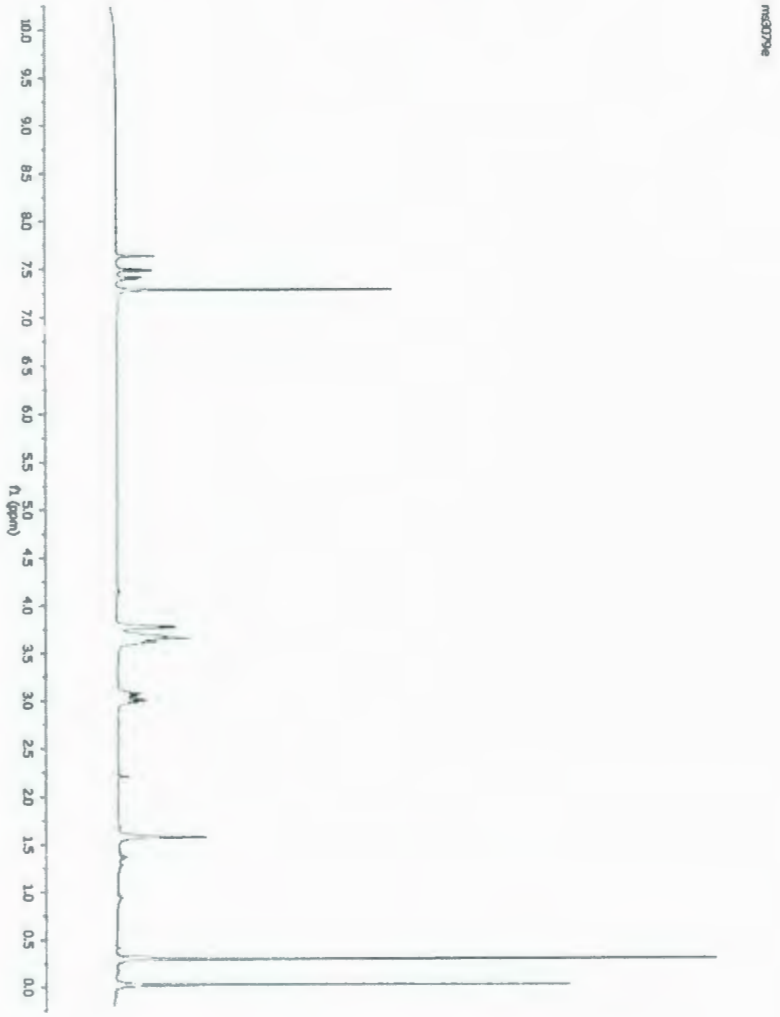

Figure A.64 ^{1}H NMR spectrum for **244.**

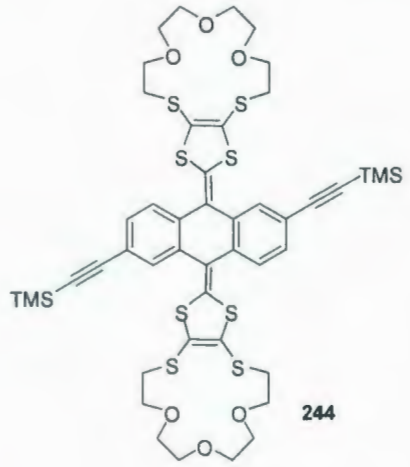

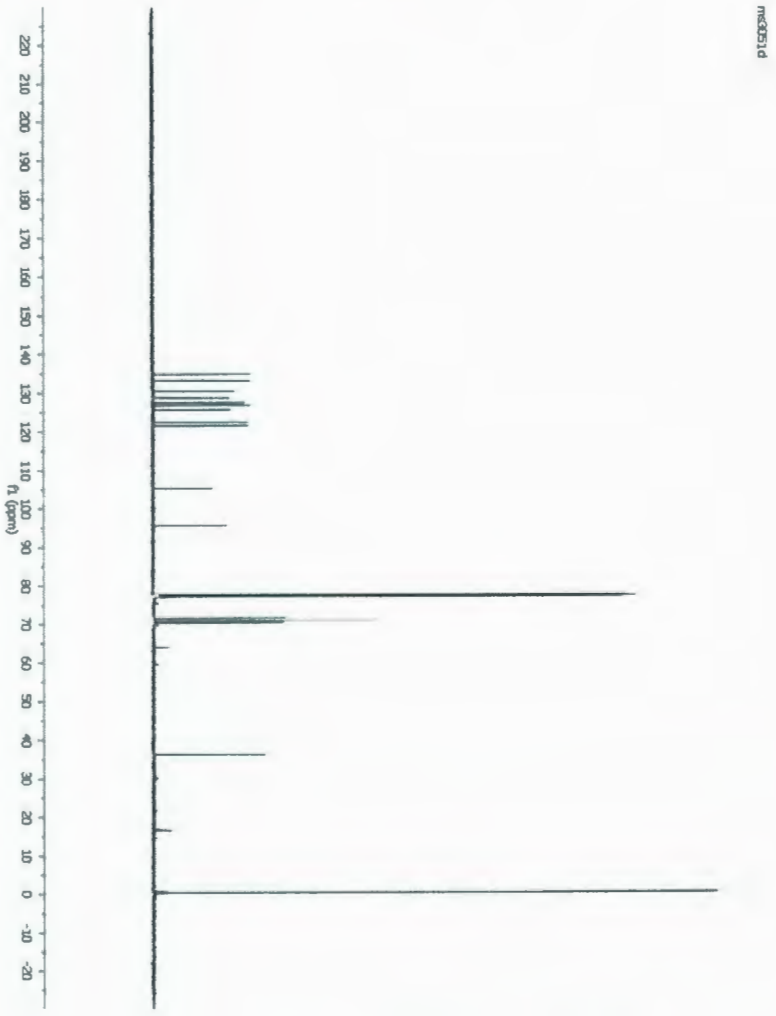

Figure A.65 ^{13}C NMR spectrum for **244.**

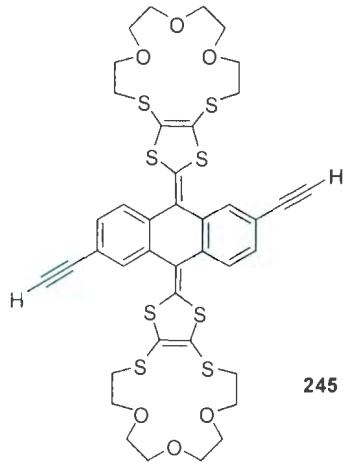

245

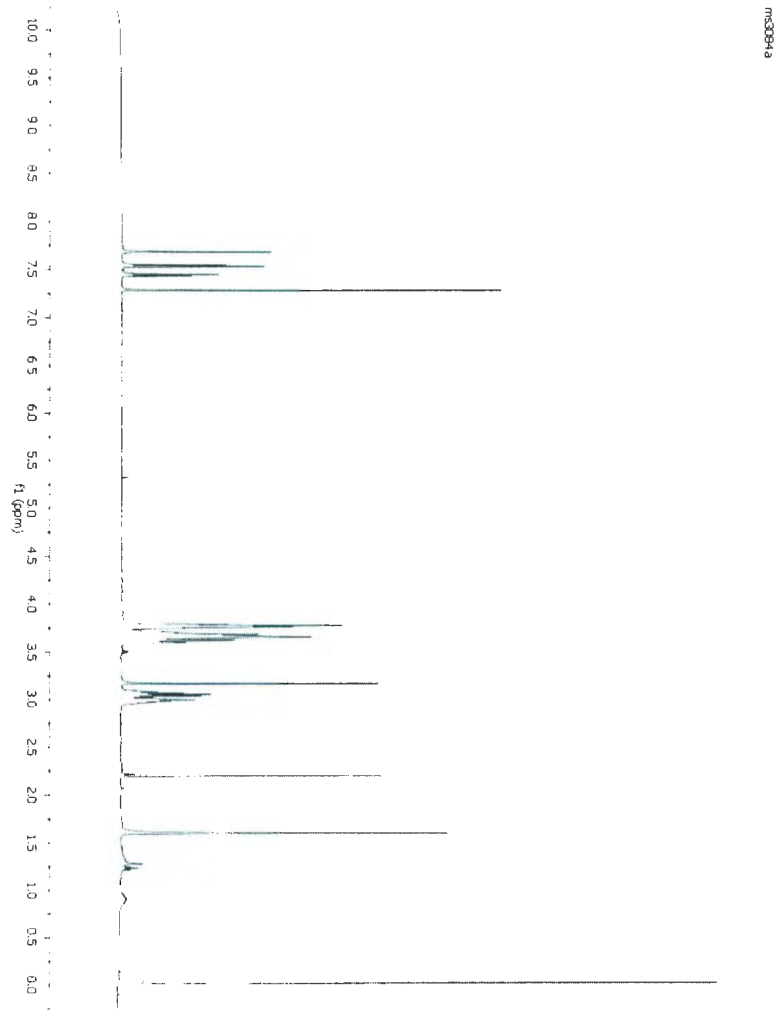

Figure A.66 ^{1}H NMR spectrum for **245.**

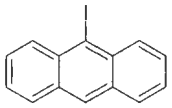

246

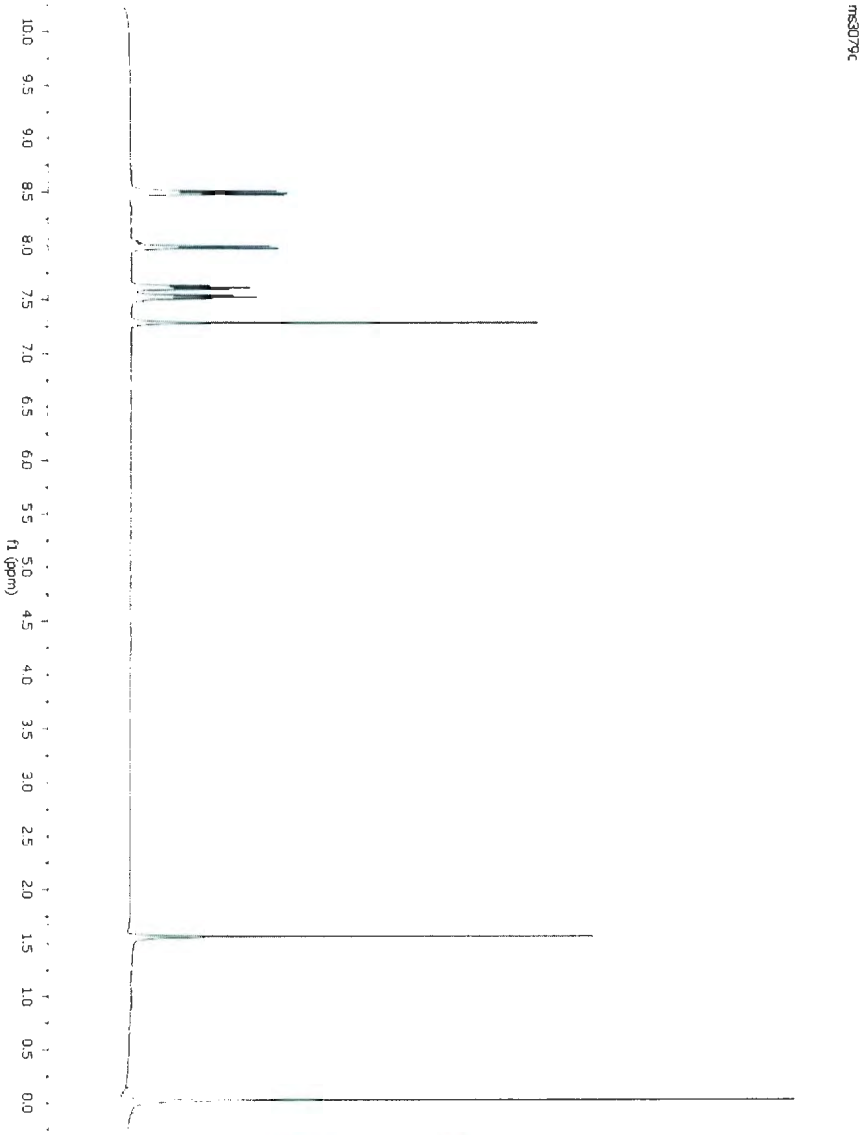

Figure A.67 ^{1}H NMR spectrum for **246**

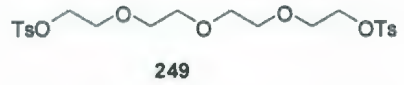

249

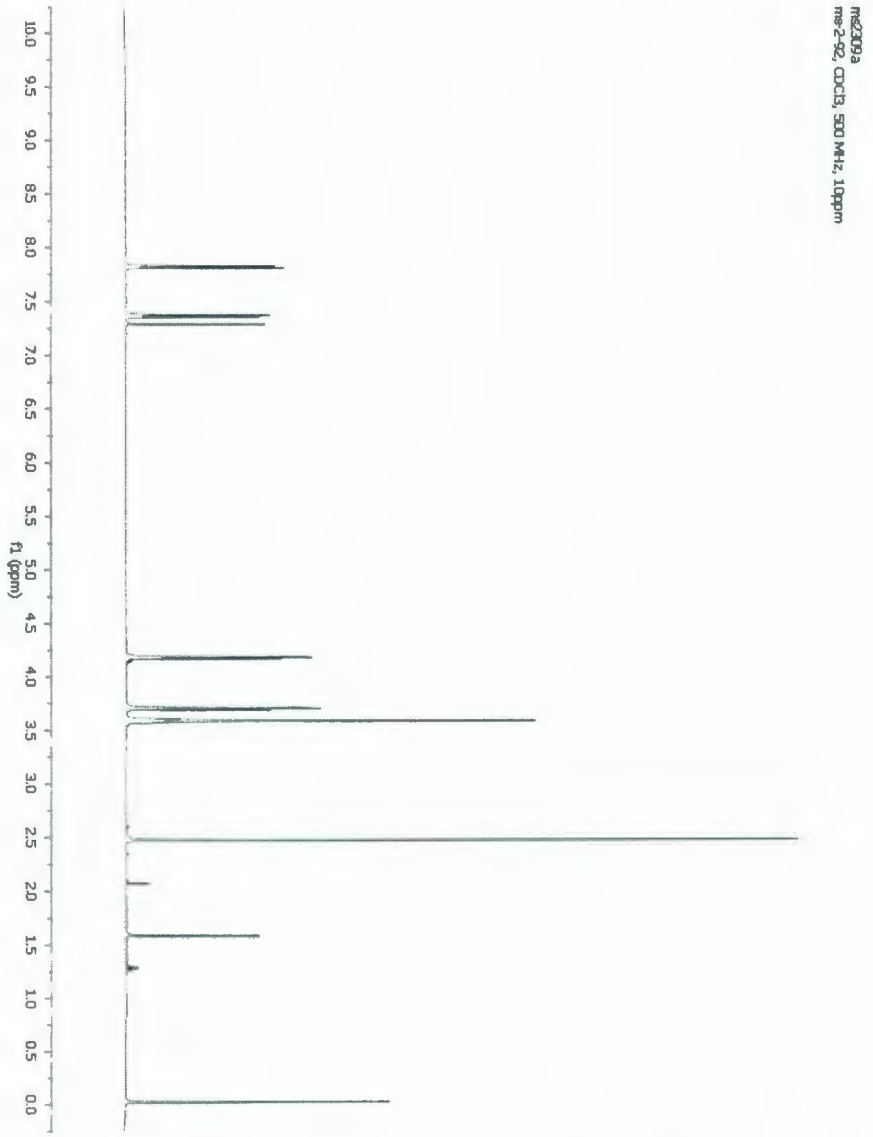

Figure A.68 ^{1}H NMR spectrum for **249.**